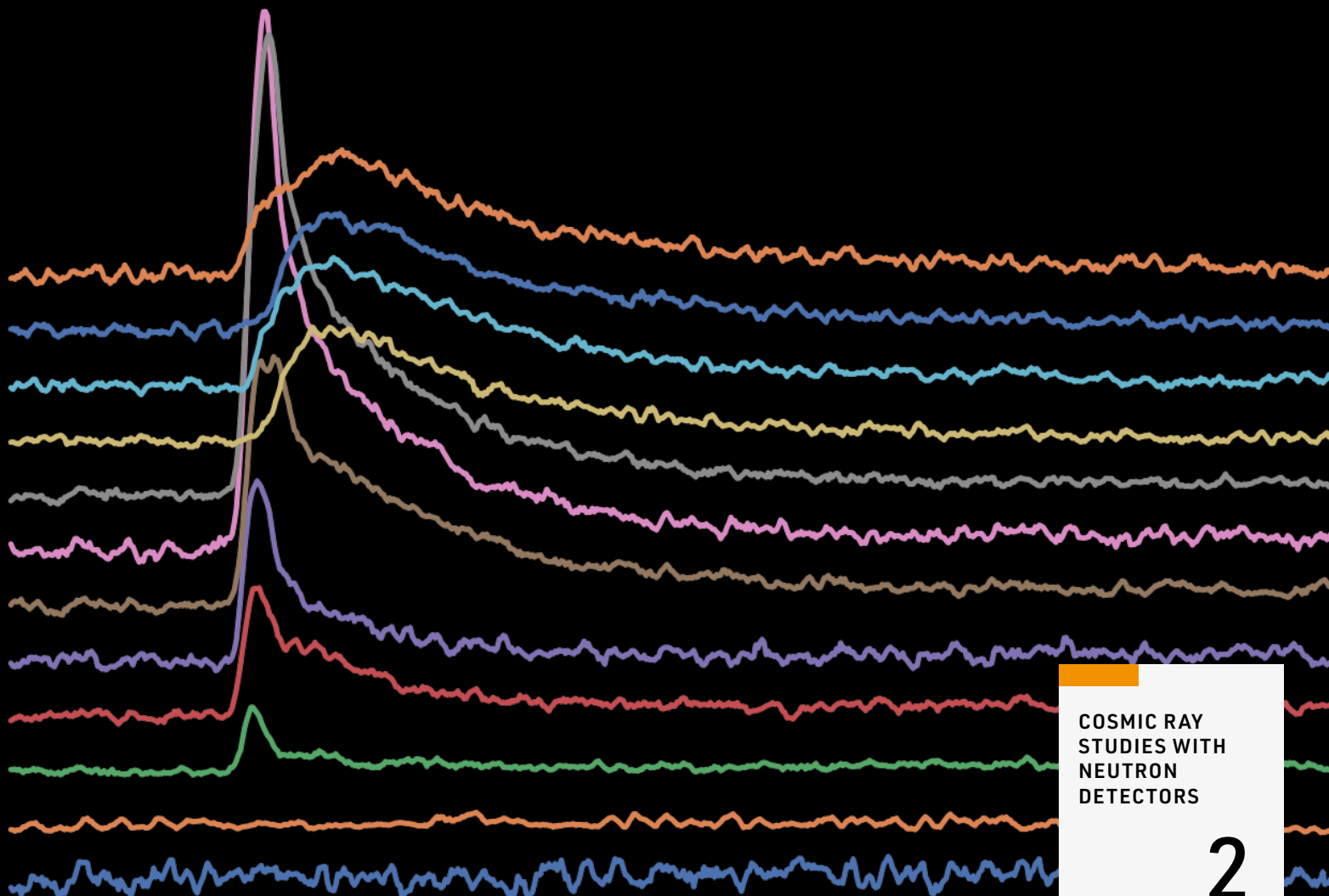


NMDB@Athens

Proceedings of the hybrid
symposium on cosmic ray studies
with neutron detectors

September 26-30, 2022



COSMIC RAY
STUDIES WITH
NEUTRON
DETECTORS

2

Cosmic ray studies with neutron detectors

Volume 2

NMDB@Athens


Proceedings of the hybrid symposium on
cosmic ray studies with neutron detectors
September 26-30, 2022


Edited by Rolf Bütikofer, Agnieszka Gil-Świderska, Karl-Ludwig Klein,
Olga Kryakunova, Monica Laurenza, Helen Mavromichalaki,
David Ruffolo, Danislav Sapundjiev, Christian T. Steigies, Du Toit Strauss

Cosmic ray studies with neutron detectors | Volume 2 (2023)


(eISSN: 2748-3150)


Editors


Rolf Bütikofer , Physics Institute, University of Bern, Switzerland


Agnieszka Gil-Świdarska , Institute of Mathematics, Siedlce University, Poland


Karl-Ludwig Klein, Observatoire de Paris, LESIA, Université Paris Sciences et Lettres, CNRS, Sorbonne Université, Université Paris Cité, France


Olga Kryakunova , Institute of Ionosphere, Almaty, Kazakhstan


Monica Laurenza , INAF – National Institute for Astrophysics, Rome, Italy

Helen Mavromichalaki , Nuclear and Particle Physics Department, Faculty of Physics, National and Kapodistrian University of Athens, Greece

David Ruffolo , Department of Physics, Faculty of Science, Mahidol University, Bangkok, Thailand

Danislav Sapundjiev , Royal Meteorological Institute of Belgium, KMI-IRM, Brussels, Belgium

Christian T. Steigies , Extraterrestrial Physics, Institute of Experimental and Applied Physics, Kiel University, Germany

Du Toit Strauss , Center for Space Research, North-West University, Potchefstroom, South Africa

Bibliographic information published by the Deutsche Nationalbibliothek

The Deutsche Nationalbibliothek lists this publication in the Deutsche Nationalbibliografie; detailed bibliographic data are available on the internet at <http://dnb.d-nb.de>.

Open Access



This book is published under the Creative Commons Attribution 4.0 International license (<https://creativecommons.org/licenses/by/4.0>). Please note that individual, appropriately marked parts of the book may be excluded from the license mentioned or may be subject to other copyright conditions. If such third party material is not under the Creative Commons license, any copying, editing or public reproduction is only permitted with the prior consent of the respective copyright owner or on the basis of relevant legal authorization regulations. The electronic open access version of this book is permanently available on MACAU: Open Access Repository of Kiel University (<https://macau.uni-kiel.de>): <https://doi.org/10.38072/2748-3150/v2>

2023 Universitätsverlag Kiel | Kiel University Publishing

Universitätsbibliothek Kiel
Leibnizstr. 9
24118 Kiel
Germany
verlag@ub.uni-kiel.de, www.universitaetsverlag.uni-kiel.de

Cover: Ground level enhancement of 2006-12-13 (GLE # 70). Plot created by Christian T. Steigies using data from the neutron monitor database (NMDB), founded under the European Union's FP7 programme (contract no. 213007) for providing data.

Typesetting: Wiebke Buckow

eISBN (PDF): 978-3-928794-99-2

Contents

Introduction

NMDB@Athens	9
Rolf Bütikofer, Agnieszka Gil-Świdarska, Karl-Ludwig Klein, Olga Kryakunova, Monica Laurenza, Helen Mavromichalaki, David Ruffolo, Danislav Sapundjiev, Christian T. Steigies, Du Toit Strauss	
Welcoming for NMDB@Athens conference	15
Helen Mavromichalaki	
Obituary: Marisa Storini (1944–2023)	21
Monica Laurenza on behalf of the Rome neutron monitor team	

Session 1: Cosmic rays in the heliosphere

Cosmic ray angular distribution dynamics during Forbush decrease in 3-4 November 2021	27
Petr Yu. Gololobov, Vladislav G. Grigoryev, Sardaana K. Gerasimova, Sergey A. Starodubtsev, Anton S. Zverev	
Magnetospheric effects on cosmic rays during the magnetic storm of March 2015	37
Elena Ntina, Maria Gerontidou, Helen Mavromichalaki, Maria Abunina, Anatoly Belov, Victor Yanke, Angelos Laoutaris	
Residual modulation of galactic cosmic rays in the heliosphere	47
Victor Yanke, Anatoly Belov, Raisa Gushchina, Pavel Kobelev, Lyudmila Trefilova	
Session 1: Abstracts	61
• Real time monitoring of the angular distribution of cosmic rays with Ring of Stations method using NMDB data	61
• Cosmic rays in the heliosphere	61
• Cosmic ray intensity and spectral changes during 27-day variations using time-delay measurements from Antarctic neutron monitors	62
• Large amplitude bidirectional anisotropy of cosmic-ray intensity observed in November, 2021	63
• Solar magnetic polarity effect on neutron monitor count rates: comparing latitude surveys and Antarctic stations	64
• Revised neutron monitor scaling factor and modulation potential determination for 1964-2021	65

Session 2: GLE analysis and space weather research and services




GOES observations of solar protons during ground level enhancements	69
Juan V. Rodriguez, Brian T. Kress	
NMDB and space weather forecasting	81
Petr Yu. Gololobov, Sergey A. Starodubtsev, Vladislav G. Grigoryev, Anton S. Zverev	
Behavior of galactic cosmic rays density and vector anisotropy before and during high-energy magnetospheric electron flux enhancements	89
Olga Kryakunova, Anatoly Belov, Botakoz Seifullina, Maria Abunina, Artem Abunin, Irina Tsepakina, Nataly Shlyk, Serik Nurakynov, Nikolay Nikolayevskiy	
The updated GLE Alert system by ANEMOS	97
Helen Mavromichalaki, Pavlos Paschalis, Maria Gerontidou, Anastasia Tezari, Maria-Christina Papailiou, Dimitra Lingri, Maria Livada, Argyris Stassinakis, Norma Crosby, Mark Dierckxsens	
The GLE # 73 on 28 October 2021: spectra, angular distribution and terrestrial effects	105
Alexander Mishev, Leon Kocharov, Sergey Koldobskiy, Nicholas Larsen, Esa Riihonen, Rami Vainio, Ilya Usoskin	

What do we learn from ground level enhancements?	113
Athanasios Papaioannou	
Session 2: Abstracts	131
• Cosmic rays and space weather	131
• Solar activity as observed by neutron monitors and muon telescopes in the same location	131
• Solar energetic particle event on 28 October 2021 as observed by the neutron monitor network	132
• 40 years of solar neutron observations from ground	132
• A relationship between rise times and decay times of relativistic solar particle events observed by neutron monitors	133
• A new reconstruction of solar energetic particle fluence for GLE events	134
• Magnetic field line path length variations and effects on solar energetic particle transport	134
• Solar energetic particle events and Forbush decreases driven by the same solar sources	135
• Investigating GLE73, the first ground level enhancement of solar cycle 25	136
Session 3: Cosmic rays and the atmosphere	137
<hr/>	
Atmospheric cosmic ray induced ionization and radiation affecting aviation	139
Panagiota Makrantonou, Anastasia Tezari, Argyris N. Stassinakis, Pavlos Paschalis, Maria Gerontidou, Helen Mavromichalaki, Ilya G. Usoskin, Norma Crosby, Mark Dierckxsens	
Session 3: Abstracts	
• Neutron monitors detecting cores of extensive air showers	151
• Local environmental effects on cosmic ray observations at Syowa Station in the Antarctic: PARMA-based snow cover correction for neutrons and machine learning approach for neutrons and muons	151
• Forbush decrease observed by nodes of SEVAN East-European particle detector network on November 2021	152
• Tutorial: cosmic rays and the atmosphere	153
Session 4: Neutron detector instrumentation and stability	155
<hr/>	
First results of the SA Agulhas II mobile mini-neutron monitor	157
Du Toit Strauss, Frederic Effenberger, Stefan Lotz, Konstantin Herbst, Helena Krüger, Corrie Diedericks	
US-based Simpson neutron monitor network	171
James Ryan, John Clem, Paul Evenson, Surujhdeo Seunarine, Veronica Bindi, Cristina Consolandi, David Ruffolo, Waraporn Nuntiyakul	
Calgary neutron monitor efficiency factor estimation after major renovation	177
Clifford John Bland, Alexei F. Kouznetsov	
Haleakala neutron monitor redeployment and calibration with AMS data	183
Cristina Consolandi, Veronica Bindi, Claudio Corti, Nikolay Nikonov, James Ryan, Jason Legere, Waraporn Nuntiyakul	
Session 4: Abstracts	191
• New registration system of cosmic ray stations of ISTR SB RAS	191
• Neutron monitor electronics for spectral information from a single neutron monitor	191
• Neural networks for identification of neutron monitor faulty tube-counts	192
• Correction of snow effects on Oulu data using local snow depth data	193
• Latitude surveys of time-delay histograms from a semi-leaded neutron monitor during 2018–2020	193

Session 5: Neutron detector response functions	195
Neutron monitor yield function: improved spectral computations of the Forbush decrease of June 2015	197
Maria Livada, Loukas Xaplanteris, Nafsika Dimosthenous, Helen Mavromichalaki	
Session 5: Abstracts	207
• Neutron monitor response functions	207
Session 6: Data bases and catalogues	209
Accessing NMDB data using NEST and pandas	211
Christian T. Steigies, Nicolas Fuller	
Session 6: Abstracts	
• The catalog of the thunderstorm ground enhancement events registered on Mt. Aragats	219
• NMDB status, a brief tutorial	220
Program of the meeting	221

NMDB@Athens

Hybrid symposium on cosmic ray studies with neutron detectors

Rolf Bütikofer ¹, Agnieszka Gil-Świdarska ², Karl-Ludwig Klein³, Olga Kryakunova ⁴,
Monica Laurenza ⁵, Helen Mavromichalaki ⁶, David Ruffolo ⁷, Danislav Sapundjiev ⁸,
Christian T. Steigies ⁹, Du Toit Strauss ¹⁰

Correspondence

- 1 International Foundation ›High Altitude Research Stations Jungfrauoch and Gornergrat‹ and Physics Institute, University of Bern, Switzerland, rolf.buetikofer@unibe.ch
 - 2 Institute of Mathematics, Siedlce University, Poland, agil@cbk.waw.pl
 - 3 Observatoire de Paris, LESIA, Université PSL, CNRS, Sorbonne Université, Université Paris Cité, France, ludwig.klein@obspm.fr
 - 4 Institute of Ionosphere, Almaty, Kazakhstan, krolganik@yandex.kz
 - 5 INAF - National Institute for Astrophysics, Rome, Italy, monica.laurenza@inaf.it
 - 6 Athens Cosmic Ray Group, Faculty of Physics, National and Kapodistrian University of Athens, Greece, emavromi@phys.uoa.gr
 - 7 Department of Physics, Faculty of Science, Mahidol University, Bangkok, Thailand, ruffolo.physics@gmail.com
 - 8 Royal Meteorological Institute of Belgium, KMI-IRM, Brussels, Belgium, dasapund@meteo.be
 - 9 Extraterrestrial Physics, Institute of Experimental and Applied Physics, Kiel University, Germany, steigies@physik.uni-kiel.de
 - 10 Center for Space Research, North-West University, Potchefstroom, South Africa, dutoit.strauss@nwu.ac.za
-

Keywords

cosmic rays; neutron detectors; solar-heliospheric physics; space weather

Abstract

A brief overview is given regarding the presentations delivered at the NMDB@Athens meeting which was held, in a hybrid fashion, in September 2022. Participants joined both remotely but also physically at the National and Kapodistrian University of Athens, Greece. Unlike traditional cosmic ray meetings and conferences where the focus is mainly on the science related to neutron monitor measurements, the ›NMDB@Athens‹ meeting uniquely also addresses hardware issues related to these instruments and, importantly, also databases where different data products can be accessed by a growing and increasingly diverse user base. The present overview outlines and introduces the more detailed articles contained in the proceedings.

1. Introduction

Neutron monitors (NMs) have been used for more than 70 years to monitor the flux of cosmic rays (CRs) in the near-Earth environment. In addition to the continuously present galactic cosmic ray (GCR) flux, occasionally solar energetic particle events with sufficient energy can trigger a so-called ground level enhancement (GLE) event. The unique long-term and highly accurate NM data record spans seven solar cycles and includes 73 GLEs until 2022. This data record is invaluable to CR and heliospheric research, but is increasingly also used in various new research areas, including Space Weather, hydrology research and many more. A major aim of the Neutron Monitor Database (NMDB) is to provide a central repository of corrected data to make NM data accessible to a wider scientific community.

Following the very successful NMDB@Home2020 virtual meeting in 2020, it was decided to continue with this meeting series, but to move to a hybrid setting, given the lingering COVID-19 uncertainties. The present paper intends to give an overview regarding the presentations and discussions during the meeting and to set the stage for the authors' contributions that follow.

2. Cosmic rays in the heliosphere: spatial and time variability

The session started with a tutorial by M. Laurenza on CRs in the heliosphere. V. Yanke presented a paper on the residual modulation of GCRs in the heliosphere. P.Yu. Gololobov studied the CR angular distribution dynamics during the Forbush decrease in November 2021. E. Ntina analysed magnetospheric effects on CRs during the magnetic storm of March 2015. Further presentations were given by K. Munakata on the bi-directional anisotropy of CR intensities, by K. Poopakun on the solar magnetic polarity effect on NM count rates, by P. Väisänen on revised NM scaling factors, by P. Muangha on CR intensity and spectral changes, and, lastly, by S. Belov on real-time monitoring the angular distribution of CRs with the Ring of Stations method.

3. Ground level enhancement analysis and space weather research and services

Space weather is a branch of space physics and heliophysics, concerned with the time varying conditions within the Solar System. The global NM network has been used successfully for space weather tasks, specifically for investigation of GLEs, as one of the most dangerous space weather phenomena. The introductory lecture (tutorial) was presented by A. Papaioannou. It was devoted to GLE events that are critical for the establishment of Space Weather services and the determination of their corresponding radiation risk. The presentation included a hands-on tutorial that demonstrated how the NMDB can be utilised for GLE analysis.

A. Papaioannou and co-workers presented an overview of the first GLE event of solar cycle 25, recorded on 28 October 2021 (GLE73). A. Mishev and co-workers also reported on GLE73. This event was detected on 28 October 2021 by several NMs, specifically those in the polar region as well as by space-borne instruments. The strongest signal at the ground was registered by the DOMC/DOMB NMs located at

the Antarctic plateau at the Concordia French-Italian research station. R. Bütikofer and Ch. Steigies also discussed the GLE event on 28 October 2021 as observed by the NM network. H. Mavromichalaki and co-workers presented the updated GLE Alert++ System of the Athens Neutron Monitor Station (A.Ne.Mo.S.). An accurate alert was issued successfully by the ESA R-ESC federated product GLE Alert Plus, as well as by the updated GLE Alert++ System. It should be emphasised that the GLE Alert++ signal was issued 45 minutes earlier than the one issued by the GOES satellites. J. Rodriguez and B. Kress presented the results of GOES observations of solar protons during GLEs. The connection between CRs and space weather was also discussed during M. Abunina's tutorial lecture.

A. Sáiz and co-workers reported about modelling the time profiles of solar energetic particle observations, while J.J. Blanco and co-authors also reported on solar activity as observed by NMs. The Oulu group (S. Koldobskiy et al.) conducted a new reconstruction of solar energetic particle fluence for GLE events. K.-L. Klein reported about the relationship between rise times and decay times of relativistic solar particle events observed by NMs. N. Shlyk and co-workers reported about solar energetic particle events and Forbush decreases driven by the same solar sources.

A new approach to study high-energy magnetospheric electron enhancements in geostationary orbit was proposed by O. Kryakunova and co-workers. Measurements of galactic CRs on the Earth's surface by the worldwide network of NMs are accurate and allow one to calculate the behaviour of their density and anisotropy beyond the magnetosphere boundary using the Global Survey Method. CRs carry important information about the state of the interplanetary medium and the near-Earth space. The behaviour of the density and anisotropy of galactic CRs before and during electron flux enhancements in events connected with the arrival at Earth of high-speed streams from coronal holes, coronal mass ejections associated with solar flares or disappearing solar filaments is revealed.

Using NMDB data, P. Gololobov and co-workers presented results from a new method for short-term forecasting of intense geomagnetic storms with an advance of 1-2 days. The success rate of this forecasting is about 80%. It is important that only with the creation of NMDB it became possible to implement it in real time mode.

E.O. Flückiger and R. Bütikofer reported on the results of solar neutron observations from ground-based detectors. The report gave a historical overview of the 3 June 1982 event and summarises its main scientific impact over the last 40 years.

4. Cosmic rays in the atmosphere

The session started with a tutorial, presented by S. Poluianov, regarding the formation of secondary particle cascades in the atmosphere. It was followed by a presentation by A. Chilingarian and co-workers regarding the observations of extensive air showers by the Aragats NM. The same group, presented by H. Martoyan and co-workers, discussed results of the SEVAN East-European particle detector network regarding the November 2021 Forbush decrease. In other talks, R. Kataoka and co-workers presented results of a machine learning method to account for local environmental effects in the NM count rate as measured at the Syowa Station in Antarctica. Lastly, P. Makrantonis and co-workers, discussed the levels of CR induced radiation at aviation altitudes.

5. Neutron detectors: instrumentation, stability, and response functions

Major renovations have been performed at the Calgary NM from 2009 until 2017. C. Bland and A. Kouznetsov presented a multiple regression method to estimate the efficiency factor which is used to scale the data to provide a continuous time series with the previous instrument, which has been in operation since the 1960s. The method takes solar modulation as well as changes in NM sensitivity into account.

J. Ryan and co-workers reported on the status of US-based NMs and the NSF funded Simpson NM network. This network will secure the operation, repair, and upgrades of the existing US stations and even plans to (again) set-up a station on the summit of Haleakala on Maui to take the network to a new operational and scientific level.

The detailed plan for the “Haleakala Neutron Monitor Redeployment and Calibration with AMS data” is given in the paper by C. Consolandi and co-workers. Not only will the Haleakala NM be redeployed near the initial station, but it will also be calibrated with AMS data and modelled by simulating the detector response. Thereby the station will be well suited to fill the large gap in the NM network in the Pacific Ocean, but also will be able to measure solar neutrons due to its high altitude and low latitude location.

A redesigned mini-NM has been installed on a South African Research vessel and performed several latitude scans from South Africa to Antarctica. R.D. Strauss and co-workers analysed effects of temperature variation and high-frequency interference on the measurements. To avoid the negative impact of these effects, the instrument will be moved to a more suitable location on the vessel where it can be operated continuously for several years.

Further presentations were given by A. Lukovnikova about new registration systems, by D. Ruffolo on electronics for deriving spectral information from a single NM, by D. Sapundjiev about neural networks to identify faulty tubes, by P. Väisänen on correcting snow effects, and by V. Yakum on latitude surveys with a “semi-leaded” NM.

6. Neutron detector response functions

A. Mishev presented different methods of determining NM response functions in a tutorial. M. Livada and co-workers calculated the GCR spectral index of the Forbush decrease in June 2015.

7. Databases and catalogues

C. Steigies gave a report on the status of NMDB and an interactive tutorial on accessing real-time data from NMDB using the programming language Python. With the scripts provided, everybody can quickly read data from the NMDB real-time file and make data analysis or generate plots. In a further presentation a small Python library was presented that allows retrieving data that is made available via NEST into Python and generates a pandas data frame. A final contribution by D. Aslanyan presented the catalogue of thunderstorm ground enhancement events registered on Mt. Aragats.

8. Conclusion

The NMDB@Athens meeting, building on the success of the NMDB@Home2020 virtual meeting, brought together NM scientists from around the world; participants attended from Africa, the Americas, Asia, Australia, and Europe, representing almost all time zones. A variety of topics were discussed, ranging from instrumental topics to space weather applications using NM measurements. Especially encouraging were discussions surrounding the opening of new stations and the refurbishing of older stations. This, along with other recent advances, will allow the NMDB to provide historical and real-time data to an ever growing and more diverse community of users.

Acknowledgements

As the scientific organisers of the hybrid symposium NMDB@Athens, we express our gratitude to the National and Kapodistrian University of Athens, Greece, who hosted the meeting. We would also like to thank Kiel University Publishing for publishing these proceedings. The NMDB project, which initially proposed the idea of the symposium, was funded by the European Union's FP7 programme (contract no. 213007).

In Memoriam

The participants of the symposium took note of the recent passing away of eminent members of the community, including Dr. Evgenia Alexandrovna Eroshenko (1940–2021), Dr. Lev Isaacovich Dorman (1929–2022), and Prof. Pieter Stoker (1927–2022). We are privileged to have known these colleagues who pioneered the field of cosmic ray research.


Peer-review statement

Each full-length conference proceeding included in this volume has been peer-reviewed by two independent reviewers.

Open Access

This paper is published under the Creative Commons Attribution 4.0 International license (<https://creativecommons.org/licenses/by/4.0/>). Please note that individual, appropriately marked parts of the paper may be excluded from the license mentioned or may be subject to other copyright conditions. If such third party material is not under the Creative Commons license, any copying, editing or public reproduction is only permitted with the prior consent of the respective copyright owner or on the basis of relevant legal authorization regulations.

Welcoming for NMDB@Athens conference

Helen Mavromichalaki 

Correspondence

Nuclear and Particle Physics Department, Faculty of Physics, National and Kapodistrian University of Athens, Greece, emavromi@phys.uoa.gr

Keywords

NMDB; conference; obituaries; Eroshenko; Dorman

Abstract

Prof. H. Mavromichalaki on behalf of the organizing committee welcomes everyone to the 'NMDB@Athens' conference. The obituaries for Dr. Evgenia Eroshenko and Prof. Lev Dorman who recently passed away are following.

1. The welcome talk

Dear Colleagues and Friends, dear Students,

On behalf of the NKUA and the Athens Cosmic Ray Group I would like to personally welcome you to the Virtual NMDB Symposium on Cosmic Ray Studies with Neutron Monitor Detectors. Our initial intent was to host this symposium in Athens and greet you in person, as we have done many times in past. However, since this was not feasible, I am pleased to organize an online symposium and provide once more the opportunity to meet you again.

From the NMDB installation meeting, lots of others have been realized here in Athens. This is the 2nd virtual Symposium organized in the frame of the NMDB consortium and is focused on researches on cosmic rays using data from the ground-based neutron detectors, the neutron detectors themselves, and the handling and distribution of these data.

A number of 95 registered participants from 33 institutes and universities of 19 countries will attend this meeting. The topics that will be addressed are organized into the following six sessions: Cosmic rays in the heliosphere, GLE analysis and space weather research and services, Cosmic rays and the atmosphere, Neutron detector instrumentation and stability, Neutron detector response functions and finally Data bases and catalogues. A series of 43 tutorials and contributed talks of some of the most significant scientists of the NM community will be provided with all the latest information on Cosmic Rays Studies and Neutron Monitors.

At this point I would like to thank you all not only for participating in this symposium but also for your continuous presence over the years in all the NMDB meetings and conferences. With our common efforts

and support, NMDB has become a useful tool for scientists all around the world and with our enduring collaboration NM community can progress even more in the future.

Last but not least, I would like to take a moment of your time and honor the memory of two of our esteemed colleagues and dear friends that have recently passed away, Prof. Lev Dorman and Dr. Eugenia Eroshenko. These two distinguished scientists have served Physics and Cosmic Rays in particular, with great zeal and determination and are irreplaceable for the scientific community. Their work will help keep their memory alive. Their knowledge and research will serve as a legacy and guideline for younger scientists. The cosmic ray and NM community mourns for the loss of these two great scientists and beloved friends.

2. Dr. Evgenia Alexandrovna Eroshenko (13/06/1940–03/06/2021)

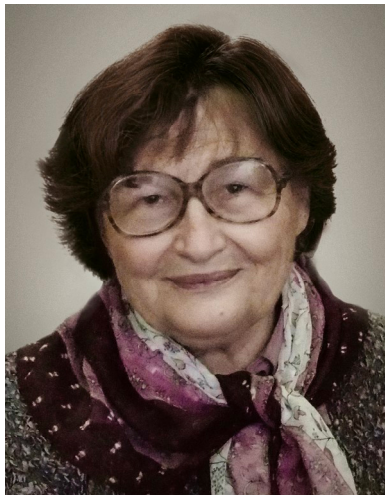


Fig.1: Dr. Evgenia Eroshenko.

2.1 Obituary by Athens Cosmic Ray Group

Dr. Evgenia Alexandrovna Eroshenko was a member of the Pushkov Institute of Terrestrial Magnetism, Ionosphere and Radio Wave Propagation (IZMIRAN) of the Russian Academy of Sciences from 1967 until 2021 and one of the founding members of the NMDB consortium.

She started her career as a Junior Scientist (1967-1981) in IZMIRAN and she was promoted to Senior Scientist (1981-2001) and finally Lead Scientist from 2001 on. Her research work addressed several issues of cosmic rays physics. Cosmic ray anisotropy, associated with transients in the interplanetary space and with the structure of the heliosphere, solar-terrestrial relations, Ground Level Enhancements, solar protons spectra during powerful solar events and Forbush effects and the search of precursors preceding these events are some of the subjects presented in her numerous publications and studies. Moreover, she was engaged in data processing (comparison and quality estimation of data from the worldwide neutron monitor network and collecting and preparing data for different tasks and databases) and investigated space weather prognosis using data from satellites and ground-based detectors.

In her long lasting career, Dr. Evgenia Alexandrovna Eroshenko collaborated with scientists from international Institutes and Universities (University of Kiel, Bartol Research Institute, University of Athens and other organizations). She participated in many international projects: Space ship Earth, NMDB (where she ensured the participation of a wide network of neutron monitors from Russia and Asia), SCOSTEP VarSITI, Interplanetary Research Virtual Laboratory disturbances and helped promote cosmic rays physics and neutron monitors through her constant and reliable presence in the NM community.

Dr. Evgenia Alexandrovna Eroshenko was an enthusiastic and dedicated scientist, a generous and patient teacher who eagerly shared her knowledge with younger scientists, a fair and diligent colleague, a conscientious, responsible and delightful person with a particular talent in painting. Her paintings and handicrafts are yet another way to keep her memory alive. Not only was she an esteemed colleague but mostly a precious friend that will be greatly missed.

2.2 Obituary by IZMIRAN Cosmic Ray Team

Eroshenko Evgenia Aleksandrovna graduated from the Orenburg Pedagogical Institute in 1962. In 1967, after post-graduate studies, she started to work at IZMIRAN. Evgenia Aleksandrovna was actively engaged in the study of cosmic ray anisotropy associated with interplanetary space transients and with the heliosphere structure, as well as in the search for precursors in the cosmic rays behavior before strong geomagnetic disturbances. She took part in the study of ground level enhancements of solar cosmic rays and in the development of methods for predicting solar proton events on Earth.

Eroshenko E.A. participated in many international projects (Spaceship Earth, NMDB, SCOSTEP VarSITI, Virtual Laboratory for Forbush Effects and Interplanetary Disturbances Analysis). For many years, she supervised the creation of modern databases for the network of cosmic ray stations in Russia and the CIS. Evgenia Aleksandrovna actively cooperated with the Japanese and American data centers, the University of Kiel, the Bartol Research Institute, the University of Athens and others.

Eroshenko E.A. was an energetic, purposeful, widely erudite person, capable of making decisions and completing the work begun, without violating the concepts of honor and conscience. Evgenia Aleksandrovna was a very sociable and charming person. She was distinguished by diligence, initiative, and a highly developed sense of duty and responsibility. We will always remember her love of life, sociability and kindness. Eroshenko E.A. was also fond of drawing art and her paintings will also remain a memory of her.

We, her colleagues and friends, express our deep condolences to her family, to everyone who knew and remembers Evgenia Aleksandrovna. We will forever keep a good memory of this bright person.

3. Prof. Lev Isaakovich Dorman (01/05/1929–27/07/2022)

3.1 Obituary by Athens Cosmic Ray Group

Dr. Lev Isaacovich Dorman was a Professor and Head of the Israel Cosmic Ray and Space Weather Centre at Tel Aviv University (TAU), Israel from 1991 until 2022 and an Honored Scientist of the Russian Federation (1989).

He held many esteemed positions over his long lasting career, including Researcher (1951-1957) and Head department (1965-1992) at IZMIRAN, Moscow, Head department at Magnetic Lab (1957-1962) and Kurchatov Institute of Atomic Energy (1962-1965), Moscow, Professor at Moscow State University (1965-1992), Director of



Fig. 2: Prof. Lev Dorman.

the Cosmic Ray Center, Tel Aviv (since 1992), President of the International Cosmic Ray Meteor Commission (1958-1987) and Cosmic Rays and Radiation Belts secretary (1981-1992), Moscow, amongst others.

He was a dedicated physicist with great contribution in the evolution of cosmic rays physics. His interests spread through a variety of topics (cosmic rays variations, precursors, space weather, etc). With over 900 publications and almost 4000 citations he was a scientist whose work and research inspired his peers and students and will continue to guide the scientific community even in his absence. As an author he published a great number of books, which were repeatedly published over the years and are considered to be valuable asset for academic libraries worldwide. His most widely acknowledged works are: Cosmic ray history (2014), Plasmas and energetic processes in the geomagnetosphere (2016/2017), Cosmic ray interactions, propagation, and acceleration in space plasmas (2006), Solar neutrons and related phenomena (2010), Cosmic rays in magnetospheres of the Earth and other planets (2009), Cosmic rays: variations and space explorations (1974), Cosmic rays in the earth's atmosphere and underground (2004) and Solar cosmic rays (1970).

Dr. Lev Isaacovich Dorman was a beloved and kind hearted person, sociable and active. He was present during conferences and meetings of our NM community at all times, always inspiring us with his knowledge, spirit and love of nature. He was a distinguished colleague and a dear friend that will be missed.

3.2 Obituary by IZMIRAN Cosmic Ray Team

Lev Isaakovich Dorman was a bright and strong man, a remarkable scientist and organizer, a truly legendary personality. His activity seemed inexhaustible, but the years do not spare even such people. Lev Isaakovich died at the age of 94.

L. I. Dorman is an outstanding scientist in the field of geophysical aspects of cosmic rays and space physics. About 70 years ago Lev Isaakovich laid the foundation for research cosmic ray variations of different origin: atmospheric, magnetospheric, and extraterrestrial. He developed theories and methods that formed the basis of a new science direction. The main results of the early period can be summarized as follows:

- discovery (with the help of cosmic ray variations) of two types of solar plasma flows: i) having relatively weak frozen-in magnetic fields with an intensity approximately constant during the solar cycle; ii) having magnetic fields approximately an order of magnitude higher and with intensity is proportional to the level of solar activity (causing strong magnetic storms on Earth and Forbush decreases in cosmic rays). Later the first type of flows was matched with the ambient solar wind, and the second – with coronal mass ejections and interplanetary shock waves (1955-1957);
- detection of the diffusion nature of solar cosmic ray propagation in interplanetary space (1957);
- discovery of resonant scattering of cosmic ray particles during propagation in cosmic plasma (1959);
- finding of the acceleration of the cosmic ray drift by shock waves (1959);
- evaluation of the heliosphere size on the basis of cosmic ray variations as about 100 AU for many years before direct space measurements (1967).

These discoveries were based on pioneering outstanding theoretical and experimental studies of cosmic ray variations, begun in 1954 (theory of meteorological effects of cosmic rays, method of coupling functions, spectrographic method). They all formed a new field of cosmic ray physics.

Lev Isaakovich Dorman took an active part in almost all International Conferences on Cosmic Rays since 1955 and COSPAR Congresses and did invited lecturing. He published many hundreds of original scientific papers and over 30 monographs.

L.I. Dorman, sparing neither effort nor time, provided scientific and organizational support to cosmic ray research in Russia. It is thanks to his efforts these studies have won international recognition and are deservedly well-known. His numerous students successfully work in many countries through the world.


We – colleagues, friends, students – express our deep condolences to relatives and friends, to every-one who knew and remembers Lev Isaakovich. We will forever keep a good memory of this outstanding man.

Open Access

This paper is published under the Creative Commons Attribution 4.0 International license (<https://creativecommons.org/licenses/by/4.0/>). Please note that individual, appropriately marked parts of the paper may be excluded from the license mentioned or may be subject to other copyright conditions. If such third party material is not under the Creative Commons license, any copying, editing or public reproduction is only permitted with the prior consent of the respective copyright owner or on the basis of relevant legal authorization regulations.

Obituary: Marisa Storini (1944–2023)

A life in cosmic ray physics

Monica Laurenza  on behalf of the Rome neutron monitor team

Correspondence

INAF - National Institute for Astrophysics, Rome, Italy, monica.laurenza@inaf.it

Keywords

NMDB; neutron monitor; obituary; cosmic ray studies; Storini

Abstract

Obituary for physicist Marisa Storini, who died in 2023.

With deep regret I inform that Dr. Marisa Storini, former senior researcher of the INAF- Istituto di Astrofisica e Planetologia Spaziali and head of the SVIRCO observatory (the Rome neutron monitor) and laboratory for terrestrial physics, passed away on 7 September 2023 at 79 years old. She was a brilliant scientist in cosmic ray physics and solar-terrestrial relationships.

Marisa was born on 4 March 1944 in Bergamo, Italy, graduated from La Plata National University in nuclear physics in 1966 and from La Sapienza University in Physics in 1969. She became a fellow of the National Research Council (CNR) of Italy in 1970–1972 when she started her pioneering studies of Forbush decreases and cosmic ray modulation.

She became staff researcher at CNR - Istituto di Fisica dello Spazio Interplanetario (IFSI) in 1972 and received the doctorate in astrophysics and ionised gas at the same university in 1983. Marisa was head of the cosmic ray section of CNR-IFSI from 1987 until 2001 and head of the international Italy/Chile collaboration for the study of cosmic rays in Antarctica from 1992 to 2005.

She was a member of the scientific committee of CNR-IFSI for the period 1998–2000 and a member of the National Committee for Research Coordination of the National Antarctic Research Program (PNRA) of Italy during 1999–2004.

Dr. Storini was one of the pioneers of the space weather and space climate discipline. She led many research projects. To name a few, she was the coordinator of A.C.QU.A. (Ares soil Characterization by Quadrupole Analysis) project of the Italian Space Agency (ASI) from 2001 to 2003, coordinator of the project ‘Cosmic rays in polar areas and associated terrestrial phenomena’ of the PNRA from 2002 to 2009, and co-investigator of the SIXS (Solar Intensity X-ray and particle Spectrometer) experiment aboard the ESA- JAXA BEPICOLOMBO mission. She was also WP leader in the Working Group 1 (Monitoring and predicting solar activity for Space Weather) and Working Group 2 (The radiation environment of the



Fig. 1: Marisa Storini (the one with sunglasses) at the IV European Cosmic Ray Symposium in 1974. Courtesy of Prof. Ester Antonucci (behind Marisa in the picture).

Earth) of the European COST ACTION 724 – developing the basis for monitoring, modelling and predicting space weather.

Marisa helped to organize several important international conferences, including the ‘IVth European Cosmic Ray Symposium’ in Frascati in 1974 (see Figure 1) and the 24th ‘International Cosmic Ray Conference’ in Rome in 1995.

Dr. Storini’s expertise extended from cosmic ray physics to solar and space physics, as well as to the solar induced effects on the terrestrial atmosphere and geomagnetic field, planets, space weather and climatology. She authored more than 200 scientific publications including an influential review of the ‘Gnevyshev gap’ in solar activity. She also obtained important results on Forbush decreases and long-term cosmic ray modulation, coronal holes, solar relativistic particles, and solar activity effects in heliosphere.

Marisa’s expertise encompassed the neutron monitor experimental set up as well as particle detectors and environmental instruments. She played a leading role in the development and upgrade of the Rome neutron monitor (NM) called SVIRCO (Studio Variazione Intensità dei Raggi COSMICI) observatory.

Thanks to Dr. Storini’s tireless efforts, the Rome neutron monitor has achieved high efficiency and reliability, is recognized as a crucial facility for space weather, and is considered to be a national asset of inestimable value and a reference station for other neutron monitors.

Marisa had a close collaboration with many neutron monitors groups. For instance, she helped in checking data from the newly installed NM in Athens in 2000. She participated actively in all NM meetings that were held in Athens, such as in the COST meeting for the creation of the ‘Neutron Monitor Data Base’ (NMDB).

Marisa was an outstanding scientist who dedicated her life to research with immense passion, but also a dear friend, with a strong character hiding a sensitive heart. She was loved and esteemed for her kindness and generosity, fruitful debate ability, honesty, and dedication to serve the community. Marisa



Fig. 2: Marisa (left) and myself (right) in one of the thousands of brain storming sessions.

was an amazing mentor (see Figure 2). Her passion for science has inspired many of us, students and collaborators, providing motivation, strength, determination to undertake our lives as researchers.

We lost a friend, an important personality, a reference for the whole community. She will be sorely missed.

Acknowledgements

Thanks to Dr. Ed Cliver, Prof. Helen Mavromichalaki, and Prof. Monica Storini for their contribution to the text and to Prof. Ester Antonucci for providing the picture in Figure 1.






Open Access

This paper is published under the Creative Commons Attribution 4.0 International license (<https://creativecommons.org/licenses/by/4.0/>). Please note that individual, appropriately marked parts of the paper may be excluded from the license mentioned or may be subject to other copyright conditions. If such third party material is not under the Creative Commons license, any copying, editing or public reproduction is only permitted with the prior consent of the respective copyright owner or on the basis of relevant legal authorization regulations.

Session 1:

**Cosmic rays
in the heliosphere**

Cosmic ray angular distribution dynamics during Forbush decrease in 3-4 November 2021

Petr Yu. Gololobov , Vladislav G. Grigoryev , Sardaana K. Gerasimova ,
Sergey A. Starodubtsev , Anton S. Zverev 

Correspondence

Yu. G. Shafer Institute of Cosmophysical Research and Aeronomy, Siberian Branch of the Russian Academy of Science, Russia, gpeter@ikfia.ysn.ru

Keywords

cosmic rays; neutron monitor; anisotropy; magnetic cloud; coronal mass ejection

Abstract

On November 3-4, 2021, there was a coronal ejection of the solar mass into the interplanetary medium. According to direct observations of the interplanetary magnetic field and the solar wind, the ejection was accompanied by a magnetic cloud. During the event, neutron monitors of the NMDB network registered a two-stage Forbush decrease with a total amplitude of up to 15%. A preliminary analysis of the NMDB data shows that the first step was due to the cosmic ray decrease behind the shock wave front, while the second step was due to the cosmic ray anisotropy formed in the magnetic cloud. This work was undertaken to study the dynamics of the angular distribution of cosmic rays in this event. The cosmic ray distribution was determined using the global survey method developed at the ShICRA in the 1960s. The method makes it possible to use the worldwide network of neutron monitors as a single multidirectional instrument and to determine the hourly dynamics of CR distribution. It is shown that unidirectional and bidirectional anisotropies of significant amplitude are observed inside the magnetic cloud. The results obtained are discussed in the framework of modern theories of the formation of magnetic clouds. The temporal dynamics of the spatial-angular distribution of cosmic rays during the Forbush decrease on November 3-4, 2021 was determined. The presence of cosmic ray anisotropy with an amplitude comparable to the magnitude of the density decrease itself was found.

1. Introduction

The flux of galactic cosmic rays (CR) coming from the interstellar medium into the heliosphere fills its entire cavity. The spatial-time distribution of CR at each point of the heliosphere is determined by its properties and structure, which depends on solar activity. Thus, in the interplanetary medium, a special CR angular distribution is formed, which is characterized by both isotropic and anisotropic components. And although the anisotropy is two orders of magnitude lower than the isotropy, it carries a valuable information about the features of GCR modulation by the solar wind.

Of particular interest are sporadic manifestations of solar activity accompanied by a large energy release into the space surrounding the Sun. One of the most striking examples of these processes are coronal mass ejections (CME). As a rule, at the moments of the passage of the Earth's by CME, the so-called Forbush decrease (FD) is observed in the data of ground-based detectors, i.e., sharp decreases in the GCR intensity followed by a gradual recovery. As a rule, on Earth, such an effect is manifested by a single sharp decrease in intensity and its subsequent gradual recovery. However, in some cases, FD can have a multi-stage time profile formed due to the so-called magnetic clouds (MC) propagating in the CME body (Xu et al. 2010). MCs are characterized by a strong regular field, which is capable of shielding GCRs, leading to a decrease in CR intensity and the formation of high-amplitude CR anisotropy (Belov et al. 2015).

2. Forbush decrease during 3-4 November 2021

On November 2, 2021, an M7.1 class solar flare occurred according to the SOHO spacecraft, as a result of which a high-velocity CME ejection was observed from the AR2891 active region (https://cdaw.gsfc.nasa.gov/CME_list/UNIVERSAL/2021_11/univ2021_11.html, last accessed June 27, 2023), which later overtook the CMEs that occurred on November 1-2 with slow velocities. As a result, according to the data of direct measurements of spacecraft (Figure 1), an interplanetary CME was observed on November 3-4. The arrival of the CME shock wave front to the observation point, which is located in close proximity to the Earth at the libration point L1, at 2021-11-03 20:00 was accompanied by a sharp jump in pressure and velocity of the solar wind, as well as an increase in the interplanetary magnetic field (IMF) module, followed by an increase in the IMF turbulence level. In the period from 2021-11-04 12:00 to 2021-11-05 04:00, a decrease in the field turbulence level and a gradual decrease in the solar wind velocity were observed, accompanied by a gradual change in the direction of the field vector. The behavior of the IMF and solar wind parameters allows us to conclude that the passage of MC was observed during the above period (Burlaga et al., 1981).

The measurement data of CR from the network of neutron monitors for November 3-6, 2021 is shown in Figure 2. As can be seen, the arrival of the ICME was accompanied by a FD, which had a two-stage character. The first stage corresponds to the moment of arrival of the shock wave to the Earth, and its depth depends inversely on vertical geomagnetic cutoff rigidities of the stations R_c . The second stage of the FD arose at the time of the passage of the MC and has an ambiguous behavior, characterized by a shift in the maximum depth, which, at the same time, does not depend on R_c . This allows us to conclude that a large CR anisotropy was observed inside the MC in this event.

3. Global survey method

To study the dynamics of the spatial-angular distribution of CRs, this work uses the global survey method (GSM) (Altukhov et al. 1970). GSM is the first method for studying the short-term dynamics of the CR angular distribution. Somewhat later, similar methods were developed by various researchers (Belov et al. 2018; Dvornikov & Sdobnov 1998; Bieber & Evenson 1989). GSM is a variant of spherical analysis of CR registration data of the world network of neutron monitors. It allows you to consider the entire global network of CR detectors as one multidirectional detector and instantly determine the CR distribution.

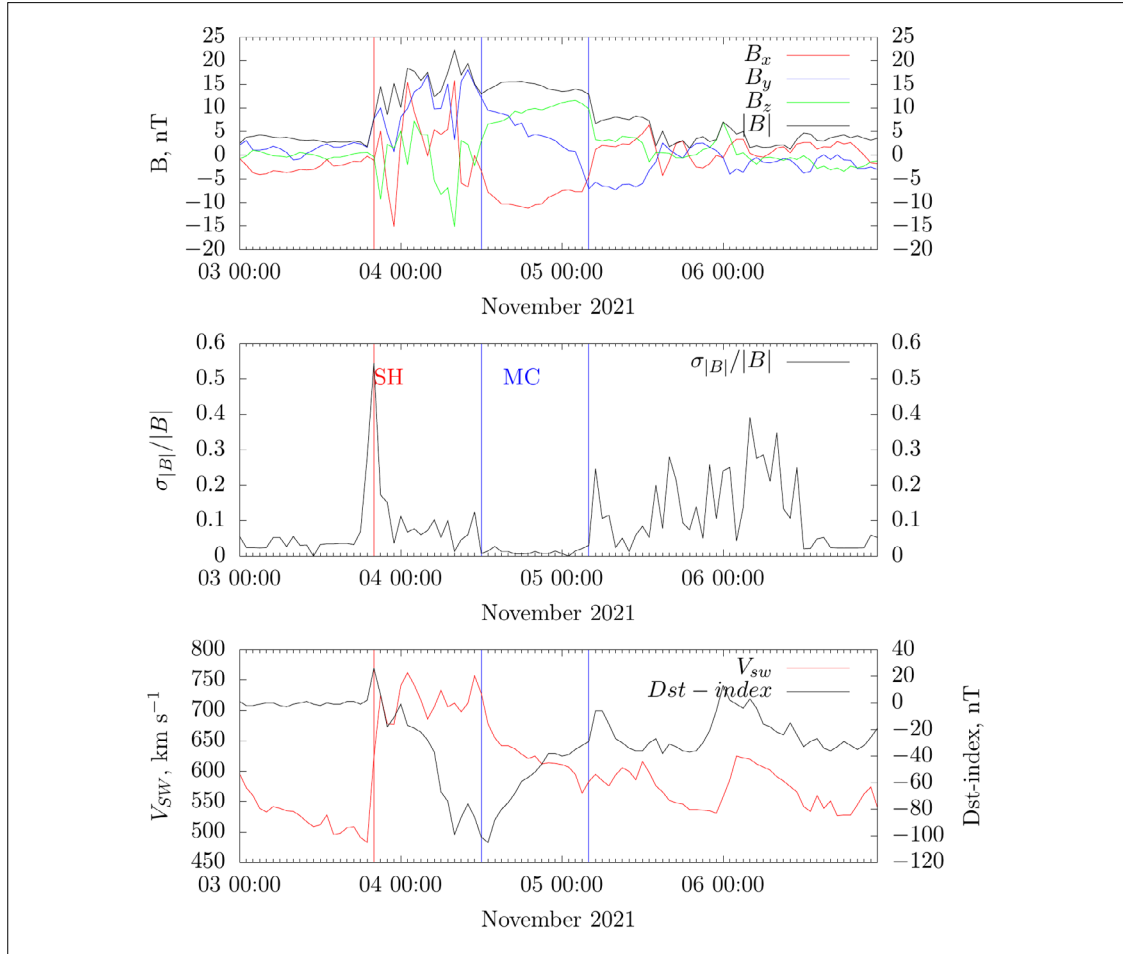


Fig. 1: The values of the components and modulus of the IMF intensity vector B , the field regularity level ($\sigma_{|B|}/|B|$) and the solar wind velocity V_{sw} and the geomagnetic activity Dst index for November 3-6, 2021 according to the OMNI catalog. The vertical red line corresponds to the moment of arrival of the shock wave to the Earth; the blue vertical lines show the MC boundaries.

Thus, the temporal resolution of determining the CR distribution is limited only by the capabilities of the detector network. In this case, 1-hour measurement data from neutron monitors included in the Neutron Monitor DataBase (NMDB) are used.

The method is based on the so-called receiving vectors (Krymsky et al. 1966), which makes it possible to establish a relationship between CR intensity variations in near-Earth outer space and the intensity of CR recorded by ground-based detectors. We will briefly describe the method below.

The CR distribution over the sphere $I(\theta, \varphi)$ when expanded into a series in terms of spherical harmonics will have the form:

$$I(\theta, \varphi) = \sum_{n=0}^{\infty} \sum_{m=0}^{\infty} (a_n^m \cos(m\varphi) + b_n^m \sin(m\varphi)) P_n^m(\sin\theta), \quad (1)$$

where θ and φ are latitude and longitude angles in the corresponding coordinate system, $P_n^m(\sin\theta)$ are associated Legendre polynomials, $0 \leq m \leq n \leq \infty$.

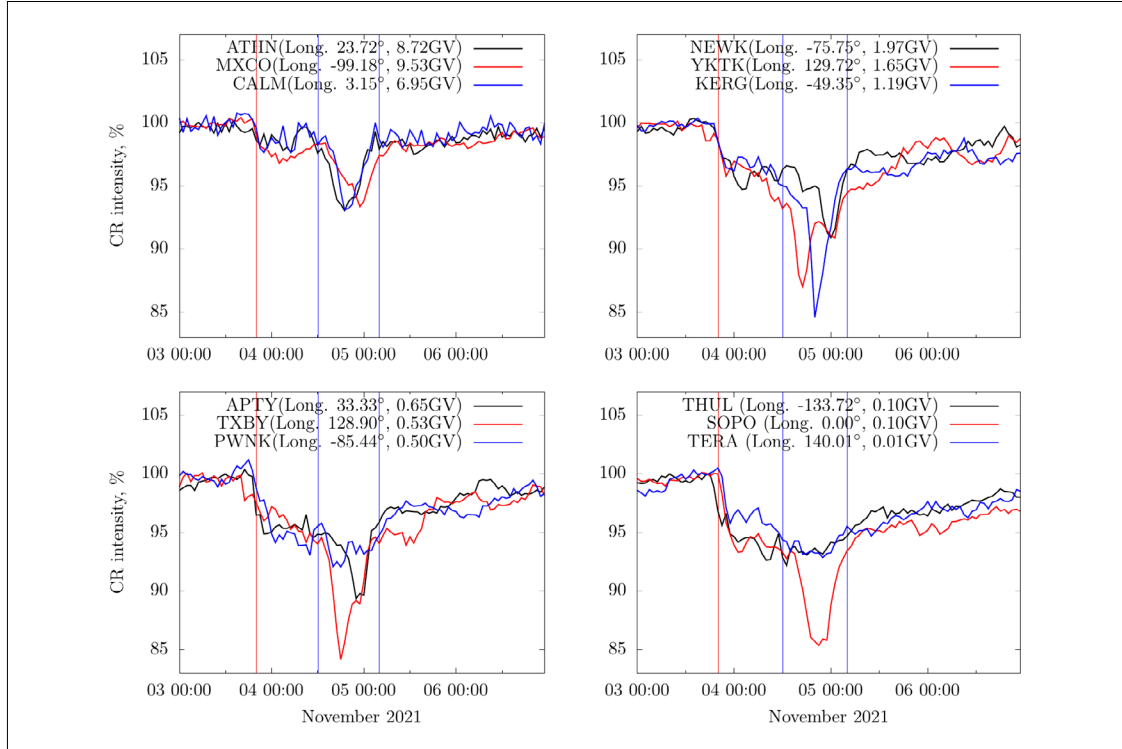


Fig. 2: Relative CR intensity recorded by the global network of neutron monitor stations according to the NMDB database for November 3-6, 2021. The stations are distributed according to the cutoff rigidities R_c . The vertical red line corresponds to the moment of arrival of the shock wave to the Earth, the vertical blue lines show the MC boundaries.

If we represent $I(\theta, \varphi)$ as a multidirectional vector $\vec{A} = (a_n^m, b_n^m)$ then the CR intensity by an individual ground-based detector will be equal to the product $I = \vec{A} \vec{R}$, where $\vec{R} = (x_n^m, y_n^m)$ is a multidimensional receiving vector.

The receiving vector for a real detector is determined taking into account its directional diagram $N(\theta, \varphi)$, CR trajectories in the geomagnetic field (asymptotic angles of arrival of particles Θ, Φ) and response functions $W(E, \theta)$:

$$z_n^m = \frac{\int_{R_c}^{\infty} \int_0^{2\pi} \int_0^{\pi/2} W(E, \theta) f_n(E) N(\theta, \varphi) e^{im\psi} P_n^m(\sin\Phi) \sin\theta dE d\varphi d\theta}{\int_{R_c}^{\infty} \int_0^{2\pi} \int_0^{\pi/2} W(E, \theta) f_n(E) N(\theta, \varphi) \sin\theta dE d\varphi d\theta}, \quad (2)$$

where $z_n^m = x_n^m + iy_n^m$, $f_n(E)$ is an energy spectrum of variations of the n -th harmonic.

As can be seen, the receiving vectors strongly depend on the form of the energy spectrum of the variations. In this particular case, it is difficult to determine the dynamics of each $f_n(E)$ during the event we are considering. However, we will rely on previously known studies of energy spectra given in the literature. We present below the spectra we have chosen and the rationale for our choice.

As was shown in (Grigoryev et al. 2014), in the growth phase of solar activity in cycle 24, it was close to a power law with indicators of 1.01 ± 0.07 . Also, long-term observations in the work of other authors (Kravtsov & Sdobnov 2013; Alania et al. 2013) show that the power-law form of the spectrum satisfac-

Tab.1: The list of NMDB neutron monitor together with their geographic locations, vertical geomagnetic cutoff rigidities and altitudes.

No.	Neutron monitor station	Latitude, deg.	Longitude, deg.	R_c , GV	Altitude, m a.s.l.
1	ATHN	37.97	23.72	8.72	40
2	MXCO	19.33	-99.18	9.53	2274
3	CALM	40.55	3.15	6.95	708
4	ROME	41.86	12.47	6.32	60
5	AATB	43.14	76.60	6.69	3340
6	BKSN	43.28	42.69	5.60	1700
7	JUNG	46.55	7.98	4.48	3550
8	LMKS	49.20	20.22	4.00	2634
9	IRK3	51.29	100.55	3.66	3000
10	IRKT	52.47	104.03	3.66	433
11	NWRK	39.68	-75.75	1.97	50
12	KIEL2	54.33	10.13	2.29	54
13	YKTK	62.02	129.72	1.65	95
14	KERG	-49.35	70.25	1.19	0
15	OULU	65.02	25.50	0.81	0
16	APTY	67.55	33.33	0.65	177
17	NRLK	69.26	88.05	0.63	0
18	TXBY	71.60	128.90	0.53	0
19	FSMT	60.02	-111.93	0.30	0
20	INVK	68.35	-133.72	0.18	21
21	NAIN	56.55	-61.68	0.40	0
22	PWNK	54.98	-85.44	0.50	0
23	THUL	76.50	-68.70	0.10	260
24	MWSN	-67.60	62.88	0.22	30
25	SOP0	-90.00	0.00	0.10	2820
26	TERA	-66.65	140.01	0.01	45

torily describes the experimental data. Although there are reasons to believe that $f_0(E)$ may have a more complex form (Kravtsova & Sdobnov 2013; Sakakibara et al. 1985), in this paper we will assume that it has a power form with exponent -1.

In a number of works (see e.g. Ahluwalia & Riker 1987; Jacklyn et al. 1970; Pomerantz & Duggal 1971) studies of the energy spectrum $f_1(E)$ have been carried out with the assumption that it has a power-law form $f_1(E) = E^\gamma$. The analysis of long-term experimental measurements of solar-diurnal variations in CR intensity by ground-based detectors, carried out in these works, showed that $f_1(E)$ can be adequately described by a power-law spectrum with an upper cutoff E_u . In this case, the exponent γ turned out to be equal to 0, and E_u , on average for a cycle of solar activity, took values close to 100 GeV. Further, a detailed analysis of $f_1(E)$ showed that the index γ varies in a narrow range from -0.3 to 0.5 (Hall et al.

1997), which also confirmed previous results. This is also confirmed by our latest studies (Gololobov et al. 2021). And although it is very likely that such a flat spectrum with an unexpected cutoff is unnatural, the main thing is that it agrees satisfactorily with experimental data.

Krivoshapkin et al. (1970) assumed that the observed semidiurnal CR variations are due to the screening effect of the regular IMF, which creates an excess of particles from the direction across the field. In this case, the energy spectrum $f_2(E)$ following from this theory has the form E^1 for $E \leq E_0$ and E^{-2} for $E > E_0$, and the characteristic energy was determined by the IMF parameters. An analysis of the experimental data made it possible to estimate at 70 GeV. A similar spectrum and values were also obtained by Zusmanovich and Mirkin (1983). On the other hand, according to the estimates of Ahluwalia and Fikani (1996), the energy spectrum indices were somewhat different values of 0.7 ± 0.3 and -0.4 ± 0.2 , and E_0 depended on the SA cycle, reaching 50 GeV at the minimum of solar activity and 150 GeV at the maximum. Despite somewhat different estimates of the energy spectrum obtained in the above papers, in general it can be argued that semidiurnal variations in the CR intensity should be observed in the energy region close to 70 GeV.

The first two angular momenta of the CR distribution function are described by 9 components $a_0^0, a_1^0, a_1^1, b_1^1, a_2^0, a_2^1, b_2^1, a_2^2, b_2^2$ and, respectively, for their determination requires at least 9 equally distributed neutron monitor stations. To implement the GSM for the FD event on November 3–4, 2022, 26 neutron monitor stations were used, providing data at that time to the NMDB. Despite their uneven distribution, the number of stations exceeds the required number by almost 3 times and is sufficient for the implementation of the GSM. The list of stations with their characteristics is presented in Table 1.

4. Results and discussions

The results of the implementation of the GSM are shown in Figure 3. As can be seen, the decrease in the isotropic component of the CR intensity had a two-stage character. The maximum of the first stage of the phase transition practically coincides with the moment of arrival of the shock and is about 5.6%, while the second step of the phase transition has a parabolic time profile and its maximum falls on the center of the MC with an amplitude of 5.3%. Also, inside the MC, there is a sharp increase in the amplitude of both diurnal and semidiurnal CR anisotropy. The maximum modulus of the CR symmetric diurnal anisotropy vector reaches 3.5%, the antisymmetric diurnal one, 5.8%, and the semidiurnal one, 3.4%. Thus, the magnitude of the CR anisotropy in the MC is comparable to the FD itself. This explains the observed fact of inconsistency in the decrease in the NM data, namely, that the second stage of the FD in the data of some neutron monitors was very deep, while in the data of others it was completely absent.

If the spatial direction of vector anisotropy can be described by three components a_1^0, a_1^1 and b_1^1 of the vector in the Cartesian coordinate system, then tensor anisotropy with its 5 components $a_2^0, a_2^1, b_2^1, a_2^2$ and b_2^2 is hard enough to represent in space. The most obvious visualization of tensor anisotropy is the tensor ellipsoid, also defined by 5 components: three semi-axes and two angles that determine the direction of one of the semi-axes. Representing it in this form, let us consider the temporal dynamics of the direction of the ellipsoid's greatest semi-line and the direction of the IMF during the passage of the CME.

The results obtained are presented in Figure 4. As can be seen, the CR tensor anisotropy amplitude has reached maximum values of the order of $\sim 7\%$ at minimum values of isotropic intensity. This moment of time corresponds to the moment when the Earth passes through the central region of the MC. The time

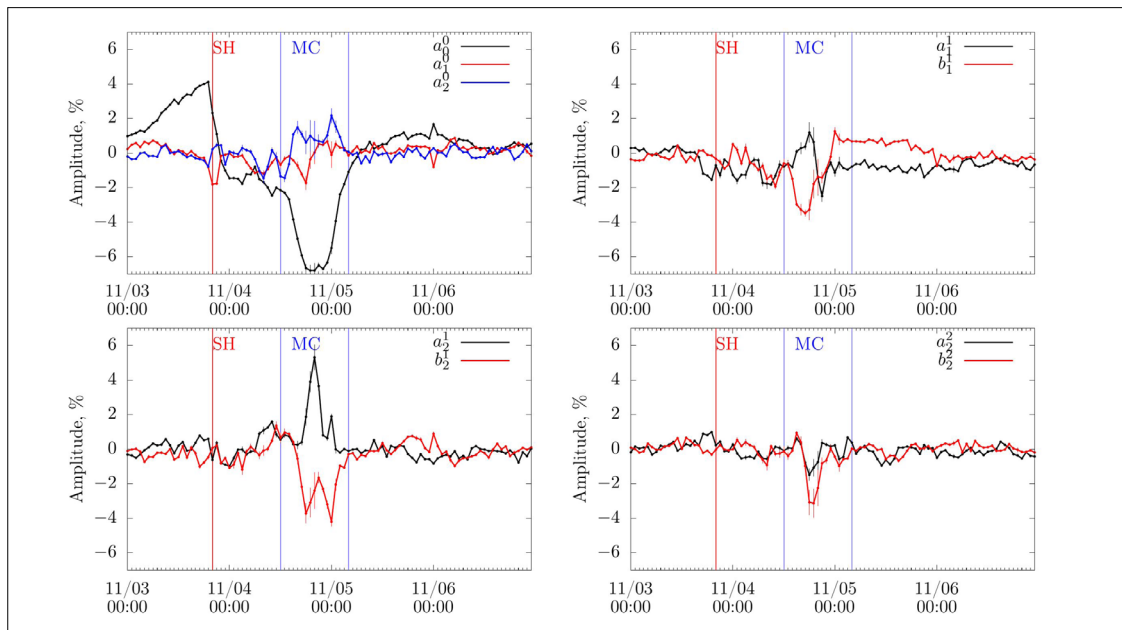


Fig. 3: The parameters of the first two spherical harmonics of the angular distribution of CR obtained using the GSM for November 3–6, 2021. The moments of arrival of the shock wave and the MC boundaries are indicated by red and blue vertical curves.

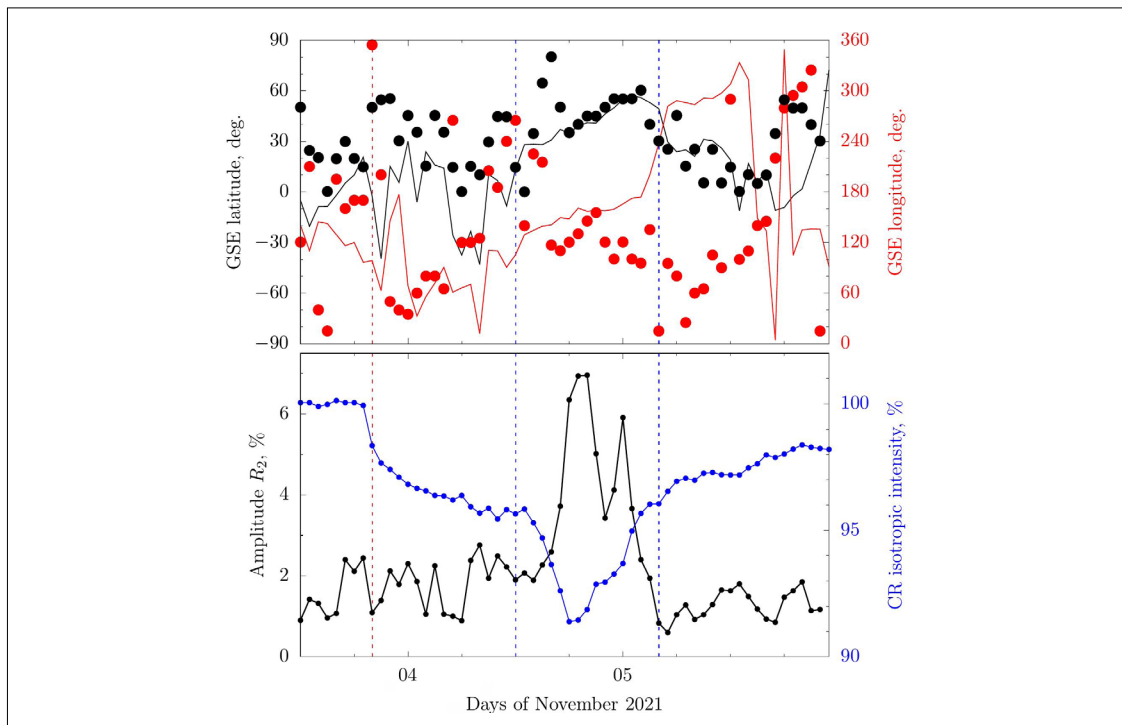


Fig. 4: Spatial angular distribution of CRs and the direction of the IMF in the space during the FD of November 3–5, 2021. The upper panel is the longitude and latitude in the in the geocentric solar ecliptic coordinate system of the direction of the IMF intensity vector (solid curves) and the second harmonic of the CR angular distribution (dots). The lower panel shows the isotropic intensity and amplitude of the second harmonic of the CR distribution. The moments of arrival of the interplanetary CME to the Earth and the boundaries of the magnetic cloud are indicated by vertical red and blue dotted lines, respectively.

profile of the second step of the FD is not typical and corresponds to the parabolic type. In other words, the phases of the decline and recovery of the CR intensity have approximately the same duration. Moreover, the direction of the maximum of tensor anisotropy and IMF in the MC region also show similar values. It can be concluded that, in the event under consideration, MC has a strong modulating effect on CR, leading to both a deep FD and a pronounced anisotropic CR distribution. It is also fair to assume that the motion of particles in the MC occurs predominantly along the force lines of the MC field.

According to the theoretical concepts of the formation of a phase transition in MC (Petukhova et al. 2019), the time profile of the decrease in the isotropic CR intensity that we found is expected. In this work, an electromagnetic mechanism for the formation of a phase transition in MC is proposed. In particular, the inductive electromagnetic field resulting from the motion of the MC leads to energy losses of positively charged particles quasi-trapped in it. In this case, the depth of modulation depends on the duration of the particle's stay inside this magnetic loop structure. It is interesting that, according to numerical calculations (Petukhova et al. 2020), the FD time profile does not depend on the structure of the magnetic field of the loop, and the anisotropy formed in it, on the contrary, is strictly determined by it. Also, in this work, it is shown what kind of CR anisotropy should be observed in MC. It is important to note that the theory predicts that a large bidirectional anisotropy should be observed in the MC. It can be assumed that our results confirm the above theory.

Acknowledgements

The work was performed under the budgetary funding of the PFSI RF project with the registration number in CITIS AAAA-A21-121011890014-0. The authors would like to thank the neutron monitor network team and the NMDB database for providing the data.

References








- Yu, X.X., Lu, H., Le, G.M., Shi, F. 2010, Influence of magnetic cloud on variations of cosmic rays in November 2004, *Solar Phys.*, 263, 223-237, <https://doi.org/10.1007/s11207-010-9522-7>
- Belov, A., Abunin, A., Abunina, M., Eroshenko, E., Oleneva, V., Yanke, V., Papaioannou, A., Mavromichalaki, H. 2015, Galactic cosmic ray density variations in magnetic clouds, *Solar Phys.*, 290, 1429-1444, <https://doi.org/10.1007/s11207-015-0678-z>
- Burlaga, L., Sittler, E., Mariani, F., Schwenn, R. 1981, Magnetic loop behind an interplanetary shock: Voyager, Helios, and IMP 8 observations, *J. Geophys. Res. Space Phys.*, 86(A8), 6673-6684, <https://doi.org/10.1029/JA086iA08p06673>
- Altukhov, A.M., Krysmky, G.F., Kuzmin, A.I. 1970, The method of "global survey" for investigating cosmic ray modulation, *Acta Physica Academiae Scientiarum Hungaricae*, 29(4), 457-460, <https://articles.adsabs.harvard.edu/pdf/1970ICRC...11d.457A> (last accessed June 27, 2023)
- Belov, A.V., Eroshenko, E.A., Yanke, V.G., Oleneva, V.A., Abunina, M.A., Abunin, A.A. 2018, Global survey method for the world network of neutron monitors, *Geomagn. Aeron.*, 58, 356-372, <https://doi.org/10.1134/S0016793218030039>
- Dvornikov, V.M., Sdobnov, V.E. 1998, Analyzing the solar proton event of 22 October 1989, using the method of spectrographic global survey, *Solar Phys.*, 17, 405-422, <https://doi.org/10.1023/a:1005069806374>
- Bieber, J.W., Evenson, P. 1998, CME geometry in relation to cosmic ray anisotropy, *Geophys. Res. Lett.*, 25, 2955-2958, <https://doi.org/10.1029/98GL51232>
- Krymsky, G.F., Altukhov, A.M., Kuz'min, A.I., Krivoschapkin, P.A., Skripin, G.V., Chirkov, N.P. 1966, Cosmic ray distribution

- and receiving vectors of detectors. *Geomagnetizm i Aeronomiya [Geomagnetism and Aeronomy]*, 6, 991–996 (in Russian)
- Grigoryev, V.G., Starodubtsev, S.A., Isakov, D.D. 2014, The energyspectrum of Forbush decreases during the growth phase of solar cycle 24, *Geomagn. Aeron.*, 54, 282–286, <https://doi.org/10.1134/S0016793214030062>
- Kravtsova, M.V., Sdobnov V.E. 2013, Rigidity spectrum of cosmic ray variations over the periods of large forbush decreases during solar cycles 22 and 23, *Journal of Physics: Conference Series*, 409, 012145, <https://doi.org/10.1088/1742-6596/409/1/012145>
- Alania, M.V., Wawrzynczak, A., Sdonov, V.E., Kravtsova, M.V. 2013, Temporal changes in the rigidity spectrum of Forbush decreases based on neutron monitor data, *Solar Phys.*, 286, 561–576, <https://doi.org/10.1007/s11207-013-0273-0>
- Sakakibara, S., Munakata, K., Nagashima, K. 1985, Rigidity spectrum of Forbush decrease, *Proceedings from the 19th International Cosmic Ray Conference*, 5, 238–241, <https://articles.adsabs.harvard.edu/pdf/1985ICRC...19e.238S> (last accessed June 27, 2023)
- Ahluwalia, H.S., Riker, J.F. 1987, Secular changes in the upper cut-off rigidity of the solar diurnal anisotropy of cosmic rays, *Planet. Sp. Sci.*, 35, 39–43, [https://doi.org/10.1016/0032-0633\(87\)90142-5](https://doi.org/10.1016/0032-0633(87)90142-5)
- Jacklyn, R.M., Duggal, S.P., Pomerantz, M.A. 1970, The spectrum of the cosmic ray solar diurnal modulation, *Proc. 11th ICRC*, 29, 47–54, <https://articles.adsabs.harvard.edu/pdf/1970ICRC...11b..47J> (last accessed June 27, 2023)
- Pomerantz, M.A., Duggal, S.P. 1971, The cosmic ray solar diurnal anisotropy, *Space Sci. Rev.*, 12, 75–130, <https://doi.org/10.1007/BF00172130>
- Hall, D.L., Duldig, M.L., Humble, J.E. 1997, Cosmic-ray modulation parameters derived from the solar diurnal variation. *ApJ*, 482, 1038–1049, <https://doi.org/10.1086/304158>
- Gololobov, P.Yu., Grigoryev, V.G., Krymsky, G.F., Gerasimova, S.K. 2021, Dynamics of energetic spectrum of solar-diurnal variations of cosmic rays in 19–24 solar activity cycles, *Cosmic ray studies with neutron detectors, NMDB@Home 2020*, Kiel University Publishing, 1, 43–48, <https://doi.org/10.38072/2748-3150/p6>
- Krivoshapkin, P.A., Krymsky, G.F., Kuzmin, A.I., Skripin, G.V., Metlyaeva, E.A. 1970, The second spherical harmonics in the distribution of cosmic rays, *Acta Physica Academiae Scientiarum Hungaricae*, 29, 147–151, 1970, <https://adsabs.harvard.edu/full/1970ICRC....2..147K> (last accessed June 27, 2023)
- Zusmanovich, A.G., Mirkin, L.A. 1983, Energy spectrum of the semidiurnal variation of cosmic rays, *Proceedings from the 18th International Cosmic Ray Conference, Bangalore, India*, 3, 333–336, <https://adsabs.harvard.edu/full/1983ICRC....3..333Z> (last accessed June 27, 2023)
- Ahluwalia, H.S., Fikani, M.M. 1996, Cosmic ray solar semidiurnal anisotropy: 1. Treatment of experimental data, *JGR: Space Phys.*, 101(A5), 11075–11086, <https://doi.org/10.1029/96JA00320>
- Petukhova, A.S., Petukhov, I.S., Petukhov, S.I. 2019, Theory of the formation of forbush decrease in a magnetic cloud: Dependence of Forbush decrease characteristics on magnetic cloud parameters, *The ApJ*, 880(1):17, <https://doi.org/10.3847/1538-4357/ab2889/meta>
- Petukhova, A.S., Petukhov, I.S., Petukhova, S.I. 2020, Forbush decrease characteristics in a magnetic cloud. *Geomagn. Aeron.*, 18(12), 1542–7390, <https://doi.org/10.1029/2020SW002616>

Open Access

This paper is published under the Creative Commons Attribution 4.0 International license (<https://creativecommons.org/licenses/by/4.0/>). Please note that individual, appropriately marked parts of the paper may be excluded from the license mentioned or may be subject to other copyright conditions. If such third party material is not under the Creative Commons license, any copying, editing or public reproduction is only permitted with the prior consent of the respective copyright owner or on the basis of relevant legal authorization regulations.

Magnetospheric effects on cosmic rays during the magnetic storm of March 2015

Elena Ntina ¹, Maria Gerontidou ¹, Helen Mavromichalaki ¹, Maria Abunina ², Anatoly Belov ², Victor Yanke ², Angelos Laoutaris ³

Correspondence

- 1 Nuclear and Particle Physics Section, Physics Department, National and Kapodistrian University of Athens, Greece, sph1600135@uoa.gr
 - 2 IZMIRAN - Pushkov Institute of Terrestrial Magnetism, Ionosphere and Radiowave Propagation, Moscow, Russia
 - 3 National Center for Scientific Research DEMOKRITOS, Institute of Nuclear and Particle Physics, Greece
-

Keywords

magnetic storm; rigidity; magnetospheric effects

Abstract

Cosmic ray variations of magnetospheric origin during the magnetic storm on 17th of March 2015 were studied. Cosmic ray intensity data were obtained from the neutron monitor database (NMDB) and the data of the Dst index were taken from World Data Center for Geomagnetism, Kyoto. The global survey method was employed for the calculation of changes in the cutoff rigidities throughout the storm. A correlation analysis between the Dst index and the calculated cutoff rigidity variations was performed for each cosmic ray station. The most essential decrease in cutoff rigidities occurred when the Dst index was around the value of -234nT . A latitudinal distribution of the cutoff rigidities was acquired, showing that the maximum effect took place at mid-latitude stations with rigidities around 8-10GV. During the examined event the maximum change in cutoff rigidity was observed at Athens station where the decrease of the cutoff rigidity reached the value of 1.07GV. Furthermore, corrections of cosmic ray intensity due to the magnetospheric effect were calculated using the derived cutoff rigidities showing a discrepancy with the observed values at mid- and low- latitude stations.

1. Introduction

Ground level cosmic ray measurements are affected by disturbances in the Earth's magnetosphere during magnetic storms. The variations in the Earth's magnetic field can alter the charge particle trajectories to such an extent that allowed trajectories become forbidden and vice versa. This has an effect on ground-level observations by changing 1) the effective cutoff rigidities and 2) the asymptotic directions of particles. For galactic cosmic rays (GCR) the first effect is the most dominant. The changes in the cutoff rigidities during magnetic storms can alter the behaviour of the observed cosmic ray intensity for a fixed station.

In this work we studied the magnetospheric effect during the magnetic storm on the 17th March 2015, which was the biggest storm during Solar Cycle 24.

The study of such events is very important for two major reasons:

1. Firstly, from a methodological point of view as these effects hinder the discrimination of primary cosmic rays variations.
2. Secondly, analysis of CR variations due to magnetospheric effects can be used to independently validate current system models during all phases of a magnetic storm. At the initial phase of the storm, which is associated with the magnetopause current system, the cutoff rigidity R_c increases relative to the quiet level, while during the main phase of the storm R_c decreases significantly. The latitudinal and longitudinal dependences of these effects reveal themselves in different ways. Cutoff rigidity variations during the main phase of the storm, which are connected to the ring current system, have a negligible dependence on longitude due to the ring symmetry. Conversely, the cutoff rigidity variations during the main phase of the storm depend significantly on latitude.

In this work a detailed study of the magnetospheric effect in cosmic rays during the major magnetic storm on 17 March 2015 has been conducted.

2. Solar activity on March 2015

The period preceding the magnetic storm of 17 March 2015 was particularly disturbed. On the 11th of March there was a X2.1 solar flare that was followed by a series of weaker flares. On the 15/03 a long duration C9 solar flare occurred at the sunspot region 2297 with a commencement at 01:15UT. The C9 flare launched a partial halo Coronal Mass Ejection (CME) that arrived at Earth around 04:00UT on the 17th. The result was a major G4 magnetic storm with the Dst index reaching a minimum value of -234nT. Aurora was observed at unusually low latitudes (<https://www.spaceweatherlive.com/en/solar-activity.html>, last accessed June 27, 2023).

3. Data and method

Hourly data from 21 stations from the Neutron Monitor Database (NMDB) have been employed in the analysis: 8 high-latitude ($R_c < 1.2\text{GV}$), 13 mid and low-latitude stations. The mid- and low- latitude stations used have a cutoff rigidity range of 2.36GV-9.15GV. The Dst-index for March 2015 was taken from the World Data Centre for Geomagnetism, Kyoto (https://wdc.kugi.kyoto-u.ac.jp/dst_final/index.html, last accessed June 27, 2023).

The Global Survey Method (GSM), which is developed by IZMIRAN, was used for the calculations of the cutoff rigidity variations. The GSM is essentially a version of spherical analysis.

In this method we use the measured ground-level cosmic ray variations to derive a set of parameters connected to the galactic cosmic ray density and anisotropy.

Generally, the measured cosmic ray variations at each neutron monitor can be written as:

$$\frac{\delta I^i}{I_0^i} = \delta_{isot}^i + \delta_{anisot}^i + \delta_{err}^i \quad (1),$$

where δ_{isot}^i and δ_{anisot}^i are the isotropic and anisotropic components of the CR variations out of the magnetosphere and δ_{err}^i the residual dispersion, which is related to possible variations due to the apparatus and the inadequate utilisation of the model.

The CR intensity out of the magnetosphere (isotropic and anisotropic part) like any function can be expressed by the expansion in spherical harmonics. Assuming only the first order harmonics for the anisotropy :

$$\delta_i = \int_{R_c}^{\infty} \frac{\delta J(R)}{J} \cdot W(R, R_c, hi) dR + C_x a_x + C_y a_y + C_z a_z \quad (2)$$

where C_i are the coupling coefficients, a_x, a_y, a_z are the three components of the first harmonic of the CR anisotropy and where $\frac{\delta J}{J} = a_0 R^{-\gamma}$ is the rigidity dependence of CR density variations and $W(R, R_c, hi)$ is the response function for a NM, located at an altitude hi with a cutoff rigidity R_c .

The system of equations (1) is solved using the least squares method relative to the unknown parameters $a_0, \gamma, a_x, a_y, a_z$. In our approach we employed a two-step method for the calculations. In the first step we solved the set of eq. (1) for the 8 high-latitude stations, where we can disregard the geomagnetic effect since $W(R, R_c, hi)$ is negligible for small R_c , and therefore eqs.(1) practically reduces to eqs.(2). In the next step we employed the derived set of parameters from the first step to correct the mid- and low-latitude stations for the variations due to the magnetospheric effect.

In our analysis, we worked separately with the residual dispersions δ_{err}^i , which can be expressed as:

$$\delta_{err}^i = \delta_{mag}^i + \delta_{mod} + \delta_H^i + \delta_L^i \quad (3)$$

The CR variation due to the magnetospheric effect can be written as $\delta_{mag}^i = -\delta R_c^i \cdot W(R_c^i, h_0^i) (1 + \frac{\delta J}{J}(R_c^i))$, δ_{mod} is connected to the inanequacy of the CR variation model (form of rigidity spectrum, contributions from higher order harmonics), δ_H^i is the error due to the statistical accuracy of the data and δ_L^i is the low-frequency component due to the possible apparatus drift. The last two terms of eq. (3) can easily be ignored if we pay particular attention to the good quality of data and δ_{mod} can also be neglected as it does not have a particular longitudinal and latitudinal distribution which is characteristic of the geomagnetic effect. Thus, we can assume that the residual discrepancies arise only from the magnetospheric effect ($\delta_{err}^i \cong \delta_{mag}^i$) such that:

$$dR_c^i = \frac{-\delta_{mag}^i}{W(R_c^i, h_0^i) (1 + \frac{\delta J}{J}(R_c^i))} \quad (4)$$

In this way, we calculated the cutoff rigidity variations at different instances during the event and at different stations independently from one another.

4. Results and discussion

Cosmic ray variations due to the magnetic storm on 17 March 2015 were evaluated using data from the worldwide neutron monitor network and the global survey method (GSM) as described above. In Fig.1 the uncorrected (upper panel) and corrected (lower panel) variations of the cosmic ray intensity data are presented for two polar stations (Mc-Murdo and Apatity) and two non-polar ones (Athens and Tsu-

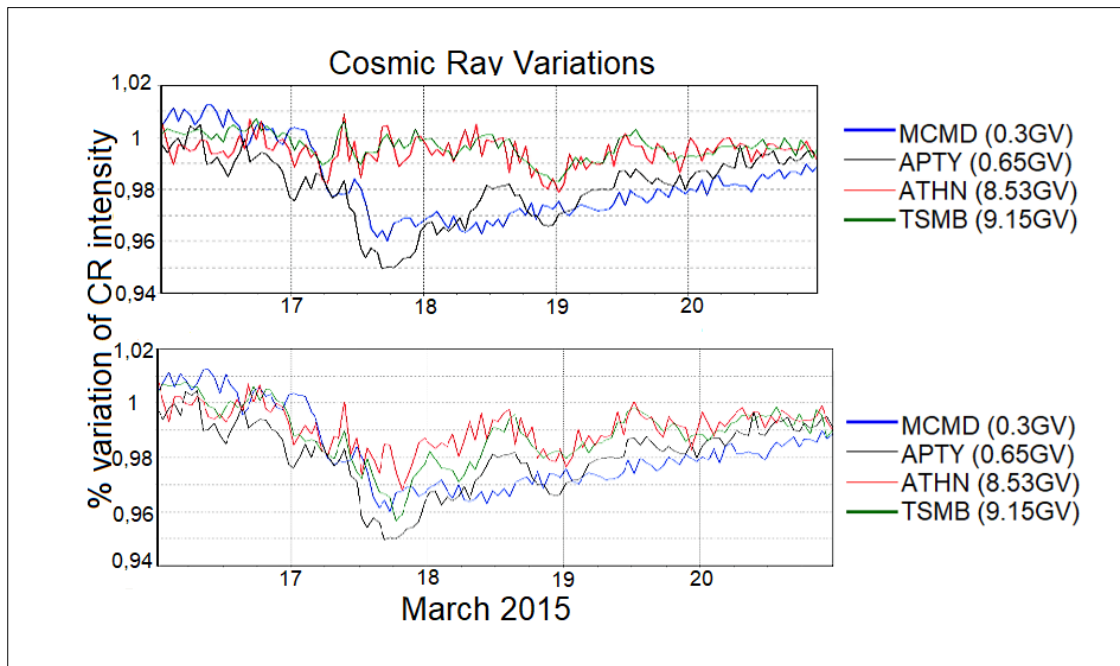


Fig. 1: Uncorrected (upper panel) and corrected (lower panel) CR variations for the magnetospheric effect for two polar station (MCMD and APTY) and non-polar stations (ATHN and TSMB).

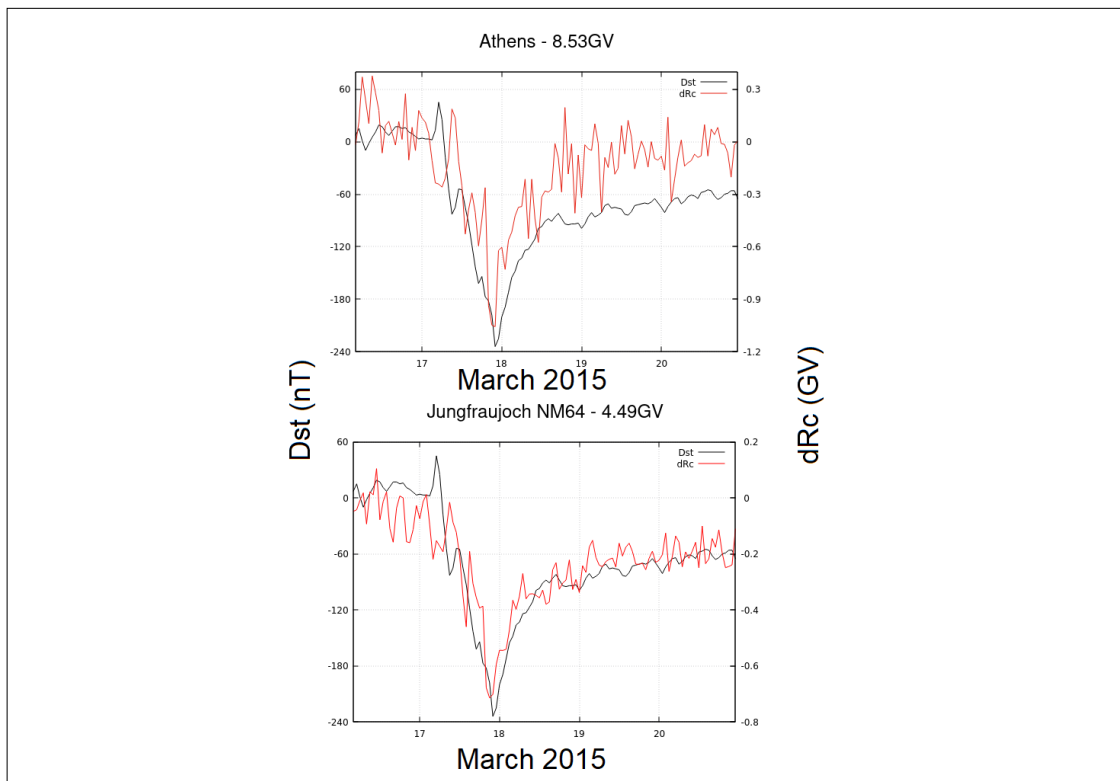


Fig. 2: Derived cutoff rigidity variations dRc and Dst indexes at Athens (ATHN) and Jungfrauoch (JUNG1) stations during the magnetic storm on 16-21 March 2015.

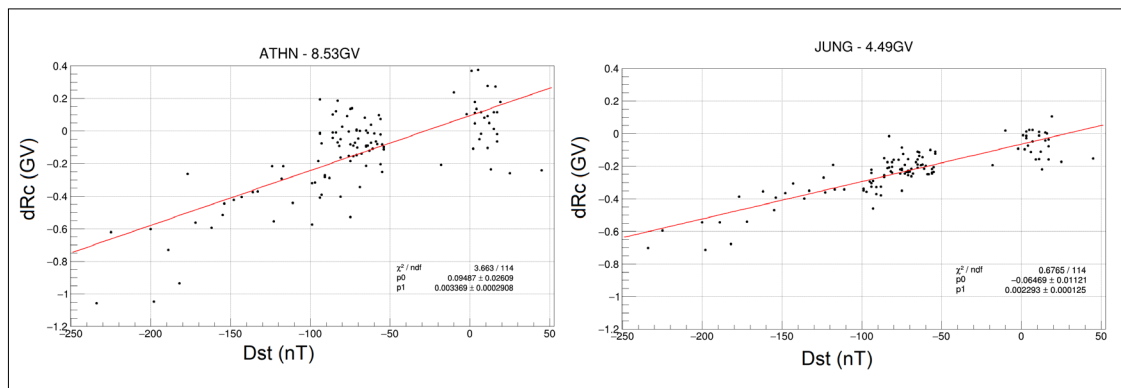


Fig. 3: Examples of regression diagrams for two stations (ATHN and JUNG1) during the magnetic storm on 16-21 March 2015.

meb). The polar and non-polar stations in the uncorrected panel have different time profiles during the magnetic storm. Specifically, for polar stations ($R_c < 1.2\text{GV}$) we observe a decrease in cosmic ray intensity of a magnitude of 3-4%, whereas this decrease is either diminished or masked completely at mid- and low-latitude stations. After the cosmic ray data are corrected for the magnetospheric effect, mid and low latitude stations (for e.g. Athens) show a similar decrease in intensity. It is evident from the comparison of the corrected and uncorrected cosmic ray graphs that the magnetospheric effect may hinder the discrimination of the primary cosmic ray intensity.

The cutoff rigidity changes were evaluated for each Neutron Monitor throughout the storm using the above method. A high correlation between the Dst index and the cutoff rigidity changes was observed during the period under consideration, as shown by the diagrams in Fig. 2. The maximum change in R_c is observed at 22:00 UT and coincides with the Dst minimum ($Dst = -234\text{nT}$) for the majority of stations. Furthermore, lower latitude stations (eg. Athens and Tsumeb) showed a higher sensitivity to the magnetospheric effect than midlatitude stations. As an example the station at Athens reached a minimum dRc value of -1.07GV compared to -0.7GV at Jungfraujoch (JUNG1) station. It has to be noted here, that during the period 15-17 of March 2015 the atmospheric conditions at the Jungfraujoch Neutron Monitors were very turbulent which might have had a minor effect on our results. The maximum effect was observed at stations with a cutoff rigidity of 8-10GV.

Regression diagrams between the Dst-index and the dRc were plotted, revealing an approximately linear dependence during the storm. The regression coefficient for Athens is 0.0034GV/nT whereas for Jungfraujoch it is 0.0023GV/nT . The latitudinal distribution of cutoff rigidity variations versus the R_c was evaluated for various instances during the main and recovery phases of the storm as shown in Appendix C. In Fig. 4 four such graphs are depicted for different phases during the event. Diagram (a) represents the results before the storm arrival while the $Dst = 25\text{nT}$ and where we can observe no significant changes in cutoff rigidities. In graph (b), which represents the commencement of the main phase of the storm, we observe a slight decrease in R_c values, while in graph (c) representing the latitudinal distribution during the maximum of the storm, we observe the maximum variations in cutoff rigidities. Specifically, the maximum effect is observed at lower latitude stations with cutoff rigidities in the range of 8-10GV as previously mentioned. Finally, after the main phase of the storm as shown in diagram (d) the cutoff rigidity values start to recover to their pre-storm values. The latitudinal distribution could have been better observed if a wider range of stations was employed (esp. subequatorial stations with $R_c > 10\text{GV}$ which are absent from our data).

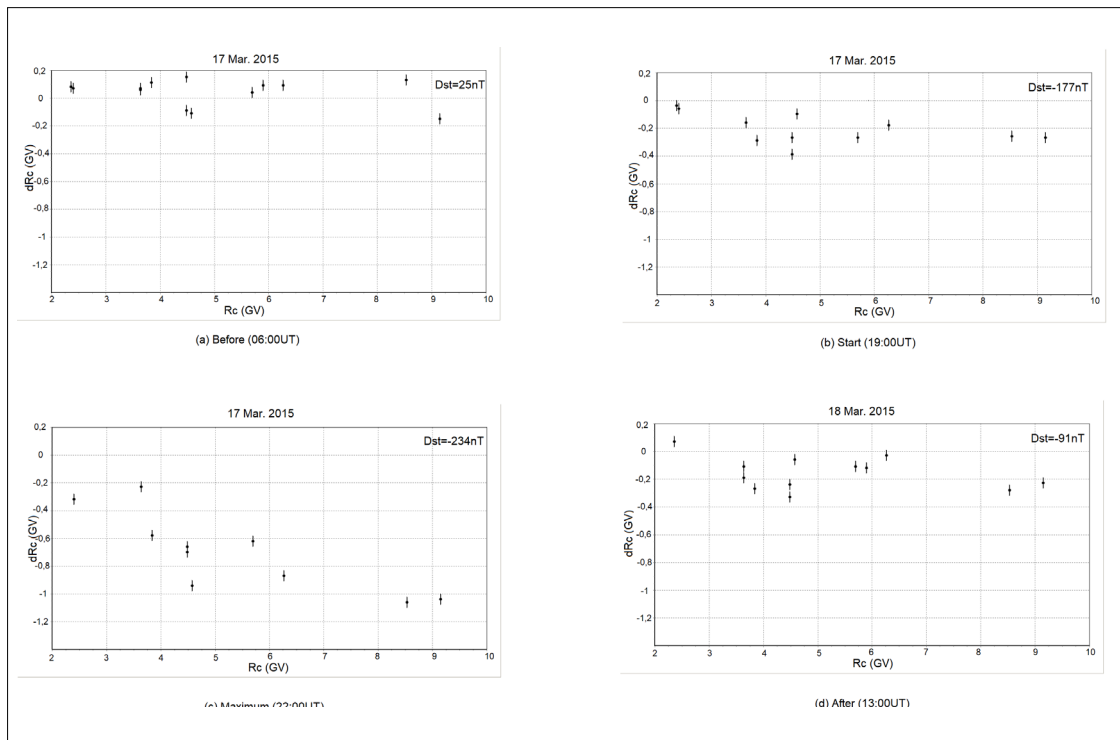


Fig. 4: Cutoff rigidity variations (dR_c) versus the cutoff rigidities (R_c) for different instances on 17-18 of March 2015.

5. Conclusions

From the above analysis, we can conclude the following:

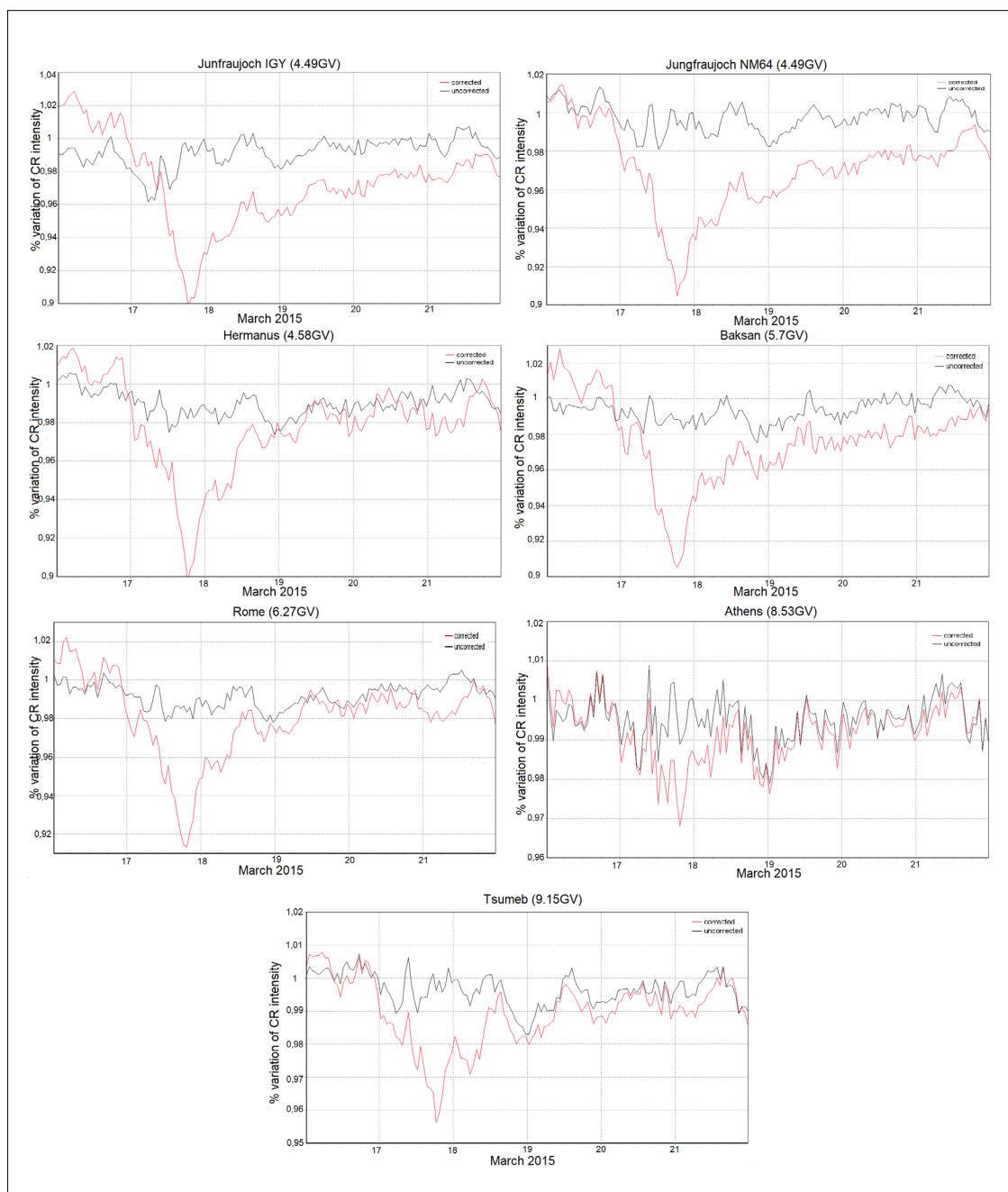
1. The maximal magnetospheric effect in CR was recorded at lower latitude stations, but not at mid-latitude stations as is the common case. Due to this anomaly the maximum change of the geomagnetic cutoff rigidity shifted from the usual values of 3-5GV to 8-10GV.
2. Variations in cutoff rigidity reached -1.07GV for Athens and -1.04GV for Tsumeb.
3. The latitudinal dependence of cutoff rigidity variations was obtained for each hour during the main and recovery phases of the geomagnetic storm. This is very useful for analysing the dynamics and evolution of the ring current system.

Acknowledgements

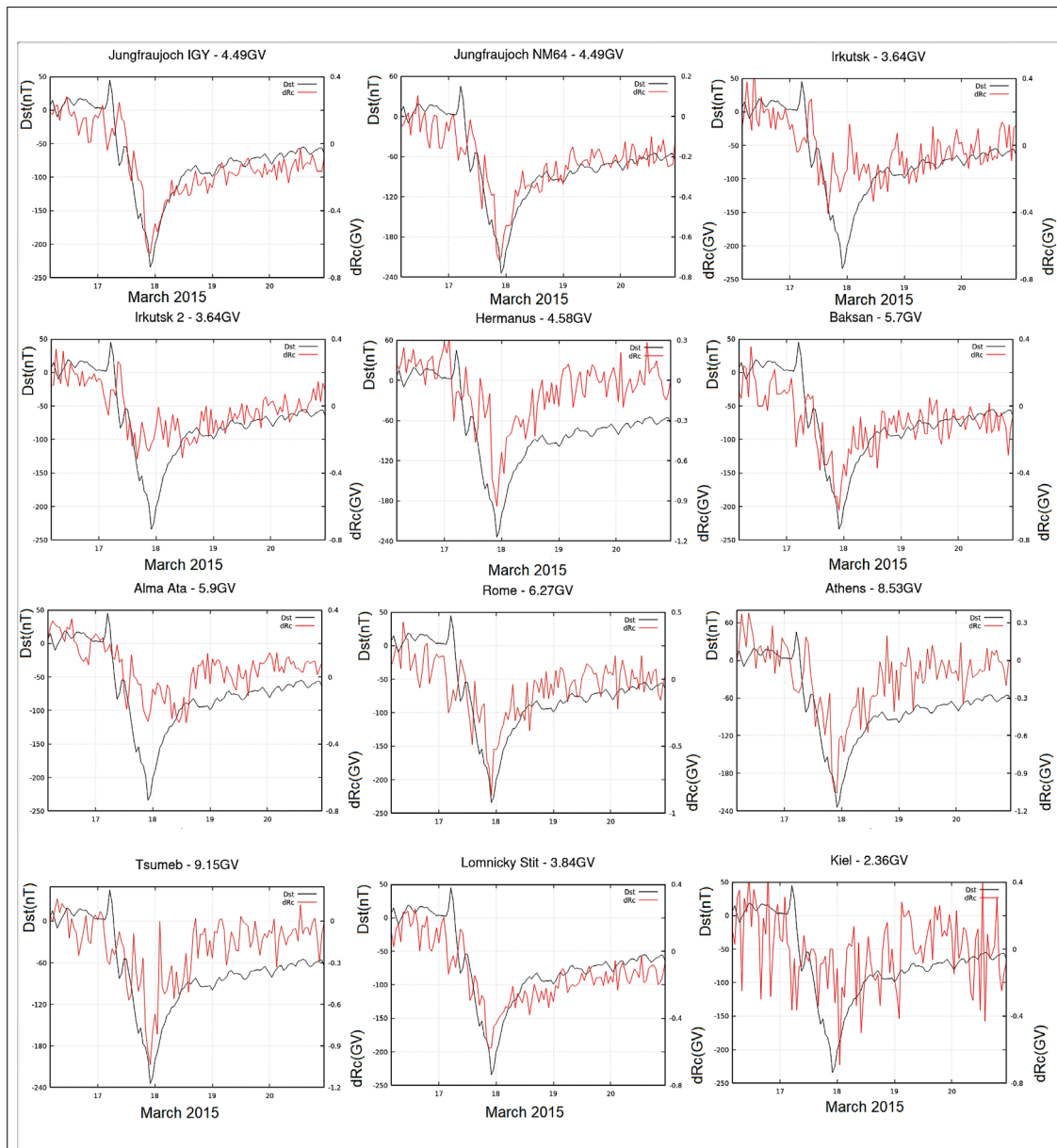
We acknowledge the NMDB database (<https://www.nmdb.eu/>), founded under the European Union's FP7 programme (contract no. 213007) for providing data, and the PIs of individual neutron monitors.

References

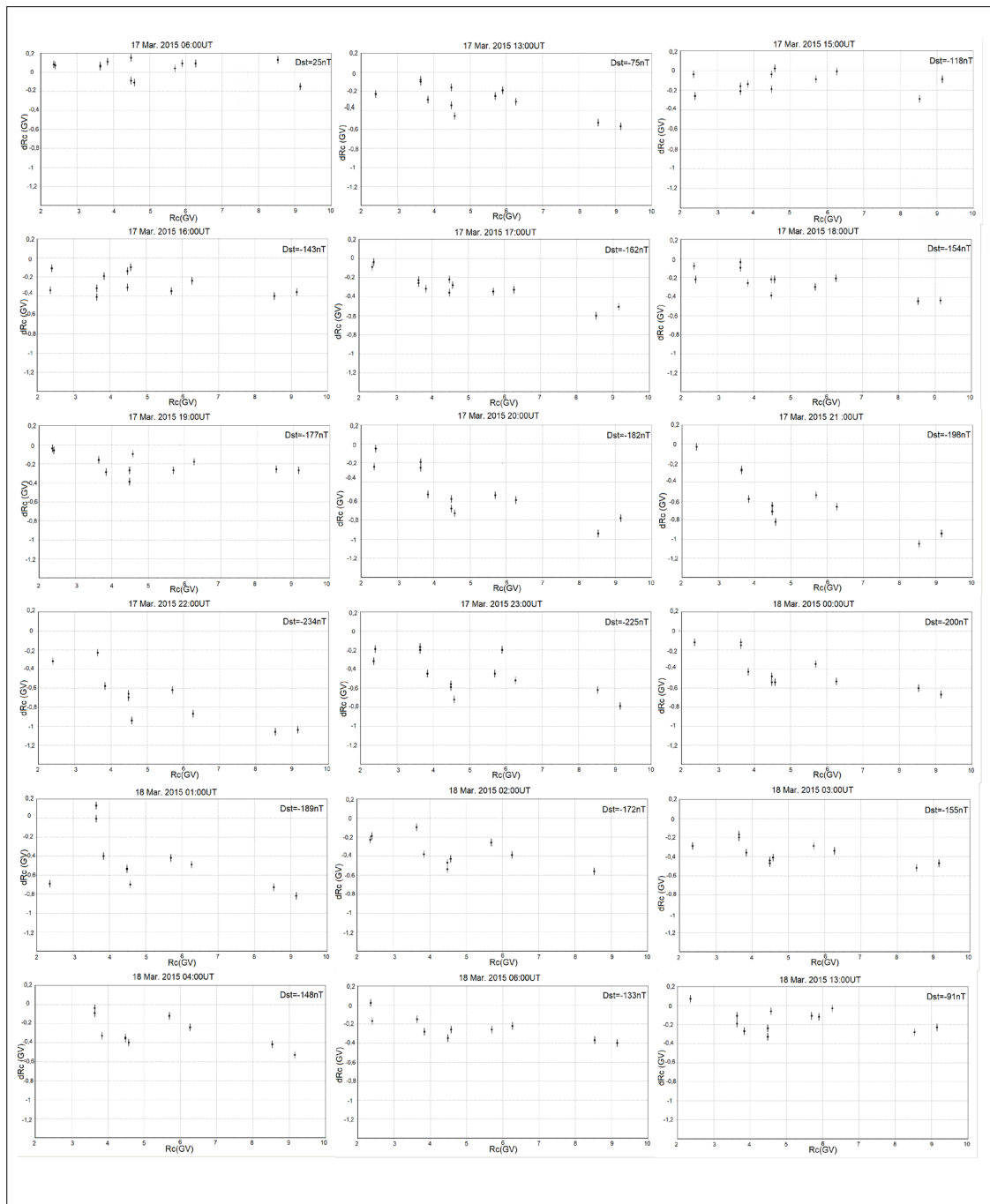
- Baisultanova, A., Belov, V., Yanke, V.G. (1995), Magnetospheric effect of cosmic rays within the different phases of magnetic storms, Proc.Int.Conf. Cosmic Rays 24th, 4, 1090.
- Belov A., Baisultanova, L., Eroshenko, E., Mavromichalaki, H., Yanke, V., Pchelkin, V., Plainaki, C., Mariatos, G. (2005), Magnetospheric effects in cosmic rays during the unique magnetic storm on November 2003, J.Geophys. Res.,100,A09S20, <https://doi.org/10.1029/2005JA011067>
- Belov, A., Eroshenko, E., Yanke, V., Oleneva, V., Abunin, A., Abunina, M., Mavromichalaki, H. (2018). The global survey method applied to ground-level cosmic ray measurements. Solar Physics, 293(4), 1-23.



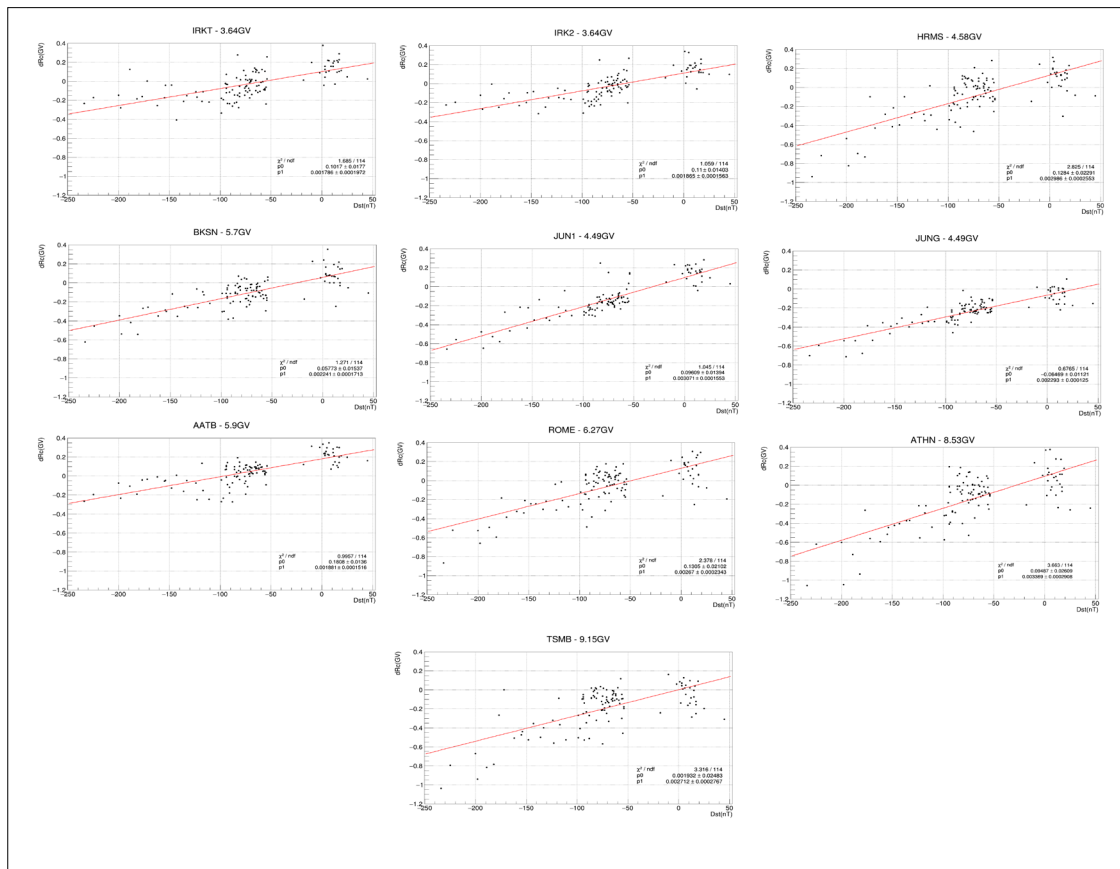
Appendix A: Cosmic ray variations for mid- and low latitude stations: uncorrected (black line) and corrected (red line).



Appendix B: Cutoff rigidity variations and Dst index from 2015/03/16 to 2015/03/21.



Appendix C: Cutoff rigidity variations versus the cutoff rigidity R_c at different instances throughout the magnetic storm on 17-18 March 2015.



Appendix D: Regression diagrams for cutoff rigidity variations dR_c and Dst index on the magnetic storm on 16-21 March.

Open Access

This paper is published under the Creative Commons Attribution 4.0 International license (<https://creativecommons.org/licenses/by/4.0/>). Please note that individual, appropriately marked parts of the paper may be excluded from the license mentioned or may be subject to other copyright conditions. If such third party material is not under the Creative Commons license, any copying, editing or public reproduction is only permitted with the prior consent of the respective copyright owner or on the basis of relevant legal authorization regulations.

Residual modulation of galactic cosmic rays in the heliosphere

Victor Yanke , Anatoly Belov , Raisa Gushchina , Pavel Kobelev , Lyudmila Trefilova 

Correspondence

IZMIRAN – Pushkov Institute of Terrestrial Magnetism, Ionosphere and Radiowave Propagation, Moscow, Russia, yanke@izmiran.ru

Keywords

long-term variations; heliosphere; PAMELA; AMS-02; Voyager-1; ground-based detectors; residual modulation

Abstract

Residual modulation of galactic cosmic rays in the heliosphere and its energy dependence are studied with data from three types of ground-based detectors, using data from PAMELA, AMS-02, and Voyager 1/2. It is shown that the residual modulation is approximately the same in magnitude as the observed variations due to the solar activity cycle, which allows us to make some conclusions about the modulation processes in the heliosphere.

1. Introduction

The concept of residual modulation, introduced at the beginning of the space age (Nagashima et al. 1980), arose when solving the problem of the size of the heliosphere, which has now been determined experimentally. The issue of residual modulation today is more related to the efficiency of the heliosphere as a whole and the contribution of its individual regions. Assuming that at the minimum of solar activity the heliosphere is completely filled with unmodulated galactic cosmic rays (CR), one can expect an insignificant residual modulation, but it is important to know the value of such residual modulation for particles of different energies.

Recent studies have shown that galactic cosmic rays intensity nowadays is significantly lower than in previous centuries (McCracken et al. 2004). The studies carried out in this work show that the sunspots number in the solar activity minima of the last 6 cycles correspond to a modulation potential of about 500 MV, while the potential during the Maunder minimum is < 100 MV. In the complete absence of modulation at the modulation potential $\Phi = 0$ MV, the local interstellar spectrum (LIS) of GCRs would be observed in the Earth's orbit, which would lead to the maximum count rate of detectors on Earth.

A powerful incentive for a detailed study of the modulation of galactic cosmic rays in the heliosphere was the exit of Voyager-1/2 (Stone et al. 2019) beyond the heliosphere, as well as accurate measurements

of particle spectra in the Earth's orbit using the PAMELA space experiments (Adriani et al. 2013) and AMS-02 (Aguilar et al. 2018).

The measurements onboard the PAMELA and AMS-02 spacecraft are carried out in a wide range of rigidities for quite a long time and make it possible to calibrate all ground-based detectors. Joint consideration of the spacecraft measurements with the results of ground-based monitoring of cosmic rays makes it possible to calibrate ground-based detectors and cover six cycles of solar activity since the beginning of ground-based CR monitoring in the 1950s.

While studying modulation for historical period from the Middle Ages to the present (McCracken 2007; McCracken et al. 2007) one can follow the time variations of the residual modulation for some effective energy. The cosmogenic data method makes it possible to obtain the residual modulation retrospectively temporal changes, but this method does not allow studying the residual modulation energy dependence. To study the residual modulation on the energy scale, it is necessary to use direct methods based on knowledge of the particles energy spectra outside the heliosphere (LIS spectra) and in the Earth's orbit. Experimental spectra outside the heliosphere were obtained using direct measurements of Voyager-1/2. Particle spectra have been measured on the Earth orbit by the AMS-02 spectrometer only since 2011. For earlier periods it is necessary to use ground-based data from various detectors that have been continuously monitoring since the middle of the last century. These are stratospheric measurements, monitoring of the neutron and muon components.

These data make it possible to consider the problem of cosmic rays residual modulation during the periods of a "quiet" Sun in order to evaluate and study quiet heliosphere modulation properties.

Studies of residual modulation on the time and energy scales are important for solving several inter-related problems: 1) determining modulation dynamics in the heliosphere of the "calm" Sun and its numerical evaluation; 2) the efficiency evaluation of the heliosphere as a whole and its individual regions; 3) verification of interstellar spectra various models of the nucleon component at low energies.

The aim of this work is to experimentally determine the spectra of the residual modulation for the last 6 solar cycles minima and to estimate the delay time of the cosmic ray response relative to the significant weakening period beginning of the heliospheric magnetic field.

2. The residual modulation determining method

The variation can be determined with respect to the selected base period of cosmic ray intensity $J_{Base} = J_{1AU}$ in the Earth's orbit (usually near the intensity maximum). In this case, the variation is defined as

$$v = J/J_{1AU} - 1, \quad (1)$$

where J is the calibrated (in this case, according to PAMELA data) intensity of cosmic rays outside the magnetosphere, obtained from the network data of a neutron monitors processed by the global spectrographic method (GSM) (Belov et.al. 2018), or from the data of individual detectors.

The variation can also be determined with respect to the unmodulated intensity of the local interstellar spectrum J_{LIS}

$$v_{LIS} = J/J_{LIS} - 1. \quad (2)$$

In (1) and in (2), the intensity is determined for one given particle rigidities. Variations v and v_{LIS} relative to different bases can be connected using the base conversion method.

Indeed, excluding J from (1) and (2), we obtain $J_{LIS}(v_{LIS} + 1) = J_{1AU}(v + 1)$. Then

$$v_{LIS} = \frac{J_{1AU}}{J_{LIS}}(v + 1) - 1 = v + \delta_{LIS}(v + 1), \quad (3)$$

where the variation relative to the LIS level is defined as

$$\delta_{LIS} = J_{1AU} / J_{LIS} - 1. \quad (4)$$

(For particles 10 GV (see table 1 below, model C2016) $\delta_{LIS} = 26.9/33.2-1=-19.0\%$.)

Residual modulation is part of the total modulation, and the modulation depth is usually expressed as a positive number, so the residual modulation is $\Delta=|\delta_{LIS}|$.

The base values for each used detector were determined as annual average intensity values for the corresponding effective rigidity.

Or in another form

$$v_{LIS} = \frac{J_{1AU}}{J_{LIS}}(v + 1) - 1 = \frac{v - \delta_{1AU}}{1 + \delta_{1AU}} \approx v - \delta_{1AU}(v + 1), \quad (5)$$

where the variation already relative to the 1AU level is defined as

$$\delta_{1AU} = J_{LIS} / J_{1AU} - 1 \quad (6)$$

(for 10 GV particles $\delta_{1AU} = 33.2/26.9-1=23.4\%$.)

Values of variation relative to the LIS level δ_{LIS} and relative to the 1AU level δ_{1AU} are connected as

$$\delta_{1AU} = -\frac{\delta_{LIS}}{\delta_{LIS} + 1} \approx -\delta_{LIS} \text{ for } |\delta_{LIS}| \ll 1.$$

3. Experimental data used

The results of the following detectors monitoring were used in the work:

PAMELA spectrometer data. For calibrating ground-based detectors and determining the basic intensity values the PAMELA magnetic spectrometer data turned out to be indispensable (Adriani et al. 2013; SSDC 2022; CRDB 2022; CRDB ultra 2022). It's operation period was on the 23/24 solar cycles minimum (2009).

The long-term detector stability and the average annual basic intensity values accuracy turned out to be sufficient for calibrating ground-based detectors (Belov et al. 2021). In addition, the PAMELA magnetic spectrometer measurements cover the detectors entire energy range we use. It is possible to use the results of magnetic spectrometers in sounding the stratosphere, but such measurements are carried out only for about 10 days during an annual expedition (Seo 2012; Maurin et al. 2020; CRDB balloon borne 2022). The average annual intensity values calibrated according to PAMELA data for 2009 and various effective rigidities R_{eff} are given in Table 1.

Ground detectors data at a distance of 1AU. These are the world network of neutron monitors (NM) data (NM Network 2022), muon telescopes (MT) data (Muon Network (GMDN) 2022), and stratospheric sounding of the ionizing component SS data (Balloon experiment 2022). The GSM global spectrographic method was carried out using data from the global NM network (Belov et.al. 2018). The result of this GSM analysis is the cosmic ray variations spectrum $v(R)$ outside the Earth's magnetosphere relative to the base period (in our case, 2009). To go to the cosmic rays intensity outside the magnetosphere, the NM network detector was calibrated using the PAMELA data for the period of 2009, i.e., calculated intensity $J = J_{\text{PAMELA}}(v_{1\text{AU}} + 1)$, where all values used depend on the particles rigidity (Belov et al. 2021). Other detectors (muon telescopes and stratospheric sounding) were calibrated in a similar way. The effective rigidities for the analyzed components are: charged component - $R_{\text{eff}}=4$ GV (Apatity and Mirny) and $R_{\text{eff}}=5.8$ GV (Moscow), muon component - $R_{\text{eff}}=41$ GV (vertical component for station Nagoya); detected particles effective rigidity for the neutron monitors ground-based network $R_{\text{eff}}=10$ GV.

LIS Spectra Models Data. The particles local interstellar spectrum is determining for calculating the cosmic rays intensity basic values outside the heliosphere for various detectors. The development of modern LIS models made it possible to estimate the residual modulation in a wide range of rigidities and to estimate their errors. There are dozens of interstellar cosmic ray spectra models made of different assumptions. We used only LIS models that relied on experimental data from Voyager-1 (Voyager Data 2022) for the lower range (<1 GV) and AMS-02 for the upper range (>100 GV) (CRDB ultra 2022). The particles modulation in the upper rigidity range was neglected, and therefore it was possible to use magnetic spectrometers on the Earth's orbit. We considered the following LIS spectra (in our notes): C2016 (Corti et al. 2016), B2019 (Bisschoff et al. 2019), B2020 (Boschini et al. 2020), V2015 (Vos & Potgieter 2015), and G1975 (Garcia-Munoz et al. 1975). The last LIS spectrum was obtained at the space age beginning. It is simple and well correlated with modern LIS measurements. Local stellar spectrum as a function of kinetic energy per nucleon $J_{\text{LIS}}^p(K)$ in units $(\text{m}^2 \text{ s sr GeV/nucleon})^{-1}$ for protons and helium nuclei is presented as

$$J_{\text{LIS}} = a(K_L + K)^{2.65}, \quad (7)$$

where $KL=b \exp(-K/K0)$ and the coefficients for the proton spectrum are defined as: $a=8900$, $b=0.78$, $K0=4$.

In Figure 1 (top panels) two models comparison of LIS rigidities spectra C2016 (Corti et al. 2016) and B2019 (Bisschoff et al. 2019) for protons and helium nuclei are made. The experimental data of Voyager 1 and the data of AMS-02high (CRDB ultra 2022) are also shown in the region of high rigidities, for which modulation can be neglected. For illustration, the modulated AMS-02 values are also shown (thin curve).

For comparison, we used only a pure power-law spectrum normalized at a rigidity of 976 GV according to the spectrometer data AMS-02 $J=8.571 \cdot 10^{-5}(R/976)^{2.82}$ in $(\text{m}^2 \text{ s sr GV})^{-1}$.

In Fig. 1, the arrows indicate the spectrum characteristic parts of the considered detectors - SS, GSM, MT. It is important that the rigidities range of 1-100 GV that is interesting for us (shaded area in Fig. 1) is in the spectrum region obtained only by interpolation, and therefore some uncertainty can be expected here. The bottom panel shows the ratios for the spectra $J_{\text{C2016}}/J_{\text{B2019}}$ and their dependence on rigidity; the discrepancy in the interest to us area reaches 10%.

Base intensities values $J_{1\text{AU}}$ and J_{LIS} for different rigidities R_{eff} by several LIS spectra data are given in Table 1.

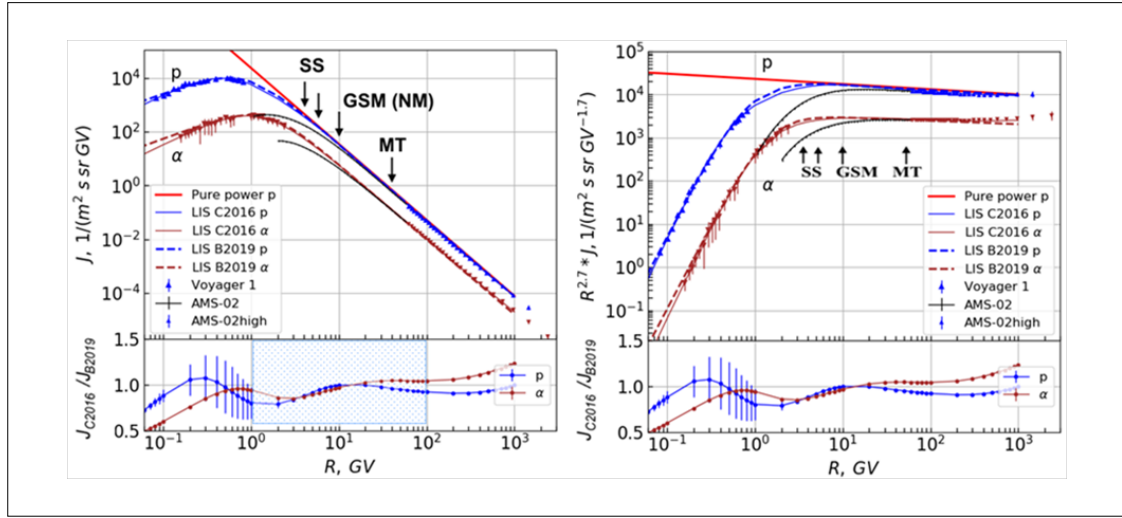


Fig. 1: Comparison of two LIS spectra models C2016 [Corti et al. 2016] and B2016 [Bischoff et al. 2019] (upper panels) and their ratios (lower panels). The Voyager 1 [Voyager Data 2022] and AMS-02high [CRDB ultra 2022] data are also shown, from which the above mentioned spectra were obtained. The purely power-law spectrum of the protons is also shown.

Tab. 1: Base (2009) intensity values J_{1AU} , calibrated according to PAMELA, intensities J_{LIS} for different effective rigidities R_{eff} found for LIS spectra and result for residual modulation Δ .

Model of spectrum $p/(m^2 s sr GV)$	R_{eff} GV						
	Stratospheric Sounding			NM		MT	
	2.6	4.0±0.1	5.8±0.2	5	10±0.3	20	41±2.5
J_{1AU} (norm PAM, 2009)	578.984	250.042	106.015	149.932	26.869	4.183	0.569
J_{LIS} (C2016)	968.016	360.295	143.745	209.172	33.184	4.653	0.596
$\Delta = J_{1AU}/J_{LIS} - 1 , \%$	40.2	30.6	26.2	28.3	19.0	10.1	4.5
J_{LIS} (B2019)	1184.428	408.766	152.580	227.744	33.225	4.669	0.597
$\Delta, \%$	51.1	38.8	30.5	34.2	19.1	10.4	4.7
J_{LIS} (B2020)	1042.240	363.382	140.727	206.688	32.617	4.611	0.585
$\Delta, \%$	44.4	31.2	24.7	27.5	17.8	9.3	2.7
J_{LIS} (V2015)	1161.200	382.719	140.068	209.978	33.460	4.627	0.595
$\Delta, \%$	50.1	34.7	24.3	28.6	19.7	9.5	4.4
$\langle \Delta \rangle \pm \text{stat} \pm \text{sys}, \%$	46 ±0.3±5	34 ±0.3±4	26 ±0.3±3	30 ±0.3±3	19 ±0.4±2	10 ±0.5±2	4.0 ±0.7±2

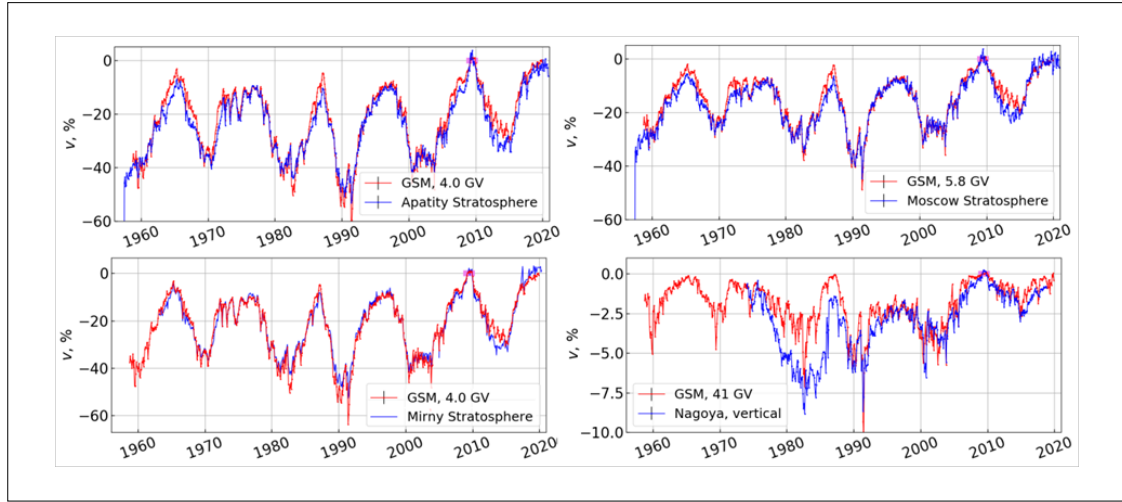


Fig. 2: Comparison of the observed variations in the charged and muon components with the results of a GSM analysis from a network of neutron monitors to determine the effective rigidity of each detector.

All the used ground-based detectors register cosmic rays with variable efficiency in a certain range of rigidities. For a comparative analysis it is necessary to have effective rigidities of each detector, the direct calculations of which are laborious and give ambiguous results, especially for the charged component. We made experimentally estimation of the effective rigidity R_{eff} , by comparing this detector variations and the neutron component $R_{eff}=10$ GV variations with the same effective rigidity R . It can be done knowing the cosmic ray variations spectrum determined by the GSM method from the data of a neutron detectors network, for example, in the work (Yanke et al. 2019). Found parameters a , γ , R_L of variation spectrum allow to determine variations for other rigidities as

$$v(R) = a_{10} \left(\frac{R_L + R}{R_L + 10} \right)^{-\gamma} \quad (8)$$

Such analysis results are shown in Fig. 2. The effective rigidities of the detectors under consideration are: for SS Apatity 4 ± 0.15 GV, for SS Mirny 4 ± 0.1 GV, for SS Moscow 5.8 ± 0.2 GV, and for MT Nagoya. V 41.0 ± 2.5 GV.

4. Discussion of results

To determine the residual modulation at any time, it is necessary to obtain the intensity J_{LS} by LIS spectra and intensity J_{IAU} at the base time for a given effective rigidities and calculate the residual modulation according to expression (4). The main results are shown in Table 1 were intensity and residual modulation values for various R_{eff} and for several LIS spectra models are given. Residual modulation for detectors with various effective rigidities is shown in Figure 3.

Each figure shows the temporal changes of cosmic ray variations relative to the 2009 base period. Variations were obtained from the calibrated intensities of each detector in accordance with (4). Variations relative to 2009 are indicated near the curves for all minima solar activity.

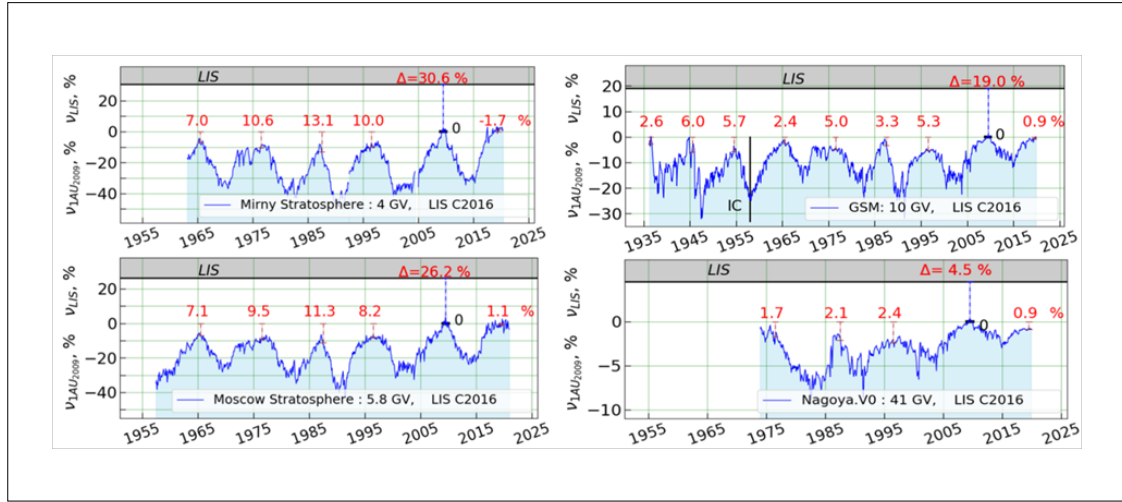


Fig. 3: A residual modulation Δ relative to the LIS level for detectors of various effective rigidities and variation relative to 2009 (curve numbers).

Fig. 3 also shows the residual modulation module Δ . Such estimates were made for several LIS spectra models (see Tab. 1), but the Fig. 3 shows the result only for the C2016 LIS spectrum (Corti et al. 2016).

The cosmic rays modulation analysis in the heliosphere showed that even during the period of the quietest Sun (for example, 2009), the residual modulation is significant. Thus, for 4.0 GV particles, the residual modulation averaged over all LIS spectra (the last line of Table 1) reaches $\Delta=34\pm 0.3(\text{stat})\pm 4(\text{sys})\%$ that is approximately equal to the modulation during the transition from minimum to maximum of solar activity. This is relevant for all rigidities. Similarly, for the rigidity of 41 GV (muon telescope) during the period of the quiet Sun, the cosmic rays residual modulation is $\Delta=4\pm 0.7(\text{stat})\pm 2(\text{sys})\%$, which is also comparable with the modulation from minimum to maximum of solar activity. Residual modulation values for other rigidities are given in Table 1.

Hence, the Sun in its most active phase is capable of modulating cosmic rays relative to quiet period, just as the quiet Sun is capable of modulating the local interstellar spectrum.

Knowing the residual modulation in the considered energy range, it is possible to form the residual modulation spectrum, i.e. the dependence of residual modulation on rigidity or energy. Such a spectrum is approximated by a power function, which is strongly modulated by an exponential function in the region of high rigidities:

$$\Delta = a_0 R^{-\gamma} \exp(-R/R_H), \quad (9)$$

It is shown in Figure 4 (left panel). The found values of the rigidity spectrum parameters for the residual modulation for the period of 2009 are equal to $a_0=(69.5\pm 1.1)\%$, $\gamma=(0.47\pm 0.05)$, $R_H=(37.7\pm 2.3)$ GV with multiple coefficient of determination $R^2=0.996$ and a small condition number of 30. At local points for rigidities of 5, 10, 20, and 41 GV (numbers in circles), the exponent of the power-law spectrum of residual modulation is ~ 0.3 , ~ 0.5 , ~ 0.9 , and ~ 1.3 , respectively. When approximating the modulation spectrum by the kinetic energy function K for the period of 2009, the parameters are determined as $a_0=(52.7\pm 1.1)\%$, $\gamma=(0.31\pm 0.08)$, $K_H=(29.3\pm 2.3)$ GeV with determination multiple coefficient $R^2=0.998$.

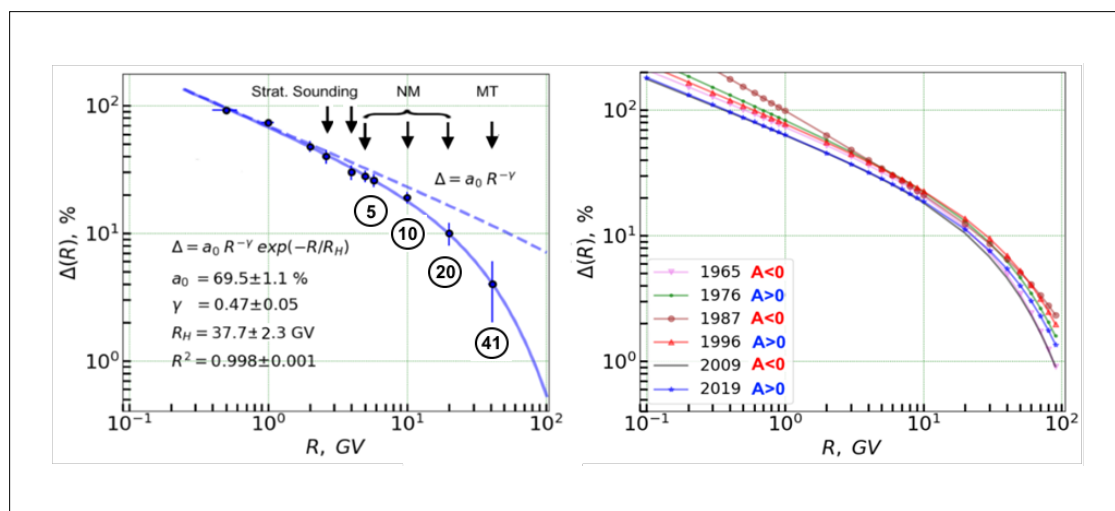


Fig. 4: Residual modulation spectrum and its approximation for the period of 2009 ($A < 0$) for the C2016 model [Corti et al. 2016] as a function of rigidity (left panel). Comparison of residual modulation spectra for various solar activity minima (right panel).

Let's consider the residual modulation spectrum behavior at different solar magnetic field polarities. The residual modulation spectra for 6 solar activity minima are shown in the right panel of Fig. 4. For any polarity, the rigidity spectrum is a power-law modulated by an exponential function in the region of high rigidities. This should be expected, since the residual modulation, in general, occurs in the far heliosphere, where the magnetic field is not even azimuthal, but is already highly turbulent. The dispersion of residual modulation values, for example, for 10 GV is about 5%, which agrees with the results shown on Figure 3.

A comparison can be made with the modulation spectrum on the Earth's orbit, determined in (Yanke et al. 2021). For the negative polarity of the solar magnetic field, such a spectrum is a power-law, modulated by an exponential function in the region of high rigidities, for positive polarity it is purely power-law. The reason is that in the first case, the particles enter the inner heliosphere through the neutral current sheet, in the second case - through the polar regions.

Above, we considered the residual modulation and its dependence on particle energy for the modern era, but its temporal changes in a historical perspective are also of interest.

5. Retrospectively determined residual modulation

Retrospectively, the residual modulation was discussed in (McCracken 2007; McCracken et al. 2007). This work was based on the combined instrumental neutron monitor data "pseudo-Climax" and cosmogenic isotope ^{10}Be data. The analysis shows that the intensity of cosmic rays steadily decreased; the residual modulation at solar cycle minima increased from 5% at the Spörer minimum in the 15th century to 18% at present for an effective rigidity of 10 GV.

Based on modern instrumental data, we obtained the residual modulation value $\Delta = 19 \pm 0.4(\text{stat}) \pm 2(\text{sys}) \%$, which resonates well with (McCracken et al. 2007).

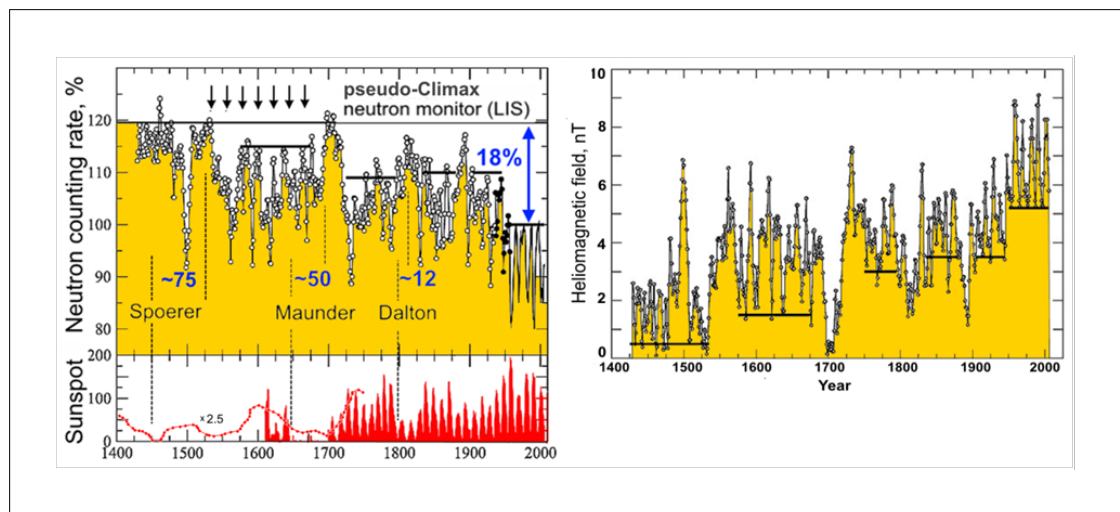


Fig. 5: Left panel - estimation (1428-1954) and observations (1951-2005) of neutron component variations for 10 GV. LIS line - calculated speed in the solar modulation absence [McCracken 2007; McCracken et al. 2007]. Solar activity indices for the period of the Middle Ages from 1400-1600 were obtained in [Usoskin et al. 2003]. Right panel - Heliomagnetic field near the Earth's orbit. The field was not obtained independently but reconstructed from the data of the previous figure of cosmic ray intensity in the heliosphere. [McCracken 2007a].

For a rigidity of 10 GV (neutron monitors), a residual modulation comparison and its time dependence is shown in Fig. 5 (left panel). A steady increase of the residual modulation is seen, which is a constant property of the galactic cosmic rays intensity on the Earth during the past five centuries.

The data in Figure 5 allow us to determine how long will it take the interstellar spectrum cosmic rays to fill the entire heliosphere if the Sun activity drops to zero.

Let's consider three known minima of solar activity: minimum of Spoerer, Maunder and Dalton.

The most famous, the Maunder minimum lasted from 1645 to 1715, and the cosmic rays intensity reached the LIS level around 1700, i.e. the delay time of the cosmic rays response to the Maunder minimum beginning is about 50 years. That is, the solar system is freed from the influence of the Maunder minimum for 50 years.

The Spoerer minimum lasted from 1415 to 1534, solar activity reached zero in ~1450, but cosmic rays reached a maximum on the Earth orbit only in ~1525 (the cosmic ray intensity reached a local maximum about 75 years later). On Fig. 5 (lower left panel) solar activity observed data are supplemented with reconstructed sunspot values for the Middle Ages by the method ^{10}Be analysis of Antarctic ice cores (Usoskin et al. 2003) (scaled by a factor of 2.5).

The Dalton minimum lasted from 1790 to 1830, but the cosmic rays intensity reached a local maximum after about 12 years, which is also noted in Fig. 5.

On Fig. 5 (right panel) shows the heliomagnetic field near the Earth's orbit (Caballero-Lopez et al. 2004). The results of this figure are based on cosmic ray intensity data (left panel) (McCracken 2007a). Three independent reconstructions of the heliomagnetic field (details in McCracken 2007) confirm this result. The most notable feature of Fig. 5 (right panel) is the steady long-term change in the interplanetary magnetic field between the 15th and 21st centuries from ~0.5 nT to the current level. Analyzing the results of Fig. 3 and Fig. 5, we can conclude that the cosmic rays residual modulation over the past 400 years has steadily increased to the current level.

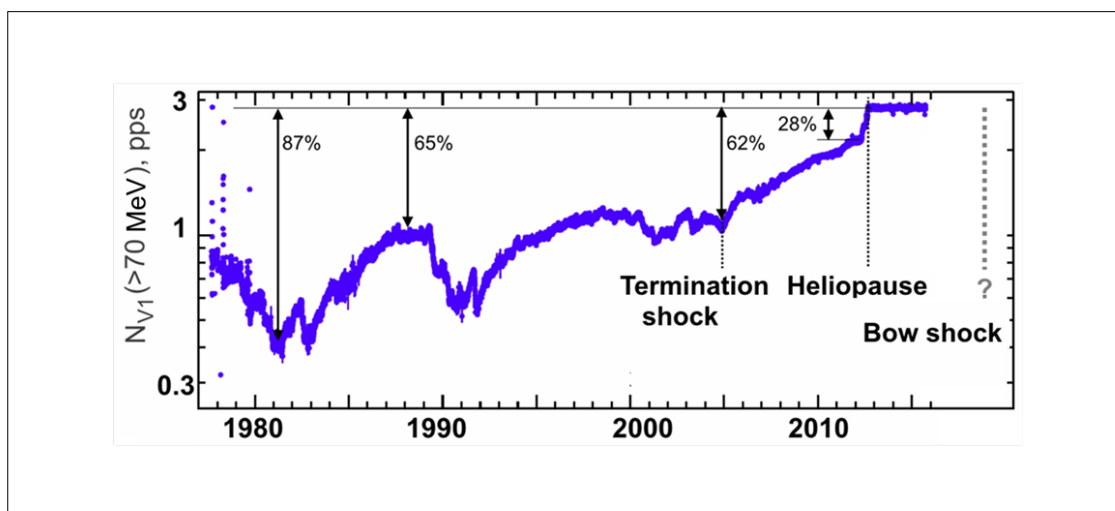


Fig. 6: Time dependence of the count rate of particles with energies >70 MeV according to Voyager-1 data [Cummings et al. 2016]. Estimation of modulation at key points of the Voyager-1 trajectory.

Based on the values of the residual modulation, we can consider two possibilities for realizing the radial dependence of the diffusion coefficient. With the active Sun, diffusion coefficient is $K \sim r$. Then, modulation $M \sim \ln(r)$ and, at velocity V_{sw} of the solar wind, according to the Parker model, the gradient is $dJ/dr = V_{sw}/K_0 \cdot J(r) \propto r^{-1}$, i.e. the modulation mainly occurs in the near heliosphere. With the quiet Sun, diffusion coefficient $K = const$. Then the modulation is linear $M \sim r$ and $grad(J) \approx 1\%/AU$. The modulation occurs throughout the entire heliosphere, and, hence, the calculated residual modulation is realistically achievable.

When analyzing the flattening of the spectrum at low energies (Fig. 1), the question may arise whether cosmic rays beyond the heliopause at a distance of 122 AU are subject to any modulation and what contribution does the region between the heliopause and the bow shock make? There are other uncertainties, some of which are discussed in (Kraimev et al. 2003; Krymsky et al. 1981).

Possible modulation of the cosmic rays outside the heliopause based on the magnetohydrodynamic model for the heliospheric medium was considered in (Strauss et al. 2013). It is shown that galactic CR modulation should persist beyond the heliosphere, where a positive CR gradient of $\sim 0.2\%/AU$ should be expected. Such a gradient can hardly be considered small, since it is not even an order of magnitude smaller than in the near heliosphere. As a result, modulation outside the heliopause can reach $25\% \div 40\%$ depending on the scenario determined by a set of CR modulation parameters. As a result, as suggested by the authors of (Strauss et al. 2013), the spectra measured by Voyager-1 are not yet true LIS spectra.

There may be another mechanism. The flattening of the CR spectrum may be due to the particles energy losses during their propagation in the Galaxy. For example, in (Werhahn et al. 2021), the stationary spectra of cosmic rays in a three-dimensional galaxy are calculated taking into account energy losses. The 3D MHD model self-consistently includes cosmic rays (protons, electrons, positrons). In the model, in particular, for protons, Coulomb and hadronic losses were taken into account and losses due to advection and diffusion (due to advection and diffusion) were estimated, provided that the diffusion coefficient depends on energy. The authors found that the spectra of protons above 10 GeV weakly depend on the

galactic radius, while at lower energies they acquire a radial dependence due to Coulomb interactions. The spectrum of protons below 1 GeV is flattened due to Coulomb interactions (which causes a spectral flattening) and turns into a reverse (a turn-over), which is consistent with the Voyager-1 data. The obtained stationary proton spectra provide excellent agreement with the observed spectra without the need for fine tuning over the entire range if the averaging was carried out for a height of 1 kpc.

Does residual modulation occur throughout the heliosphere? Direct measurements from Voyager 1 and 2 indicate that most of the residual modulation occurs between the shock wave that limits the supersonic flow of the solar wind and the heliopause. This can be seen in Fig. 6, which shows the count rate of a channel dominated by protons >70 MeV (with some fraction of electrons with energy >15 MeV) along the Voyager 1 route (Cummings et al. 2016). It can be seen that the modulation behind the shock front is comparable to the modulation from maximum to minimum in the 1980s. There are also theoretical considerations for this, since the perturbation of the medium increases behind the front of shock waves and stronger scattering and, hence, stronger modulation occurs.

6. Conclusions

1. An analysis of the modulation of cosmic rays into the heliospheres showed that even in the period of an exceptionally quiet Sun (2009), the residual modulation is significant for the entire range of rigidities under consideration (4 - 40 GV). For 10 GV particles, the residual modulation modulus is $\Delta = 19 \pm 0.4(\text{stat}) \pm 2(\text{sys}) \%$.
2. The spectrum of residual modulation at different polarities of the solar magnetic field can be described by a power function with an additional exponential dependence in the region of high rigidities.
3. The quiet Sun is capable of modulating the local interstellar spectrum by about the same magnitude as the Sun in its active phase of a relatively quiet period.
4. The resulting residual modulation for a rigidity of 10 GV is in good agreement with the results of the work based on combining data from a modern neutron monitor and cosmogenic isotope ^{10}Be data. The delay time of the response of cosmic rays relative to the moment of “disappearance” of the magnetic field of the Sun can be about 50 years.

Acknowledgments

The authors are grateful to the teams of the global network of cosmic ray stations that provide data (http://cr0.izmiran.ru/ThankYou/Our_Acknowledgment.pdf, last accessed June 27, 2023) on continuous registration of the neutron component; we thank the NMDB project (<http://www.nmdb.eu>). The work is carried out within the framework of the UNU “Russian Ground Network of Cosmic Ray Stations (CRS Network)”: <https://ckp-rf.ru/catalog/usu/433536> (last accessed June 27, 2023).

Questions and answers

Question 1: Flattening of the spectrum at low energies as a result of diffusion or energy losses - what is actually realized?

Answer 1: Both processes, but the flattening of the spectrum due to energy losses, apparently, dominates.

Question 2: Are there other options besides PAMELA data for calibrating ground detectors?

Answer 2: Yes, there is. For the period after 2011, AMS-02 data can be used; for the period from the 1970s, magnetic spectrometer data obtained during balloon measurements in the stratosphere can be used.

References

- Adriani, O. et al. (PAMELA Collaboration) 2013. Time Dependence of the Proton Flux Measured by PAMELA during the 2006 July-2009 December Solar Minimum, *ApJ*, 765, 91, <https://doi.org/10.1088/0004-637X/765/2/91>
- Aguilar, M. et al. (AMS Collaboration) 2018, Observation of Fine Time Structures in the Cosmic Proton and Helium Fluxes with the Alpha Magnetic Spectrometer on the International Space Station *Phys. Rev. Lett.*, 121, 051101, <https://doi.org/10.1103/PhysRevLett.121.051101>
- AMS-02 Data 2022, Space Science Data Center, <https://www.ssdsc.asi.it/ams>, <https://ams02.space/publications> (last accessed June 28, 2023)
- Belov, A., Eroshenko, E., Yanke, V., Oleneva, V., Abunina, M., Papaioannou, A., Mavromichalaki, E. 2018, The Global Survey Method applied to Ground Level Cosmic Ray Measurements *Solar Physics*, 293: 68, <https://doi.org/10.1007/s11207-018-1277-6>
- Belov, A.V., Gushchina, R.T., Shlyk, N.S., Yanke V.G. 2021, Using Data from a Ground-Based Network of Detectors and the PAMELA and AMS-02 Experiments to Compare Long-Term Variations in the Cosmic Ray Flux. *Bull. Russ. Acad. Sci. Phys.*, 85, 1039-1041, <https://doi.org/10.3103/S1062873821090045>
- Bischoff, D., Potgieter, M.S. and Aslam, O.P.M. 2019, New very local interstellar spectra for electrons, positrons, protons and light cosmic ray nuclei, <https://doi.org/10.3847/1538-4357/ab1e4a>
- Boschini, M.J., Della Torre, S., Gervasi, M., Grandi, D., Ohannesson, G.J., La Vacca, G., Masi, N., Moskalenko, I.V., Pensotti, S., Porter, T.A., Quadroni, L., Rancoita, P.G., Rozza, D., Tacconi, M. 2020, Inference of the Local Interstellar Spectra of Cosmic Ray Nuclei $Z \leq 28$ with the GALPROP-HELMOD Framework, <https://arxiv.org/abs/2006.01337v1>
- Caballero- Lopez, R.A., Moraal, H., McCracken, K.G., McDonald, F.B. 2004, The heliospheric magnetic field from 850 to 2000AD inferred from ^{10}Be records, *JGR*, 109, A12102, <https://doi.org/10.1029/2004JA010633>
- Corti, C., Bindi, V., Consolandi, C., and Whitman, K. 2016, Solar modulation of the local interstellar spectrum with Voyager 1, AMS-02, PAMELA and BESS, *Astrophys. J.*, 829:8, 9, <https://doi.org/10.3847/0004-637X/829/1/8>
- Cummings, A.C., Stone, E.C., Heikkilä, B.C. et al. 2016, Galactic cosmic rays in the local interstellar medium: Voyager 1 observations and model results, *The Astrophysical J.*, 831:18 (21pp), No 1, <https://doi.org/10.3847/0004-637X/831/1/18>
- CRDB (Regular stratospheric sounding) 2022, https://sites.lebedev.ru/ru/DNS_FIAN (last accessed Dec 20, 2022)
- CRDB 2022, Cosmic Rays DataBase, Dec 20, 2022, <https://tools.ssdsc.asi.it/CosmicRays/chargedCosmicRays.jsp> (last accessed June 27, 2023)
- CRDB ultra 2022, Cosmic Rays DataBase, <https://lpsc.in2p3.fr/crdb/> (last accessed Dec 20, 2022). Description: Maurin D., Dembinski H., Gonzalez J., Maris Ioana C., Melot F. Cosmic-ray database update: ultra-high energy, ultra-heavy, and antinuclei cosmic-ray data (CRDB v4.0) *Universe* 2020, XX, 5; <https://arxiv.org/pdf/2005.14663.pdf> (last accessed June 27, 2023)
- Garcia-Munoz, M., Mason, G.M., Simpson, J.A. 1977, New aspects of the cosmic ray modulation in 1974-1975 near solar minimum, *Astrophys. J.*, V. 213, P. 263-268.
- Kraiev, M.B., Kalinin, M.S. 2003, Arguments in favor of the influence of the external electric field of the heliosphere on galactic cosmic rays, *Izv. RAS, ser. Phys.*, V.67, No. 10, P. 1439-1442.
- Krymsky, G.F., Krivoshapkin, P.A., Mamrukova, V.N., Skripin, G.V. 1981, Effects of interaction of the heliomagnetosphere with the galactic field in cosmic rays // *Geomagnetism and Aeronomy*. T. 21, No. 5. P. 923-925.
- Maurin, D., Dembinski, H., Gonzalez, J., Maris Ioana, C., Melot, F. 2020, Cosmic-ray database update: ultra-

- high energy, ultra-heavy, and antinuclei cosmic-ray data (CRDB v4.0) Universe 2020, xx, 5, <https://doi.org/10.48550/arXiv.2005.14663>
- McCracken, K.G., McDonald, F.B., Beer, J., Raisbeck, G., Yiou, F. 2004, A phenomenological study of the long-term cosmic ray modulation, 850–1958 AD, JGR, 109, A12103, <https://doi.org/10.1029/2004JA010685>
- McCracken, K.G. 2007, Long Term Changes in the Residual Modulation of the Galactic Cosmic Radiation, 30th ICRC, Mexico
- McCracken, K.G., Beer, J., 2007, Long-term changes in the cosmic ray intensity at Earth, 1428–2005. Journal of Geophysical Research Atmospheres, V.112, A10101, <https://doi.org/10.1029/2006JA012117>
- McCracken, K.G. (2007a), Helimagnetic field near Earth, 1428 – 2005, JGR, 112, A09106, <https://doi.org/10.1029/2006JA012119>
- Muon Network (GMDN) 2022, <http://cosray.shinshu-u.ac.jp/crest/DB/Public/Archives/GMDN.php> (last accessed June 27, 2023)
- Nagashima, K., Morishita I., 1980, Long term modulation of cosmic rays and invariable electromagnetic state in solar modulating region, Planet. Space Sci., V. 28 (2), P. 177–194, [https://doi.org/10.1016/0032-0633\(80\)90094-X](https://doi.org/10.1016/0032-0633(80)90094-X)
- Network NM 2022 <https://www.nmdb.eu>, <https://www.nmdb.eu/nest>, or <http://cr0.izmiran.ru/common> (last accessed Dec 20, 2022)
- Seo, E.S. 2012, Direct measurements of cosmic rays using balloon borne experiments, Astroparticle Physics, 39–40, 76–87. <https://doi.org/10.1016/j.astropartphys.2012.04.002>
- SSDC 2022, Space Science Data Center <https://www.ssdsc.asi.it> (last accessed Dec 20, 2022)
- Stone, E.C., Cummings, A.C., Heikkilä, B.C. et al. 2019, Cosmic ray measurements from Voyager 2 as it crossed into interstellar space. Nat Astron 3, 1013–1018, <https://doi.org/10.1038/s41550-019-0928-3>
- Strauss, R. D., Potgieter, M. S., Ferreira, S. E. S., Fichtner, H., Scherer, K. 2013, Cosmic ray modulation beyond the heliopause: a hybrid modeling approach, ApJ, 765, L18, <https://doi.org/10.1088/2041-8205/765/1/L18>
- Usoskin, I.G., Solanki Sami K., Schüssler Manfred, Mursula Kalevi, and Alanko Katja 2003, Millennium-Scale Sunspot Number Reconstruction: Evidence for an Unusually Active Sun since the 1940s, Phys.Rev.Lett, 91, 211101 <https://doi.org/10.1103/PhysRevLett.91.211101>
- Voyager Data 2022, Science Data Access, <https://voyager.jpl.nasa.gov/mission/science/data-access>, <https://voyager.jpl.nasa.gov>, <https://voyager.jpl.nasa.gov/mission/science/bibliography/crs> (last accessed Dec 20, 2022)
- Vos, E.E., Potgieter, M.S. 2015, New Modeling of Galactic Proton Modulation during the Minimum of Solar Cycle 23/24, Astrophys. J., 815, 119, <https://doi.org/10.1088/0004-637X/815/2/119>.
- Werhahn, M., Pfrommer, C., Girichidis, P., Puchwein, E., Pakmor, R. 2021, Cosmic rays and non-thermal emission in simulated galaxies. I. Electron and proton spectra compared to Voyager-1 data, Monthly Notices of the Royal Astronomical Society, V. 505, Issue 3, P.3273–3294, <https://doi.org/10.1093/mnras/stab1324>
- Yanke, V.G., Belov, A.V., Gushchina, R.T., Zirakashvily, V.N. 2019, The rigidity spectrum of the long-term cosmic ray variations during solar activity cycles 19–24. 26th Extended ECRS + 35th RCRC. SH33. Journal of Physics: Conference Series. 1181:012007, <https://doi.org/10.1088/1742-6596/1181/1/012007>
- Yanke, V.G., Belov, A.V., Shlyk, N.S., Kobelev, P.G., and Trefilova, L.A. 2021, The Experimental Spectrum of Variations of Cosmic Rays in a Wide Range of Hardness According to AMS-02 Data. Cosmic Research, V. 59, No. 6, P. 426–431, <https://doi.org/10.1134/S0010952521060101>

Open Access

This paper is published under the Creative Commons Attribution 4.0 International license (<https://creativecommons.org/licenses/by/4.0/>). Please note that individual, appropriately marked parts of the paper may be excluded from the license mentioned or may be subject to other copyright conditions. If such third party material is not under the Creative Commons license, any copying, editing or public reproduction is only permitted with the prior consent of the respective copyright owner or on the basis of relevant legal authorization regulations.

Session 1: Abstracts

Real time monitoring of the angular distribution of cosmic rays with Ring of Stations method using NMDB data

Semyon Belov , Anatoly Belov 

Correspondence

IZMIRAN - Pushkov Institute of Terrestrial Magnetism, Ionosphere and Radiowave Propagation, Moscow, Russia

Abstract

Observing cosmic rays' angular distribution is essential to study Forbush decreases, and doing it in real time is quite helpful for space weather forecasting. By analyzing this distribution one can detect anomalies and predict possible commencement of a storm. The ring of stations method described by Abunina et al. (2020) suits really well for this task since it does not require any complicated modelling. We present an online tool built for this task. It collects hourly data from NMDB automatically and presents it visually as a longitude-time distribution plot. Apart from the plot itself, it also features the precursor index, which is intended to display likelihood of storm in the upcoming hours.

Cosmic rays in the heliosphere

Monica Laurenza 

Correspondence

INAF - National Institute for Astrophysics, Rome, Italy

Abstract

Galactic cosmic rays (GCRs) are high-energy protons and atomic nuclei entering the Heliosphere from the interstellar medium and propagating through a turbulent solar wind with an embedded heliospheric magnetic field. This leads to the so-called solar modulation, namely significant global and temporal variations in the GCR intensity and energy spectra as a function of position inside the heliosphere on long time scales (11-year solar activity cycle, 22-year magnetic polarity cycle). The modulation of GCRs involves several physical mechanisms such as diffusion, convection, adiabatic energy losses and drifts. The GCR intensity is also variable at short-term temporal scales. For instance, the large-scale magnetic field configuration

of interplanetary perturbations can produce GCR depressions called Forbush decreases. In addition, the emission at the Sun of high-energy solar particles (the so-called solar cosmic rays) produces increases in the GCR intensity. This tutorial provides an overview of GCR variability as measured by the ground-based neutron monitors and spacecraft at different locations in the Heliosphere as well as the physical processes responsible for the solar modulation and short-term variations.

Cosmic ray intensity and spectral changes during 27-day variations using time-delay measurements from Antarctic neutron monitors

Pradiphat Muangha^{1,2}, David Ruffolo¹, Alejandro Sáiz¹, Chanoknan Banglieng³, Paul Evenson⁴, Surujhdeo Seunarine⁵, Suyeon Oh⁶, Jongil Jung⁷, Marc L. Duldig⁸, John E. Humble⁸

Correspondence

- 1 Department of Physics, Faculty of Science, Mahidol University, Bangkok, Thailand
- 2 NARIT - National Astronomical Research Institute of Thailand, Chiang Mai, Thailand
- 3 Division of Physics, Faculty of Science and Technology, Rajamangala University of Technology Thanyaburi, Pathum Thani, Thailand
- 4 Department of Physics and Astronomy, University of Delaware, Newark, USA
- 5 Department of Physics, University of Wisconsin, River Falls, USA
- 6 Department of Earth Science Education, Chonnam National University, Gwangju, South Korea
- 7 Department of Astronomy, Space Science and Geology, Chungnam National University, Daejeon, South Korea
- 8 School of Natural Sciences, University of Tasmania, Hobart, Australia

Abstract

Using neutron time-delay measurements from Antarctic neutron monitors, we can extract the leader fraction, L , of neutron counts that do not follow a previous neutron count in the same counter tube due to the cosmic ray shower. L , the inverse of the neutron multiplicity, can indicate variations in the cosmic-ray spectral index over the rigidity range of the NM response function. In this presentation, a comparative analysis of L from four Antarctic NM stations at South Pole (SP), McMurdo (MC), and Jang Bogo (JB), and Mawson (MA) will be presented. We find that L is well correlated with the spectral index inferred using data from the Alpha Magnetic Spectrometer (AMS-02) aboard the International Space Station. The wavelet analysis of the count rate C , and heliosphere parameters show a strong 27-day periodicity due to high-speed solar wind streams (HSSs) and corotating interaction regions (CIRs) while L usually had a very weak variation.

Large amplitude bidirectional anisotropy of cosmic-ray intensity observed in November, 2021

Kazuoki Munakata ^{ID 1}, Masayoshi Kozai ^{ID 2}, Chihiro Kato ^{ID 1}, Yuki Hayashi ^{ID 1}, Ryuho Kataoka ^{ID 3}, Akira Kadokura ^{ID 2,3,4}, Munetoshi Tokumaru ^{ID 5}, Rafael Rodrigues Souza de Mendonça ^{ID 6}, Ezequiel Echer ^{ID 6}, Alisson Dal Lago ^{ID 6}, Marlos Rockenbach ^{ID 6}, Nelson Jorge Schuch ^{ID 7}, Jose V. Bageston ^{ID 7}, Carlos Roberto Braga ^{ID 8}, Hala K. Al Jassar ^{ID 9}, Madan Mohan Sharma ^{ID 9}, Marcus L. Duldig ^{ID 10}, John E. Humble ^{ID 10}, Ismail Sabbah ^{ID 11}, Paul Evenson ^{ID 12}, Pierre-Simon Mangeard ^{ID 12}, Takao Kuwabara ^{ID 12}, David Ruffolo ^{ID 13}, Alejandro Sáiz ^{ID 13}, Warit Mitthumsiri ^{ID 13}, Waraporn Nuntiyakul ^{ID 14}, Jozsef Kóta ^{ID 15}

Correspondence










- 1 Department of Physics, Shinshu University, Matsumoto, Nagano, Japan
- 2 Polar Environment Data Science Center, Joint Support-Center for Data Science Research, Research Organization of Information and Systems, Tachikawa, Tokyo, Japan
- 3 National Institute of Polar Research, Tachikawa, Tokyo, Japan
- 4 Department of Polar Science, School of Multidisciplinary Sciences, The Graduate University for Advanced Studies, SOKENDAI, Tachikawa, Tokyo, Japan
- 5 Institute for Space-Earth Environmental Research, Nagoya University, Nagoya, Aichi, Japan
- 6 INPE - National Institute for Space Research, São José dos Campos, Brazil
- 7 Southern Space Coordination, National Institute for Space Research, Santa Maria, Brazil
- 8 George Mason University, Fairfax, Virginia, USA
- 9 Physics Department, Kuwait University, Safat, Kuwait
- 10 School of Natural Sciences, University of Tasmania, Hobart, Australia
- 11 Department of Natural Sciences, College of Health Sciences, Public Authority of Applied Education and Training, Kuwait City, Kuwait
- 12 Bartol Research Institute and Department of Physics and Astronomy, University of Delaware, Newark, USA
- 13 Department of Physics, Faculty of Science, Mahidol University, Bangkok, Thailand
- 14 Department of Physics and Materials Science, Faculty of Science, Chiang Mai University, Chiang Mai, Thailand
- 15 Lunar and Planetary Laboratory, University of Arizona, Tucson, USA

Abstract

We analyze the cosmic-ray variations during a significant Forbush decrease observed with world-wide networks of ground-based neutron monitors and muon detectors during November 3-5, 2021. Utilizing the difference between primary cosmic-ray rigidities monitored by neutron monitors and muon detectors, we deduce the rigidity spectra of the cosmic-ray density (or omnidirectional intensity) and the first- and second-order anisotropies separately, for each hour of data. A clear two-step decrease is seen in the cosmic-ray density with the first ~2 % decrease after the interplanetary shock arrival followed by the second ~5 % decrease inside the magnetic flux rope (MFR) at 15 GV. Most strikingly, a large bidirectional streaming along the magnetic field is observed in the MFR with a peak amplitude of ~5 % at 15 GV which is comparable to the total density decrease inside the MFR. The bidirectional streaming could be explained by adiabatic deceleration and/or focusing in the expanding MFR, which have stronger effects for pitch angles near 90

degrees, or by selective entry of GCRs along a leg of the MFR. The peak anisotropy and density depression in the flux rope both decrease with increasing rigidity. The spectra vary dynamically indicating that the temporal variations of density and anisotropy appear different in neutron monitor and muon detector data.

Solar magnetic polarity effect on neutron monitor count rates: comparing latitude surveys and Antarctic stations

Kledsai Poopakun ¹, Waraporn Nuntiyakul ¹, Sidarat Khamphakdee¹, Achara Seripienlert ², David Ruffolo ³, Paul Evenson ⁴, Peng Jiang⁵, Pongpichit Chuanraksasat ², Kazuoki Munakata ⁶, Marc L. Duldig ⁷, John E. Humble ⁷, Jim Madsen⁸, Boonracksar Soonthornthum², Siramas Komonjinda¹




Correspondence

- 1 Department of Physics and Materials Science, Faculty of Science, Chiang Mai University, Chiang Mai, Thailand
- 2 NARIT - National Astronomical Research Institute of Thailand, Chiang Mai, Thailand
- 3 Department of Physics, Faculty of Science, Mahidol University, Bangkok, Thailand
- 4 Bartol Research Institute and Department of Physics and Astronomy, University of Delaware, Newark, USA
- 5 Polar Research Institute of China, Pudong, Shanghai, China
- 6 Physics Department, Shinshu University, Matsumoto, Nagano, Japan
- 7 School of Natural Sciences, University of Tasmania, Hobart, Australia
- 8 Wisconsin IceCube Particle Astrophysics Center, University of Wisconsin-Madison, USA

Abstract

The Galactic cosmic ray spectrum manifests subtle variations over the 22-year solar magnetic cycle in addition to more pronounced variations over the 11-year sunspot cycle. We conducted numerous latitude surveys by operating a neutron monitor onboard icebreakers that traveled across a wide range of geomagnetic cutoff rigidity. Here we revisit our previous work to study spectral changes using 13 annual latitude surveys from 1994 to 2007 using neutron monitor data from Mawson instead of McMurdo (closed in 2017) to allow extension to more recent latitude surveys. We confirm linear trends between count rates at different geomagnetic cutoff rigidity and changes in slope before and after the polarity reversal in 2000. We performed two more latitude surveys (in 2019 and 2020) with a monitor similar to the 3NM64 in the previous surveys but without lead rings around the central tube; a so-called “semi-leaded neutron monitor”. We found similar results for the relationship between the count rate of the semi-leaded neutron monitor and that of the Mawson neutron monitor in Antarctica. We confirm the “crossover” in spectra measured near solar minima during epochs of opposite solar magnetic polarity using recent latitude surveys and verify the absence of crossover for the same solar magnetic polarity. Thus we confirm both the change in the linear relationship and the crossover as effects of solar magnetic polarity on the cosmic ray spectrum resulting from solar modulation. Partially supported by grant RTA6280002 from Thailand Science Research and Innovation.

Revised neutron monitor scaling factor and modulation potential determination for 1964-2021

Pauli Väisänen , Ilya Usoskin , Riikka Kähkönen, Sergey Koldobskiy , Kalevi Mursula 

Correspondence

Space Physics and Astronomy, Faculty of Science, University of Oulu, Finland

Abstract

The flux of galactic cosmic rays (GCR) is considered to be constant in the local interstellar medium, but upon arriving in the heliosphere, they experience modulation due to the magnetic activity of the Sun. This variation can be observed, e.g., when measuring GCR fluxes with neutron monitors (NMs). In order to parameterize the level of modulation, the heliospheric modulation potential, ϕ , is often used. This parameter is usually evaluated from the measurements by multiple NM stations by employing models of the cosmic ray yield functions, after correcting for the geomagnetic rigidity cutoff and atmospheric effects. In this work, we employ the recently updated yield function as presented in Mishev2020 and a new method of minimized root-mean-square errors in order to compute the modulation potential and the station-specific scaling factors.

Session 2:

**GLE analysis and space
weather research and services**

GOES observations of solar protons during ground level enhancements

Juan V. Rodriguez  , Brian T. Kress 

Correspondence

CIRES – Cooperative Institute for Research in Environmental Sciences, University of Colorado Boulder, and NCEI – National Centers for Environmental Information at NOAA – National Oceanic and Atmospheric Administration, Boulder, Colorado, USA, juan.rodriguez@noaa.gov, brian.kress@noaa.gov

Keywords

solar energetic particles; ground level enhancements; galactic cosmic rays; neutron monitor; GOES

Abstract

Since 1974, the U.S. National Oceanic and Atmospheric Administration (NOAA) has observed solar proton fluxes from the Geostationary Operational Environmental Satellites (GOES). These observations frequently have served as measurements of the primary component of ground level enhancements (GLEs). Until March 2020, when GOES-14 and -15 were turned off, solar proton measurements were made by the Energetic Particle Sensor (EPS) and the High-Energy Proton and Alpha Detector (HEPAD). EPS had poor energy resolution above 100 MeV, and NOAA derived a >100 MeV integral flux from the EPS channels to support alerts issued by the Space Weather Forecast Office. HEPAD provided some energy resolution in the 330-700 MeV range and a >700 MeV integral channel. Starting with GOES-16, a new instrument called the Solar and Galactic Proton Sensor (SGPS) has replaced EPS and HEPAD. SGPS uses three solid-state telescopes to observe solar proton fluxes between 1 and 500 MeV with a >500 MeV integral channel. The >100 MeV integral flux is now derived from SGPS observations and includes the >500 MeV flux in its derivation. In this paper, we describe the older EPS and HEPAD observations and the new SGPS solar proton observations. We also compare methods for detecting solar proton event onsets currently used with GOES and neutron monitor observations and recommend some innovations.

1. Introduction

In the study of ground level enhancements (GLEs), observations of the primary population are provided by satellite observations in Earth orbit or at the first Sun-Earth Lagrange point. One source of such observations has been the series of Geostationary Operational Environmental Satellites (GOES) operated by NOAA since 1974. The GOES series of weather satellites has operated in geostationary orbit (GEO), which most of the time lies within Earth's magnetosphere, apart from brief excursions into the magnetosheath.

Access of solar energetic particles (SEPs) to GEO is affected by the geomagnetic field, more strongly at lower energies, and trapped magnetospheric proton populations are nearly always present below 2 MeV, preventing clear observations of SEPs at lower energies. However, SEP fluxes above 500 MeV, which have ground-level signatures, have unimpeded access to GEO.

The purpose of this paper is to provide an introduction to GOES observations during GLEs. These observations include the long series of Energetic Particle Sensors (EPS) and High Energy Proton and Alpha Detectors (HEPAD), which ceased operations in 2020, and the new series of Solar and Galactic Proton Sensors (SGPS), which to date have observed GLEs 72 (September 2017) and 73 (October 2021). Because the primary purpose of these space weather sensors is to support NOAA's real-time SEP event alerts, this paper compares the NOAA-issued alerts of GLEs 72 and 73 with the alerts issued by the neutron monitor-based GLE Alert Plus systems, which follow different protocols. The paper concludes with recommendations for innovations to these alert systems.

2. Detection of >100 MeV fluxes on GOES 8-15

Prior to GOES-16, SWPC issued >100 MeV proton alerts based on observations by the GOES Energetic Particle Sensor (EPS). Specifically, >100 MeV fluxes were derived from the P6 and P7 channel proton fluxes measured by the EPS Dome D5. The basic D5 design did not change from GOES-4 (launched 9 September 1980) to GOES-15 (launched 4 March 2010). It had a large fan-shaped field-of-view (70° by 130°) defined by a tungsten collimator that also shielded the sides. The outputs of two silicon surface-barrier detectors (25 mm², each 1500-micron thick) under an 8.0 g/cm² copper moderator were summed to create one energy deposition signal. The two D5 proton channels P6 and P7 were distinguished by deposited energy (P6: 3.5-28.0 MeV; P7 1.6-3.5 MeV). This relatively simple design resulted in consistent performance among the GOES 8-15 units (Rodriguez et al. 2014). However, the energy resolution was poor, and, with no anticoincidence, the observations were susceptible to contamination by protons that penetrated the structure. A copper plug on the back was penetrated by >80 MeV protons, and >120 MeV protons penetrated the tungsten collimator, resulting in a nearly omnidirectional response at the highest energies (Panametrics 1980; Sellers & Hanser 1996). The resulting energy responses were 84-200 MeV for P6 and 110-900 MeV for P7 (Onsager et al. 1996).

An algorithm developed by R. Zwickl (unpublished until documented by Rodriguez et al. 2017) estimated the >100 MeV flux by determining a piecewise power-law from the ratios of observed channel count rates. The upper integration limit of the extrapolated power law was set at 500 MeV (though P7 had a strong response to protons above 500 MeV). SWPC issued an alert when the >100 MeV flux reached 1 p/(cm² s sr) = 1 particle flux unit (pfu).

EPS P6 and P7 proton measurements do not exhibit the diurnal variations typical of 100s of keV to multiple MeV electron fluxes at geosynchronous, including during periods when the Earth's radiation belts are significantly enhanced. This lack of electron contamination in the EPS proton channels is illustrated in Figure 1, in which the GOES-13 EPS P6 and P7 fluxes from September 2017 are plotted along with the >0.8 and >2 MeV radiation belt fluxes also observed by GOES-13 EPS. In addition, solar energetic electrons are not expected to penetrate directly to GEO due to low magnetic rigidity in their characteristic energy range. Therefore, there is no evidence that GOES EPS solar proton observations are contaminated by solar electron fluxes.

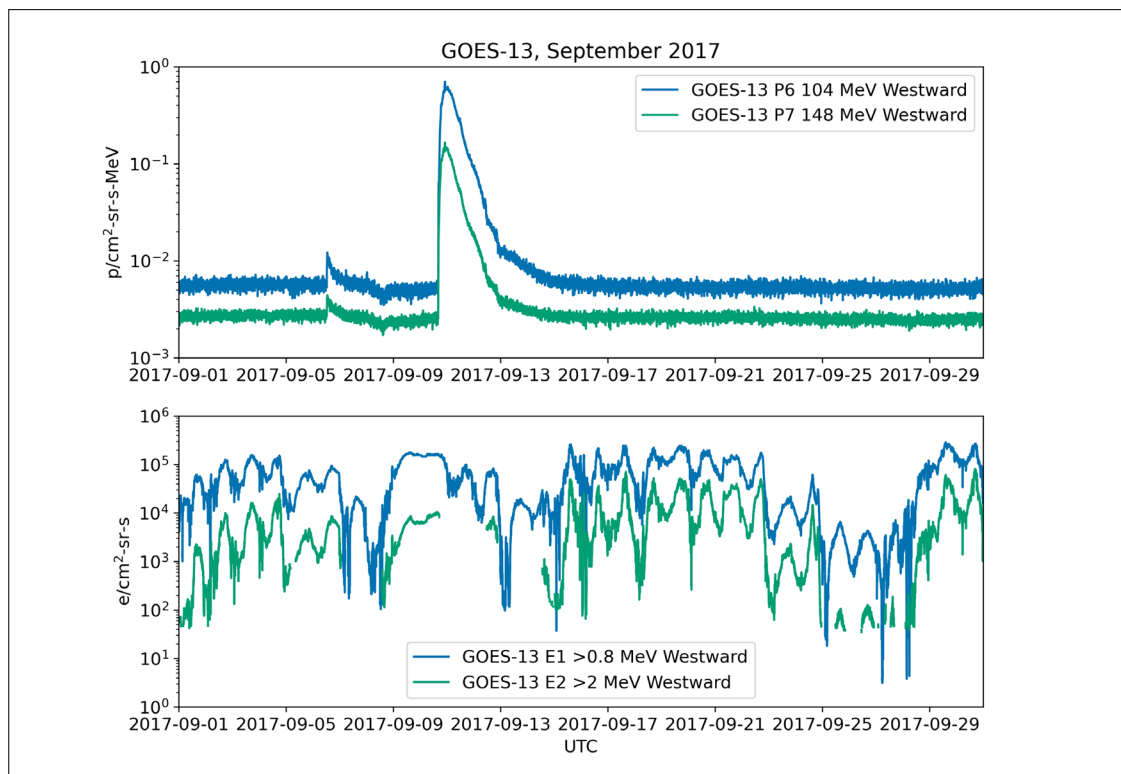


Fig. 1: GOES-13 EPS proton and electron fluxes from September 2017, illustrating the lack of electron contamination of the proton fluxes. The top panel shows the P6 and P7 channel proton fluxes observed by the westward-looking EPS. The indicated energies are from the cross-calibration by Sandberg et al. (2014). The bottom panel shows the >0.8 and >2 MeV radiation belt electron fluxes observed by the same instrument. The gaps in the >2 MeV fluxes correspond to periods when the observations are dominated by contamination from solar protons or when the electron fluxes are below background levels. While the EPS >2 MeV electron fluxes are always contaminated by proton fluxes from large SEP events, the converse is not true.

In addition to EPS, a High Energy Proton and Alpha Detector (HEPAD) solid-state telescope (70-degree full-angle conical FOV) measured >330 MeV protons on GOES 4-15. The GOES-4 and -5 HEPAD data were not archived, and the GOES-7 HEPAD failed on-orbit. Therefore, HEPAD data are available from GOES-6 and 8-15 (Sauer 1993; Sellers & Hanser 1996; Raukunen et al. 2020). The first GLE observed by GOES-6 was GLE 39 (February 1984), and the final GLE observed by GOES 13-15 was GLE 72 (September 2017). An enhancement above cosmic ray backgrounds in the HEPAD >700 MeV proton channel was a reliable signature of the primary component of a GLE, with some important exceptions (Thakur et al. 2016).

The HEPAD proton channels result from triple coincidences among two silicon detectors and the output of a photomultiplier tube illuminated by a fused silica Cherenkov radiator (Rinehart 1978). The nominal energies of the proton channel set are 330-420 MeV (P8), 420-510 MeV (P9), 510-700 MeV (P10), and >700 MeV (P11) (Sellers & Hanser 1996). In actuality, the response functions overlap substantially, and all of the channels have significant responses above their nominal energy range, those for P8 and P9 being due to rear entry (Raukunen et al. 2020). Signals above backgrounds in the two alpha particle channels are very rare and moreover are contaminated by proton fluxes, since protons in the tail of the distribution are mistaken for alpha particles (Blake & Kolasinski, n.d.). HEPAD was designed to reject <4 MeV electrons in-aperture and <7 MeV electrons out-of-aperture (Rinehart 1978) and was measured

to have no significant response below 10 MeV (Panametrics 1980). Although HEPAD proton fluxes are susceptible to contamination by >10 MeV electrons (Blake & O'Brien 2012), observable levels of such electron fluxes are rare in geostationary orbit and can be distinguished by their characteristic diurnal variations, which are not present in >330 MeV solar proton fluxes.

Comparative plots of the onsets of GLE events from Solar Cycles 23 and 24 as observed by neutron monitors and by GOES EPS (channel P7 and >100 MeV flux) and HEPAD (channels P8, P9, P10 and P11), all at 1-minute resolution, can be found in He and Rodriguez (2018; GLEs 55-71) and in Redmon et al. (2018; GLE 72).

Accurate EPS and HEPAD calibrations have been difficult to achieve. While important work on cross-calibration and incorporation of EPS and HEPAD into models has been performed recently (Sandberg et al. 2014; Bruno 2017; Rodriguez et al. 2017; Raukunen et al. 2020; Kress et al. 2021; Hu & Semones 2022), the final word on EPS and HEPAD calibrations has yet to be written.

The flow of space environment data from GOES-13 ceased on 14 December 2017. The flow of space environment data from GOES-14 and -15 ceased on 4 March 2020.

3. New solar proton detector on GOES-16+

The first of a new series of particle detection instrument suites – the Space Environment In-Situ Suite (SEISS) – was launched on GOES-16 on November 19, 2016. Subsequently, SEISS has launched on GOES-17 (01 March 2018) and GOES-18 (01 March 2022). SEISS consists of five instruments, four of which measure solar energetic particle (SEP) fluxes (Dichter et al. 2015; Kress et al. 2020). These instruments represent the first completely new designs of GOES SEP detectors directed by NOAA since the 1970's. The primary SEP instrument is the Solar and Galactic Proton Sensor (SGPS). Each satellite carries two SGPS instruments, one looking east and one looking west. The westward observations of solar protons are attenuated much less by geomagnetic cutoffs than the eastward observations (Rodriguez et al. 2010; Kress et al. 2013). SGPS observes 1-500 MeV solar proton fluxes in 13 differential channels and integral fluxes in a >500 MeV channel, and 1-224 MeV/nucleon alpha particle fluxes in 12 differential channels. From 1 to 12 MeV, its energy range overlaps the 4 highest energy channels of the proton telescopes of the Magnetospheric Particle Sensor - High Energy (MPS-HI). The Energetic Heavy Ion Sensor (EHIS) observes heavy ion fluxes in 5 differential channels spanning energy ranges that vary from 18-335 MeV/nucleon for carbon to 39-897 MeV/nucleon for copper. In addition, EHIS observes H (11-239 MeV) and He (11-154 MeV/nucleon) ion fluxes.

A more detailed description of the SGPS instrument and data, including the proton energy channels and their geometric factors, is provided by Kress et al. (2021). In brief, each SGPS consists of three passively-shielded solid state telescopes, each of which covers a different part of the 1-500 MeV energy range. The three telescopes have 60, 60 and 90 degree conical fields-of-view. The >500 MeV proton channel has a much larger geometric factor (2.5 cm² sr; Kress et al. 2021) than the HEPAD channels in a similar energy range (~0.6 cm² sr; Raukunen et al. 2020). Kress et al. (2021) include a comprehensive evaluation of the GOES-16 proton fluxes from the SEP event commencing on 10 September 2017, which included the primary component of GLE 72. Based on cross-calibrations during this SEP event, the SGPS fluxes above 100 MeV are about a factor of two greater than the equivalent EPS fluxes when the effective EPS

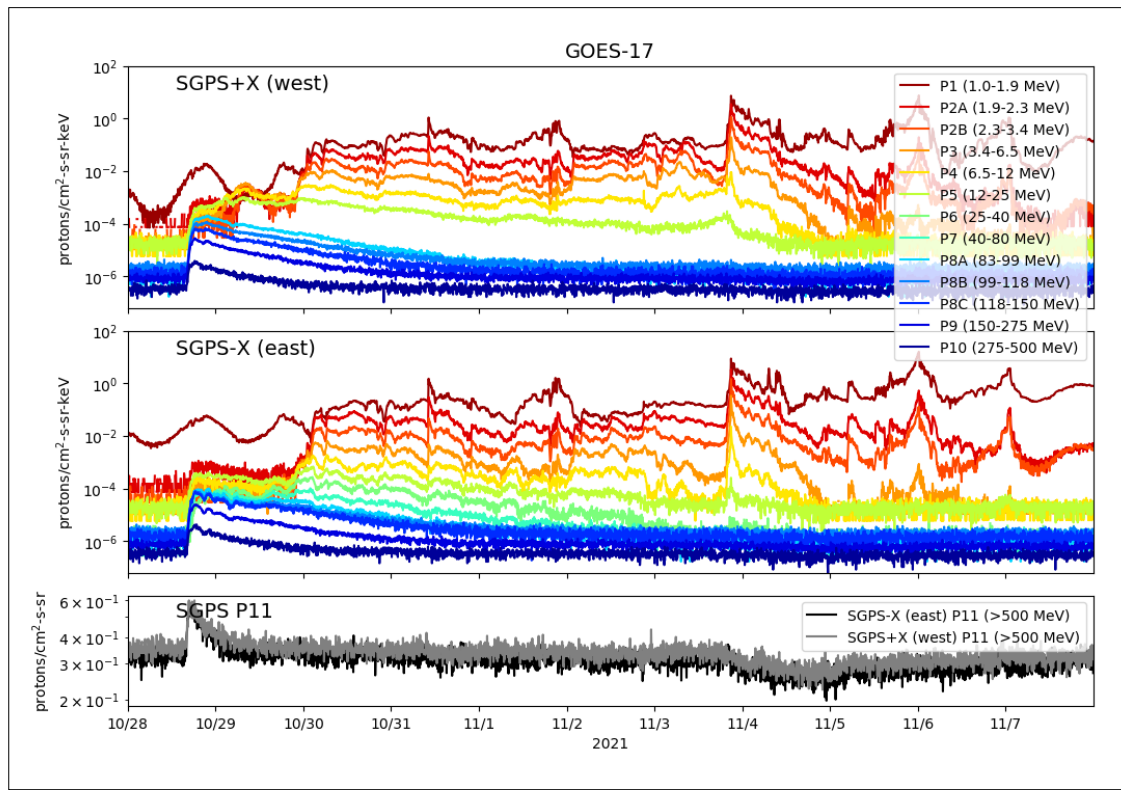


Fig. 2: GOES-17 SGPS proton fluxes from 28 October through 7 November 2021, showing the GLE 73 SEP event. The top panel shows the 1-500 MeV differential fluxes observed by the eastward-looking SGPS. The middle panel is a similar plot of the observations by the westward-looking SGPS. The bottom panel shows the >500 MeV fluxes from both the eastward and westward SGPSs.

energies derived by Sandberg et al. (2014) are used in the analysis. These effective EPS energies in turn were derived from cross-calibrations with IMP-8 observations. SWPC's >100 MeV solar proton alerts are issued based on integral fluxes derived using a new algorithm from the six channels of the third telescope of the westward-looking SGPS (Rodriguez et al. 2017; Kress et al. 2021). The EPS >100 MeV proton flux had an upper integration limit of 500 MeV, and in the absence of a SEP event, the backgrounds were residual noise from background subtractions. In contrast, the SGPS >100 MeV proton flux includes the >500 MeV P11 channel flux in the sum, and in the absence of a SEP event, the backgrounds represent the calibrated >500 MeV GCR proton flux. SGPS differential and integral fluxes are available in 1-minute and 5-minute averages.

The first GLE event of Solar Cycle 25, commencing on 28 October 2021, was observed by the GOES-16 and -17 SGPS instruments. The GOES-17 SGPS time series are shown in Figure 2. The lower energy channels from the eastward-facing sensor exhibit more fluctuations than the fluxes from the westward-facing sensor, due to time-variations in the geomagnetic cutoffs. The P11 >500 MeV channel is sensitive to the primaries of GLE 73 and to the Forbush decrease (Forbush 1937) in galactic cosmic ray (GCR) fluxes that commenced late on 3 November following the arrival of a solar wind shock at Earth.

The SGPS differential channels were designed and calibrated to observe SEP events, whose spectra decrease with energy. In the presence of a GCR spectrum, which is flat or increasing with energy over

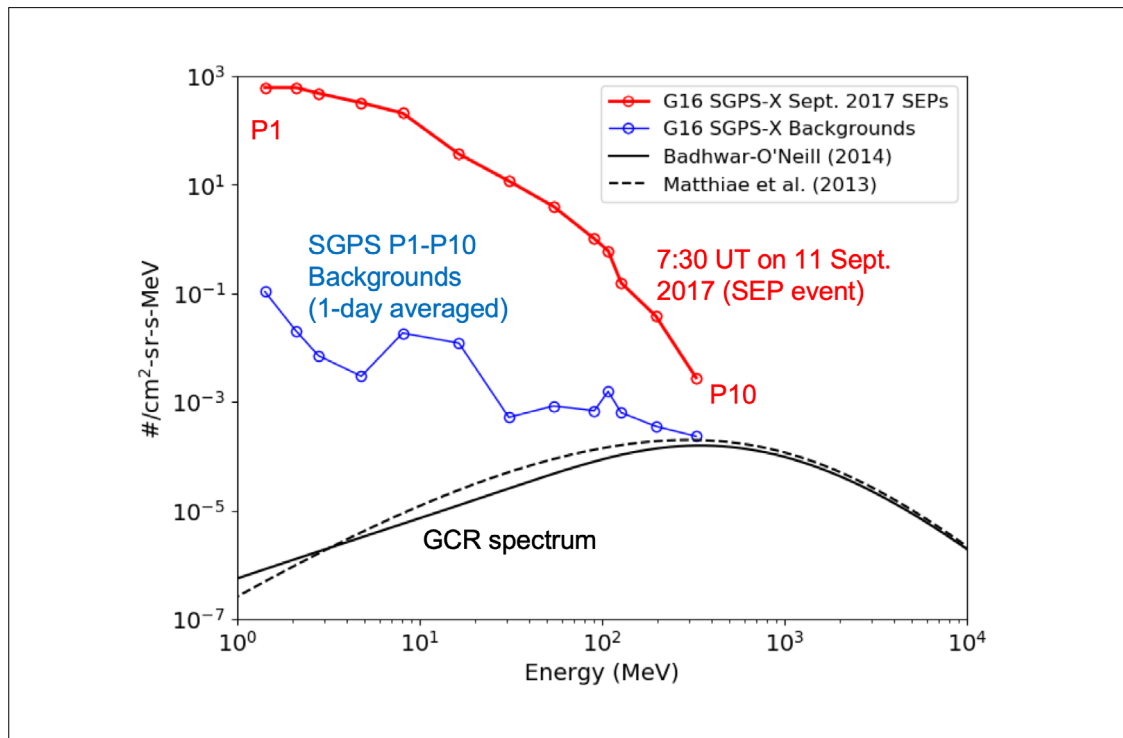


Fig. 3: GOES-16 SGPS background fluxes (blue curve), a GOES-16 SGPS solar proton spectrum from 11 September 2017, 0730 UT (red curve), and GCR model spectra from the Matthiae et al. (2013) and O'Neill et al. (2015) models (black curves). The P10 channel provides a calibrated measure of differential GCR proton fluxes in the absence of solar proton fluxes.

the SGPS energy range, the backgrounds in channels P3-P9 (3.4-275 MeV) are up to several orders of magnitude greater than the GCR flux levels at those energies, due to their sensitivity to higher-energy protons (Figure 3). In the absence of a large SEP event, the fluxes in SGPS channels P1 and P2 are dominated by trapped magnetospheric protons, which exhibit similar temporal variations to radiation belt electrons, and the SGPS P10 fluxes are within a factor of two of fluxes predicted by the Matthiae et al. (2013) and Badhwar-O'Neill 2014 (O'Neill et al. 2015) GCR models. Since the P10 energy band (276-404 MeV) bounds the GCR spectrum peak, it provides a calibrated measure of GCR flux during quiet solar conditions. SGPS channels P10 and P11 thus provide reliable GCR differential and integral proton fluxes, respectively, in their energy ranges.

The GLE 73 event was an unusual event in that the typical decreasing power law spectrum was not observed until 30 October 2021. On 28 October, the 3.4-23 MeV fluxes were sufficiently low that they were dominated by contamination from >60 MeV protons, to which the Telescope 1 channels are sensitive (Kress et al. 2021). In spectra from 28 October (18 UT), the P1 and P2A,B fluxes represent the high-energy tail of the trapped magnetospheric proton population, while P3, P4 and P5 are dominated by their >60 MeV responses (Figure 4). These low-energy SGPS fluxes should be treated with caution in the presence of a hard proton energy spectrum until a correction is put in place for this contamination.

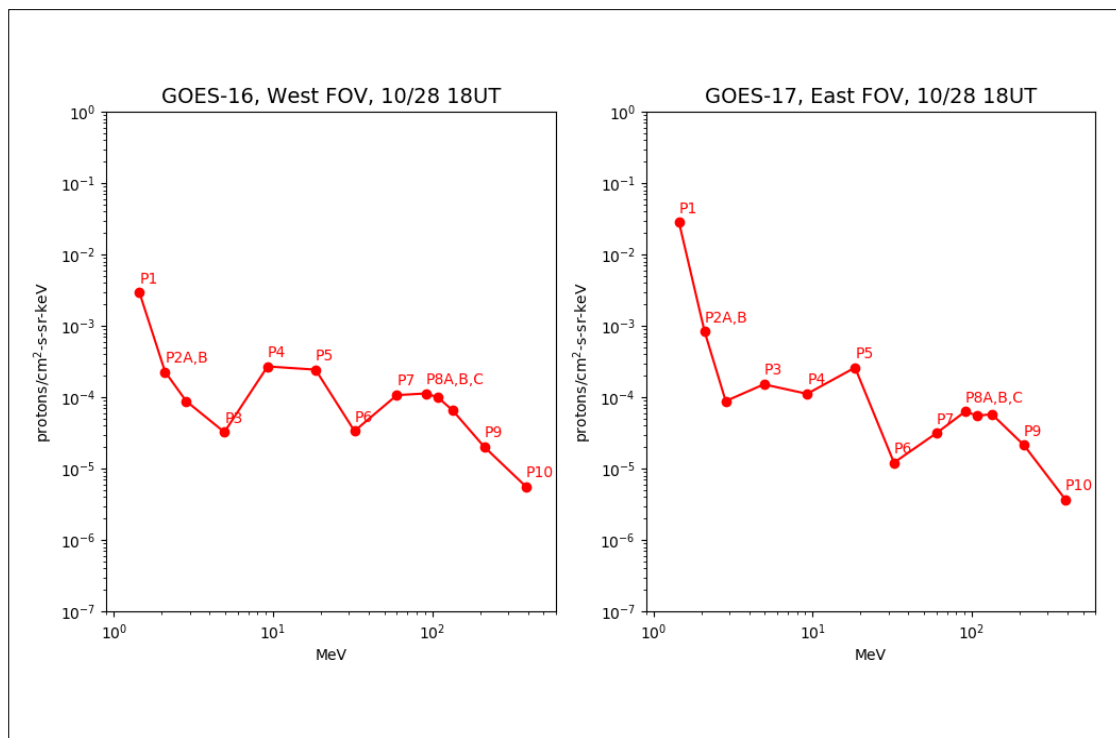


Fig. 4: SGPS proton differential number flux energy spectra from 28 October 2021, 1800 UT. (Left) Spectrum from the westward-looking SGPS on GOES-16. (Right) Spectrum from the eastward-looking SGPS on GOES-17. P3, P4, and P5 show evidence of contamination by >60 MeV protons.

4. NOAA and GLE Alert Plus alerts of GLEs 72 and 73

The NOAA SWPC and GLE Alert Plus SEP detection protocols are qualitatively different and produce different results. The NOAA method has a human forecaster in the loop. The forecaster observes 5-minute real-time averages of >10 MeV and >100 MeV proton fluxes from a single GOES satellite designated the primary satellite for space weather alerts. After three consecutive 5-minute flux averages are above a fixed threshold, an alert is issued. The first >10 MeV threshold is 10 pfu. The sole >100 MeV threshold is 1 pfu. This protocol prevents false alerts but introduces at least a 15-minute delay from the onset of a SEP event.

The GLE Alert Plus alert relies on real-time 1-minute data from multiple stations in the Neutron Monitor Database (NMDB). Following the method of Kuwabara et al. (2006), a moving threshold that is the sum of a running average and the scaled standard deviation of the count rates is calculated for each neutron monitor (NM) station (Souvatzoglou et al. 2014; Mavromichalaki et al. 2018). Depending on the value of this moving threshold, each station is at one of four alert levels (quiet, watch, warning, and alert). For a general alert to be issued, at least three stations must be in alert mode. The alert is issued automatically, and the alert status of each station is provided graphically.

GLE Alert Plus first successfully issued a real-time alert for GLE 72, whose onset was on 10 September 2017 (Mavromichalaki et al. 2018). GLE Alert Plus issued the first NM station alert (Fort Smith) at 1618 UT, and the general alert based on four stations (Kerguelen, Inuvik, South Pole Bares, Thule) was issued at 1658 UT. The

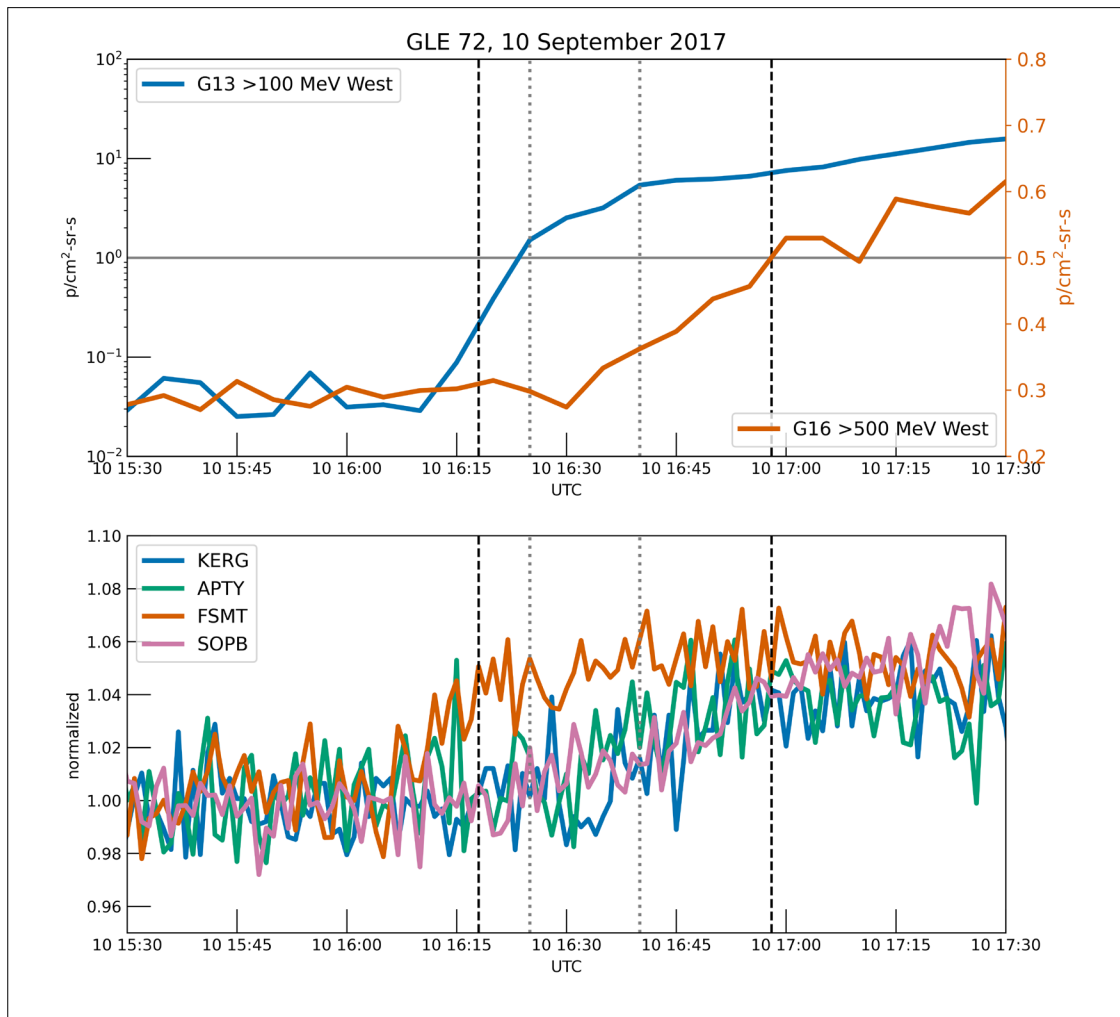


Fig. 5: The onset of GLE 72 as observed (top) by GOES-13 EPS >100 MeV and GOES-16 SGPS >500 MeV fluxes and (bottom) by the Kerguelen, Apatity, Fort Smith, and South Pole Bare neutron monitors. The GOES data are shown in integral flux units, with different scales for the two observations due to the much smaller increase in the >500 MeV fluxes. The NM data are normalized to the pre-event levels. The first vertical dashed line indicates the first NM station alert (Fort Smith) at 1618 UT. The first vertical dotted line indicates when the GOES-13 >100 MeV flux crossed the 1 pfu threshold (1625 UT). The second vertical dotted line indicates when SWPC issued the >100 MeV alert (1640 UT). The second vertical dashed line indicates when GLE Alert Plus issued the general alert (1658 UT).

GOES-13 >100 MeV flux crossed the 1-pfu threshold at 1625 UT, and SWPC issued the >100 MeV alert at 1640 UT. Therefore, though the first NM station alert preceded the NOAA alert by 7 minutes, the NOAA alert led the GLE Alert Plus general alert by 18 minutes (Figure 5). The GOES-13 >100 MeV proton flux rose above background noise similarly to the Fort Smith NM, while the rise of the GOES-16 >500 MeV solar proton flux above the GCR level was similar to some of the other NM stations like Apatity and Kerguelen. As discussed in connection with Figure 1, the early onset of the GOES-13 >100 MeV proton fluxes was not due to electron contamination. The count rates from the EPS P7 channels on GOES-14 and -15 rose less rapidly than the GOES-13 P7 count rates, from which the >100 MeV fluxes used in the SWPC alert were derived (Redmon et al. 2018). This difference among the three GOES EPS observations may indicate a longitudinal variation in geostationary orbit.

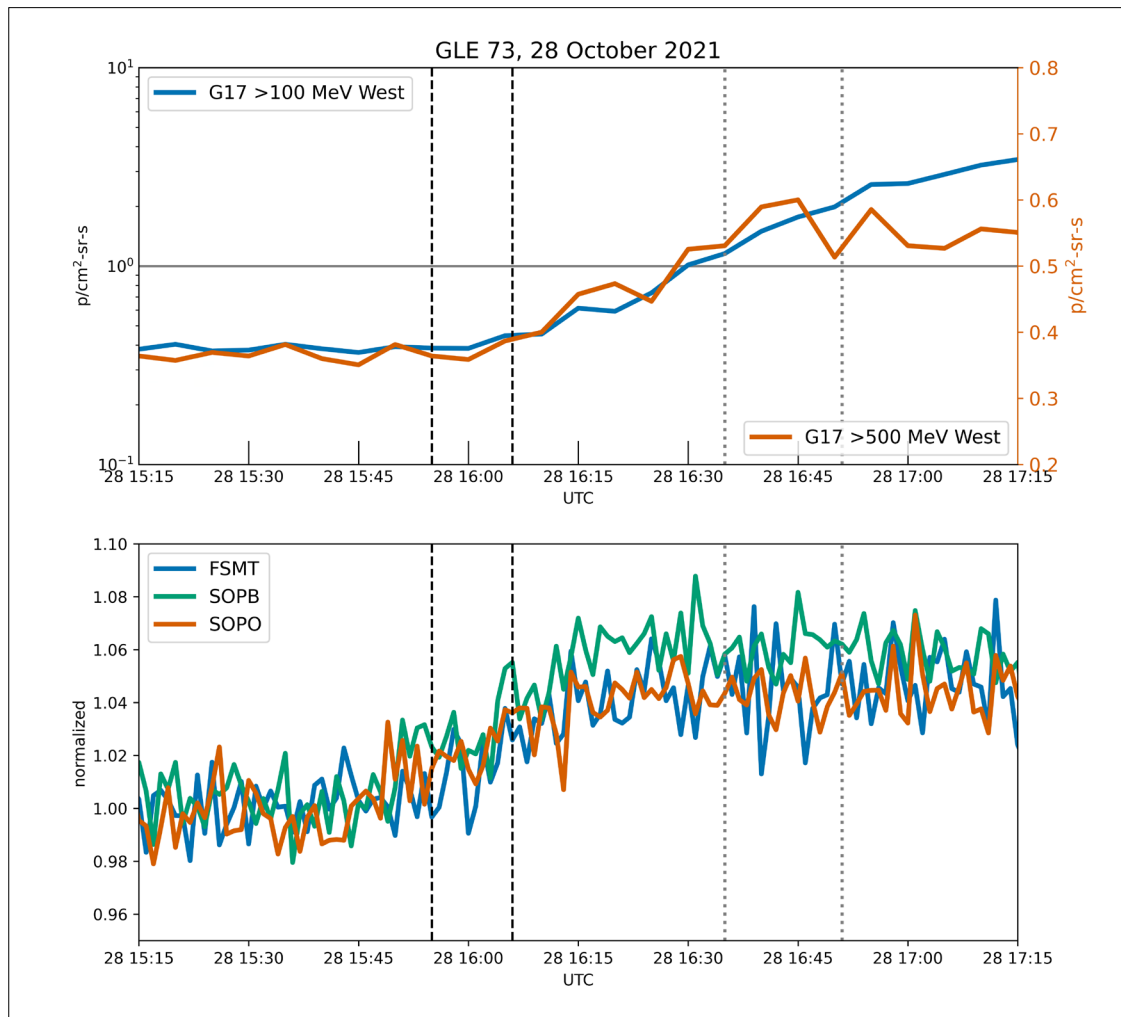


Fig. 6: The onset of GLE 73 as observed (top) by GOES-17 SGPS >100 MeV and >500 MeV proton fluxes and (bottom) by the Fort Smith, South Pole and South Pole Bares neutron monitors. The GOES data are shown in integral flux units, with different scales for the two observations due to the much smaller increase in the >500 MeV fluxes. The NM data are normalized to the pre-event levels. The first vertical dashed line indicates the first NM station alert (South Pole Bares) at 1555 UT. The second vertical dashed line indicates when GLE Alert+ issued the general alert (1606 UT). The first vertical dotted line indicates when the GOES-16 >100 MeV flux crossed the 1-pfu threshold (1635 UT). The second vertical dotted line indicates when SWPC issued the >100 MeV alert (1651 UT).

The onset of GLE 73 was on 28 October 2021. GLE Alert++ issued the first NM station alert (South Pole Bares) at 1555 UT, and the general alert based on 3 stations (Fort Smith, South Pole and South Pole Bares) was issued at 1606 UT. The GOES-16 >100 MeV flux crossed the 1-pfu threshold at 1635 UT, and SWPC issued the >100 MeV alert at 1651 UT, 45 minutes after the GLE Alert++ general alert (Figure 6). In this case, the GOES flux increases visibly occurred about 15 minutes later than the NM count rate increases, and the use of a fixed threshold based on a single satellite, rather than a moving threshold operating on data from two satellites, delayed the GOES alerts further.

5. Discussion

In a study of the onsets of GLEs 55-71 that applied a moving threshold detection method similar to that of Kuwabara et al. (2006) to 1-minute NM and GOES data, He and Rodriguez (2018) found that the median difference in the event detection times between NM and GOES was 0 minutes, with the 10th, 25th, 75th, and 90th percentiles of the differences (GOES minus NMs) being -7.2, -1.5, +2.5, and +4.2 minutes, respectively. The detection thresholds were set to avoid false alarms using a three-station coincidence for NM data and a two-satellite coincidence for GOES data. Using the same algorithm, GLE 72 was detected by some GOES 13-15 HEPAD channels within two minutes of the Fort Smith station alert (1618 UT) issued by GLE Alert Plus (Redmon et al. 2018). These differences between NMs and GOES may be due partly to energy dependencies, anisotropies and geomagnetic effects, and partly to different noise and event-to-background levels in different instruments. A deeper understanding of the causes of these differences should be pursued.

Regardless, a practical alert system should take advantage of these differences to reduce alert delays. As suggested by He and Rodriguez (2018), an alert system should be developed that relies on real-time 1-minute data from the NMDB network and from both operational GOES satellites. The >100 MeV and >500 MeV fluxes from both SGPS instruments on each satellite should be used in such an alert system, although not all GOES solar proton enhancements in these energy ranges correspond to GLEs (Thakur et al. 2016). The moving threshold method originally developed by Kuwabara et al. (2006) and implemented successfully in GLE Alert Plus (Souvatzoglou et al. 2014; Mavromichalaki et al. 2018) should be applied to both the NM and the GOES data.

6. Summary

The long series of GLE event observations by the GOES Energetic Particle Sensors (EPS) and High Energy Proton and Alpha Detectors (HEPAD) ended with GLE 72 in September 2017. That GLE was also the first observed by the series of new Solar and Galactic Proton Sensors (SGPS). To date, SGPS units on two GOES satellites have observed the primary components of GLEs 72 and 73. The GOES-based >100 MeV alert issued by NOAA at the onset of GLE 72 preceded the general alert issued by the NMDB-based GLE Alert Plus system, while the situation was reversed for GLE 73. Understanding the causes of such differences requires an investigation into the energy-, angular and propagation differences among GLE events that accounts for different instrument sensitivities and noise levels. Regardless of the causes of these differences, alert systems should be able to reduce alert delays by relying on observations by the NMDB network and the two operational GOES satellites.

Acknowledgements

We acknowledge the NMDB database (www.nmdb.eu) founded under the European Union's FP7 programme (contract no. 213 007), and the PIs of individual neutron monitors. This research was supported in part by NOAA cooperative agreement NA17OAR432010. Support was also provided by the Air Force Office of Sponsored Research (AFOSR) under grant FA9550-20-1-0339. The historical GOES-15

and earlier EPS and HEPAD data are available at <https://www.ncei.noaa.gov/data/goes-space-environment-monitor/>. The reprocessed pre-operational GOES-16 SGPS solar proton data from GLE 72 are available at https://www.ngdc.noaa.gov/stp/space-weather/satellite-data/satellite-systems/goesr/solar_proton_events/sgps_sep2017_event_data/. The operational GOES-16+ SGPS data are available in real time in JSON format at <https://services.swpc.noaa.gov/json/goes/> and retrospectively in daily netCDF files at <https://www.ncei.noaa.gov/products/goes-r-space-environment-in-situ>.

References

- Blake, J. B., and Kolasinski, W. A. (no date). Preliminary evaluation of the NOAA High Energy Proton and Alpha-Particle Detector performance, https://www.ncei.noaa.gov/data/poes-metop-space-environment-monitor/doc/reports/POES_SEM1_HEPAD_Blake-Kolasinski.pdf (last accessed September 19, 2023).
- Blake, J. B. and O'Brien, T. P. 2012. On the relativistic electron event in early April 2010. 39th COSPAR Scientific Assembly, paper D.3.4.
- Bruno A. 2017, Calibration of the GOES 13/15 high-energy proton detectors based on the PAMELA solar energetic particle observations. *Space Weather*, 15, 1191–1202, <https://doi.org/10.1002/2017SW001672>.
- Dichter, B. K., Galica, G. E., McGarity, J. O., Tsui, S., Golightly, M. J., Lopate, C., and Connell, J. J. 2015, Specification design and calibration of the space weather suite of instruments on the NOAA GOES-R program spacecraft. *IEEE Transactions on Nuclear Science*, 62(6), 2776–2783, <https://doi.org/10.1109/TNS.2015.2477997>
- He, J., and Rodriguez, J. V. 2018, Onsets of solar proton events in satellite and ground level observations: A comparison. *Space Weather*, 16, 245–260, <https://doi.org/10.1002/2017SW001743>
- Hu, S., and Semones, E. 2022. Calibration of the GOES 6–16 high-energy proton detectors based on modelling of ground level enhancement energy spectra. *J. Space Weather Space Clim.*, 12, 5, <https://doi.org/10.1051/swsc/2022003>
- Kress, B. T., Rodriguez, J. V., Mazur, J. E., & Engel, M. 2013, Modeling solar proton access to geostationary spacecraft with geomagnetic cutoffs. *Advances in Space Research*, 52, 1939–1948, <https://doi.org/10.1016/j.asr.2013.08.019>
- Kress, B. T., Rodriguez, J. V. and Onsager, T.G. 2020, The GOES-R space environment in situ suite (SEISS): Measurement of energetic particles in geospace. *The GOESR Series*, Elsevier, 243–250, <https://doi.org/10.1016/B978-0-12-814327-8.00020-2>
- Kress, B. T., Rodriguez, J. V., Boudouridis, A., Onsager, T. G., Dichter, B. K., Galica, G. E., and Tsui, S. 2021, Observations from NOAA's newest solar proton sensor. *Space Weather*, 19, e2021SW002750, <https://doi.org/10.1029/2021SW002750>
- Kuwabara, T., Bieber, J. W., Clem, J., Evenson, P., and Pyle, R. 2006, Development of a ground level enhancement alarm system based upon neutron monitors, *Space Weather*, 4, S10001, <https://doi.org/10.1029/2006SW000223>
- Matthiä, D., Berger, T., Mrigakshi, A.I. and Reitz, G. 2013, A ready-to-use galactic cosmic ray model. *Advances in Space Research*, 51(3), 329–338, <https://doi.org/10.1016/j.asr.2012.09.022>
- Mavromichalaki, H., Gerontidou, M., Paschalis, P., Paouris, E., Tezari, A., Sgouropoulos, C., et al. 2018, Real-time detection of the ground level enhancement on 10 September 2017 by A.Ne.Mo.S.: System report. *Space Weather*, 16, 1797–1805, <https://doi.org/10.1029/2018SW001992>
- Mavromichalaki, H., Paschalis, P., Gerontidou, M., Papailiou, M.C., Paouris, E., Tezari, A., Lingri, D., Livada, M., Stassinakis, A.N., Crosby, N. and Dierckxsens, M. 2022, The updated version of the A. Ne. Mo. S. GLE Alert System: The case of the ground-level enhancement GLE73 on 28 October 2021. *Universe*, 8(7), 378, <https://doi.org/10.3390/universe8070378>
- O'Neill, P. M., Golge, S., and Slaba, T. C. 2015, Badhwar-O'Neill 2014 galactic cosmic ray flux model description, NASA TP-2015-218569
- Panmetrics 1980, March 1980 HEPAD tests. SN6 and SN8 preliminary data analysis. PANA-SEM-1. https://www.ngdc.noaa.gov/stp/satellite/goes/doc/goes_nop/PANA-SEM-1_HEPAD_18Jul1980.pdf (last accessed September 14, 2023)
- Raukunen, O., Paassilta, M., Vainio, R., Rodriguez, J.V., Eronen, T., Crosby, N., Dierckxsens, M., Jiggins, P., Heynderickx, D. and Sandberg, I. 2020, Very high energy proton peak flux model. *Journal of Space Weather and Space Climate*, 10, 24, <https://doi.org/10.1051/swsc/2020024>
- Redmon, R. J., Seaton, D. B., Steenburgh, R., He, J., & Rodriguez, J.V. 2018, September 2017's geoeffective space weather and impacts to Caribbean radio communications during hurricane response. *Space Weather*, 16, 1190–1201, <https://doi.org/10.1029/2018SW001897>

- Rinehart, M. C. 1978, Cerenkov counter for spacecraft application. *Nuclear Instruments and Methods*, 154(2), 303-316, [https://doi.org/10.1016/0029-554X\(78\)90414-7](https://doi.org/10.1016/0029-554X(78)90414-7)
- Rodriguez, J. V., Onsager, T. G., & Mazur, J. E. 2010, The east-west effect in solar proton flux measurements in geostationary orbit: A new GOES capability. *Geophysical Research Letters*, 37, L07109, <https://doi.org/10.1029/2010GL042531>
- Rodriguez, J. V., Sandberg, I., Mewaldt, R. A., Daglis, I. A., & Jiggins, P. 2017, Validation of the effect of cross-calibrated GOES solar proton effective energies on derived integral fluxes by comparison with STEREO observations. *Space Weather*, 15, 290-309, <https://doi.org/10.1002/2016SW001533>
- Sandberg, I., Jiggins, P., Heynderickx, D., & Daglis, I. A. 2014, Cross calibration of NOAA GOES solar proton detectors using corrected NASA IMP-8/GME data. *Geophysical Research Letters*, 41, 4435-4441, <https://doi.org/10.1002/2014GL060469>
- Sauer H. H. 1993, GOES observations of energetic protons to E>685 MeV: Description and data comparison. In: *Proceedings of the 23rd International Cosmic Ray Conference*, Leahy DA, Hicks RB, Venkatesan D (Eds.), Vol. 3, Calgary, Canada, 250-253. <https://adsabs.harvard.edu/full/record/seri/ICRC./0023/1993ICRC....3..250S.html> (last accessed September 14, 2023)
- Souvatoglou, G., Papaioannou, A., Mavromichalaki, H., Dimitroulakos, J., & Sarlanis, C. (2014). Optimizing the real-time ground level enhancement alert system based on neutron monitor measurements: Introducing GLE Alert Plus. *Space Weather*, 12, 633-649, <https://doi.org/10.1002/2014SW001102>
- Thakur, N., Gopalswamy, N., Mäkelä, P., Akiyama, S., Yashiro, S. and Xie, H., 2016. Two exceptions in the large SEP events of solar cycles 23 and 24. *Solar Physics*, 291(2), 513-530, <https://doi.org/10.1007/s11207-015-0830-9>

Open Access

This paper is published under the Creative Commons Attribution 4.0 International license (<https://creativecommons.org/licenses/by/4.0/>). Please note that individual, appropriately marked parts of the paper may be excluded from the license mentioned or may be subject to other copyright conditions. If such third party material is not under the Creative Commons license, any copying, editing or public reproduction is only permitted with the prior consent of the respective copyright owner or on the basis of relevant legal authorization regulations.

NMDB and space weather forecasting

Petr Yu. Gololobov , Sergey A. Starodubtsev , Vladislav G. Grigoryev , Anton S. Zverev 

Correspondence

Yu.G. Shafer Institute of Cosmophysical Research and Aeronomy, Siberian Branch of the Russian Academy of Science, Russia, gpeter@ikfia.ysn.ru

Keywords

cosmic rays; neutron monitor; magnetohydrodynamic waves; fluctuations; turbulence spectrum

Abstract

From the creation of NMDB in 2007 and through the growth in the number of stations and the data accumulation, the ShICRA SB RAS group continuously has used its facilities. For the last years we have created a method for short-term forecasting of intense geomagnetic storms with an advance time 1-2 days. The probability of forecasting is around 80%. We have reported about the method in the previous NMDB: virtual symposium on cosmic ray studies with neutron detectors in 2020. The method is based on the global survey method that was developed in Yakutsk in 1960s and uses the world network of neutron monitors as a single multidirectional device. The method is intended to estimate hourly dynamics of cosmic ray anisotropy in free-space. Note that only with the NMDB creation we managed to implement it in real time mode. Now we started work on creating another method for space weather forecasting by measurements of cosmic ray fluctuations. For this purpose, we use 1-min data of NMDB. In the current report we present the first results of our investigation on forecasting of intense geomagnetic storms with $Dst < -50$ nT. The results obtained indicate the possibility of developing and implementing in real time a method for predicting strong geophysical manifestations of space weather on the basis of ground-based cosmic ray measurements.

1. Introduction

The search for effective and timely space weather forecasting is one of the most important tasks of solar-terrestrial relationships. This is due to the fact that its change and subsequent impact on the Earth is potentially negative. First of all, this concerns geomagnetic storms, which can lead to various kinds of negative effects on technological systems as, for example, communication disruption or power grid failures. With the development of modern electronic technology and space exploration, the relevance of solving this issue is as high as ever.

Observations of the state of near-Earth outer space are traditionally carried out by direct measurements of the parameters of the interplanetary medium with various detectors installed on board spacecraft. At the same time, spacecraft, as a rule, are located in relative proximity to the Earth and are able to predict with great accuracy the manifestations of changes in space weather on Earth for about 1 hour.

In this short time, it is practically impossible to take real preventive measures of any kind. On the other hand, this is possible if, for the purposes of space weather forecasting, ground-based CR measurements are used, which, due to their long mean free paths, carry information about the properties of the interplanetary medium on large scales. A similar approach for space weather forecasting has been developed by many researchers (as an example, some of them can be mentioned (Mavromichalaki et al. 2006; Bieber et al. 2004; Kudela et al. 2000)).

Since the early 2000s we are working on developing a space weather forecasting technique based on ground-based measurements of cosmic rays (Grigoryev et al. 2011; Grigoryev et al. 2015). Thus, the creation of a database of neutron monitors installed on the worldwide network of CR stations (NMDB) in 2007, which provides real-time measurement data, allowed us to begin the practical implementation of the space weather forecasting algorithm based on the global survey method developed in Yakutsk at the end of the 1960s. In particular, some of the results of this work were presented at the previous NMDB symposium in 2020 (Gololobov et al. 2020). It was shown that the spatial-angular distribution of CR experiences changes that are typical only for periods before the arrival of geoeffective solar wind disturbances, which can lead to strong geomagnetic storms with $Dst < -50$ nT. In this case, 1 hour CR registration data are used, and the method developed by us makes it possible to predict such storms with 80% probability.

Another approach to space weather forecasting is to use the recording CR intensity fluctuations (Grigoryev et al. 2008). CR fluctuations are understood as non-stationary variations with periods of less than 2-3 hours (with a frequency of more than 10^{-4} Hz), which are observed only during large-scale solar wind disturbances. In connection with this circumstance, the present work is devoted to the development of a method for predicting space weather from ground-based measurements of CR intensity fluctuations.

2. CR intensity fluctuations

As established back in the 1970s, CR fluctuations arise as a result of modulation of high-energy CR fluxes ($E > 1$ GeV) by magnetohydrodynamic (MHD) waves. In this case, the relationship between the anisotropic part of the CR distribution function and Alfvén waves was considered by Owens (1974). In this work, it was shown that the power spectra of fluctuations of CRs $P_{CR}(v, \mu, V)$ and the interplanetary magnetic field (IMF) transverse components $P_{B\perp}(v)$ are related by the relation:

$$\frac{P_{CR}(v, \mu, V)}{j_0^2} = C(v, \mu) \frac{P_{B\perp}(v)}{B_0^2} \delta_{\parallel}^2 \sim 10^{-6} \frac{P_{B\perp}(v)}{B_0^2}$$

where B_0 is the average intensity of the IMF, j_0 is the CR flux, V is the CR velocity in $\text{cm}\cdot\text{s}^{-1}$, $\delta_{\parallel} \sim U/c \sim 10^{-3}$ is the CR flux anisotropy along the magnetic field, U and c are the solar wind and light velocities, $C(v, \mu)$ is a parameter that takes into account the nonlinear interaction near resonant frequencies, μ is the pitch angle of the particle, v is the frequency.

On the other hand, in the work of Berezhko and Starodubtsev (Berezhko & Starodubtsev 1988) it was established that in the presence of fast magnetosonic waves (FMW) in the solar wind, which are capable of modulating the main, isotropic part of the CR distribution function, the spectra of CR fluctuations and the IMF modulus are related by the relation:

$$\frac{P_{CR}(\nu)}{j_0^2} = \left[\frac{(\gamma+2)C_a(C_w + U\sin\varphi)}{3\pi\sqrt{2k_\perp\nu}} \right]^2 \frac{P_B(\nu)}{B_0^2} \sim (10^{-2} \div 1) \frac{P_B(\nu)}{B_0^2}$$

where the wave velocity is $C_w = \sqrt{(C_a^2 + C_s^2)}$, C_a and C_s are the velocities of the Alfvén and magnetosonic waves, k_\perp is the transverse particle diffusion coefficient, φ is the angle between the solar wind direction and the IMF force lines.

In Berezhko & Starodubtsev (1988) it was shown for a number of events that it is relation (2) that is applicable to describe the spectrum of CR fluctuations in the frequency range above 10^{-4} Hz, which is direct evidence of the generation of CR fluctuations precisely by FMS waves. Moreover, evidence was given that this type of MHD waves is generated by flows of suprathermal particles, which are often observed ahead of the fronts of interplanetary shock waves. And since they often cause strong geomagnetic storms, the very registration of CR fluctuations in ground-based detector data can be an effective predictor of these storms.

3. Method

To determine CR intensity fluctuations in the inertial part of the turbulence spectrum, we use 1-minute measurements. It should be noted that the huge array of measurement data from neutron monitors with high temporal resolution, accumulated by the world network of CR stations, is practically not used in any way, except for the analysis of rare cases of GLE events, and lies unclaimed. Here we use barometric-corrected 1-min data from the Yakutsk (62.02°N, 129.72°E, $R_c=1.65$ GV) and Tixie Bay (71.60°N, 128.90°E, $R_c=0.53$ GV) neutron monitors. These stations are part of the Russian national network of CR ground stations, whose data are transmitted to the NMDB server in real time. Both of these stations are located fairly close to the same meridian, and the asymptotic angles of arrival of particles at them coincide fairly well.

Fluctuations in CR and the interplanetary medium were analyzed using the standard Blackman-Tukey method (Blackman & Tukey 1958). In particular, for each station we calculated auto-spectra of CR power $P_{xx}(\nu)$

$$P_{xx}(\nu) = 2\int w(\tau)R_{xx}(\tau)\cos(2\pi\nu\tau)d\tau$$

where $R_{xx}(\tau)$ is an autocovariance function, $w(\tau)$ is Tukey's correlation window, equal to

$$w_\tau(\tau) = \frac{1}{2}(1 + \cos\frac{\pi\tau}{m}), \tau \leq m$$

$$w_\tau(\tau) = 0, \tau > m$$

Also, cross power spectra of CR fluctuations were calculated for both stations. Its values can be written as the sum of the real and imaginary parts of the spectrum components:

$$P_{xy}(\nu) = C_{xy}(\nu) + j \cdot Q_{xy}(\nu),$$

where $C_{xy}(\nu)$ and $Q_{xy}(\nu)$ are cospectrum and quadrature spectrum.

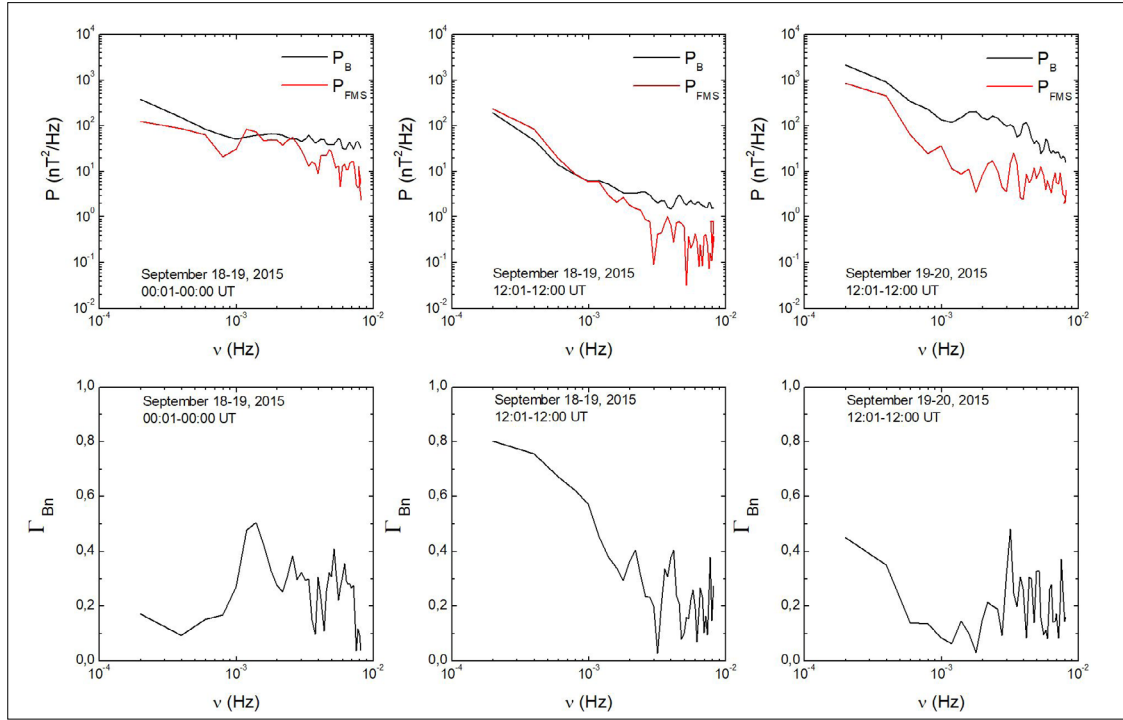


Fig.1: Power spectral densities P_B and P_{FMS} as well as coherence coefficients between Γ_{Bn} for different time periods.

In this case, along with the spectral power of the signal, the coherence coefficient Γ_{xy} was determined, which determines the tightness of the connection between the fluctuations of two quantities. The coherence coefficient is defined as the positive value of the square root of the coherence function:

$$\Gamma_{xy}(\nu) = +\sqrt{\frac{P_{xy}^2}{P_{xx}P_{yy}}}$$

The coherence factor can also be used to determine the type of MHD wave. For example, it is known that Alfvén waves are characterized by high values of the coherence coefficient between the strength of the IMF and the solar wind velocity, FMW – between the IMF strength and the solar wind density, and slow magnetosonic waves – between the solar wind velocity and density.

4. Results obtained

We have analyzed more than 100 cases of observation in the 23rd and 24th cycles of solar activity of strong geomagnetic storms characterized by $Dst < -50$ nT. Here, as an example, we will consider only one event of a strong geomagnetic storm with a Dst -index of about -80 nT that occurred on September 20, 2015. Our results are shown in Figure 1. Its analysis shows that in the time period 2015 September 18 (00:01 UT)-19 (00:00 UT), a clear increase in the coherence coefficient Γ_{Bn} was observed in the frequency range $<10^{-3}$ Hz of the considered spectrum, which indicates the predominant role of FMS waves in the formation of the spectrum of IMF fluctuations.

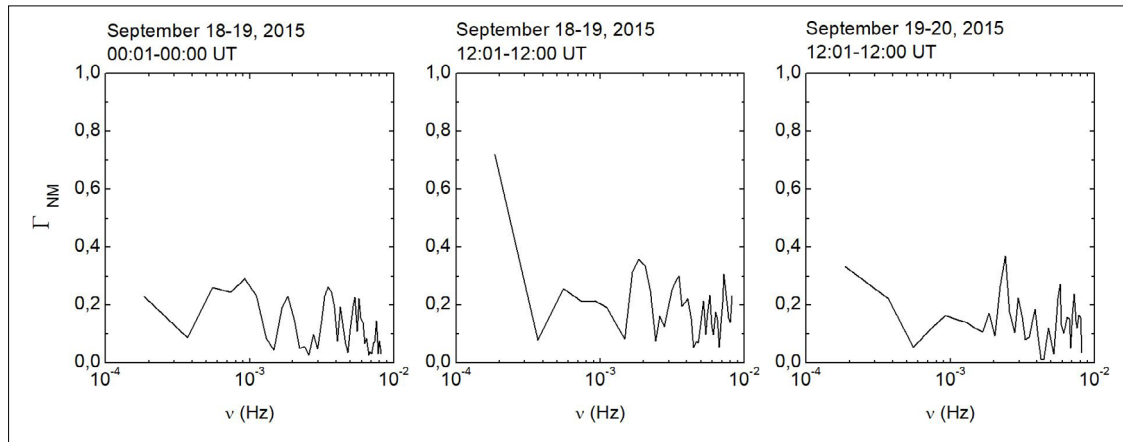


Fig. 2: Coherence coefficient between CR fluctuations according to measurements of neutron monitors Yakutsk and Tixie Bay Γ_{NM} .

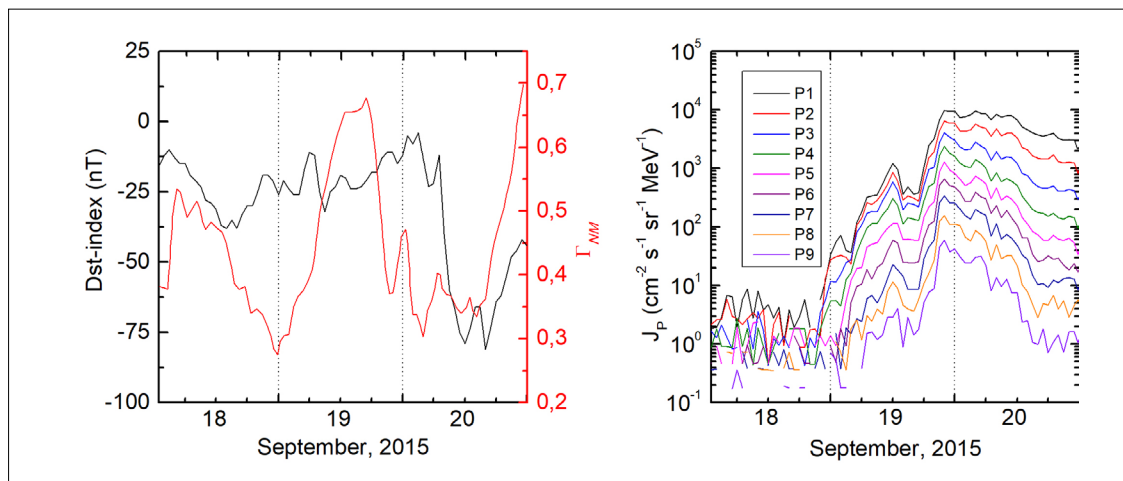


Fig. 3. Left panel: coherence coefficients Γ_{NM} and Dst-index for September 18-20, 2020. Right panel: measurement data for proton fluxes in 9 differential energy channels (P1 = 0.130-0.163 MeV, P2 = 0.163-0.233 MeV, P3 = 0.233-0.325 MeV, P4 = 0.325-0.457 MeV, P5 = 0.457-0.653 MeV, P6 = 0.653-0.884 MeV, P7 = 0.884-1.270 MeV, P8 = 1.270-1.740 MeV, P9 = 1.740-2.510 MeV) by the WIND spacecraft over a period of 18-20 September 2015.

Over the same time periods, we determined the coherence coefficients between fluctuations in the CR intensity recorded at the Yakutsk and Tixie Bay Γ_{NM} stations. The results obtained are presented in Figure 2. It is obvious that Γ_{NM} also shows high values in the low frequency region. Thus, high values of the coherence coefficient between neutron monitor stations can indicate both the presence of FMS waves in the solar wind and an impending geomagnetic storm.

Let us consider the possibility of using the coherence coefficient Γ_{NM} as a geomagnetic disturbance predictor. To do this, we will consider the highest values of the coherence coefficient Γ_{NM} in the entire spectrum range with a step of 1 hour for September 18-20, 2015. The results obtained are shown in Figure 3. As can be seen from Figure 3 (left panel), 18 hours before the storm that began on September 20, 2015, high values of Γ_{NM} were observed. At the same time, the results of measurements of the fluxes of super-thermal protons carried out on the WIND spacecraft (Figure 3, right panel, <https://omniweb.gsfc.nasa>.

[gov/form/sc_merge_min1.html](#)) show that their growth coincides with the observation of high values of Γ_{NM} . Consequently, superthermal protons can be a source of FMS waves.

Thus, taking into account the behavior of Γ_{NM} in other events, it can be assumed that it is an effective predictor of geomagnetic disturbances for medium-term space weather forecasting.

5. Conclusions

1. It is once again confirmed that before the arrival of interplanetary shocks at the Earth's orbit, in the inertial part of the solar wind turbulence spectra in the frequency range $\sim 10^{-4} \div 10^2$ Hz, FMS waves of significant amplitude are often observed.
2. FMS waves are generated by fluxes of super-thermal particles with energy $E_p \sim 1$ MeV in the vicinity of the shock front.
3. The flux of galactic CRs has been subject to modulation by FMS waves, which manifests itself in coherence as the appearance of significant CR fluctuations at frequencies $\sim 10^{-4} \div 10^2$ Hz.
4. The results obtained indicate the possibility of developing and implementing in real time a method for predicting strong geophysical manifestations of space weather based on ground-based measurements of CR intensity.

Acknowledgements

The work was carried out within the framework of the Russian Science Foundation project No. 22-22-20045. The Yakutsk CR stations and Tixie Bay are part of the unique scientific facility of the Russian Federation 'Russian Network of Cosmic Ray Ground Stations' and NMDB.

References

- Mavromichalaki, H., Souvatzoglou, G., Sarlanis, C., Mariatos, G., Plainaki, C., Gerontidou, M., Belov, A., Eroshenko, E., Yanke, V. 2006, Space weather prediction by cosmic rays, *Adv. Sp. Res.* 37, 1141-1147, <https://doi.org/10.1016/j.asr.2005.03.159>
- Bieber, J.W., Evenson, P., Dröge, W., Pyle, R., Ruffolo, D., Rujiwarodom, M., Tooprakai, P., Khumlumlert, T. 2004, Spaceship Earth Observations of the Easter 2001 Solar Particle Event, *Astrophys. J. (Lett.)*, 601, L103-L106, <https://doi.org/10.1086/381801>
- Kudela, K., Storini, M., Hofer, M.Y., Belov, A. 2000, Cosmic rays in relation to space weather, *Sp. Sci. Rev.*, 93, 153-174, https://doi.org/10.1007/978-94-017-1187-6_8
- Grigoryev, V.G., Starodubtsev, S.A. 2011, Definition of Galactic Cosmic Ray Anisotropy in the Real Time. Proc. 32-nd ICRC. Beijing, China, 11, 101-104. <https://galprop.stanford.edu/elibrary/icrc/2011/papers/SH3.3/icrc0359.pdf> (last accessed June 30, 2023)
- Grigoryev, V.G., Starodubtsev, S.A. 2015, Global Survey Method in Real Time and Space Weather Forecasting, *Bull. of the RAS: Physics*, 79, 649-653, <https://doi.org/10.3103/S1062873815050226>
- Gololobov, P.Yu., Starodubtsev, S.A., Grigoryev, V.G., Zverev, A.S. 2020, NMDB database and global survey method, Cosmic ray studies with neutron monitors, 1, 137-141, <https://doi.org/10.38072/2748-3150/p17>
- Grigoryev, A.V., Starodubtsev, S.A., Grigoryev, V.G., Usoskin, I.G., Mursula, K. 2008, Fluctuations of cosmic rays and IMF in the vicinity of interplanetary shocks, *Adv. Space Res.*, 41, 955-961, <https://doi.org/10.1016/j.asr.2007.04.044>
- Owens, A.J. 1974, Cosmic-ray scintillations .2. General Theory of Interplanetary Scintillations, *J. Geophys. Res.*, 79, 895-906, <https://doi.org/10.1029/JA079i007p00895>










Berezhko, E.G., Starodubtsev, S.A. 1988, Nature of the dynamics of the cosmic-ray fluctuation spectrum. *Izvestia AN SSSR, Ser. Fiz.*, 52, 2361-2363. (In Russian)

Blackman, R.B., Tukey, J.W. 1958, *The measurement of power spectra from the point of view of communications engineering*. New York, Dover Publications

Open Access

This paper is published under the Creative Commons Attribution 4.0 International license (<https://creativecommons.org/licenses/by/4.0/>). Please note that individual, appropriately marked parts of the paper may be excluded from the license mentioned or may be subject to other copyright conditions. If such third party material is not under the Creative Commons license, any copying, editing or public reproduction is only permitted with the prior consent of the respective copyright owner or on the basis of relevant legal authorization regulations.

Behavior of galactic cosmic rays density and vector anisotropy before and during high-energy magnetospheric electron flux enhancements

Olga Kryakunova ¹, Anatoly Belov ², Botakoz Seifullina ¹, Maria Abunina ², Artem Abunin ², Irina Tsepakina ¹, Nataly Shlyk ², Serik Nurakynov ¹, Nikolay Nikolayevskiy ¹

Correspondence

1 Institute of Ionosphere, Almaty, Kazakhstan, krolganik@yandex.ru

2 IZMIRAN – Pushkov Institute of Terrestrial Magnetism, Ionosphere and Radio Wave Propagation, Moscow, Russia

Keywords

magnetospheric electron; space weather; neutron monitor; cosmic rays

Abstract

Changes in the intensity of galactic cosmic rays on Earth and beyond the boundary of the magnetosphere occur earlier than an increase in the flux of high-energy magnetospheric electrons with energy >2 MeV in the geostationary orbit, so the behavior of galactic cosmic rays before and during electron flux enhancements can provide valuable information about the processes occurring in near-Earth space at this time. The density and vector anisotropy of galactic cosmic rays for 453 events of high-energy magnetospheric electron flux enhancements over the period 1996-2020 were calculated by the Global Survey Method (GSM). Some examples of these events, which are characteristic of different classes of solar sources, are considered. The behavior of the density and vector anisotropy of galactic cosmic rays before and during electron flux enhancements in events connected with the arrival to Earth of high-speed streams from coronal holes, coronal mass ejections associated with solar flares or disappeared solar filaments is revealed.

1. Introduction

The behavior of high-energy electrons in the Earth's magnetosphere is one of the most actual problems in the physics of magnetosphere and space weather. First of all this is due to the fact that large enhancements in relativistic electron fluxes lead to failures in the operation of spacecraft and, in some cases, led to the failure of satellites (Baker 2001; Baker et al. 2001; Belov et al. 2004; Pilipenko et al. 2006; Baker et al. 2018). The anomalies were most often associated with false commands caused by internal electrostatic discharge. Most of the anomalies were due to the accumulation of charge inside the electronic components, caused by the impact of high energy electrons (>2 MeV) at a time when the fluence of such electrons exceeded a dangerous level for two days (Wrenn, Rodgers & Ryden 2002).

Cosmic rays (CRs) carry extremely important information about the state the interplanetary medium and near-Earth space, because measurements of galactic CRs (GCRs) on the Earth's surface by the worldwide network of neutron monitors are extremely accurate and allow one to calculate the behavior of their density and anisotropy beyond the magnetosphere boundary using the Global Survey Method (GSM) (Belov et al. 2018). Forbush effects (FEs) – changes in the density and anisotropy of GCRs caused by large-scale solar wind (SW) disturbances – are part of complex processes in the interplanetary and near-Earth medium. However, changes in the CRs density and anisotropy occur earlier than enhancements in high-energy electron fluxes, so information on the behavior of GCRs can be used to predict electron flux enhancements and determine their solar sources.

2. Data used

As main characteristics of magnetospheric electron fluxes in geostationary orbits the following were chosen: the particle flux directly measured on the GOES satellites (the number of particles·cm⁻²·sr⁻¹·s⁻¹) and the diurnal fluence (total flux per day) of relativistic magnetospheric electrons with energies > 2 MeV. Information about high-energy electrons, characteristics of solar and interplanetary activity is collected in the Solar and Geomagnetic Activity (SGA) database, created and maintained at IZMIRAN. This database contains information on diurnal electron fluences obtained onboard the GOES satellites (<https://www.ngdc.noaa.gov/stp/satellite/goes/index.html>) over a 35-year period (1987-2021), information about SW parameters are taken from the OMNI database (<https://omniweb.gsfc.nasa.gov/>), information about geomagnetic activity – Kp- and Ap-indices (<https://kp.gfz-potsdam.de/en/data#c134>, Matzka et al. 2021), Dst-index (<http://wdc.kugi.kyoto-u.ac.jp>). The SGA database is updated daily.

Electron flux enhancement catalog is given by Kryakunova et al. (2022).

3. Behavior of galactic cosmic rays density and vector anisotropy before and during magnetospheric electron flux enhancements

GCRs do not affect the generation of magnetospheric electrons, nor do they affect the measurements of high-energy (> 2 MeV) electrons on the GOES satellites themselves. However, changes in the density and anisotropy of GCRs are part of a complex process of changing near-Earth outer space state, which occurs due to the arrival of various types of disturbed SW from active processes on the Sun (high-speed streams (HSS) from coronal holes (CH), coronal mass ejections (CME) associated with solar flares, and disappearances of solar filaments).

To obtain a homogeneous continuous series of CRs density variations (the isotropic part of the intensity) and vector anisotropy, a database of Forbush effects and interplanetary disturbances (FEID) was created. It includes different effects in GCRs due to large-scale SW disturbances. The capabilities of the database make it possible to carry out a correlation analysis of various parameters of the interplanetary medium (SW, interplanetary magnetic field) with the CRs parameters and to study their relationships.

To calculate the GCRs flux density and vector anisotropy the GSM is used (Belov et al. 2018), which allows one to take into account the influence of the magnetosphere and atmosphere and make calculations ac-

ording to neutron monitors of the world network of ground-based CRs stations. The GSM is a technique that combines simultaneous ground-based observations of GCRs at different points and makes it possible to obtain the main characteristics of CRs variations outside the Earth's atmosphere and magnetosphere.

The global network of CRs stations consists of individual detectors (primarily neutron monitors) located at different points on the globe and collecting particles in certain cones of asymptotic directions (reception cones). In the GSM, the entire network is used as a single multichannel device, where each channel-station provides information in a certain cone of asymptotic directions, and all channels completely cover the celestial sphere. The multi-channel nature of such a device ensures the reliability and continuity of measurements. In comparison with individual CRs stations, the statistical accuracy of the network increases markedly, and the influence of hardware effects is significantly reduced. For example, a separate neutron supermonitor provides a statistical accuracy of 0.1-0.2%/h, while the entire network of stations provides accuracy of ~0.01%/h. The GSM makes it possible to determine the density (the isotropic part of the intensity) and the anisotropy of GCRs for each hour outside the magnetosphere.

The GCRs density and vector anisotropy for 453 events of high-energy magnetospheric electron flux enhancements over the period 1996-2020 were calculated by the GSM. We considered the threshold of electron enhancements to be the day when the daily fluence exceeds 10^8 electrons·cm⁻²·sr⁻¹·day⁻¹. The choice of the period from 1996 is due to the fact that only from this time onwards can solar sources of disturbances in CRs flux be sufficiently confidently identified according to the data of Solar and Heliospheric Observatory (SOHO), launched by the European Space Agency and NASA in the end of 1995.

Let us consider some examples of these 453 events that are typical for different classes of solar sources. We divided all the events of enhancements in the flux of high-energy magnetospheric electrons into different groups according to the types of solar sources caused the SW disturbances associated with enhancements in electron flux and FEs in CRs.

In the first, most numerous group of events, we have collected events related to the disturbances of the near-Earth space caused by the arrival of HSS from CHs.

The enhancement event on March 19-26, 2006 (see Figure 1) is characterized by a high dangerous level (> 5000 particles·cm⁻²·sr⁻¹·s⁻¹) of electron flux with an energy > 2 MeV. The solar source of the enhancement was an HSS with a speed of 714 km/s from a transequatorial CH, which was in the geoeffective position for 2 days (March 16-17) and then the corresponding HSS impacted the Earth for 5 days (March 18-22). The event is characterized by a smooth behavior of the vector anisotropy (A_{xy}) and a small FE with amplitude of 1%; five three-hour periods of a small magnetic storm and two periods of a moderate magnetic storm were recorded in the geomagnetic field. In Fig. 1b and below, purple lines connect the same time points on the vector anisotropy (A_{xy}) and CR density (A_0) curves.

Now let us consider a group of electron flux enhancement events that solar sources were both HSS from CHs and CMEs associated with disappearance of solar filaments.

The event of a dangerous enhancement (> 500 particles·cm⁻²·sr⁻¹·s⁻¹) in magnetospheric electron flux on August 29 - September 2, 2000 is accompanied by an FE of more than 1% and disturbance of the geomagnetic field to the level of a moderate magnetic storm (Figure 2). The vector anisotropy A_{xy} has a more curved appearance with the rotation of the vectors due to the propagation of GCRs through the CME associated with the disappearance of the solar filament (DSF).

The event of a dangerous enhancement in magnetospheric electron flux on May 5-15, 1998 was associated with the influence on the near-Earth medium of a CME associated with a solar flare that occurred

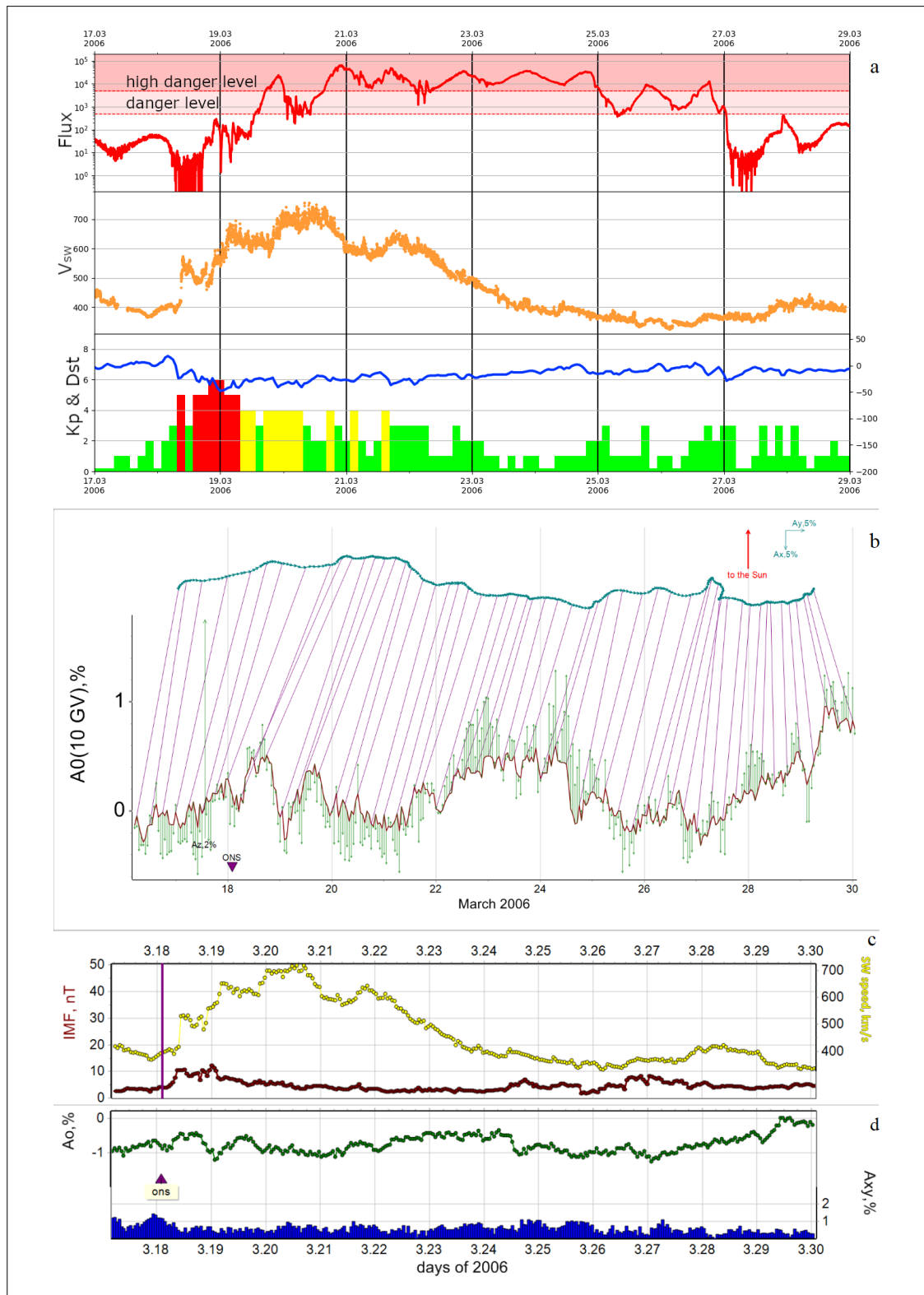


Fig. 1: An enhancement in magnetospheric electron flux and the state of the interplanetary and near-Earth medium on March 17-29, 2006. a) Magnetospheric electron flux, SW speed, Kp and Dst indices of geomagnetic activity; b) A_x and density of galactic CR; c) SW speed and interplanetary magnetic field induction; d) density A_0 of galactic CR and A_{xy} .

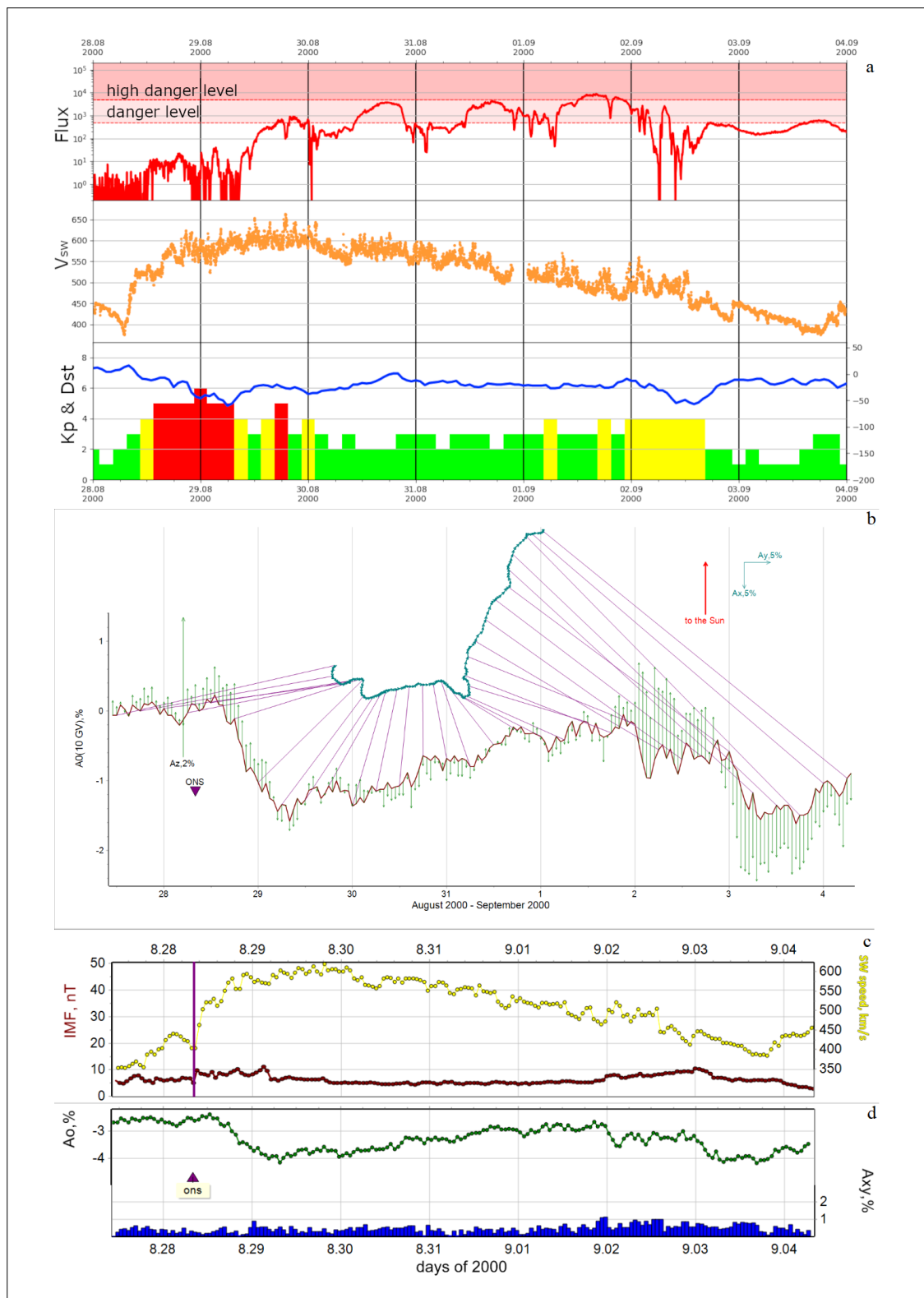


Fig. 2: An enhancement in magnetospheric electron flux and the state of the interplanetary and near-Earth medium on August 27 – September 2, 2020. a) Magnetospheric electron flux, SW speed, Kp and Dst indices of geomagnetic activity; b) A_{xy} and density of GCRs; c) SW speed and interplanetary magnetic field induction; d) density A_0 of GCRs and A_{xy} .

on April 29, 1998 at 16:06 UT. This event was accompanied by an FE of about 6% and a disturbance of the geomagnetic situation to the level of an exceptionally large magnetic storm (Figure 3). The vector anisotropy A_{xy} has a very complex curved appearance. The average SW speed in this event was 772 km/s. It should be noted that after an exceptionally large magnetic storm, the electron flux rose only to a high dangerous level ($> 5000 \text{ particles}\cdot\text{cm}^{-2}\cdot\text{sr}^{-1}\cdot\text{s}^{-1}$), practically not exceeding it.

4. Conclusion

From the analysis of 453 events of high-energy magnetospheric electron flux enhancements, in which the values of the GCRs density and anisotropy beyond the magnetosphere boundary are calculated, it can be concluded that the vast majority of electron flux enhancements are associated with the arrival of HSS from CHs to the Earth. In these events, the flux of high-energy electrons exceeds the high dangerous level most often. In this case, FEs of small magnitude (about 1%) and a smooth behavior of the vector anisotropy are observed. In events associated with other additional solar sources (two types of CMEs), an important role in increasing the electron flux is still played by HSS from CHs. In such events, a more complex, curved behavior of the GCRs vector anisotropy, large magnitudes of FEs in the CRs density, and an enhancement in the values of the equatorial component of the CRs anisotropy are observed. Single events of enhancements in high-energy electron flux caused by CMEs & solar flares are observed, however, despite large effects in the geomagnetic field, such CMEs do not cause enhancements to high dangerous levels in the electron flux.

Acknowledgements

This research is funded by the Science Committee of the Ministry of Education and Science of the Republic of Kazakhstan (Grant No. AP19678078, BR20280979) and by the Aerospace Committee of the Ministry of Digital Development, Innovations and Aerospace Industry of the Republic of Kazakhstan (BR11265408).

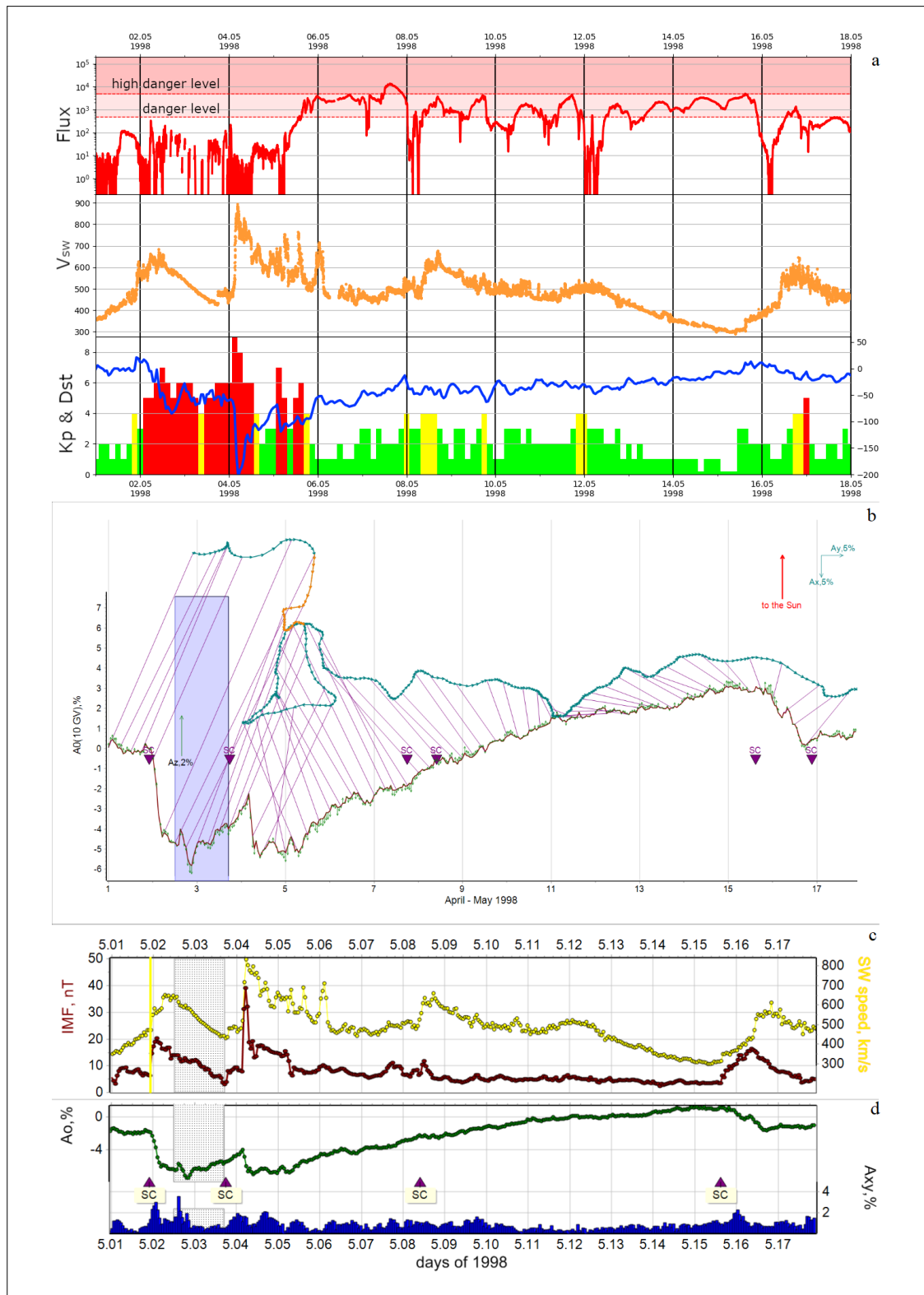


Fig. 3: An enhancement in magnetospheric electron flux and the state of the interplanetary and near-Earth medium on May 1-17, 1998. a) Magnetospheric electron flux, SW speed, Kp and Dst indices of geomagnetic activity; b) A_y and density of GCRs; c) SW speed and interplanetary magnetic field induction; d) density A_0 of GCRs and A_{xy} .

References

- Baker D.N., 2001, Satellite Anomalies due to Space Storms in Daglis I.A. ed., *Space Storms and Space Weather Hazards*. Springer Publ., New York, 285-311, https://doi.org/10.1007/978-94-010-0983-6_11
- Baker D.N., Kanekal S.G., Blake J.B., Pulkkinen T.I. 2001, The global efficiency of relativistic electron production in the Earth's magnetosphere. *Journal of Geophysical Research Atmospheres* 106(A9), 19169-19178, <https://doi.org/10.1029/2000JA003023>
- Baker D.N., Erickson P.J., Fennell J.F., Foster J.C., Jaynes A.N., Verronen P.T. 2018, Space Weather Effects in the Earth's Radiation Belts. *Space Science Reviews* 214, 17, <https://doi.org/10.1007/s11214-017-0452-7>
- Belov A., Dorman L., Lucci N., Kryakunova O., Ptitsyna N., 2004, in Daglis I.A. ed., *Effects of Space Weather on Technology Infrastructure*. The relation of high- and low-orbit satellite anomalies to different geophysical parameters, Springer Publ. 176, 147-163, https://doi.org/10.1007/1-4020-2754-0_8
- Pilipenko V., Yagova N., Romanova N., Allen J., 2006, Statistical relationships between satellite anomalies at geostationary orbit and high-energy particles. *Advances in Space Research* 37, 1192-1205, <https://doi.org/10.1016/j.asr.2005.03.152>
- Belov A., Eroshenko E., Yanke V. et al. 2018, The Global Survey Method applied to Ground Level Cosmic Ray Measurements. *Solar Physics* 293, 68-96, <https://doi.org/10.1007/s11207-018-1277-6>
- Kryakunova O.N., Belov A.V., Yakovets A.F. et al. 2022, Average characteristics of high-energy magnetospheric electron flux enhancements and the parameters of near-Earth and interplanetary medium in 1987-2021. *Monthly Notices of the Royal Astronomical Society* 516, 4782-4791, <https://doi.org/10.1093/mnras/stac2382>
- Wrenn G.L., Rodgers D.J., Ryden K.A. 2002, A solar cycle of spacecraft anomalies due to internal charging *Ann. Geophys.* 20, 953-956, <https://doi.org/10.5194/angeo-20-953-2002>

Open Access

This paper is published under the Creative Commons Attribution 4.0 International license (<https://creativecommons.org/licenses/by/4.0/>). Please note that individual, appropriately marked parts of the paper may be excluded from the license mentioned or may be subject to other copyright conditions. If such third party material is not under the Creative Commons license, any copying, editing or public reproduction is only permitted with the prior consent of the respective copyright owner or on the basis of relevant legal authorization regulations.

The updated GLE Alert system by ANEMOS

Helen Mavromichalaki ^{ID 1}, Pavlos Paschalis ^{ID 1}, Maria Gerontidou ^{ID 1}, Anastasia Tezari ^{ID 1},
Maria-Christina Papailiou ^{ID 1,2}, Dimitra Lingri ^{ID 1}, Maria Livada ^{ID 1}, Argyris Stassinakis ^{ID 1},
Norma Crosby³, Mark Dierckxsens ^{ID 3}

Correspondence

- 1 Nuclear and Particle Physics Department, Faculty of Physics, National and Kapodistrian University of Athens, Greece, emavromi@phys.uoa.gr
 - 2 Eugenides Foundation, Athens, Greece
 - 3 Royal Belgian Institute for Space Aeronomy, Brussels, Belgium, Norma.Crosby@aeronomie.be,
Mark.Dierckxsens@aeronomie.be
-

Keywords

ground level enhancements (GLEs); solar cosmic rays; neutron monitors; GLE alert

Abstract

Ground level enhancements (GLEs) of cosmic radiation are the result of solar energetic particles (SEPs) arriving at the Earth, potentially causing major damage to technological systems, but also posing a threat for human health. Intense SEPs, such as the GLE events, can influence the radiation exposure of aircrafts and consequently increase the radiation dose on human crew, but also have an impact on satellites and affect the design of space missions, i.e. electronic devices onboard the satellite platforms etc. Therefore, predicting such events is challenging and one of the most important aspects of space weather research. In this work the updated GLE Alert++ System of the Athens Neutron Monitor Station (A.Ne.Mo.S.) implemented by the Athens Cosmic Ray Group of the National and Kapodistrian University of Athens (NKUA) is being presented. Moreover, the innovations of the updated system in relation to the previous version of the GLE Alert Plus are introduced. Finally, the most recent and the first of solar cycle 25 GLE event, GLE73, is discussed. This event was registered by several stations of the worldwide ground-based neutron monitor network. An accurate alert was issued successfully by the ESA R-ESC federated product GLE Alert Plus, as well as by the updated GLE Alert++ System of the NKUA/A.Ne.Mo.S. It should be emphasized that GLE Alert++ signal by NKUA/A.Ne.Mo.S. was issued 45 minutes earlier than the one issued by GOES satellites.

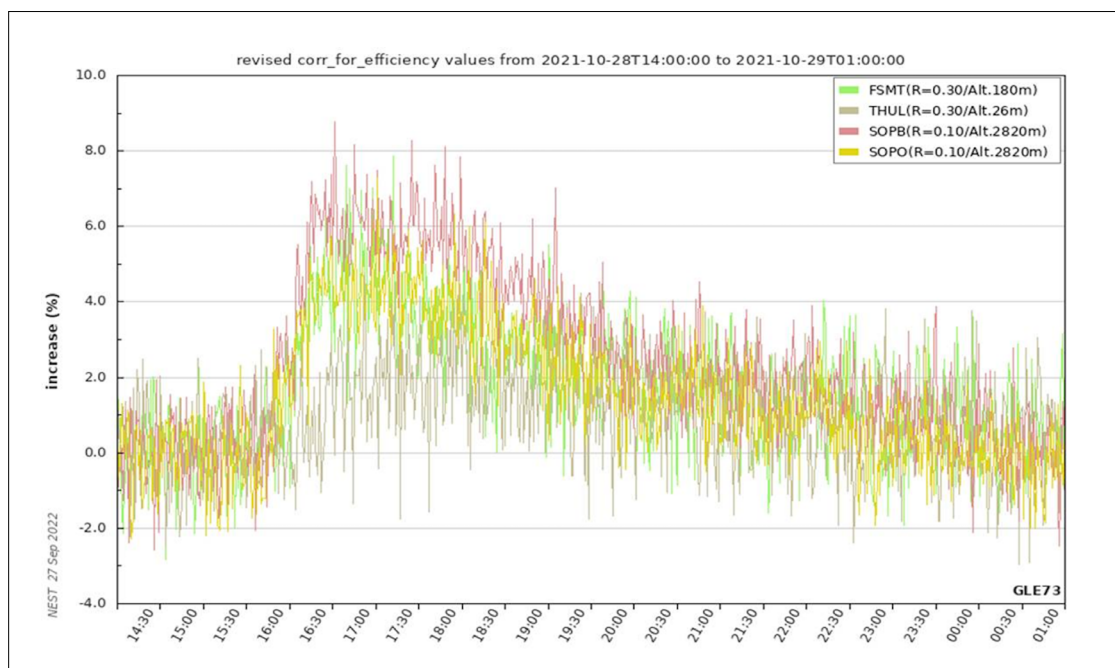


Fig. 1: The GLE73 as registered by a few neutron monitors (https://www.nmdb.eu/nest/draw_graph.php).

1. Introduction

A GLE of cosmic rays is the result of solar cosmic rays (with proton energies above 500 MeV) arriving at the Earth. It is observed as an abrupt and sharp increase in the counting rate of ground-based cosmic ray detectors and lasts several hours (Mavromichalaki et al. 2007; Anashin et al. 2009; Souvatzoglou et al. 2014) (Fig. 1).

In other words, GLEs are recorded when specific solar processes accelerate charged particles to energies high enough to be detectable by neutron monitors (NMs) or other particle detectors on the Earth (<http://www.nmdb.eu>; http://www.wdcb.ru/stp/cosmic_rays/gle.html; <https://gle.oulu.fi/#/>). Since these particles can possibly create a major problem (Mariatos et al. 2005) in microelectronic systems for satellites, spacecraft and airplanes, and biological effects on astronauts and air crews (Dorman et al. 2004; Souvatzoglou et al. 2009; 2014; Kuwabara et al. 2006), developing real-time warning systems using the neutron monitor network (<http://www.nmdb.eu>) is really important and useful.

2. Evolution of the GLE Alert system

An algorithm capable of predicting the onset of a GLE and providing an alert is created by the Athens Cosmic Ray Group. The first real-time GLE Alert system was installed and operated by Athens Neutron Monitor Data Processing (ANMODAP) Center of the Physics Department of NKUA in 2003 and was described in Mariatos et al. (2005) and Souvatzoglou et al. (2009). A few years later, in 2010, the GLE Alert system was installed and operated in the Neutron Monitor Database (NMDB) (Mavromichalaki et al. 2010).

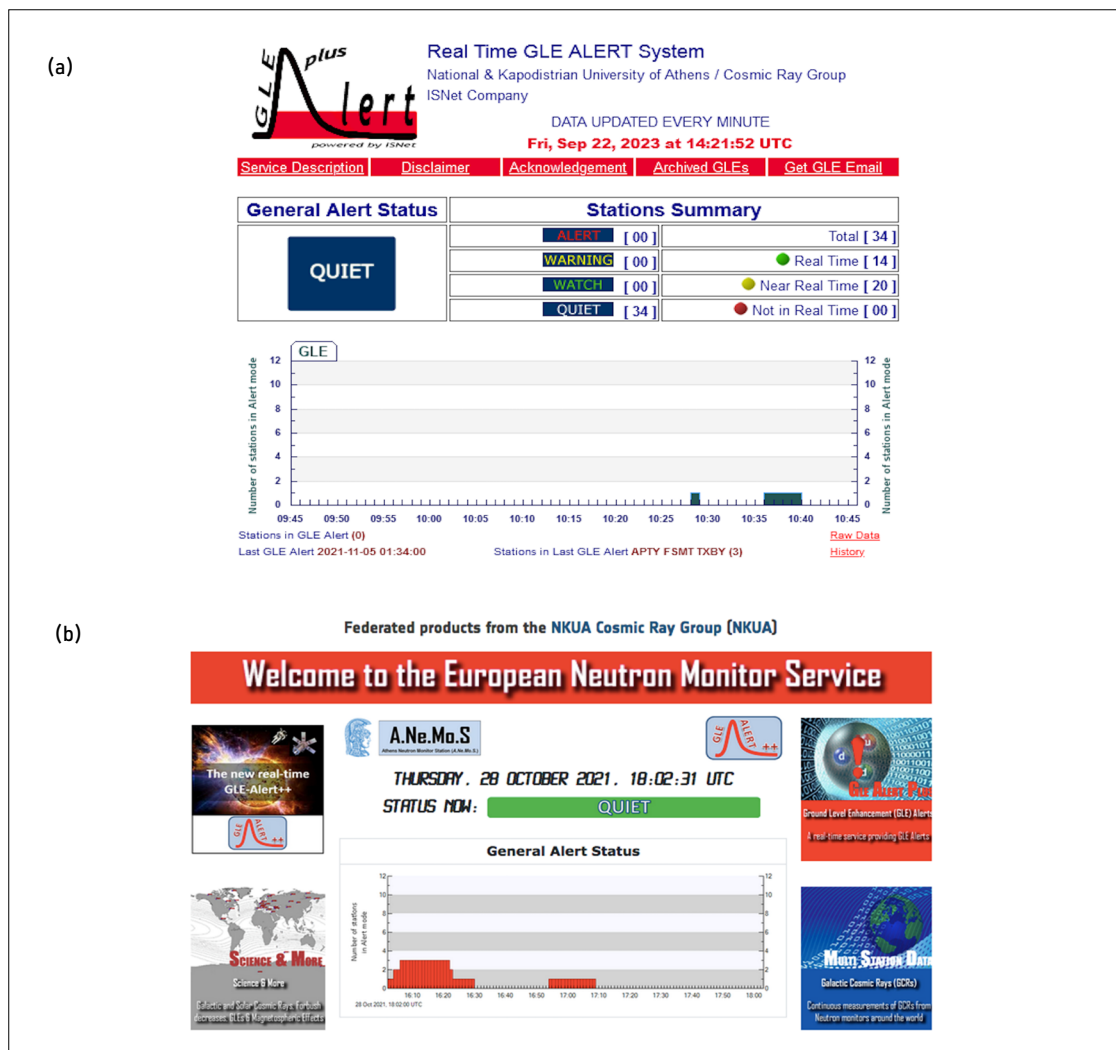


Fig. 2: (a) The previous version: GLE Alert Plus System and (b) the current version: GLE Alert++ System (<https://swe.ssa.esa.int/anemos-federated>).

GLE Alert Plus is an improved version of the previous alert system in the frame of European Space Agency (ESA) SSA P2-VIII project, operating from 2013 until now (Fig. 2). GLE Alert Plus system is developed by ISNet, uses neutron monitor data from NMDB database and is supported by NKUA and ESA. The improvements of this software are described in Souvatzoglou et al. (2014).

In 2021, an updated version of the GLE Alert Plus, GLE ALERT ++, was installed by the Athens Cosmic Ray Group and evaluated by ESA and is now operated at ESA Website (Fig. 2b). This system produces every minute a General Alert Status and station graph and status for every station participating in the network (<https://swe.ssa.esa.int/anemos-federated>).

The main core of the GLE Alert System is presented in Figure 3. As it is shown, each neutron monitor is treated separately by the GLE Alert and the general alert status is issued according to the number of stations in alert mode. However, a more extensive description of the physical concept as well as the applied algorithm are included in Mavromichalaki et al. (2010), Souvatzoglou et al. (2014), Mavromichalaki et al. (2018) and Mavromichalaki et al. (2022).

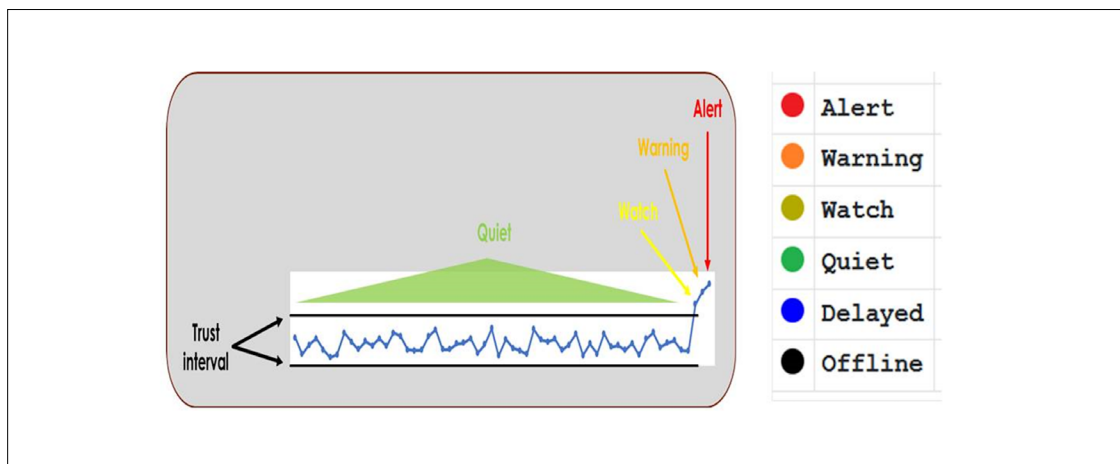


Fig. 3: GLE Alert treats each NM station separately and defines the station status. Depending on the number of stations in alert mode, GLE Alert defines the corresponding general alert status.

3. The GLE Alert ++ system

In the following a small description of the innovations in this upgraded version of the GLE Alert is presented. They refer not only to functionality but also to the web interface. Regarding functionality, the novelties are:

- Lightweight architecture that makes the process of raising an Alert faster, while at the same time the data are available in real- or near real- time.
- MySQL databases to store the one-minute measurements of the stations and the webpage content.
- SQL databases to store the GLE Alert algorithm data in daily base preventing the generation of huge databases.
- Full parameterization regarding the interface.
- Execution of the algorithm for all NM stations in only 3-4 seconds.
- Keeping history data to reproduce any past condition.

Regarding the web interface, the novelties are:

- A more user-friendly interface
- The alert status extended to a 2-hour timeslot
- Providing graphs for each NM station
- Making available raw and history data
- Providing data in CSV format

Moreover, regarding the web interface the 4 levels of real-time status have remained as in the previous version (Quiet: number of stations in ›Station Alert‹ mode = 0; Watch: number of stations in ›Station Alert‹ mode = 1; Warning: number of stations in ›Station Alert‹ mode = 2; Alert: number of stations in ›Station Alert‹ mode > 3) as is shown in [Figure 4](#).

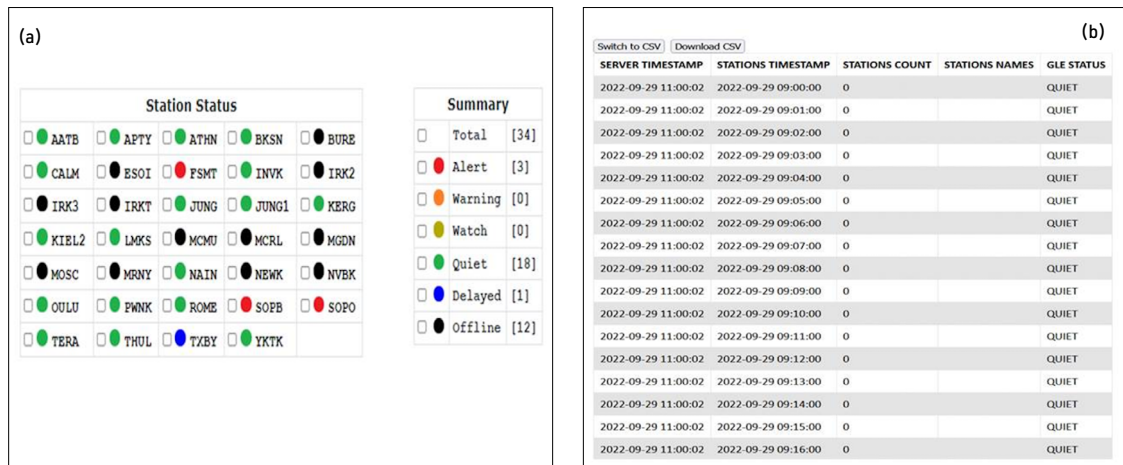


Fig. 4: (a) The station status of the NMs used in the GLE Alert ++ interface and (b) the corresponding history data.

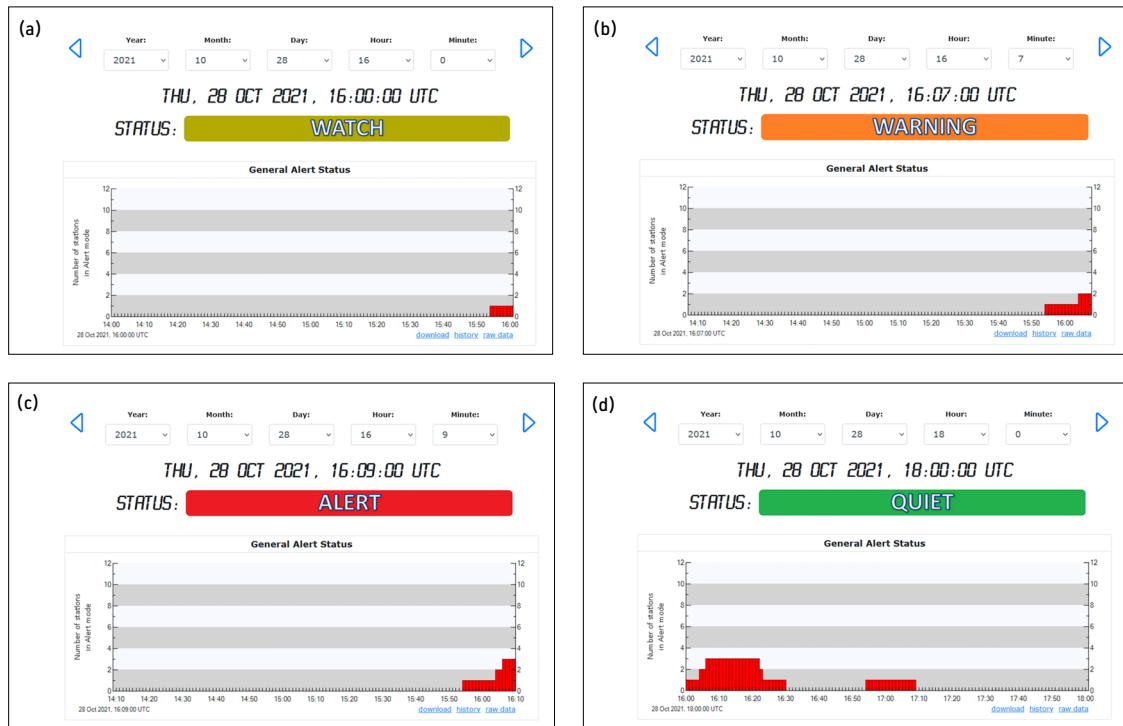


Fig. 5: The evolution of the GLE73 by the GLE Alert ++ system.

4. The first GLE Alert notification

GLE73 was detected on 28 October 2021 and was associated with the active region AR12887 on the central part of the solar disk, which produced an X1.0 solar flare. The event was registered by several stations of the worldwide ground-based neutron monitor network. The three stations that triggered the alert were Fort Smith (FSMT) Canada, South Pole Bares (SOPB), Antarctica and South Pole (SOPO) Antarctica. An accurate alert was issued successfully by the ESA R-ESC federated product GLE Alert Plus, as well as the updated GLE Alert++ System of the A.Ne.Mo.S. An overview of GLE73, the first of

solar cycle 25, as well as a post-event analysis is presented in Papaioannou et al. (2022) and in Mavromichalaki et al. (2022).

The GLE Alert ++ application produced an email notification that was sent to all subscribed users on 28 October 2021 at 16:09 UT. The GLE Alert ++ signal by NKUA/A.Ne.Mo.S. was issued 45 min earlier than the one issued by GOES. In Figure 5 the evolution of GLE73 by the GLE Alert ++ point of view is being presented.

5. Conclusions

Summarizing it can be claimed that the neutron monitors continue to be the state of the art instrumentation and a unique asset for Space Weather predictions and applications. Both of the GLE Alert Plus, as well as the updated GLE Alert ++, detected recently the first GLE of solar cycle 25, i.e. GLE73 on 28 October 2021, in real time, sending notification emails to the registered users. It should be highlighted that forecasting of the upcoming energetic particles by GLE Alert ++ precedes the alerts based on satellites' data. As it was also mentioned above, many novelties of the upgraded GLE ALERT ++ concerning the functionality as well as the web interface will help to its continuous and uninterrupted operation, providing accurate and timely signals.

Furthermore, it is underlined that the GLE Alert ++ service needs timely and reliable real time data. For this reason the need for recording assessment and a real time assessment index of data provided by the neutron monitor community is crucial for the cosmic ray studies. The assessment of the real-time availability of the NM data has to be repeated periodically, in order to update the set of the NMs used in GLE Alert ++. It is necessary, as operating issues of the stations could be raised. The next step is to incorporate to this updated system satellite data in order to avoid possible false alerts.

Acknowledgements

We acknowledge the NMDB database www.nmdb.eu, founded under the European Union's FP7 programme (contract no. 213007) for providing data. This work was supported by ESA SSA SWE Space Radiation Expert Service Centre activities (ESA contract number 4000113187/15/D/MRP). The European Neutron Monitor Services research was funded by the ESA SSA SN IV-3 Tender: RFQ/3-13556/12/D/MRP. A.Ne.Mo.S was supported by the Special Research Account of Athens University (70/4/5803).

References







- Anashin, Vasily & Belov, A. & Eroshenko, E. & Krjakunova, O. & Mavromichalaki, H. & Ishutin, I. & Sarlanis, Christos & Souvatsoglou, G. & Vashenyuk, Eduard & Yanke, Victor. 2009, 'The ALERT signal of ground level enhancements of solar cosmic rays: Physics basis, the ways of realization and development', 31st International Cosmic Ray Conference, ICRC Rome.
- Dorman, L.I., Pustilnik, L., Sternlieb, A., Zukerman, I., Belov, A., Eroshenko, E., Yanke, V., Mavromichalaki, H., Sarlanis, C., Souvatzoglou, G., Tatsis, S., Iucci, N., Villaresi, G., Fedorov, Yu., Shakhov, B. 2004, 'Monitoring and forecasting of great solar proton events using the neutron monitor network in real-time', IEEE, 32, 1478-1488, <https://doi.org/10.1109/TPS.2004.831738>

- Kuwabara, T., Bieber, J., Clem, J., Evenson, P., Pyle, R., Munakata, K., Yasue, S., Kato, C., Akahane, S., Koyama, M., Fujii, Z., Duldig, M. 2006, 'Real-time cosmic ray monitoring system for space weather', *Space Weather*, 4, S08001, <https://doi.org/10.1029/2005SW000204>
- Mariatos, G., H. Mavromichalaki, C. Sarlanis, G. Souvatzoglou, A. Belov, E. Eroshenko, and V. Yanke. 2005, 'Alert system for ground level cosmic-ray enhancements prediction at the Athens neutron monitor network in real-time', *International Journal of Modern Physics A*, 20, 6711-6713, <https://doi.org/10.1142/S0217751X05029897>
- Mavromichalaki, H., Paouris, E., Karalidi, I. 2007, 'Cosmic-Ray Modulation: An Empirical Relation with Solar and Heliospheric Parameters', *Solar Physics*, 245, 369-390, <https://doi.org/10.1007/s11207-007-9043-1>
- Mavromichalaki, H., Souvatzoglou, G., Sarlanis, C., Mariatos, G., Papaioannou, A., Belov, A., Eroshenko, E., Yanke, V. for the NMDB team. 2010, 'Implementation of the ground level enhancement alert software at NMDB database', *New Astronomy*, 15, 744-748, <https://doi.org/10.1016/j.newast.2010.05.009>
- Mavromichalaki, H.; Gerontidou, M.; Paschalis, P.; Paouris, E.; Tezari, A.; Sgouropoulos, C.; Crosby, N.; Dierckxsens, M. 2018, 'Real-Time Detection of the Ground Level Enhancement on 10 September 2017 by A.Ne.Mo.S.: System Report', *Space Weather*, 16, 1797-1805, <https://doi.org/10.1029/2018SW001992>
- Mavromichalaki, H., Paschalis, P., Gerontidou, M., Papailiou, M.-C., Paouris, E., Tezari, A., Lingri, D., Livada, M., Stassinakis, A.N., Crosby, N., Dierckxsens, M. 2022, 'The Updated Version of the A.Ne.Mo.S. GLE Alert System: The Case of the Ground-Level Enhancement GLE73 on 28 October 2021', *Universe*, 8, 378, <https://doi.org/10.3390/universe8070378>
- Papaioannou, A., Kouloumvakos, A., Mishev, A., Vainio, R., Usoskin, I., Herbst, K., Rouillard, A. P., Anastasiadis, A., Gieseler, J., Wimmer-Schweingruber, R., Kühl, P. 2022, 'The first ground-level enhancement of solar cycle 25 on 28 October 2021', *A&A*, 660, L5, <https://doi.org/10.1051/0004-6361/202142855>
- Souvatzoglou, G., Mavromichalaki, H., Sarlanis, C., Mariatos, G., Belov, A., Eroshenko, E., Yanke, V. 2009, 'Real-time GLE alert in the ANMODAP Center for December 13, 2006', *Adv. Space Res.*, 43, 728-734, <https://doi.org/10.1016/j.asr.2008.09.018>
- Souvatzoglou, G., Papaioannou, A., Mavromichalaki, H., Dimitroulakos, J., Sarlanis, C. 2014, 'Optimizing the real-time ground level enhancement alert system based on neutron monitor measurements: Introducing GLE Alert Plus', *Space Weather*, 12, 633-649, <https://doi.org/10.1002/2014SW001102>

Open Access

This paper is published under the Creative Commons Attribution 4.0 International license (<https://creativecommons.org/licenses/by/4.0/>). Please note that individual, appropriately marked parts of the paper may be excluded from the license mentioned or may be subject to other copyright conditions. If such third party material is not under the Creative Commons license, any copying, editing or public reproduction is only permitted with the prior consent of the respective copyright owner or on the basis of relevant legal authorization regulations.

The GLE # 73 on 28 October 2021: spectra, angular distribution and terrestrial effects

Alexander Mishev ¹, Leon Kocharov ¹, Sergey Koldobskiy ¹, Nicholas Larsen ¹,
Esa Riihonen², Rami Vainio ², Ilya Usoskin ¹

Correspondence

1 Sodankylä Geophysical Observatory, University of Oulu, Finland, alexander.mishev@oulu.fi, leon.kocharov@oulu.fi, sergey.koldobskiy@oulu.fi, nicholas.larsen@oulu.fi, ilya.usoskin@oulu.fi

2 University of Turku, Finland, rami.vainio@utu.fi

Keywords

solar energetic particles; ground level enhancement; neutron monitor; data analysis; terrestrial effects

Abstract

The first solar proton event observed at ground, that is ground level enhancement, of solar cycle 25 was detected on 28 October 2021 by several neutron monitors (NMs), specifically those in the polar region as well as by space-borne instruments. It was identified as the GLE (ground-level enhancement) #73 in the International GLE database. The strongest signal at the ground was registered by the DOMC/DOMB monitors located at the Antarctic plateau at the Concordia French-Italian research station. Here, we report the observations and the study of this event using the global NM network and SOHO/ERNE records. We present the derived angular and spectral characteristics of solar energetic protons, including their dynamical evolution throughout the event. Several applications are discussed, namely the terrestrial effects of the GLE particles during the event.

1. Introduction

A methodological study of high-energy particles originating from the Sun, that is, the solar energetic particles (SEPs), specifically their properties such as spectra and angular distribution provides a unique opportunity and basis to reveal important and still open questions as their acceleration and propagation in the interplanetary space (e.g. Reames 1999, Kocharov et al. 2021). A specific interest represents a particular class of SEPs, namely particles believed to be the tail of the spectrum, that is, particles with energy reaching about GeV/nucleon or even greater values. Solar protons with energy above some 300 MeV/nucleon produce, following consecutive interactions, a shower of secondary particles in the Earth's atmosphere, so that they can be registered at ground by convenient detectors, that is neutron-monitors (NMs) (for details see Dorman 2004, Mishev and Poluianov 2021). This specific class of events is known as ground-level enhancements (GLEs) (Shea and Smart 1982, Poluianov et al. 2017).

In addition, GLE particles can significantly affect the complex radiation field in the atmosphere as well as the atmospheric ionization, thus playing an important role in atmospheric chemistry and physics (Usoskin et al. 2011, Mironova et al. 2015). Since GLEs occur sporadically and differ from each other, specifically in spectra, angular distribution, duration, and geomagnetic conditions (Moraal and McCracken, 2012) they are naturally studied case-by-case. Here, we consider the latest occurred event upon the submission of the paper, that is, GLE # 73 observed on 28 October 2021.

2. GLE # 73: Observation and data analysis

The first GLE of the current solar cycle 25 was observed on 28 October 2021, notably by several low-rigidity cut-off NMs, as well as by space-borne instruments (for details see Papaioannou et al. 2022). The event was associated with an X1.0 solar flare at S28W01 and an asymmetric halo CME. The peak of the soft X-ray emission was at 15:35 UT. At ground, the peak count rate increase was registered by South Pole SOPO (5.4%) and South Pole Bare SOPB (5.7%), DOMC (7.3%) and DOMB (14%), standard and bare monitors, respectively. A detailed report of radio, and X-ray observations is given by Klein et al. (2022).

For the analysis of this event, we used the fact that NMs at different geographic locations are sensitive to a different part of the SEP spectra and arrival direction, that is, one can use the geomagnetosphere as a giant spectrometer (Bieber and Evenson, 1995; Mishev and Usoskin 2020). Using the relationship between NM count rate and primary particles given with the expression:

$$N(P_c, h, t) = \sum_i \int_{P_c}^{\infty} S_i(P, h) \cdot J_i(P, t) \cdot dP \quad (1)$$

where $N(P_c, h, t)$ is the count rate of the NM, S_i is the NM yield function, which accounts for the particle propagation in the atmosphere and the registration efficiency of the device itself, $J_i(P, t)$ is the rigidity spectrum of incoming SEPs, P_c is the rigidity cut-off of the station, we can model each NM station counting rate. Here, using Eq. (1), we model the NM count rate increase due to SEPs. Subsequently, on the basis of the method, details given in (Mishev and Usoskin, 2016; Mishev et al. 2018, 2021), which was initially developed by Cramp et al. (1997); Vashenyuk et al. (2006), we unfold the GLE characteristics, that is spectra, apparent source position and pitch angle distribution (PAD).

The method involves the computation of asymptotic directions and rigidity cut-offs of all NMs used for the data analysis; making a convenient initial guess of the optimization procedure and performing the optimization itself by minimizing the difference between modeled and recorded NM responses over a selected space of unknown parameters. Here, the rigidity cut-off and asymptotic directions were computed using a new open-source tool OTSO (Larsen et al. 2022), employing a combination of the IGRF + TSY 89 models (Tsyganenko 1989), which provides reasonable precision and straightforward computation of the needed parameters for the data analysis (Kudela et al. 2008; Nevalainen et al. 2013). An illustration of computed asymptotic directions of selected NMs is given in Fig. 1. Thus, using data from the international GLE database and the Neutron Monitor Database NMDB (Mavromichalaki et al. 2011), and the aforementioned method, we derived the spectra during GLE # 73. The best fit for the SEP spectra according to our analysis is depicted by modified power-law Eq. (2)

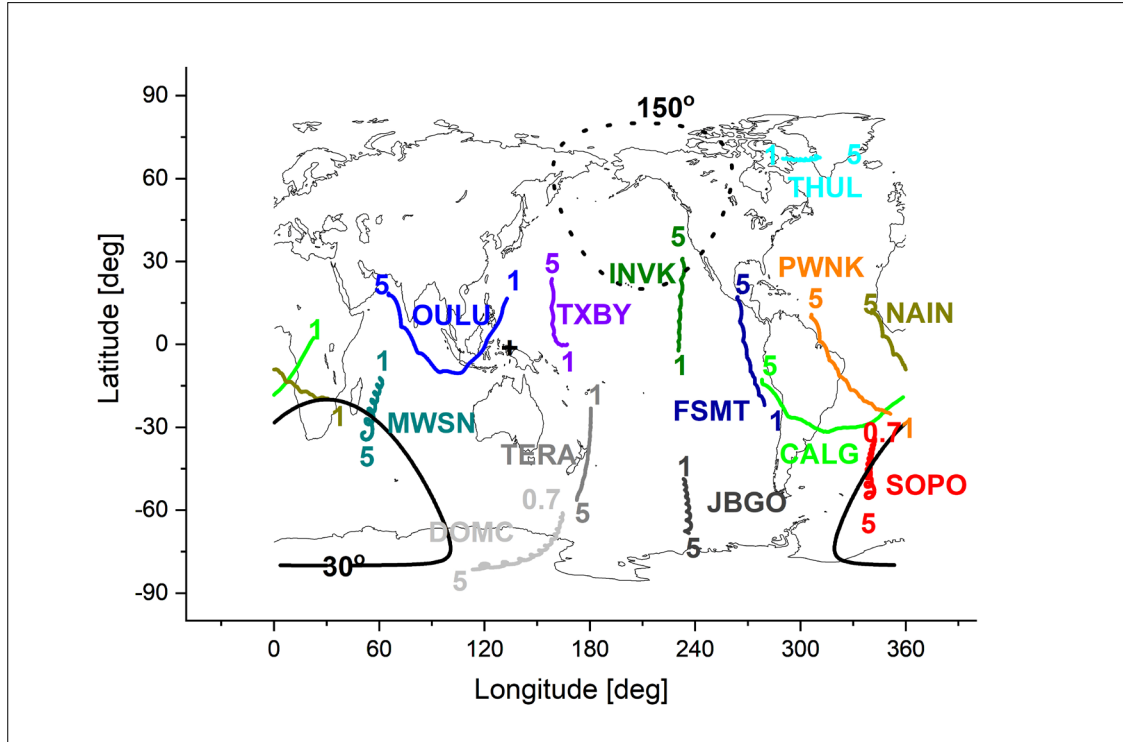


Fig. 1: Asymptotic directions of several NMs during to the event onset of GLE #73. The cross corresponds to the interplanetary magnetic field (IMF) direction obtained by the Advanced Composition Explorer (ACE) satellite. The lines of equal pitch angles relative to the derived anisotropy axis are plotted for 30° and 150° respectively.

$$J(P) = J_0 P^{-(\gamma + \delta \gamma (P-1))} \quad (2)$$

Accordingly, the angular distribution was approximated with Gaussian, see Eq. (3).

$$G(\alpha(P)) \sim \exp(-\alpha^2/\sigma^2) \quad (3)$$

The derived spectra and PAD are presented in Fig. 2, whereas the details are reported in (Mishev et al. 2022a). The derived spectra were moderately hard, with a considerable steepening during the event onset, which vanished in the late stage of the event. The SEP spectra revealed a gradual softening throughout the event. The derived PAD was relatively wide, considerably wider compared to beam-like events. In addition, analysis based on SOHO/ERNE shows that the anisotropy of relativistic protons was surprisingly low compared to the anisotropy of deka-MeV protons, notably revealing different anisotropy direction (Mishev et al. 2022a). While, the low-energy protons arrived predominantly from the north and west, which is consistent with the observed direction of the interplanetary magnetic field, the relativistic protons arrived from a location near the eruption center.

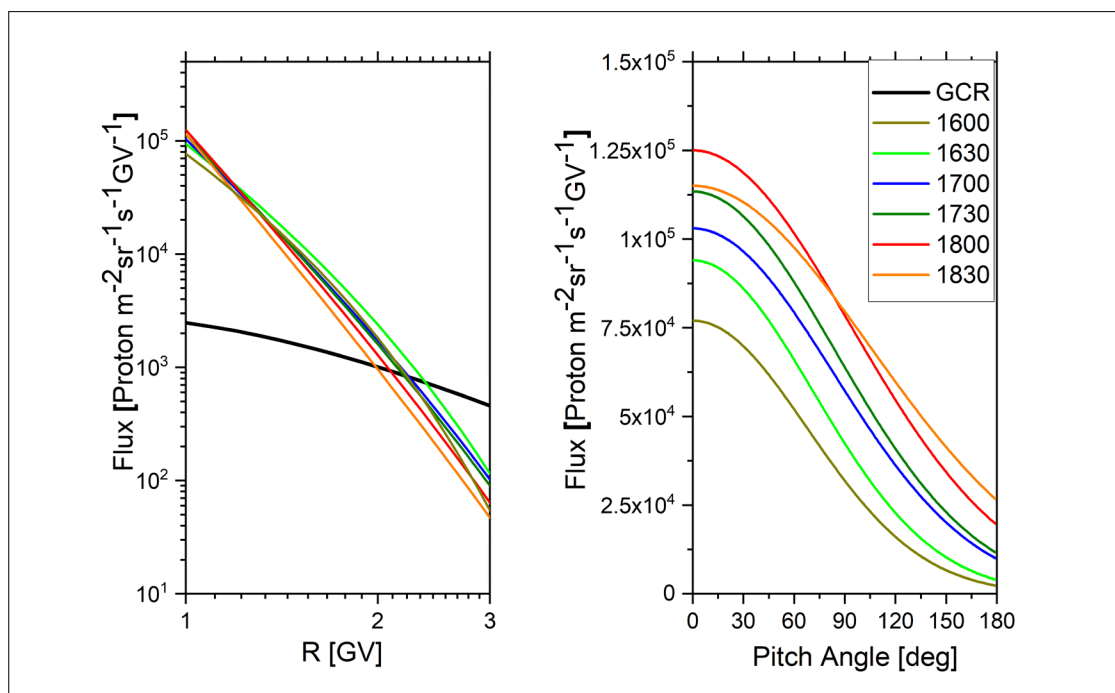


Fig. 2: Derived rigidity spectra and PAD during GLE #73. The solid black line depicts the GCR flux. Time [UT] corresponds to the start of the five-minute interval over which the data are integrated.

3. Atmospheric ionization effect

During GLEs the increased intensity of high-energy particles entering the atmosphere is greatly increased, leading to enhanced ionization, namely SEPs result in important space weather issues, specifically over the polar caps, where the geomagnetic shielding is marginal (Usoskin et al. 2011).

Using the derived spectra during the GLE # 73 and employing a model originally developed by Usoskin and Kovaltsov (2006), and recently verified by stratospheric balloon-borne measurements (Mishev et al. 2022b), we computed the ion production rate in the atmosphere due to GCRs and SEPs over the GLE # 73. In order to realistically quantify the terrestrial effects of the precipitating high-energy SEPs, specifically for atmospheric physics and chemistry studies, we normalized the ion production rate to a given period, namely to 24 hours, employing the recombination model by Krivolutsky et al. (2006) and assuming isotropic distribution (Pätsi and Mishev 2022), that is, we computed the 24h averaged ionization effect similarly to (Mishev and Velinov 2018, 2020). Employment of an isotropic distribution during these computations is reasonable, because of the wide angular distribution of incoming SEPs and none the least the fast isotropization of the event. The computed ionization effect in the upper atmosphere, that is, at a depth of 25 g/cm² is presented in Fig. 3, and in the region of Regener-Pfotzer maximum (Regener and Pfotzer 1935), at a depth of 200 g/cm², in Fig. 4.

One can see that the ionization effect was notable in the upper atmosphere (about 300% in the polar region, 120% in the sub-polar region, 40% at mid-latitudes and marginal or null in high rigidity cut-off region), yet considerably diminished at lower altitudes, e.g. at Regener-Pfotzer maximum, (less than 30% in the polar region), due to the softer SEP spectra compared to the GCRs spectra.

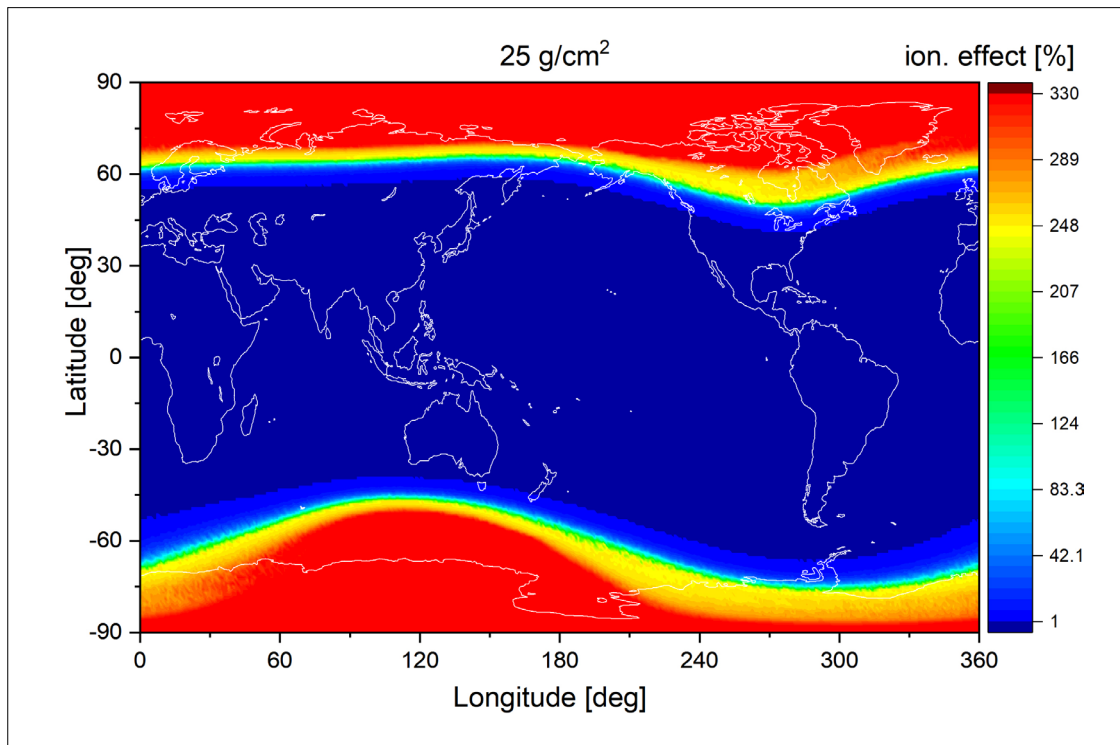


Fig.3: Averaged ionization effect during GLE # 73 at a depth of 25 g/cm².

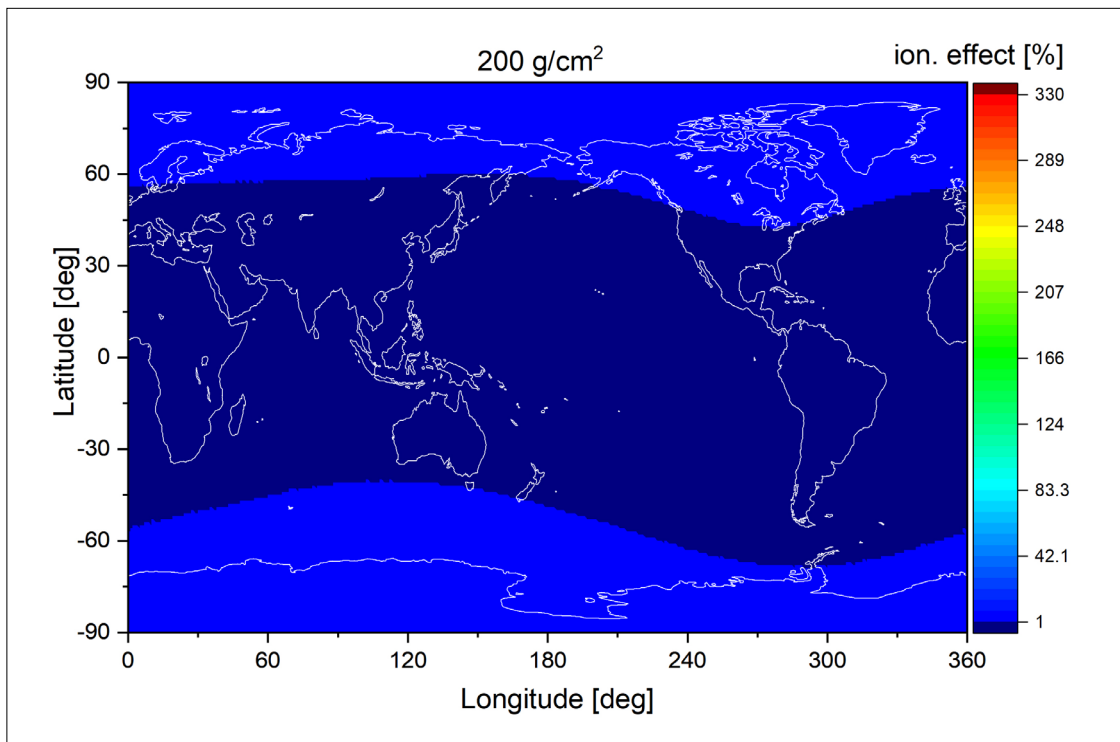


Fig.4: Averaged ionization effect during GLE # 73 at a depth of 200 g/cm².

4. Conclusion

In the present study here, we derived the spectral and angular characteristics of high-energy SEPs during the first GLE event of solar cycle 25, namely GLE# 73, which occurred on 28 October 2021. The best fit was achieved with a modified power-law in the spectrum and a simple Gaussian PAD. Moderately hard SEP spectra were derived, with considerable steepening, specifically during the event initial stage.

Subsequently, employing a Monte Carlo-based numerical model, we assessed for the first time, the atmospheric ionization effect during the GLE # 73. It is shown, that the effect was moderate in the polar region, whilst at mid- and high rigidity cut-off regions was barely seen.

The study presented here, representing full chain analysis of GLEs using NM records, namely derivation of SEP spectra and computation of terrestrial effects, provides the necessary basis to study the impact of precipitating high-energy particles in the Earth's atmosphere at different scales.

Acknowledgements

This work was supported by the Academy of Finland (projects 330064 QUASARE, 321882 ESPERA) and the University of Oulu grant SARPEDON.

References

- Bieber, J., Evenson, P. 1995, Spaceship earth – an optimized network of neutron monitors, in: Proc. of 24th ICRC Rome, Italy, 28 August – 8 September 1995, 1316–1319.
- Cramp, J.L., Duldig, M.L., Flückiger, E.O., Humble, J.E., Shea, M.A., Smart, D.F. 1997, The October 22, 1989, solar cosmic enhancement: ray an analysis the anisotropy spectral characteristics. *Journal of Geophysical Research* 102(A11), 24 237.
- Dorman, L.: 2004, *Cosmic rays in the earth's atmosphere and underground*, Kluwer Academic Publishers, Dordrecht.
- K-L. Klein, S. Musset, N.Vilmer, C. Briand, S. Krucker, A. Battaglia, N. Dresing, C. Palmroos, and D. Gary, 2022, The relativistic solar particle event on 28 October 2021: Evidence of particle acceleration within and escape from the solar corona, *Astronomy and Astrophysics* 663, A173, <https://doi.org/10.1051/0004-6361/202243903>
- Kocharov, L., Omodei, N., Mishev, A., Pesce-Rollins, M., Longo, F., Yu, S., Gary, D.E., Vainio, R., Usoskin, I. 2021, Multiple sources of solar high-energy protons. *Astrophysical Journal* 915, 12, <https://doi.org/10.3847/1538-4357/abff57>
- Kudela, K., Bučik, R., Bobik, P. 2008, On transmissivity of low energy cosmic rays in disturbed magnetosphere. *Advances in Space Research* 42(7), 1300–1306, <https://doi.org/10.1016/j.asr.2007.09.033>
- Larsen, N, Mishev, A, Usoskin, I. 2023, A New Open-source Geomagnetosphere propagation tool (OTSO) and its applications, *Journal of Geophysical Research: Space Physics*, 128, e2022JA031061, <https://doi.org/10.1029/2022JA031061>
- Mavromichalaki, H., Papaioannou, A., Plainaki, C., Sarlanis, C., Souvatzoglou, G., Gerontidou, M., Papailiou, M., Eroshenko, E., Belov, A., Yanke, V., Fluckiger, E.O., Butikofer, R., Parisi, M., Storini, M., Klein, K.-L., Fuller, N., Steigies, C.T., Rother, O.M., Heber, B., Wimmer-Schweingruber, R.F., Kudela, K., Strharsky, I., Langer, R., Usoskin, I., Ibragimov, A., Chilingaryan, A., Hovsepyan, G., Reymers, A., Yeghikyan, A., Kryakunova, O., Dryn, E., Nikolayevskiy, N., Dorman, L., Pustil'Nik, L. 2011, Applications and usage of the real-time neutron monitor database. *Advances of Space Research* 47, 2210–2222, <https://doi.org/10.1016/j.asr.2010.02.019>
- Mironova, I., Aplin, K., Arnold, F., Bazilevskaya, G., Harrison, R., Krivolutsky, A., Nicoll, K., Rozanov, E., Turunen, E., Usoskin, I. 2015, Energetic particle influence on the earth's atmosphere. *Space Sci. Rev.* 194, 1–96, <https://doi.org/10.1007/s11214-015-0185-4>
- Mishev, A., Poluianov, S. 2021, About the altitude profile of the atmospheric cut-off of cosmic rays: New revised assessment. *Solar Physics* 296(8), 129, <https://doi.org/10.1007/s11207-021-01875-5>

- Mishev, A., Usoskin, I. 2016, Analysis of the ground level enhancements on 14 July 2000 and on 13 December 2006 using neutron monitor data. *Solar Physics* 291(4), 1225-1239, <https://doi.org/10.1007/s11207-016-0877-2>
- Mishev, A., Usoskin, I., 2020, Current status and possible extension of the global neutron monitor network. *Journal of Space Weather and Space Climate* 10, <https://doi.org/10.1051/swsc/2020020>
- Mishev, A., Velinov, P. 2018, Ion production and ionization effect in the atmosphere during the Bastille day GLE 59 due to high energy SEPs. *Advances in Space Research* 61, 316-325. <https://doi.org/10.1016/j.asr.2017.10.023>
- Mishev, A., Velinov, P. 2020, Ionization effect in the earth's atmosphere during the sequence of October–November 2003 Halloween GLE events. *Journal of Atmospheric and Solar-Terrestrial Physics* 211, 105484, <https://doi.org/10.1016/j.jastp.2020.105484>
- Mishev, A., Usoskin, I., Raukunen, O., Paassilta, M., Valtonen, E., Kocharov, L., Vainio, R. 2018, First analysis of GLE 72 event on 10 September 2017: Spectral and anisotropy characteristics. *Solar Physics* 293, 136, <https://doi.org/10.1007/s11207-018-1354-x>
- Mishev, A.L., Koldobskiy, S.A., Kocharov, L.G., Usoskin, I.G. 2021, GLE # 67 event on 2 November 2003: An analysis of the spectral and anisotropy characteristics using verified yield function and detrended neutron monitor data. *Solar Physics* 296(5), 79, <https://doi.org/10.1007/s11207-021-01832-2>
- Mishev, A., Kocharov, L., Koldobskiy, S., Larsen, N., Riihonen, E., Vainio, R., Usoskin, I. 2022a, High-Resolution Spectral and Anisotropy Characteristics of Solar Protons During the GLE N 73 on 28 October 2021 Derived with Neutron-Monitor Data Analysis, *Solar Physics* 297, 5, 88, <https://doi.org/10.1007/s11207-022-02026-0>
- Mishev, A., Binios, A., Turunen, E., Leppänen, A-P., Larsen, N., Tanskanen, E., Usoskin, I., Envall, J., Linatti, T., Lakkala, P. 2022b, Measurements of natural radiation with an MDU Liulin type device at ground and in the atmosphere at various conditions in the Arctic region, *Radiation Measurements* 154, 106757, <https://doi.org/10.1016/j.radmeas.2022.106757>
- Moraal, H., McCracken, K. 2012, The time structure of ground level enhancements in solar cycle 23. *Space Sci. Rev.* 171, 85-95.
- Nevalainen, J., Usoskin, I., Mishev, A. 2013, Eccentric dipole approximation of the geomagnetic field: Application to cosmic ray computations. *Advances in Space Research* 52(1), 22-29, <https://doi.org/10.1016/j.asr.2013.02.020>
- Papaioannou, A., Kouloumvakos, A., Mishev, A., Vainio, R., Usoskin, I., Herbst, K., Rouillard, A. P., Anastasiadis, , Gieseler, J., Wimmer-Schweingruber, R., Küh, P. 2022, The first ground level enhancement of solar cycle 25 on 28 October 2021. *Astronomy and Astrophysics* 660, L5, <https://doi.org/10.1051/0004-6361/202142855>
- Pätsi, S., Mishev, A. 2022, Ionization effect in the Earth's atmosphere due to cosmic rays during the GLE # 71 on 17 May 2012, *Advances in Space Research* 69, 2893-2901.
- Poluianov, S.V., Usoskin, I.G., Mishev, A.L., Shea, M.A., Smart, D.F. 2017, GLE and sub-GLE redefinition in the light of high-altitude polar neutron monitors. *Solar Physics* 292(11), 176, <https://doi.org/10.1007/s11207-017-1202-4>
- Reames, D.V. 1999, Particle acceleration at the sun and in the heliosphere. *Space Science Reviews* 90(3-4), 413-491.
- Regener, E., Pfozter, G. 1935, Vertical intensity of cosmic rays by threefold coincidences in the stratosphere. *Nature* 136, 718-719.
- Shea, M.A., Smart, D.F. 1982, Possible evidence for a rigidity-dependent release of relativistic protons from the solar corona. *Space Science Reviews* 32, 251-271.
- Tsyganenko, N.A. 1989, A magnetospheric magnetic field model with a warped tail current sheet. *Planetary and Space Science* 37(1), 5-20, [https://doi.org/10.1016/0032-0633\(89\)90066-4](https://doi.org/10.1016/0032-0633(89)90066-4)
- Usoskin, I., Kovaltsov, G. 2006, Cosmic ray induced ionization in the atmosphere: Full modeling and practical applications. *Journal of Geophysical Research* 111.
- Usoskin, I., Kovaltsov, G., Mironova, I., Tylka, A., Dietrich, W. 2011, Ionization effect of solar particle GLE events in low and middle atmosphere. *Atmos. Chem. Phys.* 11, 1979-1988.
- Vashenyuk, E.V., Balabin, Y.V., Perez-Peraza, J., Gallegos-Cruz, A., Miroshnichenko, L.I. 2006, Some features of the sources of relativistic particles at the sun in the solar cycles 21-23. *Advances Space Research* 38(3), 411-417, <https://doi.org/10.1016/j.asr.2005.05.012>

Open Access

This paper is published under the Creative Commons Attribution 4.0 International license (<https://creativecommons.org/licenses/by/4.0/>). Please note that individual, appropriately marked parts of the paper may be excluded from the license mentioned or may be subject to other copyright conditions. If such third party material is not under the Creative Commons license, any copying, editing or public reproduction is only permitted with the prior consent of the respective copyright owner or on the basis of relevant legal authorization regulations.

What do we learn from ground level enhancements?

Athanasios Papaioannou 

Correspondence

IAASARS – Institute for Astronomy, Astrophysics, Space Applications and Remote Sensing, National Observatory of Athens, Penteli, Greece, atpapaio@astro.noa.gr

Keywords

solar energetic particles; ground level enhancements; coronal mass ejections; solar flares; neutron monitors

Abstract

Ground level enhancements (GLEs) comprise the high-energy end of solar energetic particle (SEP) events and constitute a special class in which ions are accelerated to relativistic energies, causing a significant sudden increase of cosmic rays at ground-based detectors, mainly at neutron monitors (NMs). GLEs require acceleration processes capable of producing particles with sufficient energy to allow their secondary products to reach the terrestrial ground and be detected. Moreover, due to their fast propagation, relativistic protons in GLEs are particularly useful for the identification of SEP sources at the Sun (i.e. flare, coronal mass ejections) – nonetheless, the debate about the exact nature of GLE mechanisms is still ongoing. GLEs are further critical for the establishment of Space Weather services and the accurate determination of their imposed radiation risk. In this tutorial, an overview of GLEs with respect to their historical identification, measurements from the worldwide neutron monitor network, modeling and forecasting efforts will be provided. In addition, a hands-on tutorial that will demonstrate how the Neutron Monitor Database (NMDB) can be utilized for GLE analysis will be conducted.

1. Introduction

Ground level enhancements (GLEs) are short-term increases of the cosmic ray intensity above the ever-present background of galactic cosmic rays registered at the ground by particle detectors (usually neutron monitors – NMs; Miroshnichenko, 2001; Poluianov et al. 2017) (see [Figure 1](#)). These particles originate at the Sun and are very fast (i.e. reach near-relativistic energies). GLEs are associated with solar eruptive events such as solar flares and coronal mass ejections (CMEs). A central scientific question which is still under debate up to nowadays concerns the mechanisms responsible for the production of these near-relativistic protons that give rise to GLEs.

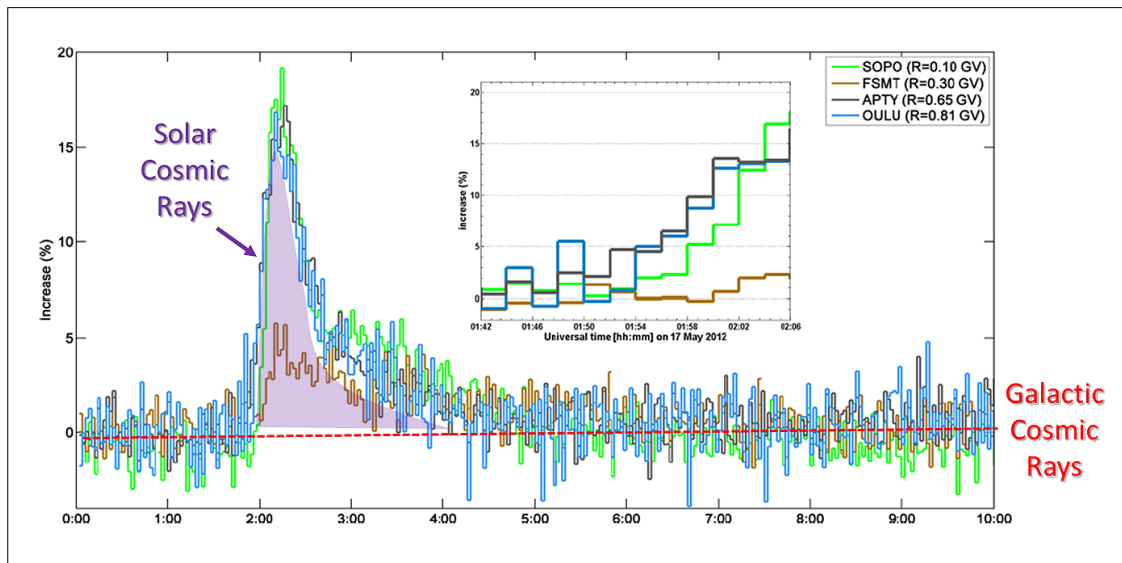


Fig. 1: Recordings of GLE71 on 17 May 2012 by South Pole (SOP0), Fort Smith (FSMT), Apatity (APTY) and Oulu (OULU) NMs. The red dashed horizontal line depicts the average galactic cosmic ray background and the shaded purple area the excess of solar cosmic ray particles that constitute this GLE event (adapted from Papaioannou et al. 2014).

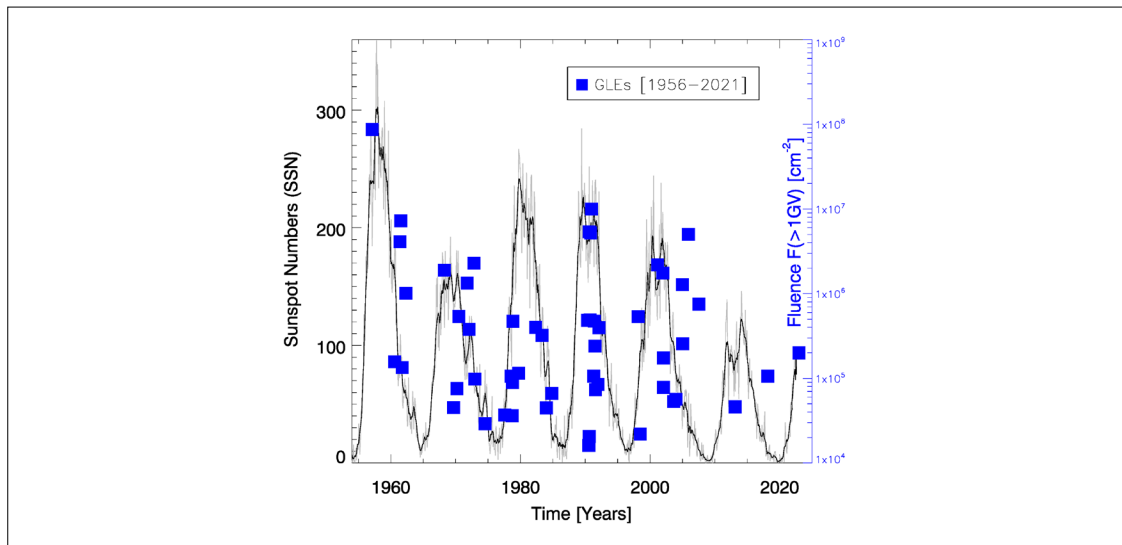


Fig. 2: Distribution over time of 68 GLEs since 1956, on the background of the evolving solar cycle. The blue squares depict the fluence $F(>1 \text{ GV})$ for each GLE.

GLEs constitute the most energetic class of solar energetic particle (SEP) events. They were first discovered by Forbush (1946) who identified three unusual cosmic ray increases and further linked them to charged particles emitted from the Sun. A few years later with the implementation of NMs Meyer, Parker and Simpson (1956) studied the GLE that was recorded on 23 February 1956 (GLE05) indicating solar flares as the driving source of these particles. GLE05 is the largest GLE event to date (see Usoskin et al. 2020, Mallios et al. 2022). GLEs are rare events since from 1946 there have only been 73 such events (or 68 if the counting starts at the NM era, i.e. GLE05 onwards) leading to a rate of ~ 1.04 GLEs/yr. Figure 2 depicts all

68 GLEs since 1956 through their achieved fluence at >1GV ($F(>1GV)$ in cm^{-2} ; y-axis on the right) plotted on the background of the evolving solar cycle which in turn is presented through the sunspot number (SSN; y-axis on the left). One may notice that GLE05 achieved a fluence almost one order of magnitude larger than all other GLEs up until today. Moreover, although GLEs follow the solar cycle (SC) evolution, in general, they seem to be present not only in the maximum but also in the ascending and declining phases of the SC. Finally, SC24 (after 2006) was the weakest SC presented and the origin of only two GLE events.

2. From the Sun to the ground

Multiple steps and building blocks need to be taken into account in order to understand and evaluate the physics of high-energy particle acceleration, injection and transport in the inner heliosphere, the interaction of these particles with the magnetosphere and the atmosphere of the planet (in our case, the Earth), as well as, the pivotal role of GLEs and ground based detectors, i.e. NMs. This is because GLE near-relativistic particles (i.e. “primary” solar cosmic ray particles) are accelerated at the Sun, propagate in interplanetary space and – once they reach the magnetopause – enter the magnetosphere where their particle trajectories bent. Consequently they enter the atmosphere and interact with its molecules creating a cascade that leads to the “secondary” solar cosmic rays. In turn, these secondary products eventually are recorded by a NM. Hence, it becomes apparent that taking all of the aforementioned steps into consideration is vital in the understanding of the underlying physics at every step. What is more, GLE recordings are most appropriate to shed light on the problem of particle acceleration, since those: (a) frame the early phase of SEP events – close to the time of acceleration and (b) the role of interplanetary transport is assumed to be minimal on the scattering of the particles (i.e. focused transport of near-relativistic particles).

2.1 The Sun is the giver of (life) particles

Paraphrasing Ramses the II, the Sun is the giver of particles. For hundreds of years people are looking at the Sun, drawing and monitoring its sunspots (Cliver and Herbst 2018). Modern instrumentation allowed scientists to get unprecedented imaging of the Sun and its dynamics, providing insights to concepts of i.e. the solar cycle variation and the eruption of solar flares and CMEs. [Figure 3](#) shows a combination of both these solar eruptive events. In particular, (from left to right), actual observations of a solar flare recorded by the Solar Dynamic Observatory (SDO) on 2012-05-17, a 2D model of stochastic acceleration in solar flares; magnetic field lines (in green) and turbulent plasma or plasma waves (as red circles) generated during magnetic reconnection (highlighted with a red circle). Blue arrows heading back to the solar surface depict accelerated particles impinging on the lower denser chromosphere, while similar arrows heading upwards present accelerated particles that may escape to interplanetary space. These are then detected as SEPs and/or GLEs (adapted from Vlahos et al. 2019; Temmer 2021) and a CME on the same date observed by the Solar and Heliospheric Observatory (SOHO); an emerging CME-driven shock (black arc) that may also accelerate SEPs/GLEs (black dots) in the corona or heliosphere via diffusive shock acceleration (highlighted with a red circle; adapted from Mikić and Lee 2006; Temmer 2021).

During a solar flare, electromagnetic radiation covering the whole electromagnetic spectrum is generated by the hot plasma and the non-thermal particles and travels at the speed of light through the interplanetary space. Usual indicators of solar flares lie in the X-ray and the radio emissions. This type of

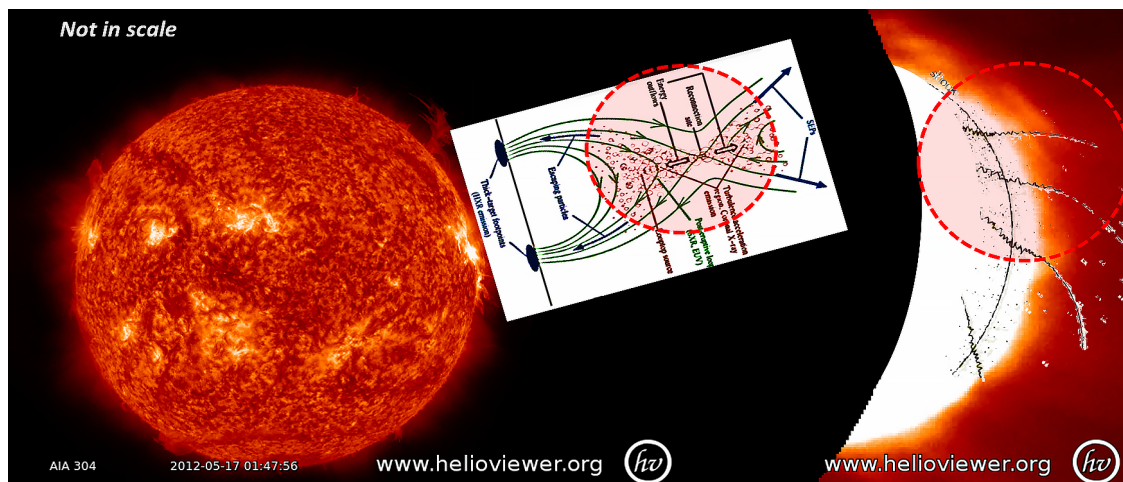


Fig. 3: A composite figure demonstrating the two major solar eruptive events (i.e. solar flare and CME) for GLE71 (17/05/2012) (made with <https://www.jhelioviewer.org>), as well as the dominant acceleration mechanisms, i.e. stochastic acceleration in solar flares (adapted from Vlahos et al. 2019) and DSA in propagating bow shocks (adapted from Mikić and Lee 2006). The red dashed circles demonstrate the acceleration sites.

radiation travels radially from the Sun to the Earth and requires ~ 8.33 minutes to reach the observing point (at Earth). The onset of an increase in soft X-ray (SXR) emission detected by sensors on the Earth-orbiting spacecraft is approximately simultaneous with the visual observations of a solar flare (see Figure 3, left panel) usually made in the H α wavelength. CMEs are sudden expulsions of magnetized plasma into the solar wind from regions initially magnetically closed. These form in the low corona (below $\sim 2 R_s$) and their energies range up to $\sim 10^{31} - 10^{32}$ erg, and their mass up to $\sim 10^{35}$ erg. The average speed of CMEs is ~ 500 km/s and their width is ~ 50 degrees (Vourlidas 2021). Most CMEs are in general associated with some level of X-ray emission, although, there are many more flares than CMEs. Nonetheless the strongest flares (in terms of magnitude) are most probably associated with CMEs, since solar eruptive events do not evolve in isolation but in concert, as a result of changes in the magnetic field (Yashiro et al. 2006). Radio waves from the Sun indicate electron acceleration, primarily to energies of tens of keV, and such electrons are likely to be accelerated at any time that high energy ions are accelerated. The characteristics of solar radio emissions as a function of frequency and time, at frequencies below a few hundred MHz, have been described in terms of five main types of bursts named type I through V (Wild et al. 1963). The most common types are: (a) type III burst, a classic signature of the so-called “impulsive phase” of flares which signify the opening of the magnetic field lines allowing the release of particles to the interplanetary medium¹ and (b) type II bursts denoted by their slow drift, implying speeds appropriate for coronal shock waves, and thus related to CMEs (Klein 2021a,b).

2.2 The Sun-Earth connection for energetic particles

Unlike solar electromagnetic radiation, those particles that are accelerated and injected into interplanetary space need to be directed to the appropriate interplanetary magnetic field (IMF) line that connects the source at the Sun to the observer at Earth. That said, both the onset time and the obtained maximum

¹ Type III bursts trace electron streams as they propagate along open field lines from flaring regions near the Sun into the interplanetary medium. Nonetheless, a study by e.g. Benz et al. (2005) suggests that only in a third (33%) of all flares (>C5.0) at least one of the four ends of reconnecting field lines is open.

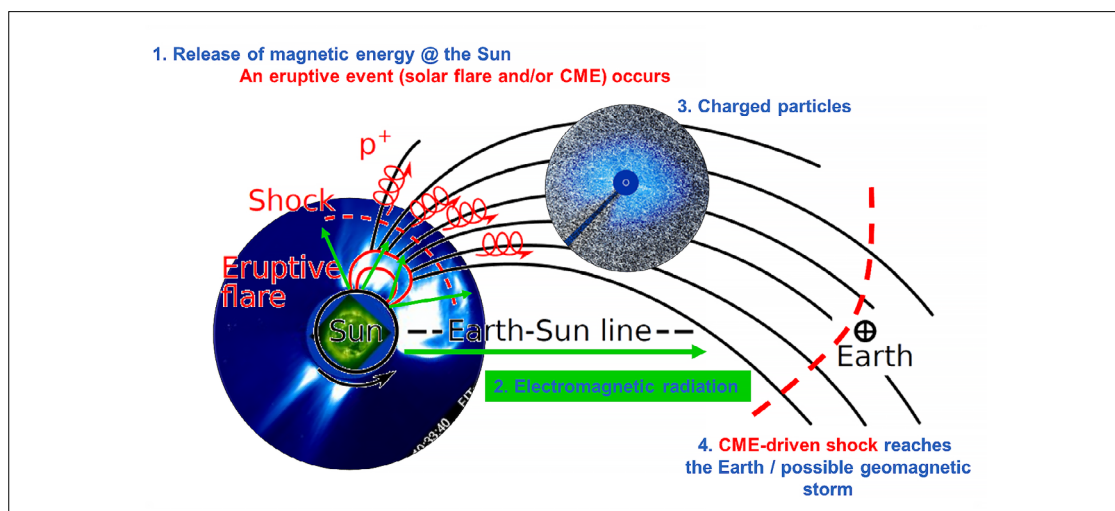


Fig. 4: A schematic of the solar storm scenario divided into 4 steps. A solar eruptive event initiates the scenario [1], its electromagnetic signatures arrive at the detector/observer [2], charged particles [3] are released and spiral along the IMF lines and if the CME drives a shock, when that reaches the Earth a geomagnetic storm may occur [4].

intensity of an SEP/GLE at a given (detection) point in the interplanetary space is dependent on the particles' source. This means that the location (i.e. helio-longitude) of the parent solar flare of an SEP/GLE with respect to the detection point is very important. This is explained as follows: first of all, as it is known, the IMF topology is governed by the solar wind outflow and the rotation of the Sun. As a result, during so-called “quiet” conditions (when the solar wind speed ranges from 300-400 km/s) the IMF can be approximated by an Archimedean (or a Parker) spiral, the nominal length of which is ~ 1.2 AU. Second of all, the previously accelerated and injected particles into the interplanetary medium, being charged, spiral along the IMF lines. Thereby, a favorable magnetic connection is established between the Earth and solar flares that occur at the Sun's W50-W70 helio-longitude, being termed as “well-connected” ones. In this picture one may further add a propagating CME that drives a shock. SEPs time-intensity profiles are organized in terms of the longitude of the observer with respect to the solar source (Cane and Lario 2006), in general, and the CME-driven shock (Cane et al. 1988), in particular, and thus particles are able to propagate to remote observers within the inner heliosphere.

Another important aspect is the energy of the released particles. For example, for the propagation along a nominal Archimedean spiral (i.e. scatter-free propagation) from the Sun to the Earth, 10 MeV protons take ~ 70 minutes; 100 MeV ~ 24 minutes and 450 MeV ~ 14 minutes to cover the same distance. That said, the higher the energy of the particles the less time they require to reach the Earth and in turn, near-relativistic protons recorded by NMs offer a prime sample for the investigation of the acceleration mechanisms at play. Figure 4 presents a combined scenario distributed over 4 steps taking into account the aforementioned facts.

2.3 Flare versus CME-shocks for GLEs

The open scientific question that rose decades ago and is still under debate focuses on the dominant acceleration mechanism for GLEs. For example, studies indicated that relativistic particles can be accelerated either through a coronal shock driven by the CME (see e.g. Vainio & Laitinen 2007, Afanasiev et

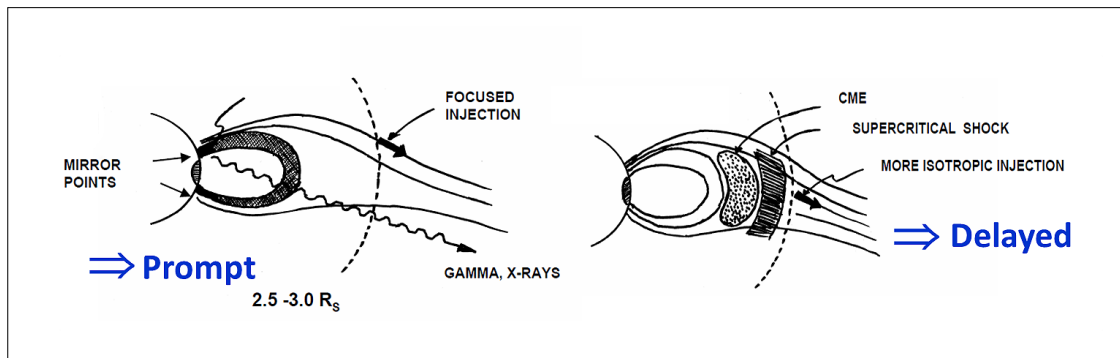


Fig. 5: A schematic of the prompt and focussed injection of particles following a solar flare giving ground to the “prompt” component of GLEs, followed by the expansion of a CME that leads to supercritical shock and results in a more isotropic injection giving ground to the “delayed” component of a GLE (adapted from Moraal and McCracken 2012).

al. 2018), or through magnetic reconnection during a flare (see a recent review in e.g. Vlahos et al. 2019). The observational findings that point to a flare origin are summarized as: (a) powerful flares are always present during GLEs; (b) the flare versus GLE timing has an excellent correlation; (c) no (significant) correlation of the fluence of GLEs with the CME speed and (d) favorable longitudinal distribution of the parent flares (the majority for GLEs are “well-connected” ones). On the opposite site, observational findings pointing to a CME origin are: (a) the majority of GLEs is associated with most powerful CMEs; (b) close connection with a type II radio emission which is indicative of a shock; (c) a delay between the flare’s timing and the particle’s escape into interplanetary space – depending on energy and (d) long injection comparatively to the impulsive phase of a flare. Nonetheless, since GLEs always occur after a very strong solar flare and a fast and wide CME (see e.g. Gopalswamy et al. 2012) a clear-cut separation has not been achieved up until today. Thereby each GLE event is treated separately (see some recent studies in e.g. Klein et al. 2022; Mishev et al. 2022; Papaioannou et al. 2022). Moreover, the pioneer work of Vashenyuk et al. (2011) introduced the so-called “prompt” and the “delayed” components scenario for GLEs, with the former being driven by the flare and the latter by the CME (see also McCracken et al. 2012; Figure 5).

2.4 Propagation in the magnetosphere

The motion of a charged particle in the magnetosphere is governed by the Lorentz force, that is, that the trajectories of particles are bent by the Earth’s magnetic field. Numerical methods employing a model of the magnetic field are required for the calculation of the particles’ trajectories in the magnetosphere (Smart et al. 2000). The magnetic field of the Earth is represented with two parts: the inner one generated by an internal dynamo and the outer part induced by different current systems in the ionosphere and the magnetosphere accounting for the interaction of the Earth’s magnetic field with the solar wind (e.g. Büttiker 2018 and references therein). For the internal magnetic field, the International Geomagnetic Reference Field (IGRF) model is usually employed while for the external magnetic field the semi-empirical model by Tsyganenko et al. (1989) (TSY89) requiring as the only input the geomagnetic activity index K_p is usually used (see e.g. discussion in Herbst 2021 and references there in). The geomagnetic field provides a shield against charged particles, which is most effective near the geomagnetic equator and marginal or almost non-present near the geomagnetic poles. Therefore, the access of energetic particles at a specific point of observation within the magnetosphere is determined by: (a) the Earth’s magnetic field, (b) the energy

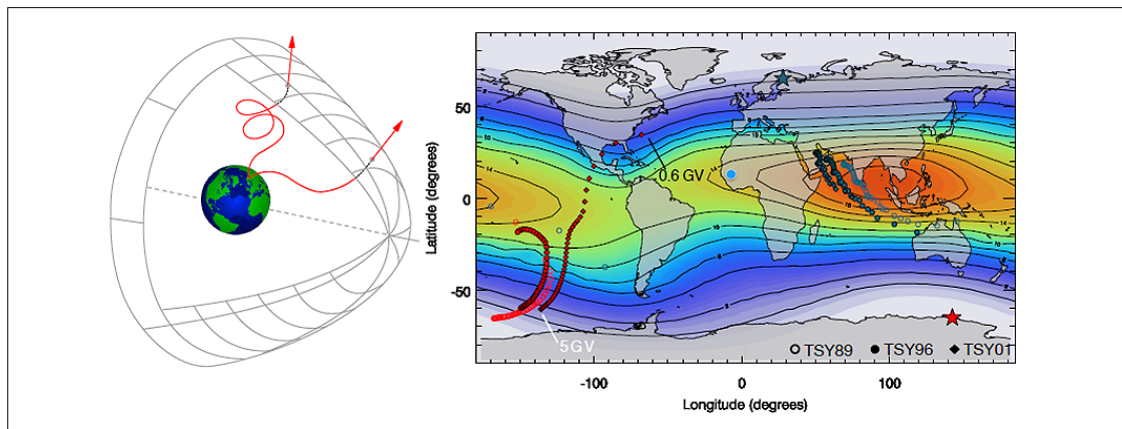


Fig. 6: An illustration of the concept of the asymptotic cones (taken from Herbst 2021).

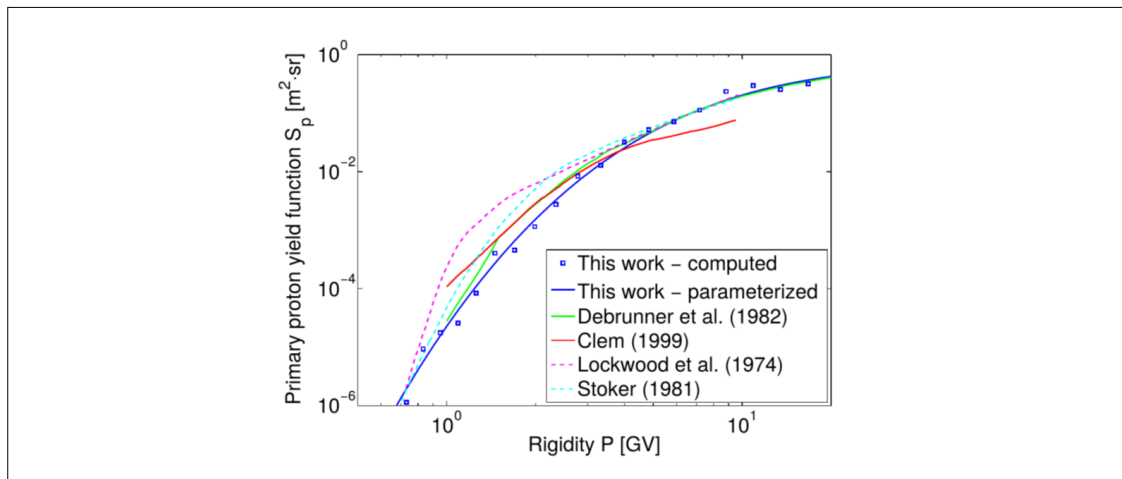


Fig. 7: Comparison of the NM yield function (taken by Flückiger et al. 2008).

and (c) the incidence angle of the particle. Usually, this access is quantified by the effective cut-off rigidity, R_c ($R_c = pc/Z_e$, where p is the momentum, c is the speed of light and Z_e is the charge of the particle; units GV), which is defined as the rigidity below which particles have no access to this location. Therefore, the trajectories of particles with rigidities greater (below) than R_c are “allowed” (“forbidden”). Moreover, the asymptotic direction of the incoming particles is used as the particle’s trajectory direction of approach at the boundary of the magnetosphere. The geomagnetic cut-off varies from 0 to 17 GV (~ 17 GeV in energy for protons).

2.5 Propagation in the atmosphere

The transport of particles in the Earth’s atmosphere depends on the atmospheric depth or atmospheric cut-off which is the lower energy limit of particles that can reach a given location on the ground and be registered by a NM. This cut-off is about 1 GV (~ 433 MeV in energy for protons). Nonetheless, the atmospheric cut-off decreases with altitude, and thus provides additional sensitivity of high-altitude polar neutron monitors to low-energy particles, mainly during GLEs pushing the lower-energy limit to ~ 300 MeV (see Poluianov and Batalla 2022). As noted here above, once a “primary” particle enters the atmosphere it

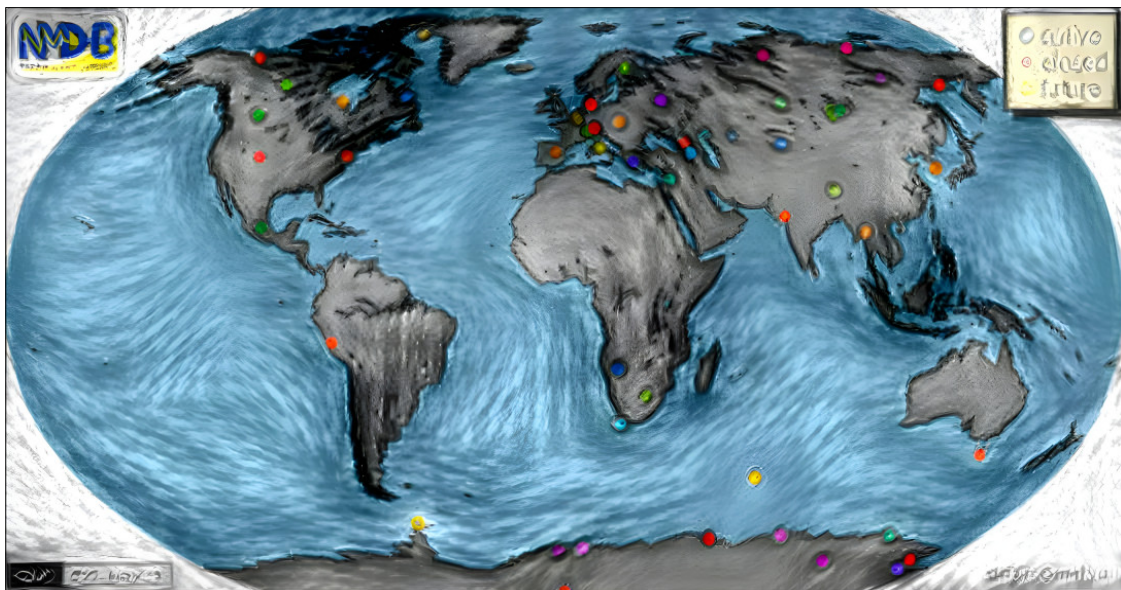


Fig. 8: Image of the distribution of the neutron monitors on the world map (credit: NMDB; <http://nmdb.eu>) treated with an artificial intelligence filter called Deep Dream technology (<https://deepdreamgenerator.com/>).

interacts with its molecules producing an atmospheric cascade and results to “secondary” particles. The intensity of the cascade (i.e. the number of secondary particles) grows with the growing atmospheric depth, until a maximum is reached. Thereafter it exponentially decreases. That said, it becomes apparent that a more energetic “primary” particle induces a stronger atmospheric cascade with a higher probability to reach the ground, and be measured by a NM. The unfolding of the cascade in the atmosphere and the NM detection efficiency for secondary cosmic ray particles are combined in the NM yield function (see Figure 7) (Flückiger et al. 2008; Mishev et al. 2013, 2020).

3. Analysis of GLEs by neutron monitor measurements

3.1 The neutron monitor network

Neutron monitors record secondary particles and the NM location corresponds to primaries: (a) with energies covering a specific part of the primary spectrum depending on the cut-off rigidity of the location and (b) coming from a specific set of directions. Thereby the usage of all available neutron monitors offers a more complete picture of the angular and energy distribution of the primary particles. That said the Network of NMs (Figure 8) serves as a Multi-directional tool, revealing the properties of primary particles reaching the Earth’s atmosphere. Almost 15 years ago, the implementation of the Neutron Monitor Database (NMDB; <https://www.nmdb.eu>) provided the opportunity to gather high-quality fine resolution (1-min) NM data in real-time mode, directly addressing the need for timely Space Weather related applications and archived data with higher time resolution that facilitates long-term investigations of the solar-terrestrial relations (Mavromichalaki et al. 2011; Steigies and Fuller 2023).

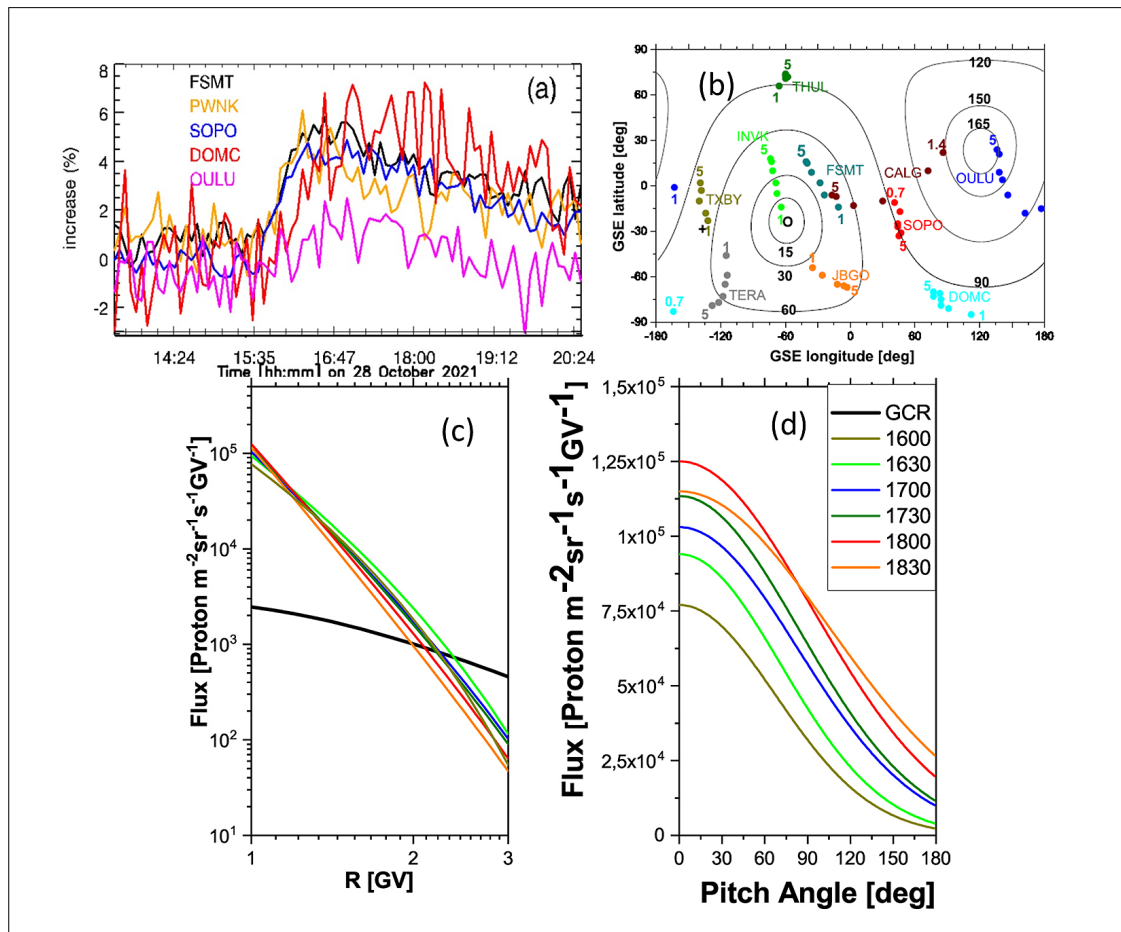


Fig. 9: Composite picture of the GLE analysis/modeling: (a) GLE73 recordings of NMs; (b) calculated asymptotic directions for GLE73 (from Mishev et al. 2022); (c) modeled spectrum of GLE73 and (d) modeled pitch-angle distribution for GLE73 (from Papaioannou et al. 2022).

3.2 Modeling GLEs

The analysis of GLEs requires the modeling of the response (i.e. recordings) of an adequate (optimally a significant number of NMs with good spatial coverage around the world and with quality data) number of NMs aiming at determining an optimal fit for the SEP spectrum and the angular distribution at 1 AU (see Mishev et al. 2022 and references therein). The usage of the worldwide network of neutron monitors is ideal for this task, since NMs situated in different geographic regions are sensitive to a different part of the solar particle spectra and arrival direction (Mishev and Usoskin 2020). This is basically achieved via a three-step procedure:

- *First step:* Compute the asymptotic directions and the cut-off rigidity of NM stations, i.e. simulate the propagation of the charged particles in a modeled magnetosphere.
- *Second step:* Make an initial guess of the inverse problem by viable assumptions keeping in mind that functions need to represent the physical processes involved.
- *Third step:* Apply an optimization method and identify the energy spectrum, the anisotropy axis direction and the pitch-angle distribution.

The model of the global response of NMs during a GLE has been developed over many years (e.g. Shea and Smart 1982; Flückiger & Kobel 1990; Belov et al. 2005; Bieber et al. 2013; Bombardieri et al. 2008; Bütikofer et al. 2008, 2016; Plainaki et al. 2007, 2010; Vashenyuk et al. 2011; Mishev et al. 2018, 2022) and is described in detail by Cramp et al. (1997). This method employs a least-squares fitting technique to determine the axis of symmetry of the particle arrival, the spectrum and the anisotropy of the high-energy solar protons that give rise to the increased neutron monitor response.

The spectral shape of the “primary” particles needs to be assumed in such a process. This is directly related to the acceleration process involved. Several such forms have been investigated, as pure and modified power laws, as well as spectra based on theoretical expectations (Ellison and Ramaty 1985). An empirical functional form that can be employed to fit the neutron monitor observations is the so-called: “modified power-law” spectrum which incorporates the change of the power law exponent ($\delta\gamma$), leading to a spectrum that steepens with increasing rigidity (see Mishev et al. 2022; Papaioannou et al. 2022 and references therein).

The propagation of particles through the interplanetary medium results in a distribution of pitch angles which can be described using a functional form. Formally, the particle pitch angle is defined as the angle between the axis of symmetry of the particle distribution and the asymptotic direction of view. The most widely-used functions have been cosine or Gaussian relationships (see Cramp et al. 1997; Mishev et al. 2022). [Figure 9](#) depicts results from the analysis and modeling of the recent GLE73.

3.3 Forecasting solar storms

Since the propagation of particles is governed by their energy (speed) the near-relativistic particles that are recorded by NMs are the fastest and establish a distinguishable enhancement at the ground level prior to the arrival of the bulk of the several 10's of MeV particles that follow. Therefore one can make use of the particle recordings at NMs in order to forecast the arrival of lower energy protons (see details in e.g. Kuwabara et al. 2006; Souvatzoglou et al. 2014), as this is illustrated in [Figure 10](#) (left panel) which shows the NM recordings of GLE60 on 15 April 2001 compared to the GOES spacecraft measurements at $E>10$ and $E>100$ MeV (Kuwabara et al. 2006). As it can be seen, the first arriving particles at the ground provide an earlier onset compared to the time when the enhancement was clearly identified in spacecraft measurements. Thereby, the time difference provides a window of reliable forecasting based solely on NM measurements giving ground to the so-called “GLE Alert”. [Figure 10](#) (right panel) shows the velocity dispersion analysis (VDA; Vainio et al. 2013; Paassilta et al. 2017) for GLE31 on 07 May 1978. VDA assumes that particles at all energies exhibit a simultaneous release into the interplanetary medium follow the IMF lines and arrive promptly to the observer (i.e. Earth). Due to this scenario (see also Section 2) the onset times of these solar particles at different energies as a function of their inverse velocity leads to a linear fit, with the slope of the fit providing the path length travelled by the particles and the intersection with the y-axis denoting the solar release time.

Once a “GLE Alert” is established then NMs can further provide an estimation of the expected spectrum down to lower-energies and most importantly can inform about the radiation hazard at flight altitudes due to the forthcoming increased exposure, particularly during long flights at low cut-off rigidities, e.g. over the polar and sub-polar regions (Mishev and Velinov 2020).

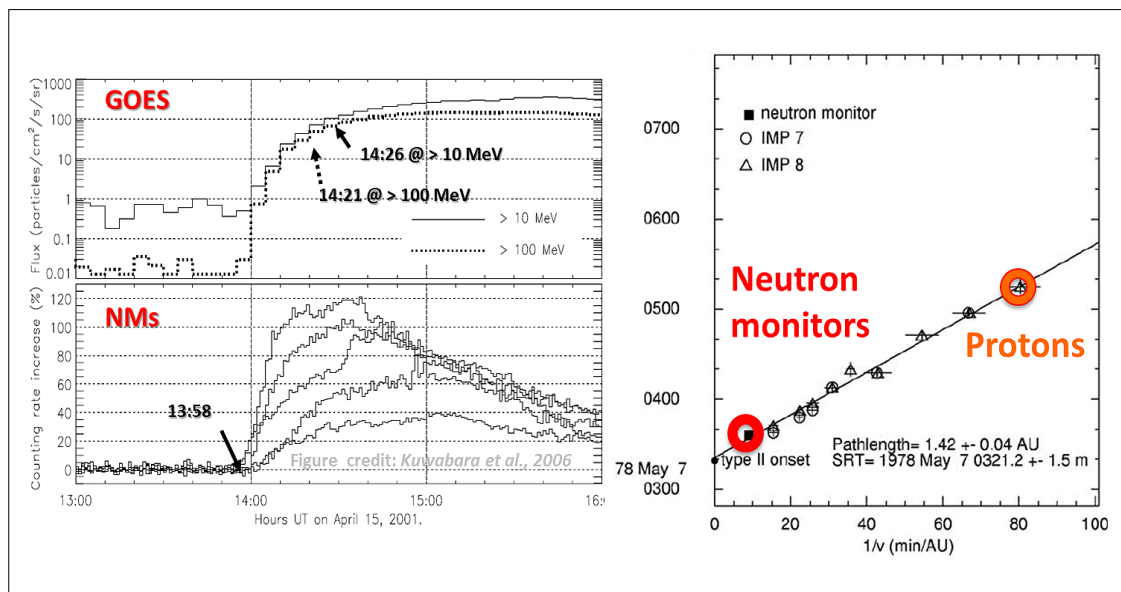


Fig. 10: Left panel: Recordings of the GLE60 on 15 April 2001 by NMs (bottom) and by GOES spacecraft (upper plot; adapted from Kuwabara et al. 2006). Velocity Dispersion Analysis (VDA) of GLE31 on 07 May 1978 based on spacecraft (IMP7 & IMP8) and neutron monitor measurements (adapted from Reames 2009).

4. Analysis of GLEs in the inner heliosphere

Particles emitted from the Sun, reaching to GLE energies ($E > 430$ MeV or $E > 300$ MeV for high altitude polar NMs) are recorded as excesses of solar particles above the background since the start of the space era. These data have been obtained from particle sensors on near-Earth satellites and on space probes throughout the heliosphere. When these observations are coupled with NM recordings they greatly increase our understanding of the fundamental processes of the generation of solar energetic particles and their propagation in the interplanetary medium.

4.1 Recordings at spacecraft detectors

From the patrol measurements offered by the Geostationary Operational Environmental Satellite (GOES) series, the High Energy Proton and Alpha Detector (HEPAD) could register particles up to 700 MeV. Thereby, GOES observations have been used for the identification of a number of GLEs at a range from ~ 10 -700 MeV (Figure 11, left panel; e.g. Mishev et al. 2018; Rodriguez and Kress 2023). Moreover, such recordings led to the unfolding of the spectrum during GLEs and demonstrated a double power-law behavior with a characteristic “break” energy (Figure 11, right panel, see details in Mewaldt et al. 2012; Cohen and Mewaldt 2018) which has been explained either on the basis of the CME-shock acceleration, transport of solar particles and/or on the existence of two distinct components: one CME related for lower energies and a second one for higher energies which is flare related (for the latter see the detail discussion in Kiselev et al. 2022).

Recent re-calibrations of science grade instruments further expanded the capabilities of space based detectors. For example, Kühl et al. (2017) demonstrated that the Electron Proton Helium Instrument (EPHIN) on board SOHO recorded 42 SEP events from 1997 to 2015 that reached a mean energy up to 610

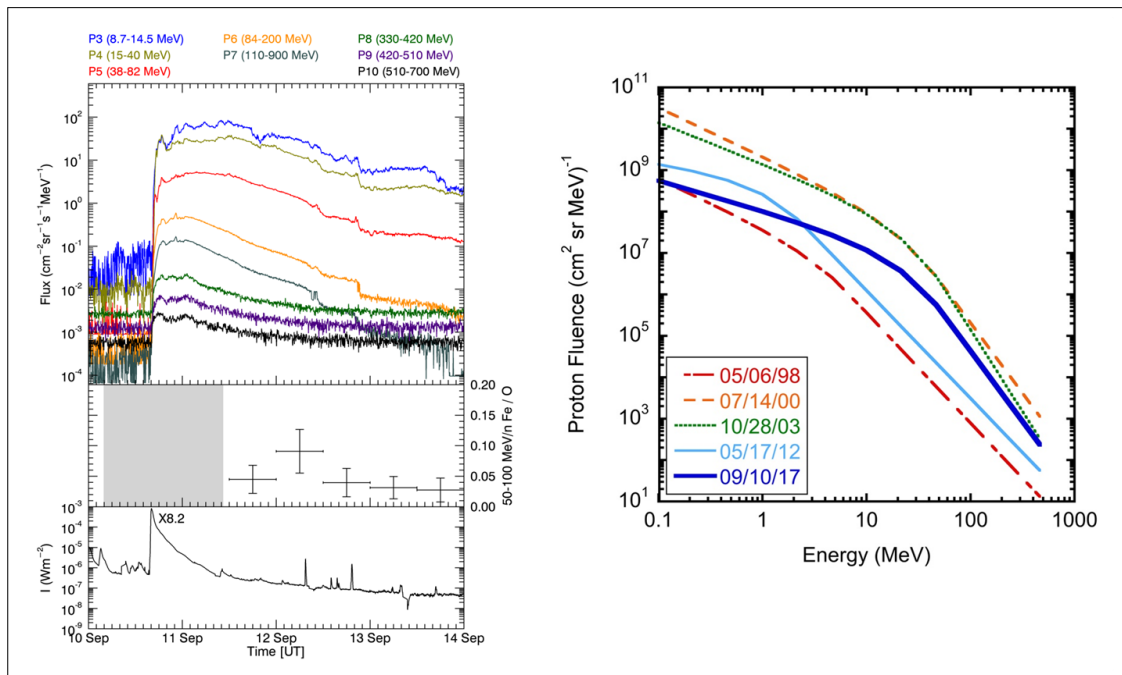


Fig. 11: Left panel: Recordings of the GLE72 on 10 September 2017 by (from top to bottom) GOES (8.7-700 MeV), SOHO/ERNE Fe/O at 50-100 MeV/n and GOES SXR denoting the driving X8.2 solar flare (from Mishev et al. 2018). Right panel: Proton fluence spectrum for 5 GLEs obtained by GOES measurements demonstrating the double power law behavior (from Cohen and Mewaldt 2018).

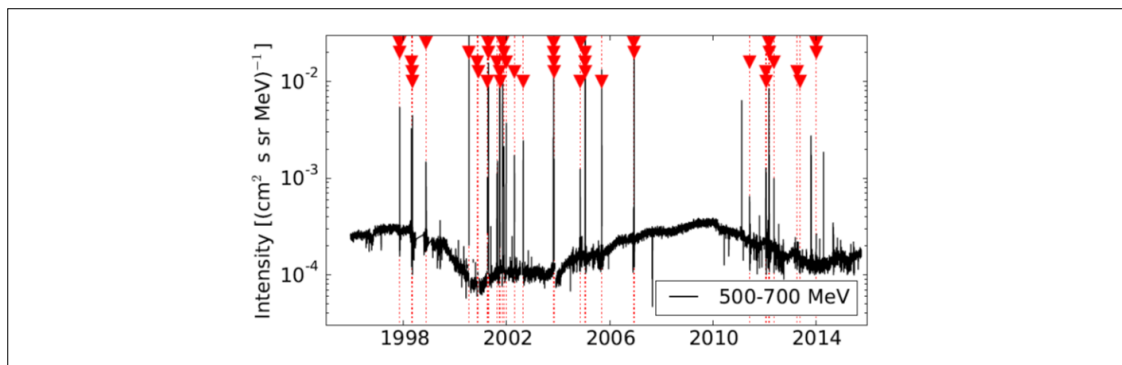


Fig. 12: Recordings of SOHO/EPHIN at 500-700 MeV from 1995-2015. The red triangles and the vertical lines denote the identified SEP events in these measurements (from Kühl et al. 2017).

MeV (Figure 12). A few of these SEP events were further recorded on the ground by NMs and thus were labeled as GLEs. Nonetheless, this paper gave rise to the identification of mildly relativistic particles and added context to the previously reported term: “sub-GLEs”.² Moreover, most recently similar work has taken place for Solar Orbiter/HET and showed that particles up until ~890 MeV can be recorded, with most trusted ones reaching ~300 MeV. Both SOHO/EPHIN and Solo/HET measurements have been used in the identification of GLE73 (see Kouloumvakos et al. 2023). In addition, measurements from Payload for Antimatter Matter

² See details in <https://www.issibern.ch/teams/heroic/>.

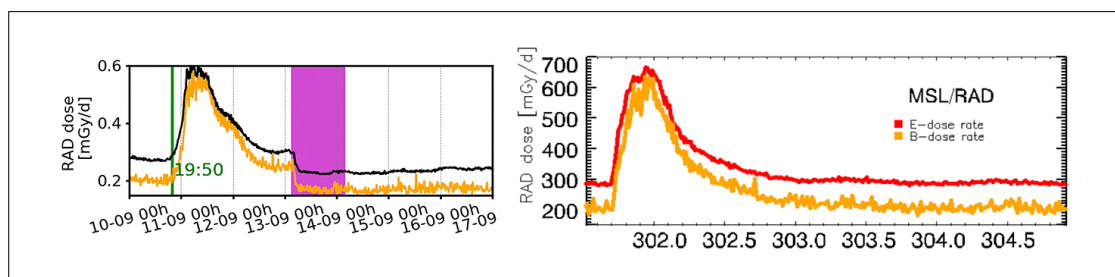


Fig. 13: Recordings of MSL/RAD at $E>150$ MeV demonstrating GLE72 (left panel; from Guo et al. 2018) and GLE73 (right panel; from Kouloumvakos et al. 2023).

Exploration and Light-nuclei Astrophysics (PAMELA) and the Alpha Magnetic Spectrometer (AMS)-02 payloads added significant information that bridges the critical gap in the spectra from the low-to-high energy particles (typically from about ~ 100 MeV to the NM range) (see e.g. Whitman et al. 2017; Bruno et al. 2018).

4.2 Recordings at different planets

100 years since the discovery of Cosmic Rays by Victor Hess in 1912, the Radiation Assessment Detector (RAD) onboard the Mars Science Laboratory (MSL) (Hassler et al. 2012) measures for the first time Cosmic Rays on the surface of another planet. This allowed us to observe solar particles reaching Mars at a few cases up to now with two of them being GLEs, i.e. GLE72 (Guo et al. 2018) and GLE73 (Kouloumvakos et al. 2023). As it can be seen in Figure 13 RAD onboard MSL on the surface of Mars recorded a distinguishable increase at both E- and B-dose rates (Hassler et al. 2012; Guo et al. 2015) for both GLEs. It should be noted that the required energy for the initiation of a proton triggering a GLE recorded by RAD located in Gale crater on Mars is $\sim E>150$ MeV (see Guo et al. 2018).

5. Future directions

5.1 GLEs as the stepping stone for super events

GLEs are hard spectrum events (Asvestari et al. 2017) and pose a significant threat for the radiation environment. Although, the Carrington event and its corresponding particle fluence were seen as the worst-case estimate of radiation hazard in the near-Earth environment that the Sun is capable of producing (Miroshnichenko & Nymmik 2014), with the help of cosmogenic radionuclide records, it became clear that much more extreme events (e.g. the event around AD774/775) might have occurred on the Sun (Miyake et al. 2012). Hence, these solar driven “super-events” are modeled on the basis of a multiplication factor of the measured GLE05 spectra. That said, GLEs provide direct context for the quantification and specification of the radiation environment during these “worst-case” scenario events.

5.2 GLEs contribution to the Sun-Earth-atmosphere system

The Sun-Earth connection is an intensive field of research for the past decades, GLEs provide a direct link to the atmospheric processes. For example, several works have focused on the ozone depletion (see the detailed work of Mironova et al. 2015) explaining the proposed mechanisms by which penetrating particles (i.e. not only of solar origin) can affect the atmosphere, including chemical changes in the upper atmo-

sphere and lower thermosphere, chemistry-dynamics feedbacks, the global electric circuit (GEC) and cloud formation. Most recently, a study by Mallios et al. (2022) proposed a model of the atmospheric electricity and its variability during strong GLEs, demonstrating that in the case of fair weather conditions, GLE events enhance the atmospheric electrical conductivity, reduce the columnar resistance, and modify the fair weather electric field, air–earth conduction current, and possibly the Ionospheric Potential (IP) in a way that depends on the geomagnetic cut-off rigidity of the location and the altitude of the observer.

6. Conclusions

An overall presentation of Ground Level Enhancements (GLEs) has been provided in this work. Their historical identification and evolution of ideas for their origin; measurements from the worldwide neutron monitor network; modeling and forecasting efforts as well as their imprint in the inner heliosphere (on space based detectors and on the surface of Mars) together with a few future research directions have been presented. Thereby, if the question is, “What do we learn from GLEs?”, the answer is that GLEs provide us with a direct link to access acceleration mechanisms at the Sun, to understand the solar storm evolution and to quantify their impact in the inner heliosphere and the near-Earth space, in particular. Additionally, GLEs pave the way for the understanding of the “worst-case” scenario for extreme SEP events and have further a direct impact on the atmospheric processes, which in turn, are directly related to the habitability of our planet and beyond.

Further contents

A Jupyter Notebook was implemented for this tutorial, accessible at: <https://github.com/atpapaio/GLE-NMDB>. It makes use of the script by C.T. Steigies ([nest.py](#)) to call NMDB and download data from the neutron monitor (NM) stations selected by the user (see also Steigies and Fuller 2023). The notebook (GLE_tutorial.ipynb) provides three plots:

- *First plot*: A percentage increase plot of the selected stations. In order to make the percentage a baseline (taken simply as the 1 hour, i.e. the first 60 minutes from the selected interval).
- *Second plot*: A plot of the North-South latitudinal anisotropy. Similar as before, in order to make the percentage a baseline (taken simply as the 1 hour, i.e. the first 60 minutes from the selected interval). Then, it makes a plot of two stations including their difference (the idea here is to directly evaluate the North-South latitudinal anisotropy. For this THULE and JBGO (or MCMU for earlier GLEs) should be selected, see also https://www.aanda.org/articles/aa/full_html/2022/04/aa42855-21/F10.html for an example).
- *Third plot*: This script provides the longitudinal anisotropy. Similar as before, in order to make the percentage a baseline (taken simply as the 1 hour, i.e. the first 60 minutes from the selected interval). The script makes a sum of all selected stations except the first one and then provides the difference between the first one and the rest of the NMs. The idea is to have all NM stations with a nominal cut-off $R_c < 1.4$ GV in order to evaluate the longitudinal anisotropy see also https://www.aanda.org/articles/aa/full_html/2022/04/aa42855-21/F11.html for an example).

Acknowledgements

I would like to gratefully acknowledge the organizers for giving me the opportunity to give this tutorial on GLEs. The never-ending continuous efforts of the Neutron Monitor community at large and the Neutron Monitor Database (NMDB) in particular, without which our knowledge and understanding would be significantly hampered, are deeply appreciated. Constructive comments by Priv. Doc. Dr. Konstantin Herbst and the Organizing Committee of the NMDB@Athens 2022 (<https://conf2022.nmdb.eu/>) significantly improved the current manuscript. Discussions and exchange of ideas with Dr Christian T. Steigies and Mr George Vasalos helped shaping the accompanied python jupyter notebook on the analysis of GLEs for this tutorial. The present work benefited from discussions within the context of the ISSI International Team 441: High Energy solar particle Events Analysis (HEROIC; <https://www.issibern.ch/teams/heroic/>).

References

- Afanasiev, A., Vainio, R., Rouillard, A. P., Battarbee, M., Aran, A., & Zucca, P. (2018). Modelling of proton acceleration in application to a ground level enhancement. *Astronomy & Astrophysics*, 614, A4, <https://doi.org/10.1051/0004-6361/201731343>
- Asvestari, E., Willamo, T., Gil, A., Usoskin, I. G., Kovaltsov, G. A., Mikhailov, V. V., & Mayorov, A. (2017). Analysis of Ground Level Enhancements (GLE): Extreme solar energetic particle events have hard spectra. *Advances in Space Research*, 60(4), 781-787, <https://doi.org/10.1016/j.asr.2016.08.043>
- Belov, A., Eroshenko, E., Mavromichalaki, H., Plainaki, C., & Yanke, V. (2005). Solar cosmic rays during the extremely high ground level enhancement on 23 February 1956. In *Annales Geophysicae* (Vol. 23, No. 6, 2281-2291). Göttingen, Germany: Copernicus Publications, <https://doi.org/10.5194/angeo-23-2281-2005>
- Benz A. O., Grigis P. C., Csillaghy A., Saint-Hilaire P. (2005). Survey on solar X-ray flares and associated coherent radio emissions. *Solar Phys* 226:121-142, <https://doi.org/10.1007/s11207-005-5254-5>
- Bieber, J. W., Clem, J., Evenson, P., Pyle, R., Sáiz, A., & Ruffolo, D. (2013). Giant ground level enhancement of relativistic solar protons on 2005 January 20. I. Spaceship Earth observations. *The Astrophysical Journal*, 771(2), 92, <https://doi.org/10.1088/0004-637X/771/2/92>
- Bombardieri, D. J., Duldig, M. L., Humble, J. E., & Michael, K. J. (2008). An improved model for relativistic solar proton acceleration applied to the 2005 January 20 and earlier events. *The Astrophysical Journal*, 682(2), 1315, <https://doi.org/10.1086/589494>
- Bruno, A., Bazilevskaia, G. A., Boezio, M., Christian, E. R., de Nolfo, G. A., et al. (2018). Solar energetic particle events observed by the PAMELA mission. *The Astrophysical Journal*, 862(2), 97, <https://doi.org/10.3847/1538-4357/aacc26>
- Bütikofer, R., Flückiger, E. O., Desorgher, L., & Moser, M. R. (2008). The extreme solar cosmic ray particle event on 20 January 2005 and its influence on the radiation dose rate at aircraft altitude. *Science of the total environment*, 391(2-3), 177-183, <https://doi.org/10.1016/j.scitotenv.2007.10.021>
- Bütikofer, R., Agueda, N., Heber, B., Galsdorf, D., & Vainio, R. (2016). Assessment of Source and Transport Parameters of Relativistic SEPs Based on Neutron Monitor Data. arXiv preprint, <https://doi.org/10.48550/arXiv.1612.08922>
- Bütikofer, R. (2018). Cosmic ray particle transport in the Earth's magnetosphere. *Solar Particle Radiation Storms Forecasting and Analysis: The HESPERIA HORIZON 2020 Project and Beyond*, 79-94, https://doi.org/10.1007/978-3-319-60051-2_5
- Cane, H. V., Reames, D. V., & Von Rosenvinge, T. T. (1988). The role of interplanetary shocks in the longitude distribution of solar energetic particles. *Journal of Geophysical Research: Space Physics*, 93(A9), 9555-9567, <https://doi.org/10.1029/JA093iA09p09555>
- Cane, H. V., & Lario, D. (2006). An introduction to CMEs and energetic particles. *Space science reviews*, 123(1-3), 45-56, https://doi.org/10.1007/978-0-387-45088-9_4
- Cliwer, E. W., & Herbst, K. (2018). Evolution of the sunspot number and solar wind B time series. *Space Science Reviews*, 214(2), 56, <https://doi.org/10.1007/s11214-018-0487-4>
- Cohen, C. M. S., & Mewaldt, R. A. (2018). The ground level enhancement event of September 2017 and other large solar energetic particle events of Cycle 24. *Space Weather*, 16(10), 1616-1623, <https://doi.org/10.1029/2018SW002006>

- Cramp, J. L., Duldig, M. L., Flückiger, E. O., Humble, J. E., Shea, M. A., & Smart, D. F. (1997). The October 22, 1989, solar cosmic ray enhancement: An analysis of the anisotropy and spectral characteristics. *Journal of Geophysical Research: Space Physics*, 102(A11), 24237-24248, <https://doi.org/10.1029/97JA01947>
- Ellison, D. C., & Ramaty, R. (1985). Shock acceleration of electrons and ions in solar flares. *The Astrophysical Journal*, 298, 400-408, <https://doi.org/10.1086/163623>
- Forbush, S. E. (1946). Three unusual cosmic-ray increases possibly due to charged particles from the Sun. *Physical Review*, 70(9-10), 771, <https://doi.org/10.1103/PhysRev.70.771>
- Flückiger, E. O., & Kobel, E. (1990). Aspects of combining models of the Earth's internal and external magnetic field. *Journal of geomagnetism and geoelectricity*, 42(9), 1123-1136, <https://doi.org/10.5636/jgg.42.1123>
- Flückiger, E. O., Moser, M. R., Pirard, B., Bütikofer, R., & Desorgher, L. (2008). A parameterized neutron monitor yield function for space weather applications. In *International Cosmic Ray Conference (Vol. 1, 289-292)*, ID1182 (last accessed September 14, 2023)
- Gopalswamy, N., Xie, H., Yashiro, S., Akiyama, S., Mäkelä, P., & Usoskin, I. G. (2012). Properties of ground level enhancement events and the associated solar eruptions during solar cycle 23. *Space Science Reviews*, 171, 23-60, <https://doi.org/10.1007/s11214-012-9890-4>
- Guo, J., Zeitlin, C., Wimmer-Schweingruber, R. F., et al. (2015). Modeling the variations of dose rate measured by RAD during the first MSL Martian year: 2012-2014. *The Astrophysical Journal*, 810(1), 24, <https://doi.org/10.1088/0004-637X/810/1/24>
- Guo, J., Dumbović, M., Wimmer-Schweingruber, R. F., et al. (2018). Modeling the evolution and propagation of 10 September 2017 CMEs and SEPs arriving at Mars constrained by remote sensing and in situ measurement. *Space Weather*, 16(8), 1156-1169, <https://doi.org/10.1029/2018SW001973>
- Hassler, D. M., Zeitlin, C., Wimmer-Schweingruber, R. F., et al. (2012). The radiation assessment detector (RAD) investigation. *Space science reviews*, 170, 503-558, <https://doi.org/10.1007/s11214-012-9913-1>
- Herbst K. (2021). Exploring the Radiation and Particle Environment of Cool Stars and Their Impact on (Exo) Planetary Habitability, Habilitation Thesis, Christian-Albrechts-Universität zu Kiel.
- Kiselev, V. I., Meshalkina, N. S., & Grechnev, V. V. (2022). Relationships Between the Spectra of Near-Earth Proton Enhancements, Hard X-Ray Bursts, and CME Speeds. *Solar Physics*, 297(5), 53, <https://doi.org/10.1007/s11207-022-01986-7>
- Klein, K. L. (2021a). Radio astronomical tools for the study of solar energetic particles I. Correlations and diagnostics of impulsive acceleration and particle propagation. *Frontiers in Astronomy and Space Sciences*, 7, 580436, <https://doi.org/10.3389/fspas.2020.580436>
- Klein, K. L. (2021b). Radio Astronomical Tools for the Study of Solar Energetic Particles II. Time-Extended Acceleration at Subrelativistic and Relativistic Energies. *Frontiers in Astronomy and Space Sciences*, 7, 580436, <https://doi.org/10.3389/fspas.2020.580445>
- Klein, K. L., Musset, S., Vilmer, N., et al. (2022). The relativistic solar particle event on 28 October 2021: Evidence of particle acceleration within and escape from the solar corona. *Astronomy & Astrophysics*, 663, A173, <https://doi.org/10.1051/0004-6361/202243903>
- Kouloumvakos, A., Papaioannou, A., Vainio, R., Waterfall, C.O., Dalla, S., et al. (2023). The multi-spacecraft solar particle event on 28 October 2021. *Astronomy & Astrophysics*, under review.
- Kühl, P., Dresing, N., Heber, B., & Klassen, A. (2017). Solar energetic particle events with protons above 500 MeV between 1995 and 2015 measured with SOHO/EPHIN. *Solar Physics*, 292, 1-13, <https://doi.org/10.1007/s11207-016-1033-8>
- Kuwabara, T., Bieber, J. W., Clem, J., Evenson, P., & Pyle, R. (2006). Development of a ground level enhancement alarm system based upon neutron monitors. *Space Weather*, 4(10), <https://doi.org/10.1029/2006SW000223>
- Mallios, S. A., Papaioannou, A., Herbst, K., Papangelis, G., & Hloupis, G. (2022). Study of the Ground Level Enhancements effect on atmospheric electric properties and mineral dust particle charging. *Journal of Atmospheric and Solar-Terrestrial Physics*, 233, 105871, <https://doi.org/10.1016/j.jastp.2022.105871>
- Mavromichalaki, H., Papaioannou, A., Plainaki, C., et al. (2011). Applications and usage of the real-time Neutron Monitor Database. *Advances in Space Research*, 47(12), 2210-2222, <https://doi.org/10.1016/j.asr.2010.02.019>
- McCracken, K. G., Moraal, H., & Shea, M. A. (2012). The high-energy impulsive ground-level enhancement. *The Astrophysical Journal*, 761(2), 101, <https://doi.org/10.1088/0004-637X/761/2/101>
- Meyer, P., Parker, E. N., & Simpson, J. A. (1956). Solar cosmic rays of February, 1956 and their propagation through interplanetary space. *Physical Review*, 104(3), 768, <https://doi.org/10.1103/PhysRev.104.768>
- Mewaldt, R. A., Lopper, M. D., Cohen, C. M. S., et al. (2012). Energy spectra, composition, and other properties of ground-level events during solar cycle 23. *Space Science Reviews*, 171, 97-120, <https://doi.org/10.1007/s11214-012-9884-2>
- Mironova, I. A., Aplin, K. L., Arnold, F., et al. (2015). Energetic particle influence on the Earth's atmosphere. *Space science reviews*, 194, 1-96, <https://doi.org/10.1007/s11214-015-0185-4>

- Miroshnichenko, L. I. (2001). *Solar cosmic rays* (Vol. 2). Dordrecht/Boston: Kluwer Academic Publishers, <https://doi.org/10.1007/978-94-015-9646-6>
- Miroshnichenko, L. I., & Nymmik, R. A. (2014). Extreme fluxes in solar energetic particle events: Methodological and physical limitations. *Radiation Measurements*, 61, 6-15, <https://doi.org/10.1016/j.radmeas.2013.11.010>
- Mikić, Z., & Lee, M. A. (2006). An introduction to theory and models of CMEs, shocks, and solar energetic particles. *Coronal Mass Ejections*, 57-80, https://doi.org/10.1007/978-0-387-45088-9_5
- Mishev, A. L., Usoskin, I. G., & Kovaltsov, G. A. (2013). Neutron monitor yield function: New improved computations. *Journal of Geophysical Research: Space Physics*, 118(6), 2783-2788, <https://doi.org/10.1002/jgra.50325>
- Mishev, A., Usoskin, I., Raukunen, O., Paassilta, M., Valtonen, E., Kocharov, L., & Vainio, R. (2018). First analysis of ground-level enhancement (GLE) 72 on 10 September 2017: Spectral and anisotropy characteristics. *Solar Physics*, 293, 1-15, <https://doi.org/10.1007/s11207-018-1354-x>
- Mishev, A., & Usoskin, I. (2020). Current status and possible extension of the global neutron monitor network. *Journal of Space Weather and Space Climate*, 10, 17, <https://doi.org/10.1051/swsc/2020020>
- Mishev, A. L., & Velinov, P. I. Y. (2020). Ionization effect in the Earth's atmosphere during the sequence of October–November 2003 Halloween GLE events. *Journal of Atmospheric and Solar-Terrestrial Physics*, 211, 105484, <https://doi.org/10.1016/j.jastp.2020.105484>
- Mishev, A. L., Koldobskiy, S. A., Kovaltsov, G. A., Gil, A., & Usoskin, I. G. (2020). Updated neutron monitor yield function: Bridging between in situ and ground based cosmic ray measurements. *Journal of Geophysical Research: Space Physics*, 125(2), e2019JA027433, <https://doi.org/10.1029/2019JA027433>
- Mishev, A. L., Kocharov, L. G., Koldobskiy, S. A., Larsen, N., Riihonen, E., Vainio, R., & Usoskin, I. G. (2022). High-resolution spectral and anisotropy characteristics of solar protons during the GLE N° 73 on 28 October 2021 derived with neutron-monitor data analysis. *Solar Physics*, 297(7), 88, <https://doi.org/10.1007/s11207-022-02026-0>
- Miyake, F., Nagaya, K., Masuda, K., & Nakamura, T. (2012). A signature of cosmic-ray increase in AD 774–775 from tree rings in Japan. *Nature*, 486(7402), 240-242, <https://doi.org/10.1038/nature11123>
- Moraal, H., & McCracken, K. G. (2012). The time structure of ground level enhancements in solar cycle 23. *Space Science Reviews*, 171, 85-95, <https://doi.org/10.1007/s11214-011-9742-7>
- Paassilta, M., Raukunen, O., Vainio, R., et al. (2017). Catalogue of 55–80 MeV solar proton events extending through solar cycles 23 and 24. *Journal of Space Weather and Space Climate*, 7, A14, <https://doi.org/10.1051/swsc/2017013>
- Papaioannou, A., Souvatzoglou, G., Paschalis, P., Gerontidou, M., & Mavromichalaki, H. (2014). The first ground-level enhancement of solar cycle 24 on 17 May 2012 and its real-time detection. *Solar Physics*, 289, 423-436, <https://doi.org/10.1007/s11207-013-0336-2>
- Papaioannou, A., Kouloumvakos, A., Mishev, A., et al. (2022). The first ground-level enhancement of solar cycle 25 on 28 October 2021. *Astronomy & Astrophysics*, 660, L5, <https://doi.org/10.1051/0004-6361/202142855>
- Plainaki, C., Belov, A., Eroshenko, E., Mavromichalaki, H., & Yanke, V. (2007). Modeling ground level enhancements: Event of 20 January 2005. *Journal of Geophysical Research: Space Physics*, 112(A4), <https://doi.org/10.1029/2006JA011926>
- Plainaki, C., Mavromichalaki, H., Belov, A., Eroshenko, E., Andriopoulou, M., & Yanke, V. (2010). A new version of the Neutron monitor based anisotropic GLE model: application to GLE60. *Solar Physics*, 264, 239-254, <https://doi.org/10.1007/s11207-010-9576-6>
- Poluianov, S. V., Usoskin, I. G., Mishev, A. L., Shea, M. A., & Smart, D. F. (2017). GLE and sub-GLE redefinition in the light of high-altitude polar neutron monitors. *Solar Physics*, 292(11), 176, <https://doi.org/10.1007/s11207-017-1202-4>
- Poluianov, S., & Batalla, O. (2022). Cosmic-ray atmospheric cutoff energies of polar neutron monitors. *Advances in Space Research*, 70(9), 2610-2617, <https://doi.org/10.1016/j.asr.2022.03.037>
- Reames, D. V. (2009). Solar energetic-particle release times in historic ground-level events. *The Astrophysical Journal*, 706(1), 844, <https://doi.org/10.1088/0004-637X/706/1/844>
- Rodriguez, J., & Kress, B. (2023). GOES Observations of Solar Protons during Ground Level Enhancements, this volume, <https://doi.org/10.38072/2748-3150/p32>
- Shea, M. A., & Smart, D. F. (1982). Possible evidence for a rigidity-dependent release of relativistic protons from the solar corona. *Space Science Reviews*, 32, 251-271, <https://doi.org/10.1007/BF00225188>
- Smart, D. F., Shea, M. A., & Flückiger, E. O. (2000). Magnetospheric models and trajectory computations. In *Cosmic Rays and Earth: Proceedings of an ISSI Workshop*, 21–26 March 1999, Bern, Switzerland (305-333). Springer Netherlands, <https://doi.org/10.1023/A:1026556831199>
- Souvatzoglou, G., Papaioannou, A., Mavromichalaki, H., Dimitroulakos, J., & Sarlanis, C. (2014). Optimizing the real time ground level enhancement alert system based on neutron monitor measurements: Introducing GLE Alert Plus. *Space Weather*, 12(11), 633-649, <https://doi.org/10.1002/2014SW001102>

- Steigies C.T. and Fuller N. (2023). Accessing NMDB data using NEST and pandas, this volume, <https://doi.org/10.38072/2748-3150/p44>
- Temmer, M. (2021). Space weather: the solar perspective: An update to Schwenn (2006). *Living Reviews in Solar Physics*, 18(1), 4, <https://doi.org/10.12942/lrsp-2006-2>
- Tsyganenko, N. A. (1989). A magnetospheric magnetic field model with a warped tail current sheet. *Planetary and Space Science*, 37(1), 5-20, [https://doi.org/10.1016/0032-0633\(89\)90066-4](https://doi.org/10.1016/0032-0633(89)90066-4)
- Usoskin, I., Koldobskiy, S., Kovaltsov, G. A., Gil, A., Usoskina, I., Willamo, T., & Ibragimov, A. (2020). Revised GLE database: Fluences of solar energetic particles as measured by the neutron-monitor network since 1956. *Astronomy & Astrophysics*, 640, A17, <https://doi.org/10.1051/0004-6361/202038272>
- Vainio, R., & Laitinen, T. (2007). Monte Carlo simulations of coronal diffusive shock acceleration in self-generated turbulence. *The Astrophysical Journal*, 658(1), 622, <https://doi.org/10.1086/510284>
- Vainio, R., Valtonen, E., Heber, B., et al. (2013). The first SEP Server event catalogue~ 68-MeV solar proton events observed at 1 AU in 1996–2010. *Journal of space weather and space climate*, 3, A12, <https://doi.org/10.1051/swsc/2013030>
- Vashenyuk, E. V., Balabin, Y. V., & Gvozdevsky, B. B. (2011). Features of relativistic solar proton spectra derived from ground level enhancement events (GLE) modeling. *sAstrophysics and Space Sciences Transactions*, 7(4), 459-463, <https://doi.org/10.5194/astra-7-459-2011>
- Vlahos, L., Anastasiadis, A., Papaioannou, A., Kouloumvakos, A., & Isliker, H. (2019). Sources of solar energetic particles. *Philosophical Transactions of the Royal Society A*, 377(2148), 20180095, <https://doi.org/10.1098/rsta.2018.0095>
- Vourlidas, A. (2021). Improving the Medium-Term Forecasting of Space Weather: A Big Picture Review From a Solar Observer's Perspective. *Frontiers in Astronomy and Space Sciences*, 8, 651527, <https://doi.org/10.3389/fspas.2021.651527>
- Whitman, K., Bindi, V., Consolandi, C., Corti, C., & Yamashiro, B. (2017). Implications of improved measurements of the highest energy SEPs by AMS and PAMELA. *Advances in Space Research*, 60(4), 768-780, <https://doi.org/10.1016/j.asr.2017.02.042>
- Wild, J. P., Smerd, S. F., & Weiss, A. A. (1963). Solar bursts. *Annual Review of Astronomy and Astrophysics*, 1(1), 291-366, <https://doi.org/10.1146/annurev.aa.01.090163.001451>
- Yashiro, S., Akiyama, S., Gopalswamy, N., & Howard, R. A. (2006). Different power-law indices in the frequency distributions of flares with and without coronal mass ejections. *The Astrophysical Journal*, 650(2), L143, <https://doi.org/10.1086/508876>

Open Access

This paper is published under the Creative Commons Attribution 4.0 International license (<https://creativecommons.org/licenses/by/4.0/>). Please note that individual, appropriately marked parts of the paper may be excluded from the license mentioned or may be subject to other copyright conditions. If such third party material is not under the Creative Commons license, any copying, editing or public reproduction is only permitted with the prior consent of the respective copyright owner or on the basis of relevant legal authorization regulations.

Session 2: Abstracts

Cosmic rays and space weather

Maria Abunina 





Correspondence

IZMIRAN - Pushkov Institute of Terrestrial Magnetism, Ionosphere and Radiowave Propagation, Moscow, Russia

Abstract

When we speak on Space Weather we are commonly meaning the radiation and electromagnetic conditions in the near Earth space. Cosmic ray variations define directly a radiation situation. And they are also related to the variations of electromagnetic conditions in the interplanetary space and Earth's magnetosphere. This makes cosmic ray variation one of the important recourses for validating the space weather state and forecasting its changes. Cosmic ray observations till now are not sufficiently used in the space weather tasks. The main reason of such inefficiency is inaccessibility of different cosmic ray data for an operative analysis. Fortunately, this situation is now changing fast to the better. In particular, data from 26 ground level cosmic ray stations now are available in real time. It gives a hope that in the nearest years we shall see more wide and effective use of the cosmic ray characteristics for space weather forecasting.

Solar activity as observed by neutron monitors and muon telescopes in the same location

Juan José Blanco , Alejandro López-Comazzi , Ignacio García Tejedor , Sindulfo Ayuso ,
Óscar García Población 

Correspondence

Department of Physics and Mathematics, University of Alcalá, Madrid, Spain

Abstract

In this paper we present the advantage of observing solar activity with neutron monitors and muon telescopes operated from the same location. This combination of detectors multiplies the information that would be collected with only one of these instruments. Not only the observation of different types of secondary cosmic rays but also the observation at different energy thresholds with some information on the directionality of muons. As an example of the above, we analyze the GLE73 and the Forbush decrease associated with the same solar event.

Solar energetic particle event on 28 October 2021 as observed by the neutron monitor network

Rolf Bütikofer ¹, Christian T. Steigies ²


Correspondence

- 1 International Foundation “High Altitude Research Stations Jungfrauoch and Gornergrat” and Physics Institute, University of Bern, Switzerland
- 2 Extraterrestrial Physics, Institute of Experimental and Applied Physics, Kiel University, Germany

Abstract

The first solar energetic particle event during the current solar cycle 25 observed on ground, i.e. GLE#73, was detected on 28 October 2021 by a few neutron monitors of the worldwide network. Although GLE#73 showed only a small, gradual increase in the cosmic ray intensity near Earth, the Athens GLE Alert system issued successfully an automatic alert at 16:09 UT. We present the outcome of our GLE analysis of this SEP event based on neutron monitor data and assess the additional radiation doses that may be acquired at different locations at a typical flight altitude. In addition, we compare our results with the findings published by Mishev et al. 2022.

40 years of solar neutron observations from ground

Erwin O. Flückiger, Rolf Bütikofer 

Correspondence

International Foundation “High Altitude Research Stations Jungfrauoch and Gornergrat” and Physics Institute, University of Bern, Switzerland

Abstract

In association with the X8 /2B solar flare on 3 June 1982, the neutron monitors at Jungfrauoch, Lomnický štít, and Rome were the only ones in the worldwide neutron monitor network to record simultaneously a short, small increase in the counting rate. The analysis of these records and of observations of solar electromagnetic emissions implied that these count rate increases were due to the impact of high energy solar neutrons into the Earth’s atmosphere. This first observation of terrestrial effects by neutrons of solar origin not only provided supporting evidence for a theory pointed out by Biermann et al. in 1951, but it triggered an intense activity in the theoretical study of particle acceleration and emissions in high-energy processes at the Sun, as well as in the development of dedicated solar neutron detectors. The establishment of global networks

of such detectors enables the detection of an eventual solar neutron event around the clock. In addition, the identified need for real-time data with high time resolution initiated the Neutron Monitor Data Base, NMDB. The presentation gives a historical overview of the 3 June 1982 event and summarizes its main scientific impact over the last 40 years.

A relationship between rise times and decay times of relativistic solar particle events observed by neutron monitors

Karl-Ludwig Klein¹, Sophie Musset², Nicolas Fuller¹, Gaelle Khreich¹, Antonin Wargnier¹

Correspondence



1 Observatoire de Paris, Université Paris Sciences et Lettres, Paris, France

2 European Space Research and Technology Centre, ESA/ESTEC, Noordwijk, The Netherlands

Abstract

The most energetic particles accelerated in solar eruptive events are protons with energies up to a few tens of GeV (ground level enhancements, GLEs). Their study is relevant on the one hand because the high particle energies pose particularly strong challenges on the understanding of the acceleration processes. On the other hand, the secondary particles from the atmospheric cascade constitute a source of irradiation in the atmosphere that may temporarily exceed the permanent dose rate from galactic cosmic rays. The monitoring of radiation doses received by aircrew from GLEs is one issue of space weather services for aviation, which since 2019 has also been established as a permanent real-time service for international aviation under the auspices of the United Nations agency ICAO. In this contribution we report an empirical investigation of the rise times and decay times of historical GLEs, focussing on the time profile (corrected to sea-level) observed by the neutron monitor of the worldwide network with the strongest response, which is presumably best-connected to the Sun by the interplanetary magnetic field at the time of the event. Data from the neutron monitor database (<https://www.nmdb.eu/>) at the University of Kiel (Germany) and the GLE database at the University of Oulu (<https://gle oulu.fi/#/>), Finland are used. As previous studies by Strauss and coworkers (Solar Phys. 2017) we find an empirical correlation between the observed rise times and decay times of the neutron monitor count rate profiles. We identify possible evidence of different types of events and compare them with previous work (Vashenyuk, McCracken, Moraal and coworkers) on the contribution of prompt and delayed particle releases to GLEs. Ideas on the origin of the relationship between rise times and decay times and on its usefulness for space weather services will be discussed.

A new reconstruction of solar energetic particle fluence for GLE events

Sergey Koldobskiy ¹, Osku Raukunen ^{2,3}, Rami Vainio ², Gennady Kovaltsov ¹, Ilya Usoskin ¹






Correspondence

- 1 Space Physics and Astronomy, Faculty of Science, University of Oulu, Finland
- 2 Department of Physics and Astronomy, University of Turku, Finland
- 3 Aboa Space Research Oy, Turku, Finland

Abstract

A ground level enhancement (GLE) is defined as a strong event with high-energy solar energetic particles (SEPs) detected by the network of ground-based neutron monitors. Until now, 73 GLEs have been registered. In this work, we report a new reconstruction of the event-integrated spectra (fluences) of SEPs during 59 moderate and strong GLE events detected by NM network and satellite experiments. The reconstructions of SEP fluences are based on the "bow-tie" method employing the latest advances in NM data analysis (time-dependent GCR background and the use of the altitude-dependent NM yield function directly verified with the AMS-02 experiment data) and a detailed study of different uncertainties. As a result of this work, we obtained fluences of SEPs in the energy range from 30 MeV to a few GeV for GLE events since 1956, which were fitted with the modified Band-function (a double power-law function with two exponential cutoffs). An easy-to-use presentation of SEP fluences in the form of an analytical expression makes a solid basis for new studies in various fields, such as the influence of SEPs on the atmosphere and a statistical study of extreme solar activity.

Magnetic field line path length variations and effects on solar energetic particle transport

Alejandro Sáiz ¹, Wirin Sonsrettee ², Piyanate Chuychai ³, Achara Seripientert ⁴, Paisan Tooprakai ⁵, David Ruffolo ¹, William Matthaeus ⁶, Rohit Chhiber ⁶

Correspondence

- 1 Department of Physics, Faculty of Science, Mahidol University, Bangkok, Thailand
- 2 Panyapiwat Institute of Management, Faculty of Engineering and Technology, Pak Kret, Thailand
- 3 Independent scholar, Thailand
- 4 NARIT - National Astronomical Research Institute of Thailand, Chiang Mai, Thailand
- 5 Department of Physics, Faculty of Science, Chulalongkorn University, Bangkok, Thailand
- 6 Bartol Research Institute and Department of Physics and Astronomy, University of Delaware, Newark, USA

Abstract

Modeling of time profiles of solar energetic particle (SEP) observations typically considers transport along a large-scale magnetic field with a fixed pathlength from the source to the observer. Chhiber et al. (2021) pointed out that the path length along a turbulent magnetic field line is longer than that along the large scale field, and that the path along the particle gyro-orbit can be substantially longer again; they also considered the global variation in these quantities. Here we point out that variability in the turbulent field line path length can affect the fits to SEP data and the inferred mean free path and injection profile. To explore such variability, we perform Monte Carlo simulations in representations of homogeneous 2D MHD + slab turbulence in spherical geometry and trace trajectories of field lines, particle guiding centers, and full particle orbits, considering ion injection from a narrow or wide angular region near the Sun, corresponding to an impulsive or gradual solar event, respectively. We analyze our simulation results in terms of path length statistics within and among square-degree pixels in heliolatitude and heliolongitude at 0.35 and 1 AU from the Sun. For a given representation of turbulence, there are systematic effects on the path lengths vs. heliolatitude and heliolongitude. Field line path lengths relate to the fluctuation amplitudes experienced by the field lines, which in turn partly relate to the local topology of 2D turbulence. There are also systematic patterns in the mean path lengths of energetic particles arriving at different locations, because of variations in the underlying magnetic field line path lengths and variations in the pitch angle scattering experienced by the particles. We describe the effects of such path length variations on observed time profiles of solar energetic particles, both in terms of path length variability at specific locations and motion of the observer with respect to turbulence topology during the course of the observations. This research was partially supported by Thailand Science Research and Innovation grant RTA6280002 and the Parker Solar Probe mission under the ISOIS project (contract NNN06AA01C) and a subcontract to University of Delaware from Princeton University (SUB0000165). Additional support is acknowledged from the NASA LWS program (NNX17AB79G) and HSR program (80NSSC18K1210 & 80NSSC18K1648).

Solar energetic particle events and Forbush decreases driven by the same solar sources

Nataly Shlyk ¹, Anatoly Belov ¹, Maria Abunina , Elena Belova ¹, Artem Abunin , Athanasios Papaioannou ²

Correspondence

1 IZMIRAN - Pushkov Institute of Terrestrial Magnetism, Ionosphere and Radiowave Propagation, Moscow, Russia












2 IAASARS - Institute for Astronomy, Astrophysics, Space Applications and Remote Sensing, National Observatory of Athens, Penteli, Greece

Abstract

The characteristics of Forbush decreases (FDs) and solar energetic particle (SEP) events driven by the same solar source (i.e. coronal mass ejection & associated solar flare) are investigated. The part of the solar disk (E04–W35)

was chosen in which most of the solar events lead both to an FD and SEP event at Earth. SEPs for different energies ($E > 10$ MeV, $E > 100$ MeV, and ground level enhancements) and with different flux thresholds were considered independently. The obtained results were compared with the control group of FDs that had solar sources within the same longitudinal range but were not accompanied with any SEPs. It is shown that coronal mass ejections (CMEs) followed by SEPs have a very high probability to create a large FD in the Earth's orbit and further to cause a geomagnetic storm. It is also obtained that the accelerative and modulating efficiencies of such driving solar events are well correlated; this can be explained mostly by high speeds of the corresponding CMEs.

Investigating GLE73, the first ground level enhancement of solar cycle 25

Athanasios Papaioannou ¹, Athanasios Kouloumvakos ², Alexander Mishev ³, Rami Vainio ⁴, Ilya Usoskin ³, Konstantin Herbst ⁵, Alexis P. Rouillard ⁶, Anastasios Anastasiadis ¹, Jan Gieseler ⁴, Robert Wimmer-Schweingruber ⁵, Patrick Kühl ⁵

Correspondence

- 1 IAASARS - Institute for Astronomy, Astrophysics, Space Applications and Remote Sensing, National Observatory of Athens, Penteli, Greece, atpapaio@astro.noa.gr
- 2 The Johns Hopkins University Applied Physics Laboratory, Maryland, USA
- 3 Space Physics and Astronomy Research Unit and Sodankylä Geophysical Observatory, University of Oulu, Finland
- 4 Department of Physics and Astronomy, University of Turku, Finland
- 5 Extraterrestrial Physics, Institute of Experimental and Applied Physics, Kiel University, Germany
- 6 IRAP, Université Toulouse III-Paul Sabatier, CNRS, CNES, Toulouse, France

Abstract

We present an overview of the first ground level enhancement (GLE) event of solar cycle 25, recorded on 28 October 2021 (GLE73), based on the available neutron monitor (NM) network observations and on data from near-Earth spacecraft (GOES, SOHO, SoLd). The maximum increase was 7.3% for DOMC (Dome C NM at Concordia station) and 5.4% for SOPO (South Pole) conventional NMs located on the Antarctic plateau. Bare (lead-free) NMs at the same sites detected a higher response (14.0% for DOMB and 6.6% for SOPB). The Fort Smith (FSMT) NM shows the earliest increase among the high-latitude NMs, indicating a moderate anisotropy in the first phase of the GLE event. The maximum rigidity of accelerated protons did not exceed 2.4 GV. We estimated the solar release time (SRT) of >1 GV protons into open magnetic field lines at 15:40 UT. In-situ proton observations from near-Earth spacecraft were combined with the detection of a solar flare in soft X-rays (SXR), a coronal mass ejection (CME), radio bursts and extreme ultraviolet (EUV) observations to identify the solar origin of the GLE. Around the 1 GV proton SRT the CME-driven shock was located at a height of 2.33 Rs. The timing of the EUV wave evolution towards the field lines magnetically connected to Earth seem to be in good agreement with the inferred release time of 1 GV protons.

Session 3:

**Cosmic rays
and the atmosphere**

Atmospheric cosmic ray induced ionization and radiation affecting aviation

Panagiota Makrantonis¹, Anastasia Tezari², Argyris N. Stassinakis¹, Pavlos Paschalis¹, Maria Gerontidou¹, Helen Mavromichalaki¹, Ilya G. Usoskin³, Norma Crosby⁴, Mark Dierckxsens⁴

Correspondence

- 1 Athens Cosmic Ray Group, Faculty of Physics, National and Kapodistrian University of Athens, Greece, pmakrantonis@phys.uoa.gr, a-stassinakis@phys.uoa.gr, ppaschalis@phys.uoa.gr, mgeront@phys.uoa.gr, emavromi@phys.uoa.gr
 - 2 Eugenides Foundation, Athens, Greece, anatez@med.uoa.gr
 - 3 Space Physics and Astronomy Research Unit and Sodankylä Geophysical Observatory, University of Oulu, Finland, ilya.usoskin@oulu.fi
 - 4 Royal Belgian Institute for Space Aeronomy, Brussels, Belgium, Norma.Crosby@aeronomie.be, Mark.Dierckxsens@aeronomie.be
-

Keywords

cosmic rays; atmosphere; ionization; radiation; solar cycle; flight level; aviation

Abstract

Cosmic radiation is a major factor of ionization of the Earth's atmosphere. Both solar and galactic cosmic rays, which depend on solar activity and geomagnetic field, affect the radiation exposure in the atmosphere. Several models have been created for the estimation of the ionization and radiation dosimetry. In this work, as regards the ionization rate computations the CRAC:CR11 model by the University of Oulu (<https://cosmicrays.oulu.fi/CR11/CR11.html>) was used, while for the estimation of the ambient equivalent dose rate ($dH^*(10)/dt$) we used the validated software DYASTIMA / DYASTIMA-R by the University of Athens (<http://cosray.phys.uoa.gr/index.php/applications/dyastima>). Both tools are of great importance as they allow us to calculate the respective quantities all over the globe, at the entire atmosphere and for different time periods and solar cycle phases. The study concerns the last two solar cycles 23 and 24 (1996–2019) and specific flight levels of commercial aviation (FL310, FL350 and FL390). The dependence of CR11 and $dH^*(10)/dt$ on geomagnetic cut-off rigidity, solar activity, cosmic ray intensity, as well as the altitude inside the atmosphere, affect the radiation exposure of the air crew members and frequent flyers, which make the results very interesting for the aviation industry.

1. Introduction

Cosmic rays are highly energetic particles of extraterrestrial origin, with two main components, Galactic Cosmic Rays (GCR) which originate from outside of our Solar System and Solar Energetic Particles (SEPs) which are accelerated during eruptive processes on the Sun. As cosmic rays travel through the interplanetary space, they reach and penetrate the Earth's atmosphere, colliding with nuclei of atoms and ions of the atmosphere, creating nucleonic, muonic and electromagnetic cascades named secondary cosmic rays. Primary particles are absorbed inside the atmosphere due to ionization losses. In this way, cosmic rays affect the physical–chemical properties of the atmosphere. The Earth's magnetic field acts as a charge discriminator and modulates the cosmic ray flux that reaches each location on the Earth.

Cosmic rays contribute significantly to the atmospheric ionization (Cosmic Ray Induced Ionization – CRII). CRII is affected by the GCR and the 11-year solar cycle. Specifically, CRII is anti-correlated with the solar activity, while a significant dependence on SEPs is also observed at high latitude regions, at high altitude (Usoskin et al. 2009). The CRII may affect the Earth's climate, as many studies suggest that CRII may affect in numerous ways different climate parameters such as cloud cover, precipitation, cyclogenesis in mid- to high-latitude regions atmospheric transparency aerosol formation (Bazilevskaya et al. 2008, and references therein), the avionic electronic systems, as well as the human health of aircrews and / or passengers (Berger et al. 2008; Flückiger and Bütikofer 2011).

The major contributor to the aircrews' health is the occupational exposure to the ionizing cosmic radiation, during the flights. Aircrews and passengers are constantly exposed to the permanent GCR background, as well as to the unpredictable SEPs. Similarly, to the CRII, the radiation exposure is greater during conditions of minimum solar activity, as well as during strong events (SEPs, ground level enhancements – GLEs). For this reason, the radiation assessment of aircrews is of great importance and it can be performed by using several software tools and models.

The purpose of this work is the calculation of the CRII and the estimation of the radiation exposure of aircrews for different flying levels and different periods of solar activity. In order to perform the aforementioned calculations, the CRAC:CRII model and the DYASTIMA software have been used respectively.

2. Technical analysis and data selection

Regarding the calculations of the Cosmic Ray Induced Ionization (CRII) the CRAC:CRII model of the University of Oulu was used. CRAC:CRII is a numerical model, based on the CORSIKA code and the FLUKA Monte Carlo package, which allows extensive calculations of CRII from the Earth's surface to the upper limit of the atmosphere for every location on Earth. The computations derived from the model coincide with direct fragmentary measurements of the ionization in the atmosphere in a full range of parameters, covering all latitudes and altitudes during different solar cycle phases confirming its reliability and validity. Full details of the CRAC:CRII model are given in Usoskin and Kovaltsov (2006) and Usoskin et al. (2010).

For the calculations of the ambient dose equivalent rate $dH^*(10)/dt$, the Dynamic Atmospheric Shower Tracking Interactive Model Application (DYASTIMA) of the National and Kapodistrian University of Athens was used. The DYASTIMA software is based on Monte Carlo simulation techniques using the Geant4 toolkit (Agostinelli et al. 2003; Allison et al. 2006, 2016). It simulates air showers and cosmic ray secondary

particles cascades inside the atmosphere of a planet and it is a federated product on the ESA SWE Portal (<https://swe.ssa.esa.int/dyastima-federated>), validated according to ICRP / ICRU criteria (ICRP 2007, 2016; ICRU Report 84 2010; ESA 2019). Moreover, the radiobiological quantities were calculated with the DYASTIMA-R extension. The full details of DYASTIMA software are given in Paschalis et al. (2014) and the DYASTIMA Software User Manual (2019).

The input parameters required for the DYASTIMA / DYASTIMA-R software are the characteristics of the planet and its atmosphere, we used the International Standard Atmosphere (ISA) model (ISO 2533:1975/ISO 2007), the differential spectrum of the incoming primary cosmic ray particles at the top of the atmosphere, the ISO15390 model was used (ISO 15390:2004/ISO, 2004), the appropriate physics list, the FTFP_BERT_HP GEANT4 list was used, the magnetic field components, obtained from the National Oceanic and Atmospheric Administration (NOAA) portal (<https://www.ngdc.noaa.gov/geomag/>), the particle detection altitudes and the settings concerning the realization of dosimetric calculations.

3. Results

In this work, both the CRAC:CRII model and the DYASTIMA/DYASTIMA-R software were applied globally, from cut-off rigidity 0-17 GV, during the last two solar cycles 23 and 24, i.e. years 1996-2008, 2009-2019, and were focused on specific altitudes that correspond to the most common commercial flight levels, i.e. FL310 (9.45 km a.s.l.), FL350 (10.67 km a.s.l.), FL390 (11.89 km a.s.l.).

The results obtained are depicted on maps. [Figure 1](#) shows the CRII rate, globally, during the solar minima and maxima of the last two solar cycles, SC23 (1996-2008) and SC24 (2009-2019), at FL390, while [Figure 2](#) and [3](#) show the same quantities for FL350 and FL310 respectively. It is obvious that the CRII rate was greater during the solar minima than during the solar maxima for both solar cycles 23 and 24. This fact is due to the CRII following the cosmic ray intensity behavior with which it is positively correlated, while it is negatively correlated with the solar activity. This means that the greater the solar activity, the lower the intensity of the CRII and vice versa (Forbush 1954; Gleeson and Axford 1968; Mavromichalaki et al. 1998; Makrantonis et al. 2013, 2021, 2022).

Moreover, if we compare the values of solar cycles 23 and 24, it is clear that during both the solar minima and maxima they were greater during solar cycle 24 than these of solar cycle 23. This coincides with the fact that solar cycle 24 was a quiet solar cycle, while solar cycle 23 was a very active one. As depicted on the maps, it is observed that, at polar regions the ionization rate has maximum values, while at equatorial regions, the ionization rate has minimum values. Responsible for this is the magnetic field of the Earth and thus the different geomagnetic cut-off rigidity (R_c) that corresponds to each location. At polar regions, where the geomagnetic cut-off rigidity is lower ($R_c=0$ GV), more cosmic rays penetrate the magnetosphere and the atmosphere of the Earth, which lead to atmospheric ionization, than at equatorial regions, where the geomagnetic cut-off rigidity is greater ($R_c=17$ GV). All the aforementioned maps were generated via the rigidity maps of Smart and Shea (2007a; 2007b; 2019) and (Gerontidou et al. 2021).

Comparing the maps for FL390 in [Figure 1](#), with the respective maps for FL350 in [Figure 2](#) and FL310 in [Figure 3](#), it is evident that the CRII rate significantly increases with altitude, as expected up to the Regener-Pfotzer maximum. More to that, the same pattern between the two solar cycles is observed; the CRII rate is higher during solar cycle 24 where the solar activity is lower.

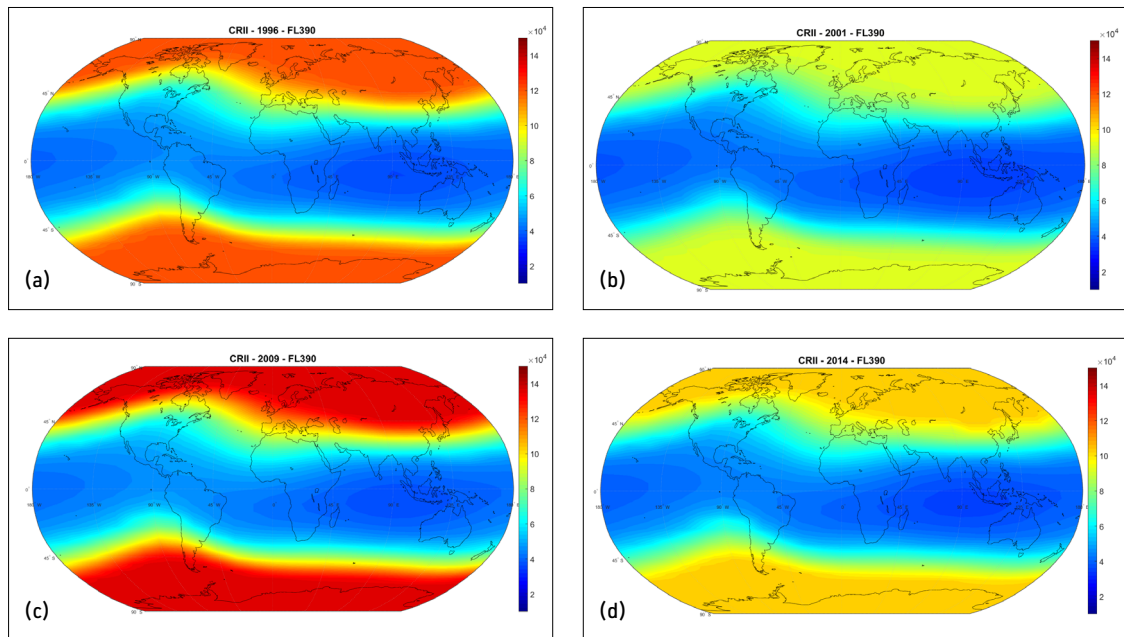


Fig. 1: Maps of CRII rate (ion pairs/(g*s)) at FL390: (a) during the minimum of solar cycle 23; (b) during the maximum of solar cycle 23; (c) during the minimum of solar cycle 24; (d) during the maximum of solar cycle 24.

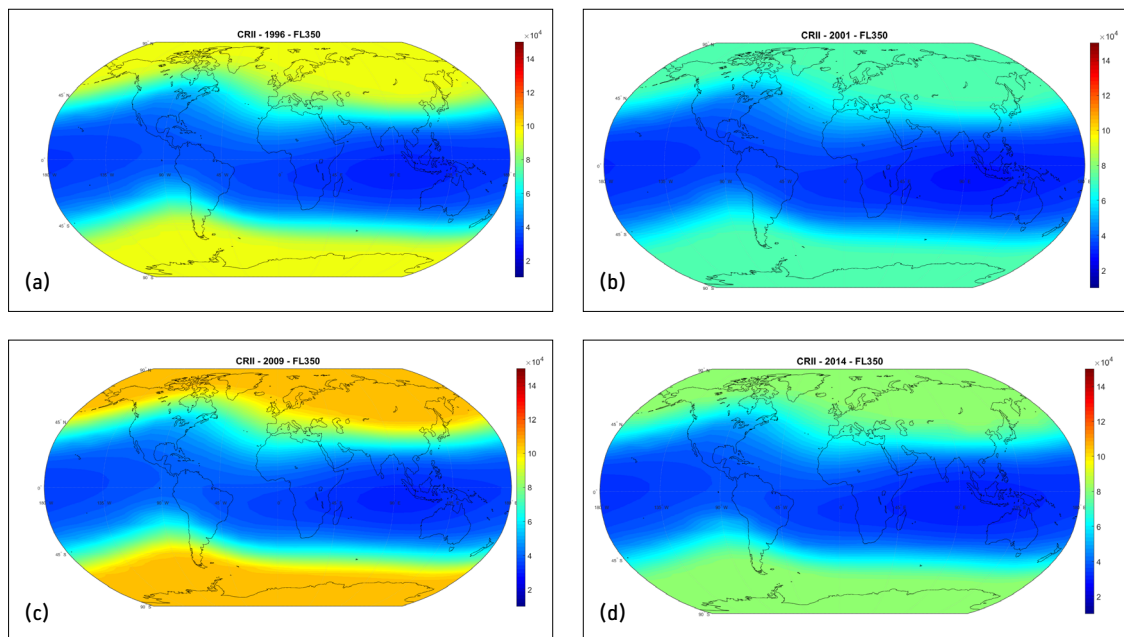


Fig. 2: Maps of CRII rate (ion pairs/(g*s)) at FL350: (a) during the minimum of solar cycle 23; (b) during the maximum of solar cycle 23; (c) during the minimum of solar cycle 24; (d) during the maximum of solar cycle 24.

The ambient dose equivalent rate during the solar minimum and maximum of solar cycle 23 at all three FLs is presented in Figures 4 and 5 respectively. The dependence of the radiation levels on the cosmic ray intensity at the different atmospheric altitudes (Tezari et al. 2020, 2022), eventuates in the $dH^*(10)/dt$ behaving the same way as CRII does, i.e., minimum values are found at equatorial regions

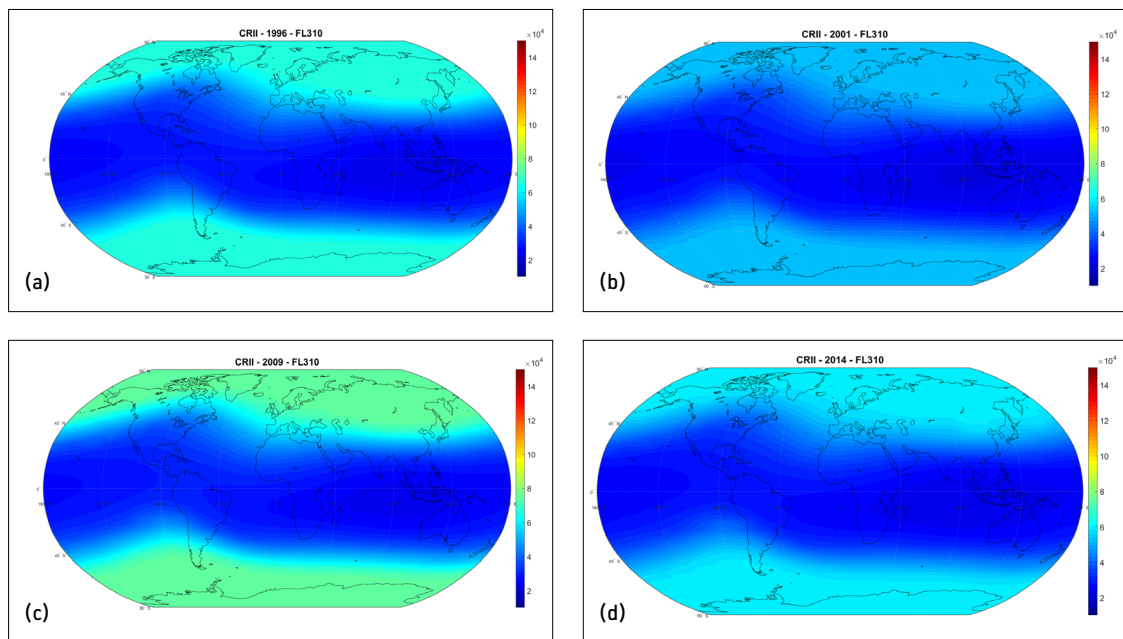


Fig. 3: Maps of CRII rate (ion pairs/(g*s)) at FL310: (a) during the minimum of solar cycle 23; (b) during the maximum of solar cycle 23; (c) during the minimum of solar cycle 24; (d) during the maximum of solar cycle 24.

($R_c=15-17$ GV) whereas maximum values at polar regions ($R_c=0-2$ GV). Furthermore, it is observed that the radiation exposure during the solar minimum was greater than that during the solar maximum, due to the negative correlation between the intensity of the incoming cosmic ray particles and the solar activity. Once again, comparing the maps of the three flight levels, it is evident that the ambient dose equivalent rate also significantly increases with altitude.

Figure 6 presents time profiles of the annual values of CRII rate and ambient dose equivalent rate for the same period of time (year 1996 to 2019) for the three typical FLs and for four different geomagnetic cut-off rigidities (0.1 GV, 3.1 GV, 8.5 GV and 14.9 GV). It is observed that both CRII rate (blue lines, left axis) and ambient dose equivalent rate (red lines, right axis) follow an 11-year modulation, at all the locations, the same way the Galactic Cosmic Ray intensity does (Makrantonis et al. 2021, 2022; Tezari et al. 2022; Mavromichalaki et al. 1995), as the intensity of the cosmic radiation directly affects the radiation exposure of the aircrew.

Moreover, as regards the time profiles of the three different flight levels, we observe that the CRII and ambient dose equivalent rates increase as the flight level of the aircraft increases. This is due to the fact that the shielding effect of the atmosphere reduces with height and consequently the radiation exposure of the aircrew and frequent flyers is higher. Additionally, it is noted that the difference among the values of the three FLs is larger towards lower rigidities, i.e., polar regions, and reduces towards higher rigidities, i.e., equatorial regions. Specifically, regarding the CRII, it is observed that during all phases of solar cycle 23, the values were smaller than those of the respective phases of solar cycle 24, eventuated from the fact that solar cycle 23 was very active whereas solar cycle 24 was a quiet one. Nonetheless, as one reaches equatorial regions, this difference becomes very small, which indicates that mostly low-rigidity regions are affected by solar activity.

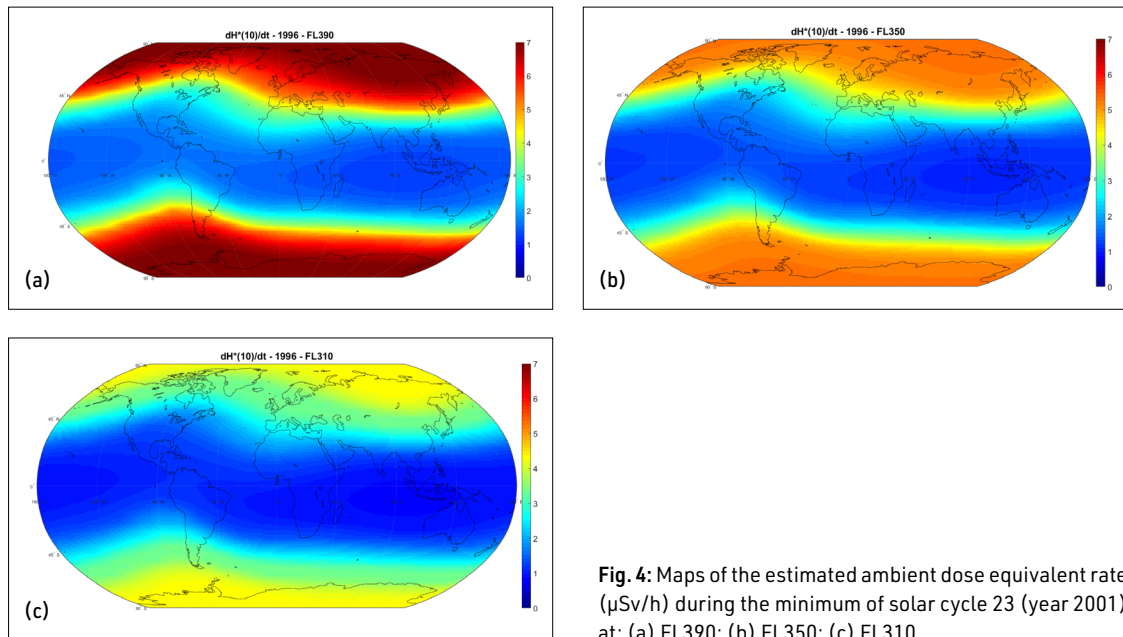


Fig. 4: Maps of the estimated ambient dose equivalent rate ($\mu\text{Sv/h}$) during the minimum of solar cycle 23 (year 2001) at: (a) FL390; (b) FL350; (c) FL310.

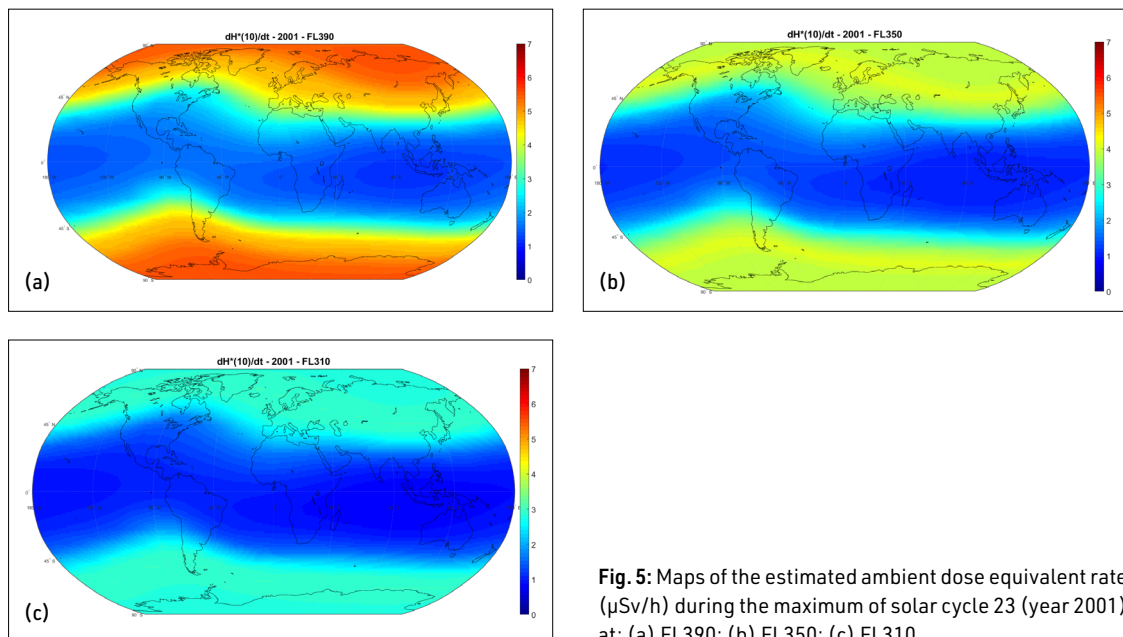


Fig. 5: Maps of the estimated ambient dose equivalent rate ($\mu\text{Sv/h}$) during the maximum of solar cycle 23 (year 2001) at: (a) FL390; (b) FL350; (c) FL310.

The correlation between the annual distribution of the CRII and the $dH^*(10)/dt$ for all four rigidities mentioned before, for all three FLs, from 1996 to 2019, is illustrated in [Figure 7](#). We observe a positive correlation between these two physical quantities, with a correlation coefficient of $R^2=0.97$. This confirms the contribution of CRII to the radiation deposited at different locations and altitudes.

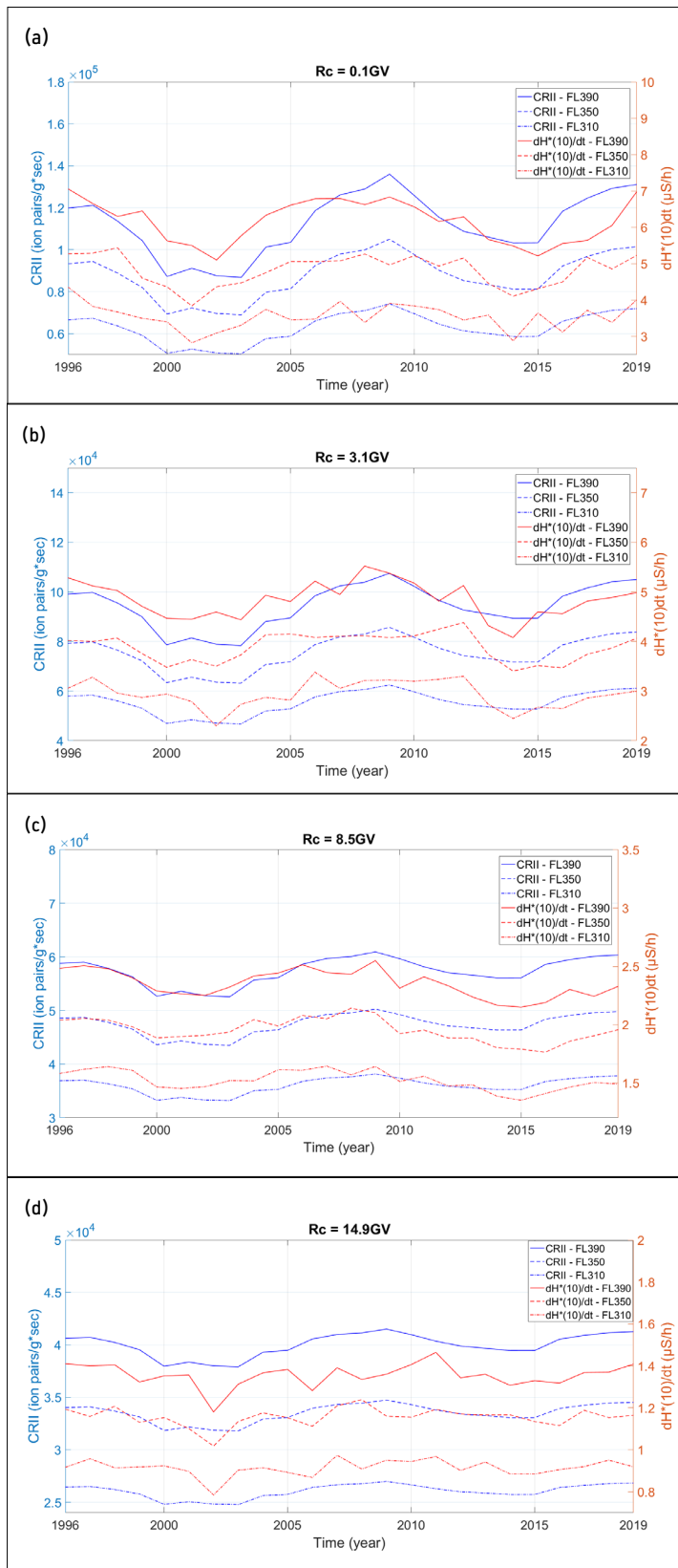


Fig. 6: Annual distribution of the CRII rate (left axis, blue lines) and ambient dose equivalent rate (right axis, red lines) at three different flight levels (FL310, FL350, FL390), during solar cycles 23 and 24 (years 1996–2019): (a) at a polar region with cut-off rigidity 0.1 GV; (b) a region with cut-off rigidity 3.1 GV; (c) at a region with cut-off rigidity 8.5 GV (Athens); (d) an equatorial region with cut-off rigidity 14.9 GV.

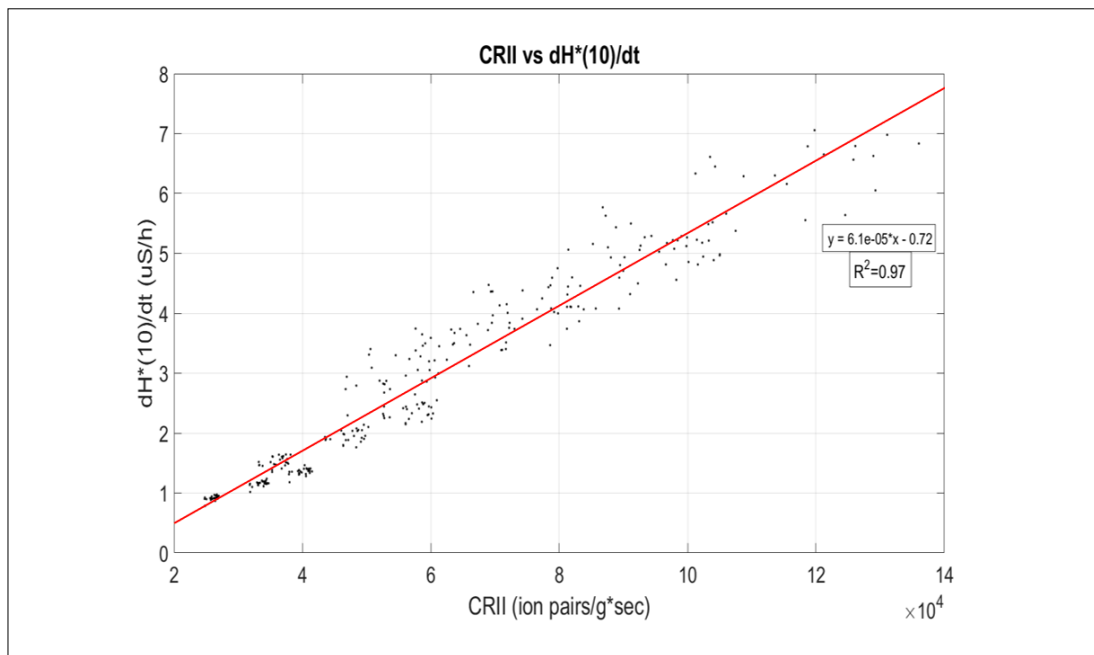


Fig. 7: Scatter plot of the annual distribution of the CRII rate and the ambient dose equivalent rate for the time period 1996–2019 at FL390, FL350, FL310.

4. Discussion and conclusions

Concluding, CRII and $dH^*(10)/dt$ follow the behavior of the cosmic ray intensity and are negatively correlated with the solar activity. The maximum values are observed during the solar minima and at polar regions ($\sim 7 \mu\text{Sv/h}$ at FL390, $5 \mu\text{Sv/h}$ at FL350 and $4 \mu\text{Sv/h}$ at FL310), while the minimum values during the solar maxima and at the equatorial regions ($\sim 1.2 \mu\text{Sv/h}$ at FL390, $1 \mu\text{Sv/h}$ at FL350 and $0.8 \mu\text{Sv/h}$ at FL310). It is observed that the higher the flight level, the higher the CRII and the radiation exposure of air-crew and frequent flyers, since the provided shielding of the atmosphere is reduced in higher atmospheric altitudes. Finally, comparing the CRII and $dH^*(10)/dt$ calculations the correlation is positive ($R^2 = 0.97$).

The CRAC:CRII and DYASTIMA tools are reliable and give useful results for the study of the impact of the ionization and radiation induced by cosmic rays on the environment, space weather, climate change (Dorman 2016; Todd and Kniveton 2001) and human health (Singh et al. 2011; Meier et al. 2020). As the number of flights keeps increasing and air traffic is elevated, commercial aircraft are forced to fly at higher flight levels, which leads to a variation of the CRII and the radiation exposure, according to the flight route and the FLs chosen during each flight. This field of research could be very useful to the aviation industry for updating safety measures and regulations, as well as the air traffic flow and capacity management.

Acknowledgements

This work is supported by the ESA Space Safety Programme's network of space weather service development and pre-operational activities, under ESA Contract 4000134036/21/D/MRP, in the context of the

Space Radiation Expert Service Centre. I.G.U. acknowledges partial support from the Academy of Finland (projects ESPERIA No. 321882). Thanks are due to the Special Research Account of the University of Athens for supporting the Cosmic Ray research. Thanks are also due to the Oulu Cosmic ray colleagues for kindly providing cosmic ray data as well as the CRAC:CRII model.

Questions and answers

Question 1: How does your evaluation of radiation dose rates compare with those of commonly used models as EPCARD?

Answer: The comparison of radiation dose rates values with some other models (for example, CARI-7) has been performed indicatively during the validation process of the DYASTIMA-R tool. We have not yet performed a comparison with the results of EPCARD. Details about the validation process and the results (not the comparison with other models) may be found in Tezari A., Paschalis P., Mavromichalaki H., Karaiskos P., Crosby N., and Dierckxsens M. at Oxford Academic Journal Radiation Protection Dosimetry (<https://dx.doi.org/10.1093/rpd/ncaa112>).

Question 2: How did you calculate the CR fluxes arriving at the upper atmosphere at all locations on Earth?

Answer: Concerning the CRAC:CRII model, the differential energy spectrum of galactic cosmic rays is parameterized by the force field model which has only one parameter, the modulation potential, for a given local interstellar spectrum. Full details may be found at Usoskin and Kovaltsov (2006) and Usoskin et al. (2005, 2010, 2011). Concerning the DYASTIMA software, the differential spectrum of the incoming primary galactic cosmic rays at the top of the atmosphere, we used the ISO15390 model (ISO 15390:2004ISO, 2004).

Question 3: Do you have an idea how strong a GLE must be to give a significant signal in your models?

Answer: We haven't worked on GLEs yet.

References

- Agostinelli, S.; Allison, J.; Amako, K.A.; Apostolakis, J.; Araujo, H.; Arce, P.; Asai, M.; Axen, D.; Banerjee, S.; Barrand, G.; et al. 2003, Geant4-A simulation toolkit. Nucl. Instrum. Methods A, 506(3), 250-303, [http://doi.org/10.1016/S0168-9002\(03\)01368-8](http://doi.org/10.1016/S0168-9002(03)01368-8)
- Allison, J.; Amako, K.; Apostolakis, J.; Araujo, H.; Dubois, P.A.; Asai, M.; Barrand, G.; Capra, R.; Chauvie, S.; Chytracsek, R.; et al. 2006, Geant4 developments and applications. IEEE Trans. Nucl. Sci., 53(1), 270-278, <http://doi.org/10.1109/TNS.2006.869826>
- Allison, J.; Amako, K.; Apostolakis, J.; Arce, P.; Asai, M.; Aso, T.; Bagli, E.; Bagulya, A.; Banerjee, S.; Barrand, G.; et al. 2016, Recent developments in Geant4. Nucl. Instrum. Methods A, 835, 186-225, <http://doi.org/10.1016/j.nima.2016.06.125>
- Athens Cosmic Ray Group, 2019, DYASTIMA Software User Manual, <http://cosray.phys.uoa.gr/index.php/dyastima> (last accessed July 5, 2023)
- Bazilevskaya, G.A.; Usoskin, I.G.; Flückiger, E.O.; et al. 2008, Cosmic Ray Induced Ion Production in the Atmosphere. Space Sci Rev, 137, 149-173, <https://doi.org/10.1007/s11214-008-9339-y>
- Berger, T., Meier, M., Reitz, G. and Schridde, M. 2008, Longterm dose measurements applying a human anthropomorphic phantom onboard an aircraft. Radiat. Meas., 43(2-6), 580-584, <https://doi.org/10.1016/j.radmeas.2007.12.004>
- Dorman, L. I. 2016, Space Weather and Cosmic Ray Effects, Chapter 30, Climate Change, 513-544, <https://doi.org/10.1016/B978-0-444-63524-2.00030-0>
- ESA <https://swe.ssa.esa.int/dyastima-federated> (last accessed July 5, 2023).
- ESA 2019, ESA SSA P3 SWE-III Acceptance Test Report, R.137 Dynamic Atmospheric Tracking Interactive Model Application (DYASTIMA); ESA: Paris, France.

- Flückiger, E. and Bütikofer, R. 2011, Radiation doses along selected flight profiles during two extreme solar cosmic ray events. *Astrophys. Space Sci. Trans.*, 7(2), 105–109, <https://doi.org/10.5194/astra-7-105-2011>
- Forbush, S. E. 1954, World wide cosmic ray variations, 1937–1952, *J. Geophys. Res.*, 59(4), 525–542, <https://doi.org/10.1029/JZ059i004p00525>
- Gerontidou, M.; Katzourakis, N.; Mavromichalaki, H.; Yanke, V.; Eroshenko, E. 2021, World grid of cosmic ray vertical cut-off rigidity for the last decade. *Adv. Space Res.*, 67(7), 2231–2240. <http://doi.org/10.1016/j.asr.2021.01.011>
- Gleeson, L. J. and Axford, W. I. 1968, Solar Modulation of Galactic Cosmic Rays. *Astrophysical J.*, 154, 1011–1026, <https://doi.org/10.1086/149822>
- International Commission on Radiation Units and Measurements 2010, Reference data for the validation of doses from cosmic-radiation exposure of aircraft crew. ICRU Report 84. *J. Int. Comm. Radiat. Units Meas.*, 10.
- International Commission on Radiological Protection 2007, The Recommendations of the International Commission on Radiological Protection. *Ann. ICRP*, 37, 103.
- International Commission on Radiological Protection 2016, Radiological protection from cosmic radiation in aviation. *Ann. ICRP*, 45, 132.
- ISO 2533:1975 ISO Standard Atmosphere, International Organization for Standardization: Geneva, Switzerland, 2007.
- ISO 15390:2004 ISO Space Environment (Natural and Artificial)—Galactic Cosmic Ray Model, International Organization for Standardization: Geneva, Switzerland, 2004.
- Makrantonis, P.; Mavromichalaki, H.; Usoskin, I. G.; Papaioannou, A. 2013, Calculation of the cosmic ray induced ionization for the region of Athens, *J. Physics, Conf. Series* 409, 2232, <http://doi.org/10.1088/1742-6596/409/1/012232>
- Makrantonis, P.; Mavromichalaki, H.; Paschalis, P. 2021, Solar cycle variation of the ionization by cosmic rays in the atmosphere at the mid-latitude region of Athens, *Astrophys. Space Sci.*, 366:70 <https://doi.org/10.1007/s10509-021-03978-8>
- Makrantonis, P.; Tezari, A.; Stassinakis, A.N.; Paschalis, P.; Gerontidou, M.; Karaiskos, P.; Georgakilas, A.G.; Mavromichalaki, H.; Usoskin, I.G.; Crosby, N.; et al. 2022, Estimation of Cosmic-Ray-Induced Atmospheric Ionization and Radiation at Commercial Aviation Flight Altitudes. *Appl. Sci.*, 12(11), 5297, <https://doi.org/10.3390/app12115297>
- Mavromichalaki, H.; Marmatsouri, L.; Vassilaki, A. 1995, On reproduction of long term cosmic-ray modulation as seen by neutron monitor stations, *Astrophys. and Space Sci.*, 232, 315–326, <https://doi.org/10.1007/BF00658302>
- Mavromichalaki, H.; Belehaki, A.; Rafios, X. 1998, Simulated effects at neutron monitor energies: evidence for a 22-year cosmic-ray variation. *Astron. Astrophys.*, 330, 764–772.
- Meier, M.M.; Copeland, K.; Klobbe, K.E.J.; Matthia, D.; Plettenberg, M.C.; Schennetten, K.; Wirtz, M.; Hellweg, C.E. 2020, Radiation in the atmosphere. A hazard to aviation safety? *Atmosphere*, 11(12), 1358. <http://doi.org/10.3390/atmos11121358>
- National Oceanic and Atmospheric Administration, <https://www.ngdc.noaa.gov/geomag/> (last accessed July 5, 2023)
- OMERE, <http://www.trad.fr/en/space/omere-software/> (last accessed July 5, 2023)
- Paschalis, P.; Mavromichalaki, H.; Dorman, L.I.; Plainaki, C.; Tsirigkas, D. 2014, Geant4 software application for the simulation of cosmic ray showers in the Earth's atmosphere. *New Astron.*, 33, 26–37, <https://doi.org/10.1016/j.newast.2014.04.009>
- Singh, A.K.; Singh, D.; Singh, R.P. 2011, Impact of galactic cosmic rays on earth's atmosphere and human health. *Atmos. Environ.* 2011, 45(23), 3806–3818, <http://doi.org/10.1016/j.atmosenv.2011.04.027>
- Smart, D.F.; Shea, M.A. 2007a, World grid of calculated cosmic ray vertical cutoff rigidities for epoch 1995.0. In *Proceedings of the 30th International Cosmic Ray Conference*, Yucatán, Mexico, 3–11 July.
- Smart, D.F.; Shea, M.A. 2007b, World grid of calculated cosmic ray vertical cutoff rigidities for epoch 2000.0. In *Proceedings of the 30th International Cosmic Ray Conference*, Yucatán, Mexico, 3–11 July.
- Smart, D.F.; Shea, M.A. 2019, Vertical Geomagnetic Cutoff Rigidities for Epoch 2015. In *Proceedings of the 36th International Cosmic Ray Conference*, Madison, WI, USA, 24 July –1 Aug.
- Tezari, A.; Paschalis, P.; Mavromichalaki, H.; Karaiskos, P.; Crosby, N.; Dierckxsens, M. 2020, Assessing Radiation Exposure Inside The Earth's Atmosphere. *Radiat. Prot. Dos.*, 190(4), 427–436, <https://doi.org/10.1093/rpd/ncaa112>
- Tezari, A.; Paschalis, P.; Stassinakis, A.; Mavromichalaki, H.; Karaiskos, P.; Gerontidou, M.; Alexandridis, D.; Kanellakopoulos, A.; Crosby, N.; Dierckxsens, M. 2022, Radiation Exposure in the Lower Atmosphere during Different Periods of Solar Activity. *Atmosphere*, 13(2), 166, <https://doi.org/10.3390/atmos13020166>
- Todd, M.C.; Kniveton, D.R. 2001, Changes in cloud cover associated with Forbush decreases of galactic cosmic rays. *J. Geophys. Res.*, 106(D23), 32031–32042, <http://doi.org/10.1029/2001JD000405>
- Usoskin, I.G.; Alanko-Huotari, K.; Kovaltsov, G.A.; Mursula, K. 2005, Heliospheric modulation of cosmic rays: Monthly reconstruction for 1951–2004. *J. Geophys. Res.*, 110, A12108, <http://doi.org/10.1029/2005JA011250>

Usoskin, I.G.; Kovaltsov, G.A. 2006, Cosmic ray induced ionization in the atmosphere: Full modeling and practical applications. *J. Geophys. Res.*, 111, D21206, <http://doi.org/10.1029/2006JD007150>

Usoskin, I.G.; Desorgher, L.; Velinov, P.; Storini, M.; Flueckiger, E.O.; Buetikofer, R.; Kovaltsov, G.A. 2009, Ionization of the Earth's atmosphere by solar and galactic cosmic rays. *Acta Geophys.*, 57, 88-101, <http://doi.org/10.2478/s11600-008-0019-9>

Usoskin, I.G.; Kovaltsov, G.A.; Mironova, I.A. 2010, Cosmic ray induced ionization model CRAC: CRIL: An extension to the upper atmosphere. *J. Geophys. Res.*, 115, D10302. <http://doi.org/10.1029/2009JD013142>

Usoskin, I. G.; Bazilevskaya, G. A.; Kovaltsov, G. A. 2011, Solar modulation parameter for cosmic rays since 1936 reconstructed from ground-based neutron monitors and ionization chambers, *J. Geophys. Res.*, 116, A02104, <http://doi.org/10.1029/2010JA016105>

Open Access

This paper is published under the Creative Commons Attribution 4.0 International license (<https://creativecommons.org/licenses/by/4.0/>). Please note that individual, appropriately marked parts of the paper may be excluded from the license mentioned or may be subject to other copyright conditions. If such third party material is not under the Creative Commons license, any copying, editing or public reproduction is only permitted with the prior consent of the respective copyright owner or on the basis of relevant legal authorization regulations.

Session 3: Abstracts

Neutron monitors detecting cores of extensive air showers

Ashot Chilingarian 

Correspondence





Artem Alikhanyan National Lab (Yerevan Physics Institute), Yerevan, Armenia

Abstract

We identify and analyzed EAS events by the registration of the neutron bursts in the Aragats NM. We relate these bursts to the EAS cores hitting the ground nearby NM. All bursts were observed as sequences of microsecond pulses temporally isolated from other pulses on a time scale of at least 100 microseconds. The burst duration, defined as a time interval between the first and last detectable pulses in the sequence was (2.5 ms +/- 0.6) ms. Thus, NM is enlarging the EAS core particle lifetime (usually not more than 20 - 30 ns) by 5 orders of magnitude by registering multiple secondary neutrons born in the lead absorber and soil by relativistic particles from the EAS core. In this way, NM registers EASs and enables the estimation of primary particle energy by measuring the event multiplicity (number of isolated pulses in NM) and relating it to the primary particle energy. Although the sensitive area of NM is only several tens of m², multiyear operation of the NM network will provide sufficient statistics for the physics around the knee of all particle energy spectrum (3-4 PeV) and beyond. The largest cosmic ray experiments confirm the neutron bursts from EAS cores without any relation to lightning occurrences. The network of near 50 neutron monitors (NM) operates 24/7 around the globe at different altitudes, latitudes, and longitudes for more than 60 years. Maintenance of such detectors is very cheap and they are providing data for many years with minimal intervention of personnel. The data from neutron monitors are collected in databases with open access and a user-friendly interface. After a very simple modernization of NM electronics, it will be possible to recover the energy spectra of galactic cosmic rays with detectors located all around the globe.

Local environmental effects on cosmic ray observations at Syowa Station in the Antarctic: PARMA-based snow cover correction for neutrons and machine learning approach for neutrons and muons

Ryuhō Kataoka ^{1,2,3}, Tatsuhiko Sato ⁴, Chihiro Kato ⁵, Akira Kadokura ^{6,1,2}, Masayoshi Kozai ⁶,

Shoko Miyake ⁷, Kiyoka Murase ², Lihito Yoshida², Yoshihiro Tomikawa ^{1,2}, Kazuoki Munakata ⁵

Correspondence

- 1 National Institute of Polar Research, Tokyo, Japan
- 2 The Graduate University for Advanced Studies, SOKENDAI, Hayama, Japan
- 3 Okinawa Institute of Science Technology Graduate University, Zancha, Onna, Japan
- 4 Japan Atomic Energy Agency, Tōkai, Japan
- 5 Shinshu University, Matsumoto, Nagano, Japan
- 6 Polar Environment Data Science Center, Joint Support-Center for Data Science Research, Research Organization of Information and Systems, Tokyo, Japan
- 7 KOSEN - National Institute of Technology, Ibaraki College, Tokyo, Japan

Abstract

We would like to briefly introduce our paper submitted to the Journal of Space Weather and Space Climate: Solar modulation of galactic cosmic rays around the solar minimum in 2019-2020 looks different in the secondary neutrons and muons observed at the ground. To compare the solar modulation of primary cosmic rays in detail, we must remove the possible seasonal variations caused by the atmosphere and surrounding environment. As such surrounding environment effects, we evaluate the snow cover effect on neutron count rate and the atmospheric temperature effect on muon count rate, both simultaneously observed at Syowa Station in the Antarctic (69.01 S, 39.59 E). A machine learning technique, Echo State Network (ESN), is applied to estimate both effects hidden in the observed time series of the count rate. We show that the ESN with the input of GDAS data (temperature time series at 925, 850, 700, 600, 500, 400, 300, 250, 200, 150, 100, 70, 50, 30, and 20 hPa) at the closet position can be useful for both the temperature correction for muons and snow cover correction for neutrons. The corrected muon count rate starts decreasing in late 2019, earlier than the corrected neutron count rate, which starts decreasing in early 2020, possibly indicating the rigidity-dependent solar modulation in the heliosphere.

Forbush decrease observed by nodes of SEVAN East-European particle detector network on November 2021

H. Martoyan

Correspondence

Yerevan Physics Institute, Yerevan, Armenia

Abstract

On November 3-4, 2021, CME hit the magnetosphere, sparking a strong G3-class geomagnetic storm and auroras as far south as California and New Mexico. European particle detector SEVAN registered Forbush decrease (Fd) coherently at all nodes. We present the results of a comparative analysis of the variations of different species of cosmic rays, and the surface electric field obtained in November 2021 at three observation sites Aragats (Armenia), Lomnický štít (Slovakia), and Musala (Bulgaria) mountains. We discuss the characteristics of the variations of the charged and neutral components of cosmic rays registered by the SEVAN particle detectors at 3 sites and the near-surface electric field (NSEF). We made a correlation analysis of the geomagnetic field and NSEF at the start and maximum of particle flux depletion.

Tutorial: cosmic rays and the atmosphere

Stepan Poluianov 

Correspondence

Sodankylä Geophysical Observatory, University of Oulu, Finland

Abstract





Cosmic rays are high-energy nuclei of elements (hydrogen, helium and heavier species) travelling in space with relativistic speeds. The atmosphere of the Earth is constantly bombarded by them. When a cosmic ray particle enters the atmosphere, it likely experiences an interaction(s) with ambient atoms such as nitrogen, oxygen, argon and others. If the energy of the incident particle is high, the interaction can lead to a nuclear reaction with production of secondary particles. Those secondaries are often also highly energetic and are able to produce consequent reactions leading to production of even higher number of secondaries. Such chains of reactions form a cosmic-ray induced cascade also called as an air shower. The tutorial covers the topics of basics of the cascade formation, its composition and development over the altitude. It will be also explained what we can learn studying the cascade, particularly, with ground-based neutron monitors.

Session 4:

**Neutron detector
instrumentation and stability**

First results of the SA Agulhas II mobile mini-neutron monitor

Instrumental characterization and environmental sensitivity

Du Toit Strauss ¹, Frederic Effenberger ², Stefan Lotz ³, Konstantin Herbst ⁴, Helena Krüger¹, Corrie Diedericks¹

Correspondence

- 1 Center for Space Research, North-West University, Potchefstroom, South Africa, dutoit.strauss@nwu.ac.za, helenakruger6@gmail.com, 27863840@nwu.ac.za
 - 2 Institut für Theoretische Physik, Lehrstuhl IV: Plasma-Astroteilchenphysik, Ruhr-Universität Bochum, Germany, fe@tp4.rub.de
 - 3 South African National Space Agency, Hermanus, South Africa, slotz@sansa.org.za
 - 4 Extraterrestrial Physics, Institute of Experimental and Applied Physics, Kiel University, Germany, herbst@physik.uni-kiel.de
-

Keywords

neutron monitor; cosmic rays; heliosphere; modulation; instrumentation

Abstract

We present the first results of a new redesigned version of the mini-neutron monitor installed on the South African Research vessel, the SA Agulhas II. Measurements taken from the 2019/2020 relief voyages are presented. We show that the instrument is very sensitive to temperature variations when the ambient temperature is below 3°C. This is believed to be an instrumental effect. Additionally, we show the presence of high-frequency interference in the calculated waiting time distributions when the vessel reaches polar latitudes. We show that these periodic variations are only present in the intensity of secondary atmospheric particles and most likely related to the operation of the vessel's ice radar. We are currently looking at moving the instrument to a more suitable location on board the SA Agulhas II where we will hopefully be able to operate the instrument in a continuous fashion for several years to come.

1. Introduction

Neutron monitors (NMs) have been used for more than 70 years to monitor the indirect flux of cosmic rays in the near-Earth environment. Primary cosmic ray particles that enter the Earth's atmosphere produce showers of secondary particles (including protons, neutrons, and other particles and sub-atomic particles).



Fig. 1: The left panel shows the SA Agulhas II unloading supplies in Antarctica with the location of the mini-NM circled. The right panel shows the monitor, emphasizing the newly installed vibration dampeners.

These secondary particles are registered on the ground level by the NM, so that the NM count rate N can be expressed as

$$N(P_c, t) = \sum_i \int_{P_c}^{\infty} j_i(P, t) Y_i(P, t, \dots) dP$$

where P_c is the cut-off rigidity (minimum rigidity particle that can reach the detector due to deflection by the geomagnetic field), j_i is the primary cosmic ray flux at the top of the atmosphere, i represents the particle distribution under consideration, and Y is the so-called yield function that represents the response of the instrument on the unit flux of primary cosmic rays with rigidity P , including atmospheric and instrumental effects. The latter therefore depends on various parameters that are unique to each monitor (Caballero-Lopez 2016; Clem and Dorman 2000). The rigidity dependence of Y can, however, be calculated experimentally by placing the monitor (or at least some tubes making up the large monitors) on a ship that crosses multiple latitudes (and thereby sampling different regions of P) in a relatively short time (e.g. Caballero-Lopez and Moraal 2012, amongst many others). This is referred to as a latitude scan and has been carried out many times in the past by various groups.

The mini-NM is a small and compact version of the standard NM (Simpson 2000; Bütikofer 2018), originally envisioned to serve as a *calibration* NM (Moraal et al. 2001; Krüger et al. 2003). However, under the right conditions, it was realized that the mini-NM could supplement the existing network of traditional NMs (Krüger et al 2015). Mini-NMs have been operated successfully by several research groups for several years (Poluianov et al. 2015; Usoskin et al. 2015; Heber et al. 2015). Due to their small size and autonomous operation, the mini-NM is ideally suited to be used for latitude scans, which has been done before by Heber et al. (2015) and Krüger et al. (2008).

In this paper we present initial results from a newly re-designed mini-NM, using a ^3He counting tube, installed on the South African Antarctic research vessel, the SA Agulhas II. This instrument uses a new version of the electronics system described by Strauss et al. 2020. Results from this system, featuring very high temporal resolution, were recently reported by Similia et al. (2020), Strauss et al. (2021) and Strauss et al. (2022)

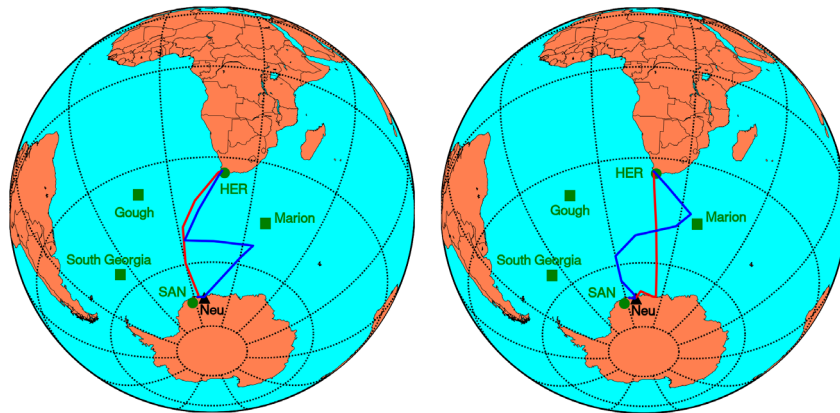


Fig. 2: The four latitude scans performed by the SA Agulhas II during the 2019/2020 Antarctic relief voyages. Voyages starting in Cape Town are coloured red.

The redesigned mini-NM was installed on the SA Agulhas II in early December 2019. An unused, and un-heated, storeroom on the upper deck was selected. This region of the ship is circled in the left panel of Fig. 1 which shows the SA Agulhas II anchored at the Fimbul ice shelf in Antarctica, and uploaded materials for the yearly relief voyage to the South African Antarctic base, SANAE IV. The right panel of Fig. 1 shows an image of the monitor, with the newly installed mechanical vibration dampeners circled.

2. The 2019/2020 SANAE IV relief voyage

The 2019/2020 Antarctic relief voyage was ideally suited to test the working of the redesigned mini-NM as two voyages were performed; a first relief voyage to the SANAE IV base, and a second to the German Neumayer-Station III. This gives a total of four latitude scans, although not a very wide range of magnetic rigidities were covered. The four latitude scans are illustrated in Fig. 2, with red showing voyages starting in Cape Town. Also shown on the map is the position of the SANAE IV base (SAN), the Hermanus NM (HER), located near Cape Town, Neumayer (Neu), and other regular stops for the SA Agulhas II (South Georgia, Marion, and Gough Islands).

The entire raw data set for the 2019/2020 takeover season is presented in Fig. 3 in minute cadence. The red and green shading indicate different periods; green shading indicates the time when the ship moves between Cape Town harbour and the SANAE ice shelf, while red shading indicated periods when the ship is anchored. The naming convention for these periods are included in the top panel.

3. Temperature and pressure corrections

It is well-known that the count rate of an NM depends on the temperature of the instrument, and this has also been confirmed to be the case for the mini-NM (e.g. Moraal et al. 2003; Krüger et al. 2008; Heber et

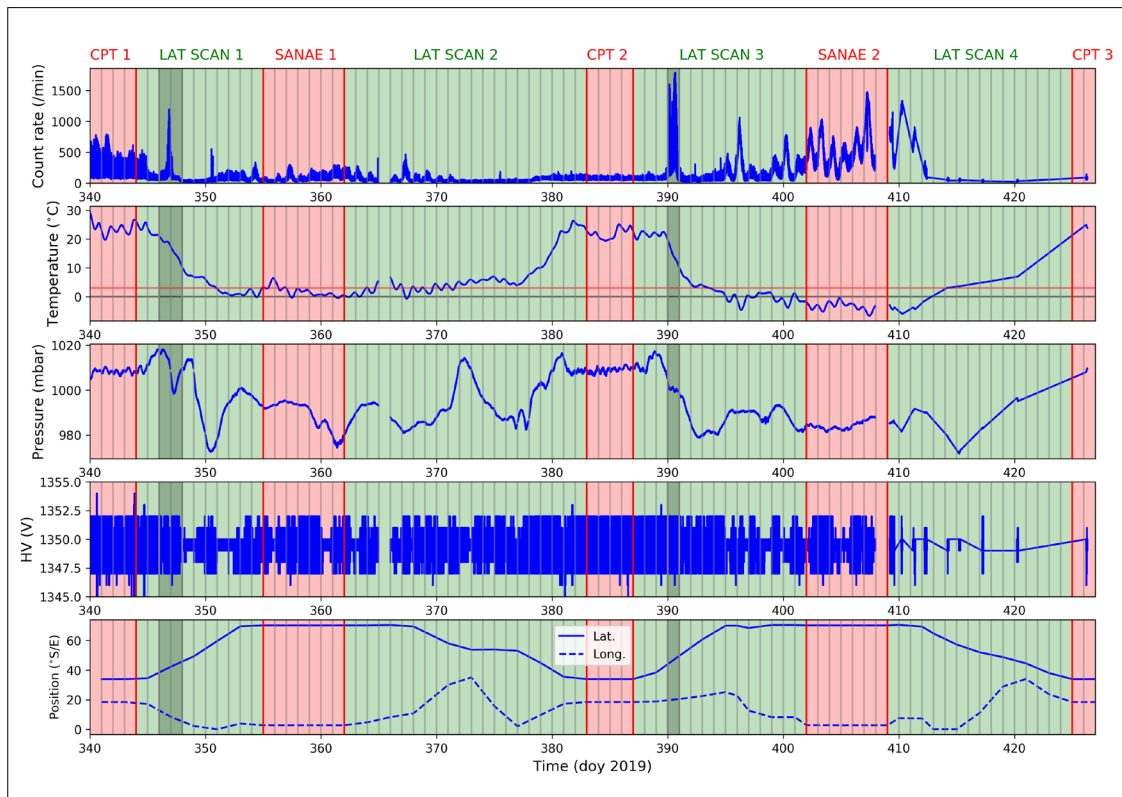


Fig. 3: An overview of the mini-NM measurements taken during the 2019/2020 Antarctic relief voyages.

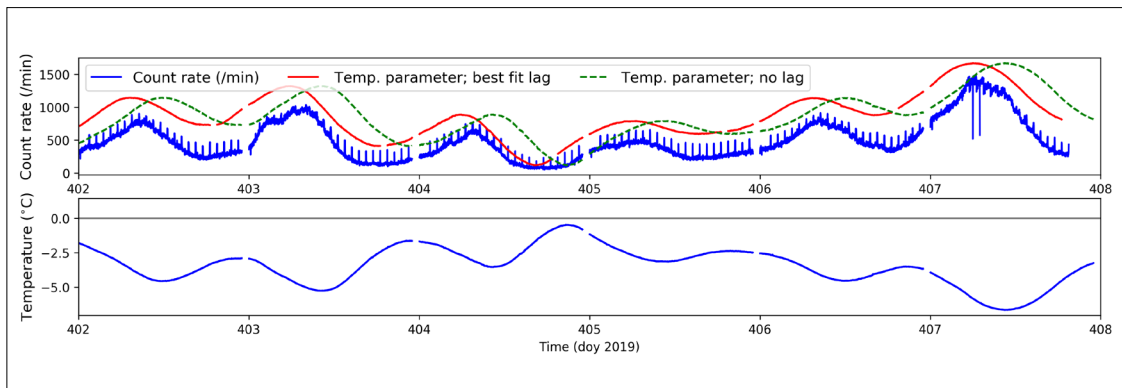


Fig. 4: The top panel shows the uncorrected count rate (blue curve) and the absolute temperature (with an offset), referred to as the temperature parameter, uncorrected for any temporal lag effects (green dashed curve) and corrected with the optimized time lag value (red curve). The bottom panel shows the measured temperature.

al. 2015). The temperature dependence of an NM, however, is complex as the different components react differently to temperature variations leading to different absorption and attenuation lengths, and also possibly different neutron production rates (Evenson et al. 2005).

In Fig. 4 we show, in the top panel, the uncorrected (for pressure) count rate for the period 2019 DOY 402 to 2019 DOY 408 the so-called SANAE 2 time period where the ship was anchored at the ice shelf. In the bottom panel, the corresponding temperature is shown, illustrating a definite correlation with the

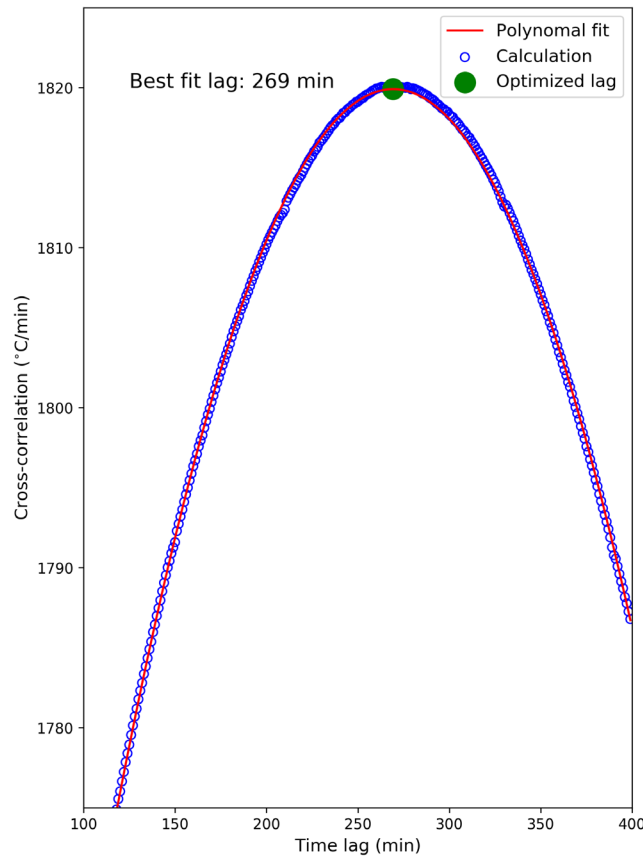


Fig. 5: A cross correlation between the temperature and count rate for various temporal lags (blue symbols). A second order polynomial is fitted (red curve) to find the optimal lag value (indicated by the green symbol).

count rate; lower temperatures generally lead to high count rates. The absolute temperature (with an offset for clarity) is shown in the top panel (green dashed curve), illustrating that there is also a lag between the temperature and the count rate. This lag is because of the large thermal mass of the mini-NM and the fact that the temperature probe is inserted against the ^3He tube (see also the discussion by Evenson et al. 2005).

To correct for this time-lag between the count rate and the temperature, the cross-correlation between these two quantities are calculated for various level of temporal lag, i.e.

$$N * T(n) = \sum_{m=0}^M N(m) \circ T(m + n)$$

where N and T are the count rate and temperature time series, n is the lag (in minutes) and there are M counts in the series. The results of the cross-correlations analysis are shown as the blue symbols in Fig. 5. There is a maximum correlation at ~ 270 min. To better quantify the magnitude of the lag, a second order polynomial is fitted to the cross-correlation results, and its maximum value is obtained, giving an optimized lag value of 269 min. This time lag is applied to the temperature measurements (which are now shifted 269 min earlier), and the resulting time series is shown as the red curve in the top panel of Fig. 5. This *lag corrected temperature* time series is used for the calculations in the next section.

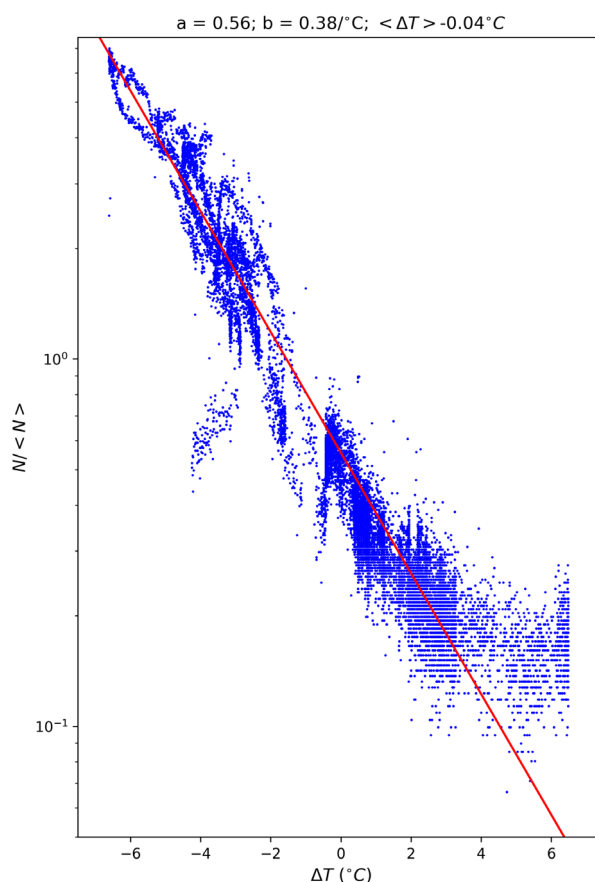


Fig. 6: The measured count rate (blue symbols) during the SANAE 2 time interval is well described by an exponential function (red curve).

Now that we have accounted for any lag effects, the temperature dependence of the mini-NM count rate for the SANAE 2 time period can be evaluated. Following the usual approach (e.g. Krüger et al. 2008), an exponential relationship is assumed, where

$$\frac{N}{\langle N \rangle} = a \exp(-\beta_T \Delta T)$$

with $\Delta T = T - \langle T \rangle$, β_T the temperature coefficient, a is a fit constant, and the angle brackets $\langle \rangle$ indicating average values. Note that this equation can be approximated by a linear function when either β_T or ΔT is small. However, as shown the left panel of Fig. 6, the measurements (blue symbols) during the SANAE 2 time period can be very well described by an exponential regression line (red curve). We find an extremely large temperature coefficient of $\beta_T \sim 40\%/^{\circ}\text{C}$ which is much larger than the value of $\beta_T \sim 0.1\%/^{\circ}\text{C}$ from Moraal et al. (2003) and Krüger et al. (2008) for the same monitor (although using older electronics) at ambient temperatures larger than $\sim 10^{\circ}\text{C}$. As this very large exponential increase in the count rate below $\sim 3^{\circ}\text{C}$ is therefore most likely due to noise from the electronics and these data were not used for the rest of the analysis. Further temperature tests in the laboratory confirms that this is an instrumental effect at very low temperatures.

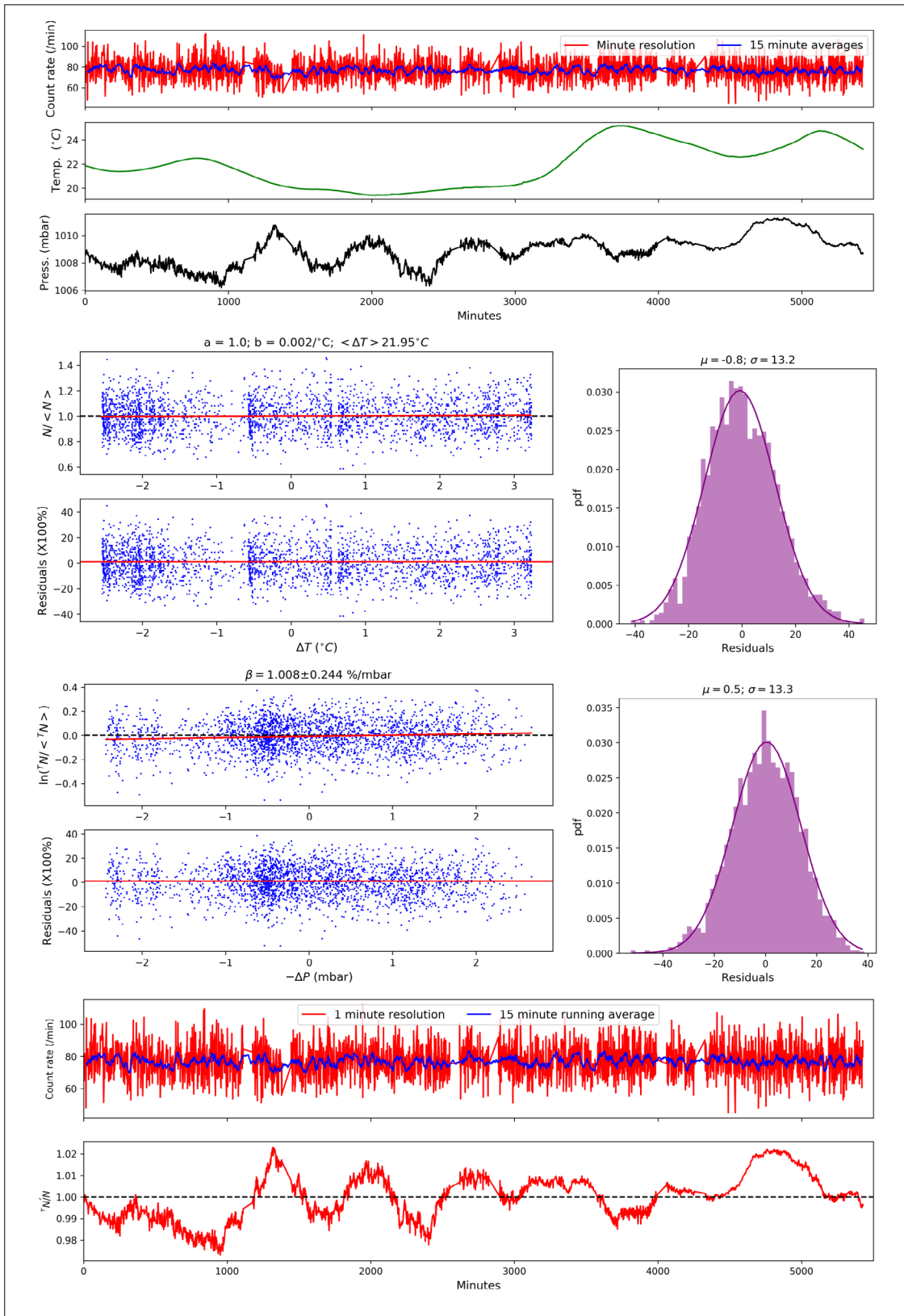


Fig. 7: An example of how the daily measurements were processed, including temperature and pressure correction details.

The following analysis was performed for each day's data. As an example, we show here the data taken during the period labelled CPT 2, i.e. DOY 383 – 387. For these five days the ship was anchored at Cape Town harbour for refueling and loading of cargo. The top panel of Fig. 7 shows the measured count rate, temperature, and pressure in minute resolution. As the temperature varied very little in this interval (and this is in general also true when looking only at daily periods of data), a linear temperature correction is then performed, where

$$\frac{N}{\langle N \rangle} = a - \beta_T \Delta T.$$

Once β_T is known, the temperature-corrected count rate can be calculated, with results shown in the middle panel, where, for this case, the temperature coefficient is $\sim 0.2\%/^{\circ}\text{C}$. This value is more in line with previous measurements by Krüger et al. (2008). We also show the residuals of this linear fit, and the distribution of the residuals, in the middle panel. The probability density function (pdf) of the residuals (purple histogram) is fitted by a Gaussian function (purple curve). The mean and variance of the Gaussian function are indicated in the figure's legend.

The temperature-corrected count rate varies as

$$N = \langle N \rangle \exp(-\beta \Delta p)$$

where β is the pressure coefficient and $\Delta p = P - \langle P \rangle$. The resulting $\beta \sim 1\%/mbar$ is indicated in the figure title. Regression residuals are again shown. The bottom panels of Fig. 7 show the pressure and temperature corrected count rate and the uncorrected to corrected count rate ratio.

The analysis discussed in the previous section was repeated for every day of the 2019/2020 relief voyage that produced reliable measurements. I.e., only days with a temperature larger than 3°C . For each such day, the daily average temperature- and pressure-corrected count rate was calculated and compared to the geomagnetic cut-off, calculated from the daily average position of the ship, using the online calculator <http://nearfld.com/util/rigidity.php> (last accessed July 5, 2023). The results of this are presented in the top left panel of Fig. 8 for the three latitude scan. The solid curve is the prediction from Caballero-Lopez and Moraal (2012) using their Eq. (13) with the 1987 sea level (SL) parameters and normalized to $N_0 = 90$ counts/min. Above $\sim 2.8\text{GV}$, the measured latitude profile seems consistent with the expectation and previous results. However, below $\sim 2.8\text{GV}$, and shaded gray, there is a clear discrepancy with lower-than-expected NM counts. By also examining the count rate against the latitude of the ship (bottom left panel), it is clear that there is a discrepancy when the ship passes above the 45°S latitude mark. The reason for this discrepancy is presented in the next section.

The top right panel of Fig. 8 shows the calculated pressure coefficient as a function of the geomagnetic cut-off. The vertical dashed line indicates the average value of $\sim 1.3\%/mbar$. Given the relatively low count rate of the mini-NM, and the associated large errorbars in β , we did not find any latitude dependence.

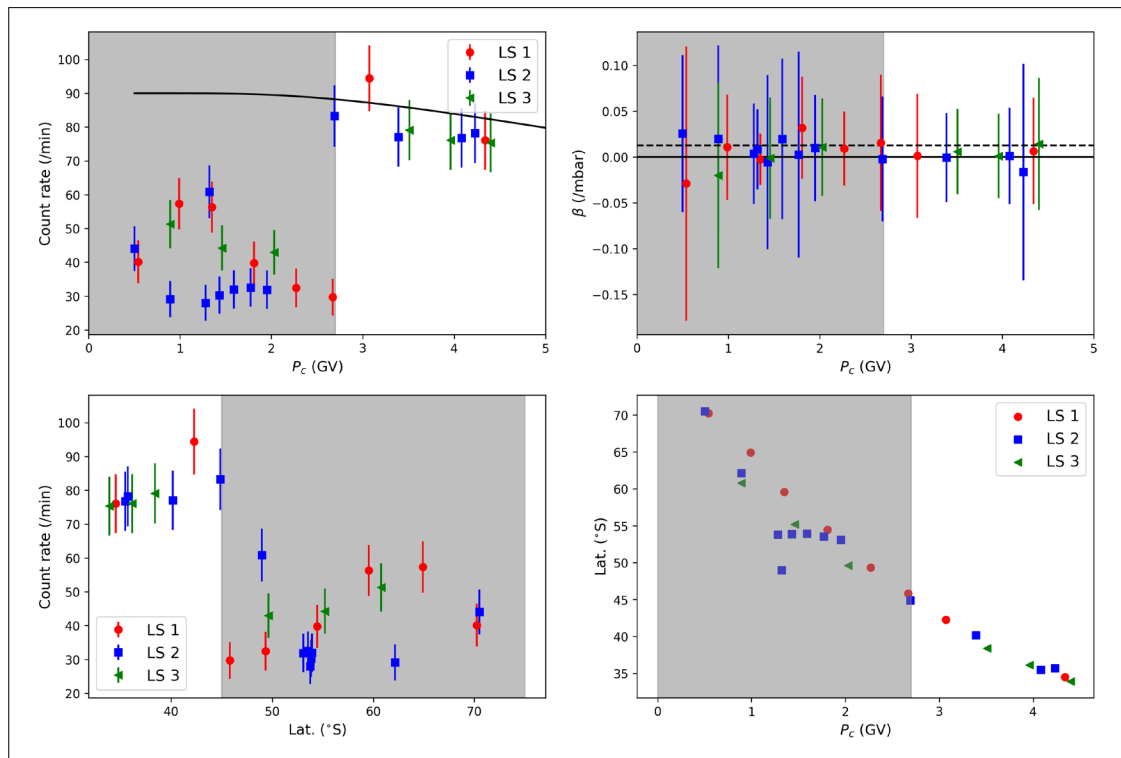


Fig. 8: Daily average temperature- and pressure-corrected count rates as a function of geomagnetic cut-off rigidity (top left panel) and latitude (bottom left panel). The cut-off rigidity dependence of the pressure coefficient is presented in the top right panel, and the relationship between the cut-off rigidity and the latitude is in the bottom right panel.

4. Waiting time distribution and high-frequency interference

The outer moderator surrounding the NM blocks thermal particles from entering the detector. In the lead producer, some of the non-thermal atmospheric particles interact with the lead nuclei to form a new low-energy neutron component, so the particle spectrum here consists of two components: The original incident particles that did not undergo any additional reactions and neutrons produced inside the lead producer. These non-thermal distributions now pass through the inner moderator forming a thermal distribution. These thermal neutrons can now be captured by the ^3He gas during a neutron capture reaction. The protons or alpha particles formed during the capture process are then accelerated, via an applied voltage, towards the positive cathode where they can be counted as a pulse by appropriate electronics. It does, however, also happen that some accelerated particles interact with the walls of the ^3He tube and deposit some energy there (the so-called *wall effect*, Knoll 2010) so that the recorded neutron distribution appears to have a tail towards lower pulse lengths. However, it is important to note that the recorded pulse width from the NM has no relation to the energy of the incident neutrons: Due to a combination of thermalization by the moderators, and by the nature of the neutron capture process, all information regarding the energy of the incident proton and neutron is lost.

However, low- and high-energy protons interact with the lead producer differently. Low energy protons and neutrons interact with the lead producer, and thus the ^3He gas, in a random fashion and their observed pulses show a stochastic nature with subsequent pulses unrelated to each other. A high-energy

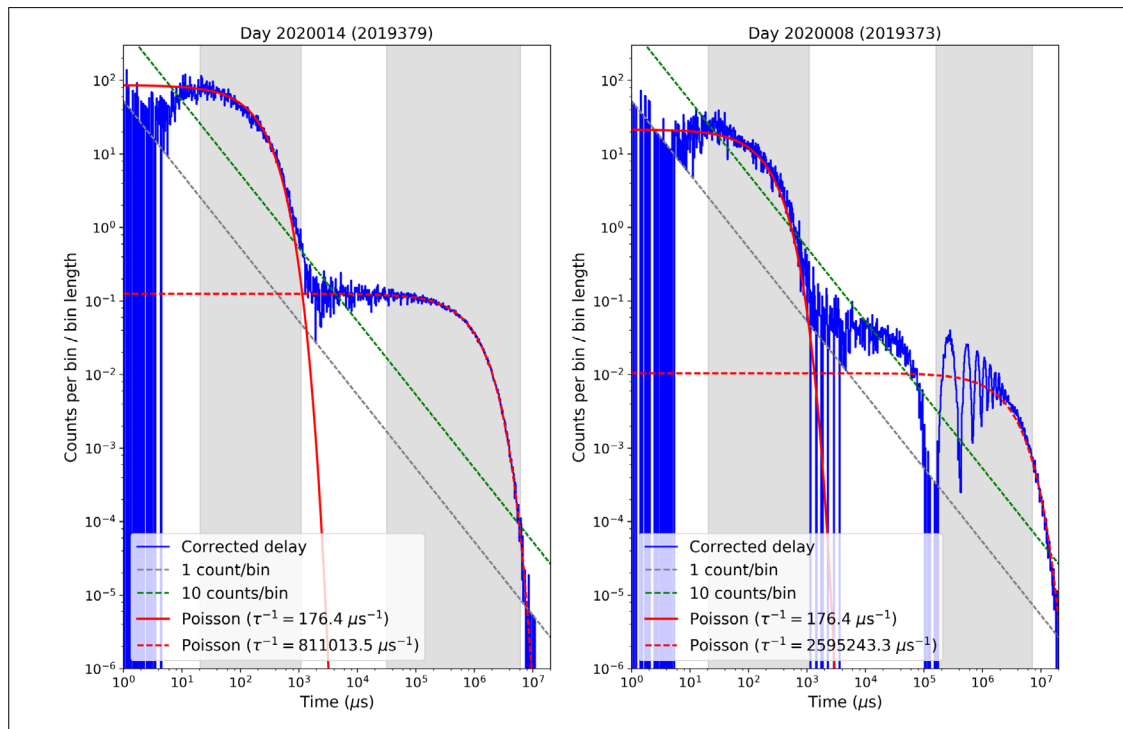


Fig. 9: Multiplicity of the observed count rate as measured during two different days. The waiting time distributions are fitted by two Poisson-like distributions, with the fit results indicated in the legend.

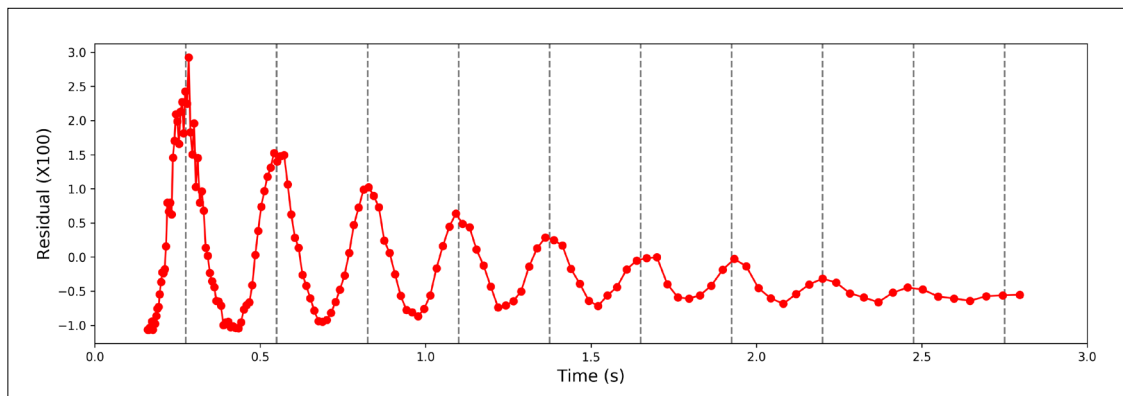


Fig. 10: The deviation of the observed waiting time distribution from a fitted Poisson distribution. The vertical dashed lines have a periodicity of 0.275 s.

proton, on the other hand, can interact with the lead nuclei to form a number of low-energy *evaporation neutrons* (e.g. Bieber et al. 2004). These neutrons are observed as several pulses over a short period, showing a high temporal correlation. This is usually expressed in terms of the waiting time distribution (i.e. the time between subsequent pulses observed in the monitor) as the level of multiplicity. Thus, looking at the waiting time distribution, as an indication of the multiplicity, observed by the monitor these two components are clearly distinguishable. By looking at the ratio of these components some information about the incident particle spectrum can be reconstructed (see e.g. Ruffolo et al. 2016; Mangeard et al. 2016; Banglieng et al. 2020).

As discussed in the previous section, a discrepancy in the mini-NM count rate is visible when the ship crosses 45°S in latitude; a deficiency of counts is observed. This coincides with the activation of the ship's ice radar. We, therefore, suspect that the rotating radar dish blocks some of the incoming atmospheric protons and neutrons. Note that the monitor is installed directly below this dish, as shown in Fig. 1. In order to test the blocking hypothesis, we examine the waiting time distribution of the monitor on two different days, 2020008 (2019373) and 2020014 (2019379), using the YEARD0Y notation (year followed by the day-of-year), during latitude scan 2 when the ship was on route to Cape Town harbour. On both days, only minor temperature effects are noticeable and needs to be corrected for. During 2020008, the ship was ~53°S, and on 2020014, it was at ~42°S. The calculated waiting time distribution are shown in Fig. 9 as blue curves. The green and gray dashed lines show the 1 and 10 counts/bin limits. The high multiplicity part of the distribution (i.e., the part with shorter waiting times) forms due to high-energy protons producing multiple neutrons in the lead producer. The low multiplicity part (at longer waiting times) are neutrons and protons that are captured randomly with the counts unrelated. We fit the waiting time distributions with two Poisson-like distributions for each multiplicity component. The results are shown in Fig. 10 as the red curves. The grey-shaded areas indicate the data used to fit each distribution. The spectrum for 2020014, which is during a time when no discrepancies in the data are observed, shows the expected two component Poisson distribution. The spectrum for 2020008, which coincides with a day showing such a discrepancy, shows additional features: The high multiplicity part of the distribution is lower than for 2020014 but interestingly has the same shape. The low multiplicity part, however, shows quasi-periodic decreases in counts. This, at least partially, confirms our suspicion that the radar periodically blocks some of the incident atmospheric protons and neutrons: At fixed time values, there is a deficiency of particles in the low part of the waiting time distribution. However, only of the high multiplicity part of the distribution is reduced (due to the reduced incoming proton/neutron flux) while the shape remains the same, clearly showing that only the incident particles are affected and not the neutrons produced inside the lead producer.

We can further analyse the blocking of incident particles by examining the residuals in the low multiplicity part of the 2020008 distribution (the right panel of Fig. 10). Here, we define the residual as the difference between the measured waiting time distribution and that predicted by the fitted Poisson-like distribution, normalized to the average difference. This quantity is shown, as a function of Δt , in Fig. 10. The vertical dashed lines, corresponding to the different peaks in the residual, are placed every 0.275 s revealing the quasi-periodic behaviour of the inference of incident particles. The overhead ice radar rotates at a rate of 40 rotations-per-minute. As this instruments consists of two rotating fins, we can expect a fin to pass over the monitor every 0.75 s. This is about 3 times the observed signal period. At the moment a direct correlation between the ice radar and the mini-NM cannot be proven. However, as we observe interference only at latitudes greater than ~45°S, with co-insides with the operation of the ice radar system, we still believe the radar system is the main suspect in influencing the operation of the NM.

5. Discussion and future outlook

A newly redesigned version of a mini-NM was placed on the SA Agulhas II during its 2019/2020 annual relief voyage between Cape Town, South Africa, and the Antarctic ice shelf near the South African Antarctic base SANAE IV. Four such latitude scans were performed in 2019/2020, giving us a good opportunity

to test several new modifications to the instrument, including new (and much more sensitive) electronics and a redesigned cradle featuring vibration dampeners.

During the SANAE 2 time interval, when the ship was anchored against the ice shelf, the average temperature measured inside the monitor was $T \sim 0^\circ\text{C}$. It is found that, during such extremely low temperatures, the mini-NM count rate increases exponentially with a decrease in temperature. An extremely large temperature coefficient of $\beta_T \sim 40\%/^\circ\text{C}$ is found for such scenarios, which is believed to be caused by noise from the electronics. However, when the temperature of the detector rises above $\sim 3^\circ\text{C}$, a small to moderate temperature dependence is found with $\beta_T \sim 0.2\%/^\circ\text{C}$, or even smaller. The significant temperature dependence, and hence the corresponding correction needed for periods with temperatures less than 3°C , introduce large uncertainties into the temperature-corrected count rate and essentially makes these periods unusable for further analysis.

Daily measurements allow us to study the relationship between the count rate and the geomagnetic cut-off. In contrast to what was expected, we measured a decrease in the counting rate below $\sim 2.7\text{GV}$. This is, however, not related to the physics of cosmic ray transport through the geomagnetic field, but is rather caused by, presumably, interference from the ship's ice radar which is activated below $\sim 45^\circ\text{S}$. We can study this high-frequency interference by looking at the measured waiting time distribution. This allowed us to confirm that incident protons and neutrons are blocked periodically from reaching the detector. In addition, we can determine that this interference occurs with a frequency of $\sim 3.6\text{Hz}$. This shows, for the first time, that the multiplicity derived from the NM observations, can be used to test the stability of the mini-NM observations.

Due to both the large temperature effect and the interference from the ice radar at the mini-NM's current position, we are currently looking at moving it to a more suitable location on board the SA Agulhas II. There, hopefully, we will be able to operate the instrument in a continuous fashion for several years.

Acknowledgements

This work is based on the research supported in part by the National Research Foundation of South Africa. Support from the NRF's South African National Antarctic Programme (SANAP; grant number 110741) is especially acknowledged. Opinions expressed and conclusions arrived at are those of the authors and are not necessarily to be attributed to the NRF. We acknowledge support from the Alexander von Humboldt Foundation's Group Linkage Program.

References

- Banglieng, C., Janthaloet, H., Ruffolo, D., et al., 2020, Tracking Cosmic-Ray Spectral Variation during 2007 - 2018 Using Neutron Monitor Time-delay Measurements. *Astrophys. J.* 890, 21, <https://doi.org/10.3847/1538-4357/ab6661>
- Bieber, J.W., Clem, J.M., Duldig, M.L., et al. 2004, Latitude survey observations of neutron monitor multiplicity. *J. Geophys. Res.* 109, A12106, <https://doi.org/10.1029/2004JA010493>
- Bütikofer, R., 2018, Solar Particle Radiation Storms Forecasting and Analysis: The HESPERIA HORIZON 2020 Project and Beyond. Ground-Based Measurements of Energetic Particles by Neutron Monitors, ed. by O.E. Malandraki and N.B. Crosby, 95 - 111, Springer International Publishing
- Caballero-Lopez, R.A. and Moraal, H., 2012, Cosmic-ray yield and response functions in the atmosphere. *J. Geophys.*









- Res. 117, A12103, <https://doi.org/10.1029/2012JA017794>
- Caballero-Lopez, R.A., 2015, An estimation of the yield and response functions for the mini neutron monitor. *J. Geophys. Res.* 121, 7461 – 7469, <https://doi.org/10.1002/2016JA022690>
- Clem, J.M. and Dorman, L.I., 2000, Neutron Monitor Response Functions. *Space Sci. Rev.* 93, 335 – 359, <https://doi.org/10.1023/A:1026508915269>
- Evenson, P., Bieber, J.W., Clem, J., et al. 2005, Neutron Monitor Temperature Coefficients: Measurements for BF₃ and ³He Counter Tubes. *Proceedings of the 29th International Cosmic Ray Conference*, 2, 485
- Heber, B., Galsdorf, D., Gieseler, J., et al. 2015, Mini neutron monitor measurements at the Neumayer III station and on the German research vessel Polarstern. *Proceedings of the 34th International Cosmic Ray Conference*, 34, 122
- Knoll, G.F., 2010, *Radiation Detection and Measurement*, 4th ed. Wiley, New Jersey
- Krüger, H., Moraal, H., Bieber, J.W., et al. 2003, First Results of a Mobile Neutron Monitor to Intercalibrate the Worldwide Network. *Proceedings of the 28th International Cosmic Ray Conference*, 6, 3441
- Krüger, H., Moraal, H., Bieber, J.W., et al. 2008, A calibration neutron monitor: Energy response and instrumental temperature sensitivity. *J. Geophys. Res.* 113, A08101, <https://doi.org/10.1029/2008JA013229>
- Krüger, H., Moraal, H., Nel, R. et al. 2015, The mini neutron monitor programme. *Proceedings of the 34th International Cosmic Ray Conference*, 34, 223
- Mangeard, P.-S., Ruffolo, D., Saiz, A., et al., 2016, Dependence of the neutron monitor count rate and time delay distribution on the rigidity spectrum of primary cosmic rays. *J. Geophys. Res.* 121, 11620 – 11,636, <https://doi.org/10.1002/2016JA023515>
- Moraal, H., Benadie, A., de Villiers, D., et al. 2001, A mobile neutron monitor to intercalibrate the worldwide network. *Proceedings of the 27th International Cosmic Ray Conference*, 10, 4083
- Moraal, H., Kruger, H., Benadie, A., et al. 2003, Calibration of the Sanae and Hermanus Neutron Monitors. *Proceedings of the 28th International Cosmic Ray Conference*, 6, 3453
- Poluianov, S., Usoskin, I., Mishev, A., et al. 2015, Mini Neutron Monitors at Concordia Research Station, Central Antarctica. *J. Astron. and Space Sci.* 32, 281 – 287, <https://doi.org/10.5140/JASS.2015.32.4.281>
- Ruffolo, D., Saiz, A., Mangeard, P.-S., et al. 2016, Monitoring Short-term Cosmic-ray Spectral Variations Using Neutron Monitor Time-delay Measurements. *Astrophys. J.* 817, 38, <https://doi.org/10.3847/0004-637X/817/1/38>
- Simila, M., Usoskin, I., Poluianov, S., et al. 2021, High-altitude polar NM with the new DAQ system as a tool to study details of the cosmic-ray induced nucleonic cascade. *J. Geophys. Res.* 126, e2020JA028959, <https://doi.org/10.1029/2020JA028959>
- Simpson, J.A., 2000, The Cosmic Ray Nucleonic Component: The Invention and Scientific Uses of the Neutron Monitor. *Space Sci. Rev.* 93, 11 – 32, <https://doi.org/10.1023/A:1026567706183>
- Strauss, R.D., Poluianov, S., van der Merwe, C., et al., 2021, The mini-neutron monitor: a new approach in neutron monitor design. *J. Space Weather and Space Climate*, 10, 39, <https://doi.org/10.1051/swsc/2020038>
- Strauss, R.D., van der Merwe, C., Diedericks, C., et al. 2021, The updated SANAe neutron monitor. *Adv. Space Res.*, 68, 2661 – 2675, <https://doi.org/10.1051/swsc/2020038>
- Strauss, R.D., Giday, N.M., Seba, E.B., et al. 2022, First results from the ENTOTO neutron monitor: Quantifying the waiting time distribution. *Adv. Space Res.*, in press
- Usoskin, I., Poluianov, S., Moraal, H., et al., 2015, A mini neutron monitor in Central Antarctica (Dome Concordia). *Proceedings to the 34th International Cosmic Ray Conference*, 34, 217

Open Access

This paper is published under the Creative Commons Attribution 4.0 International license (<https://creativecommons.org/licenses/by/4.0/>). Please note that individual, appropriately marked parts of the paper may be excluded from the license mentioned or may be subject to other copyright conditions. If such third party material is not under the Creative Commons license, any copying, editing or public reproduction is only permitted with the prior consent of the respective copyright owner or on the basis of relevant legal authorization regulations.

US-based Simpson neutron monitor network

”Back to the future“

James Ryan ¹, John Clem ², Paul Evenson ², Surujhdeo Seunarine ³, Veronica Bindi ⁴,
Cristina Consolandi ⁴, David Ruffolo ⁵, Waraporn Nuntiyakul ⁶

Correspondence

- 1 Space Science Center, Institute for the Study of Earth, Oceans and Space, University of New Hampshire, Durham, USA, james.ryan@unh.edu
 - 2 Department of Physics and Astronomy, University of Delaware, Newark, USA
 - 3 Department of Physics, University of Wisconsin, River Falls, USA
 - 4 Department of Physics and Astronomy, University of Hawaii at Manoa, Honolulu, USA
 - 5 Department of Physics, Faculty of Science, Mahidol University, Bangkok, Thailand
 - 6 Department of Physics and Materials Science, Faculty of Science, Chiang Mai University, Thailand
-

Keywords

space weather; ground level enhancements; solar flare neutrons; instrument; neutron monitor

Abstract

The status and condition of the various neutron monitors operated by the US reached its nadir in the mid 2000s. Now with significant investments by the National Science Foundation, the existing network will be repaired, upgraded and selectively modernized. Furthermore, a key site on the summit of Haleakala will be outfitted once again with a monitor, supported by a Space Weather Center in Honolulu. We report on the start of this work, plans for the near future with funds from the NSF and longer-term plans to take the network to a new operational and scientific level. We also report on a complementary deployment of a new portable monitor on the summit of Haleakala on Maui – a joint effort between Thai and US institutions.

1. Introduction

The years 1957–1958 were named the International Geophysical Year. Global scientific collaboration attacked a variety of puzzling phenomena, one of which was to understand cosmic-ray variability that showed dependence on location and time. The clearest way to address this phenomenon and others was to conduct a contemporaneous global study. Being prior to the space age, cosmic rays could only be studied from the ground, typically with neutron monitors. To this end, the world was well equipped for

Tab. 1: List of NM stations within the Simpson Network that were at risk.

	Station	pre-Simpson	Now
U New Hampshire	Mount Washington	Threatened	secure
	Climax	Lost	Replaced by Leadville
	Haleakala	Lost	to be redeployed
U Delaware	Inuvik	Threatened	secure
	Fort Smith	Threatened	secure
	Peawanuck	Threatened	secure
	Nain	Threatened	secure
	McMurdo	Lost	moved to Jang Bogo
	South Pole	Threatened	secure (UWRF)
	Goosebay	decommissioned	moved to Daejeon

the task with dozens of neutron monitors at a variety of locations and latitudes, covering many longitude ranges. This global system did what was intended, i.e., making key measurements that greatly expanded our understanding of cosmic rays. However, for several reasons, this global network atrophied over the years. Many scientists saw their investment in neutron monitors wither. The problem became acute in the US in the 2000s. In the mid 2010s, the National Science Foundation recognized the problem, noting that neutron monitor data usage was widespread, while US-based stations were being de-commissioned, abandoned or given away. This concern along with new and increased national interest in space weather culminated with the funding of the Simpson Neutron Monitor Network in 2021. Its intent is the securing and revitalizing the remaining US stations, investigating new deployments and training new scientists, all the while conducting science. We report here on the status of the Simpson network. Table 1 is a list of US-based stations that were de-commissioned, abandoned, lost or threatened, circa 2020. Many are now in the new Simpson Network.

2. The network

The network is the responsibility of three collaborating US institutions: the University of New Hampshire, the University of Delaware and the University of Wisconsin-River Falls. Also listed in the Table 1 is the current status of those stations with many now secure from funding cuts. The legacy station at Climax has been functionally replaced by a new station at Leadville CO, 20 km to the south and 300 m lower in altitude. The McMurdo station is now in the hands of South Korea (now Jang Bogo), still operating, but no longer part of the US network.

The tasks the collaboration has defined for itself follow. For operating stations, these objectives for the network include:

- Secure, repair, maintain existing NM stations, including structures, power and data connections.
- Increase reliability where necessary.

- Improve the capabilities of stations with improved electronics.
- Improve spectroscopic sensitivity.
- Cross calibrate with spacecraft instruments (PAMELA, AMS-02).

Periodic maintenance was long overdue at many stations. That backlog of attention is now being addressed with many stations now restored to their earlier operating condition. Some of the electronics, in particular the front-end discriminators and amplifiers, date back decades and they rely on parts that are no longer available. These electronic boards have now been mostly replaced with front-end electronics of more modern designs. In addition, the capability of detecting and measuring multiple coincident signals is being implemented in several stations. This capability effectively constitutes a new data channel with a different yield function that can be used for an independent spectral measurement. Finally, with spacecraft instruments that cover the same energy range as neutron monitors, we can actually confirm the response of the monitors.

While these tasks are being undertaken, science data still flow from the array of monitors. This enables the researchers to continue to conduct studies, such as those listed here:

- Continue studies of ground level enhancements, solar neutron events, Forbush decreases and heliospheric modulation.
- Examine means to predict onset and severity of geomagnetic storms.
- Collaborate with domestic and international ground-based observatories, such as Ice Top and muon telescopes.
- Study possible new station sites and augmenting existing ones to optimize coverage in rigidity and longitude.
- Provide greater input to space weather problem through collaborations with US agencies.

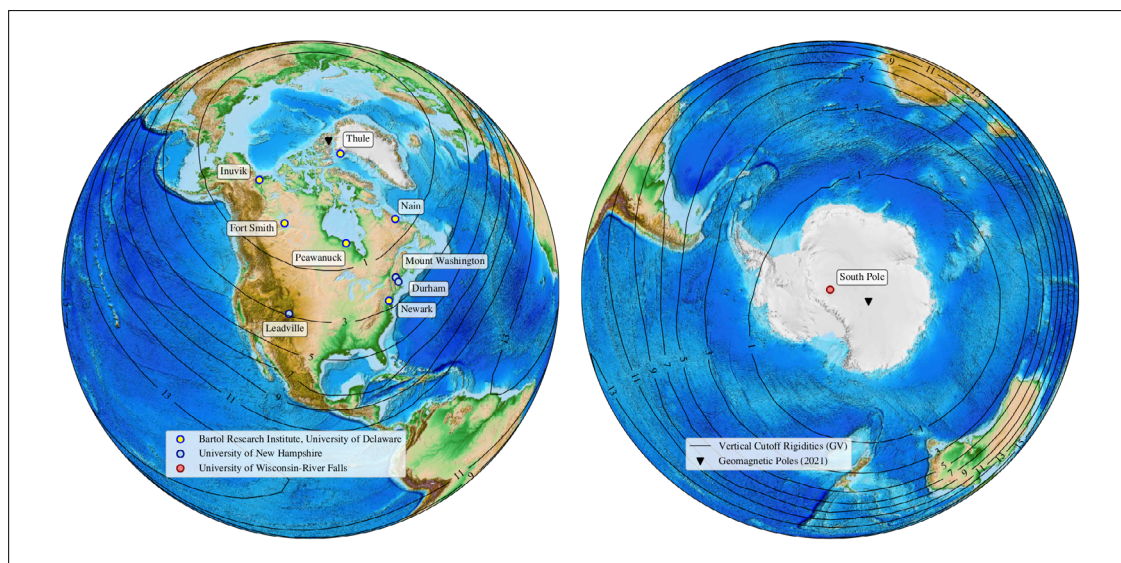
Some of the more important uses for neutron monitors have become commonplace in recent years. We note that low-latitude stations can be particularly important for detecting and measuring direct high-energy solar-flare neutrons for more than a few hours per day and more than a few weeks around the solstices. The redeployment of the Maui instrument, as discussed more below, enables these measurements and provides a high-rigidity measure of solar modulation. Also, using neutron monitors in conjunction with other ground-based detectors greatly increases the utility of the monitors, as well as the complementary detectors. Two examples of this have been to use Climax with the Milagro ground-based TeV gamma-ray detector and the use of Ice Top with the South Pole detectors. Because these are fundamentally different instruments with significantly different yield functions, they can provide single point spectral measurements that have been historically difficult or impossible, in particular, for ground level enhancements (GLE) in their highly anisotropic phase.

Because the gyroradius of neutron monitor protons is so large, they can sense changes in the interplanetary medium at great distances. Consequently, neutron monitors coupled with higher energy instruments, such as muon telescopes, can detect the presence of an approaching, otherwise invisible, CME shock. This could enable advanced warning of geomagnetic storms or Forbush decreases.

The current status of the monitors in the network is given in [Table 2](#) and their locations are illustrated in [Figure 1](#).

Tab. 2: List of stations in the Simpson network and their attributes. Cutoff calculations, courtesy of Don Smart, February 2023.

	Station	Altitude (m)	2020 Cutoff (GV)*	Gas	Type	Features
U New Hampshire	Mt. Washington	1900	1.88	$^{10}\text{BF}_3$	12 IGY	
	Durham	20	2.21	$^{10}\text{BF}_3$	18 NM64	
	Leadville	3030	2.96	$^{10}\text{BF}_3$	3 NM64	
U Delaware	Newark	50	2.63	$^{10}\text{BF}_3$	6 NM64	
				^3He	3 LND-NM64	
	Thule	16	~0	^3He	9 LND-NM64	
				$^{10}\text{BF}_3$	9 NM64	
	Nain	46	0.60	^3He	18 LND-NM64	
	Ft. Smith	206	0.32	^3He	18 LND-NM64	
	Inuvik	21	0.10	$^{10}\text{BF}_3$	18 NM64	
	Peawanuck	53	0.51	^3He	8 LND-NM64	
U Wisconsin-River Falls	South Pole	2820	0.06	^3He	3 LND-NM64	
	South Pole (Polar Bare)			^3He	12 LND	no Pb
	*Don Smart (priv. comm.)					

**Fig. 1:** Locations of neutron monitors in the Simpson Network. Iso-cutoff contours are approximate.

Various types of monitors are listed in Table 2. The standard NM-64 design is based on the Chalk River BP-28 BF₃ tubes. Recently, however, tubes provided by LND replace the Chalk River tubes, but still retain the BF₃ gas with no significant change in dimensions or operating voltage. The oldest design employs IGY tubes built into an assembly of Pb and paraffin. Only the Mount Washington station in the Simpson network is of that design. When ³He was not prohibitively expensive and available, several NM-64 configurations were filled with helium. The only operating site in the network without lead is the Polar Bare station. As with others, it uses polyethylene as the moderator and as the outer reflector, but the Pb converter is absent.

3. Future additions

3.1 The Haleakala neutron monitor (HLEA)

The 18NM-64 monitor on the summit of Haleakala since 1991 was de-commissioned in 2007 because of lack of funds. Under a different NSF grant (see Consolandi et al., this volume: <https://doi.org/10.38072/2748-3150/p42>), a new monitor is in the early stages of construction on the summit (3000 m a.s.l.). It will be either a 3- or 6NM-64 configuration, depending on construction costs. Upon completion, this will restore measurements in the mid-Pacific at a low latitude (21°N), several time zones removed from the nearest other low-latitude station. This places it at an ideal location for detecting and measuring direct solar-flare neutrons, because the Sun will be at a high elevation during the summer months and a workable elevation for much of the year. Placed in proximity to the Daniel K Inouye Solar Telescope (DKIST) observatory of the National Solar Observatory, contemporaneous optical imaging will be available, provided there is acceptable seeing. DKIST is the ideal neighbor with its capability of polarimetry, magnetographs and fast tracking of active regions, allowing researchers to link the detected neutrons with coronal and flare activity.

3.2 US-Thai collaboration

Chang Mai University has led latitude ocean-based surveys. A sea container designed for such a survey, complete with a 3NM-64 instrument, minus the BF₃ tubes, now resides in Honolulu, with no immediate plans for a sea-based survey. Thimon, as it is called, will be placed on the summit of Haleakala then outfitted with BP-28 tubes from the original Maui station. When outfitted with tubes and supporting electronics, it will be a fully functional 3NM-64 instrument that will work in tandem with the new US station (6NM-64). Together they will have half the effective area of the original Maui station, still large enough to address the objectives listed above, but with consequently poorer count statistics and small event sensitivity. The station on Haleakala will be expandable and modular, housed in sea containers, each with three or six tubes. Utilizing the remainder of the original BP-28 tubes will require additional sea containers with the appropriate configuration of BP-28 tubes, Pb and polyethylene.

4. Discussion and conclusions

The Simpson Neutron Monitor Network by 2024 should resemble that of 2020, but secure for decades to come. Data archiving and availability will exist for all stations. Temporal resolution will be 10s for all stations, along with multichannel count rates for spectral sensitivity in several stations. Locations and

features of prospective monitors will be studied in the event of the availability of future funding. The Haleakala station will begin operating as tubes come online. Plans to refurbish and re-deploy the Climax legacy station will be studied for possible future work.

Acknowledgements

The authors and collaborators acknowledge the generous support by the National Science Foundation in grants 1925016, 1931300, 2112437, 2112439, 2112441, 2149809 and 2149811. Thai support comes from Targeted Research Initiatives from faculty of science, Chiang Mai University and grant RTA6280002 from Thailand Science Research and Innovation. The authors are grateful to Don Smart who computed cutoff rigidities (2020) for this presentation.

Open Access

This paper is published under the Creative Commons Attribution 4.0 International license (<https://creativecommons.org/licenses/by/4.0/>). Please note that individual, appropriately marked parts of the paper may be excluded from the license mentioned or may be subject to other copyright conditions. If such third party material is not under the Creative Commons license, any copying, editing or public reproduction is only permitted with the prior consent of the respective copyright owner or on the basis of relevant legal authorization regulations.

Calgary neutron monitor efficiency factor estimation after major renovation

Clifford John Bland, Alexei F. Kouznetsov 

Correspondence

Department of Physics and Astronomy, University of Calgary, Canada, john@altoinstruments.com,
akouznet@ucalgary.ca

Keywords

neutron monitor; efficiency; multiple regression

Abstract

Neutron monitor data which are used for studies of long-term variations, require a means for correcting for changes in efficiency following major renovations. We propose a means to obtain the required “efficiency factor” using multiple regression which, to a first-order approximation, considers solar modulation as well as any changes in the Neutron Monitor sensitivity over time.

1. Introduction

The Calgary neutron monitor has been in operation since the 1960s. Digital records have been available since 1979. Operations were suspended from 2009 until major renovations were completed in 2017. In order to share data with the Neutron Monitor Data Base (NMDB) an “efficiency factor” must be provided whenever operating conditions have changed. To normalize our data before and after the gap, account must be taken of the cycles of solar activity which modulate the arriving galactic cosmic rays. In addition, any long-term drift in the sensitivity of the detectors or other time-dependent variations should be included.

2. Method

[Fig. 1](#) shows the variation of the count-rates of the Calgary neutron monitor over the years of interest and, for comparison, the solar cycles as revealed by monthly sunspot numbers. Following the multiple regression technique (Cooper 1969), we assume that the NM count rates c_i to the first order of approximation is given by:

$$c_i = T \cdot t_i + S \cdot s_i + E + r_i,$$

where t_i are elapsed times (number of months since the beginning of the observation), s_i to be some convenient measure of solar activity (sunspot number from the website <http://www.sidc.be/silso/home>, last accessed July 4, 2023). E is the constant level sought, and r_i is the residual error. Finally, we chose c_i to be the NM pressure-corrected monthly average count rate.

Minimizing the sum of residual error squares, we obtain and solve a matrix equation in the form:

$$\begin{pmatrix} \sum_i (c_i - \bar{c})(t_i - \bar{t}) \\ \sum_i (c_i - \bar{c})(s_i - \bar{s}) \end{pmatrix} = \begin{pmatrix} \sum_i (t_i - \bar{t})^2 & \sum_i (t_i - \bar{t})(s_i - \bar{s}) \\ \sum_i (t_i - \bar{t})(s_i - \bar{s}) & \sum_i (s_i - \bar{s})^2 \end{pmatrix} \times \begin{pmatrix} T \\ S \end{pmatrix} = (M_{TS}) \times \begin{pmatrix} T \\ S \end{pmatrix}$$

Then the inverse matrix $(M_{TS})^{-1}$ provides estimates of the variance and covariance of the parameters when multiplied by the residual variance about the fit.

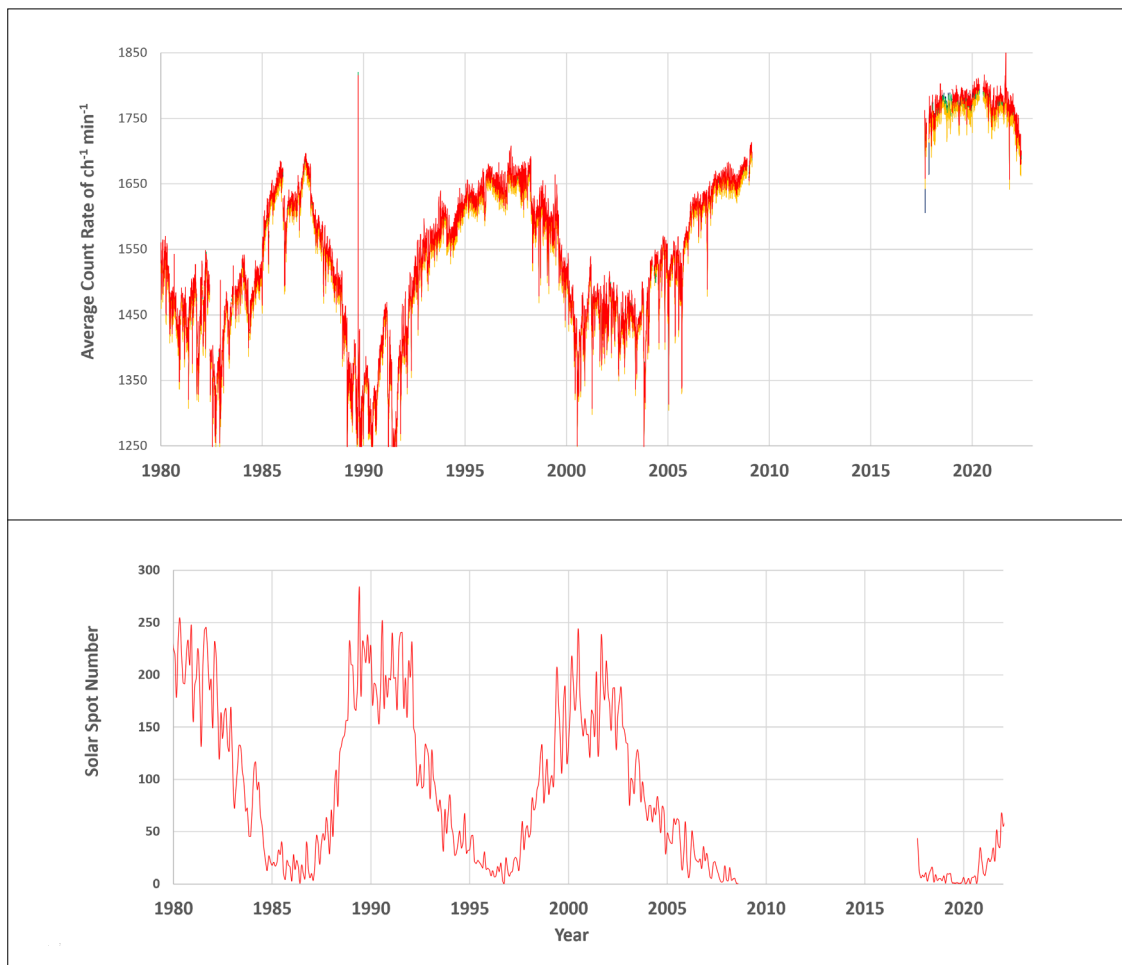


Fig. 1: Calgary NM mean count-rate change due to new data acquisition system.

3. Results

Values of the constants T (time), S (solar activity), and E (constant shift) and their respective standard deviations were obtained in the multiple regression calculations for two consecutive time periods and are shown in Tab. 1. Subscripts appended to the constants indicate the first or second period. The T_1 value may reflect not only drift in the count rate due to a decrease in detector sensitivity but also gradual changes in solar modulation. As a test, an artificial steady drift ($= 0.01 \cdot t$) was subtracted from the actual count rates for the 29-year data and was exactly reflected in the new computed value of T_1 (not shown here). However, there was no resultant change in either S_1 or E_1 . Despite the few years of data during decreased solar activity (2017-22), the values for S_1 and S_2 are remarkably close within error estimates.

Tab. 1: Constants T , S , and E evaluated before (column 1) and after (column 2) Calgary NM major renovations.

1979–2008	2017–2022
$S_1 = 1.494 \pm 0.066$	$S_2 = 1.392 \pm 0.215$
$T_1 = 0.006 \pm 0.036$	$T_2 = 0.345 \pm 0.142$
$E_1 = 1625.6 \pm 63.2$	$E_2 = 1783.8 \pm 16.1$

Fig. 2 shows the results of applying the calculated first-order correction for solar activity. The standard deviation of the ratio E_2/E_1 is given by the standard formula:

$$\sigma_R = \frac{E_2}{E_1} \sqrt{\left(\frac{\sigma_{E1}}{E_1}\right)^2 + \left(\frac{\sigma_{E2}}{E_2}\right)^2}$$

where any covariance σ_R has not been included. Inserting values from the previous slide, we obtain the estimation of the ratio E_2/E_1 and its standard deviation:

$$E_2/E_1 = 1.097 \pm 0.042$$

We conclude therefore that the renovation of the NM has resulted in an increase in the pressure-corrected count rate. However, it should be noted that the latest data coincides with several years of minimum solar activity only.

In order to verify this multiple regression method, we performed the same procedure by splitting Calgary data from 1979 to 2008 into two equal blocks. Again, the constants T , S , and E and their respective standard deviations are shown in Tab. 2. A few high values of solar activity during the early months may be responsible for the negative T_2 value. Future data points will hopefully clarify this statement.

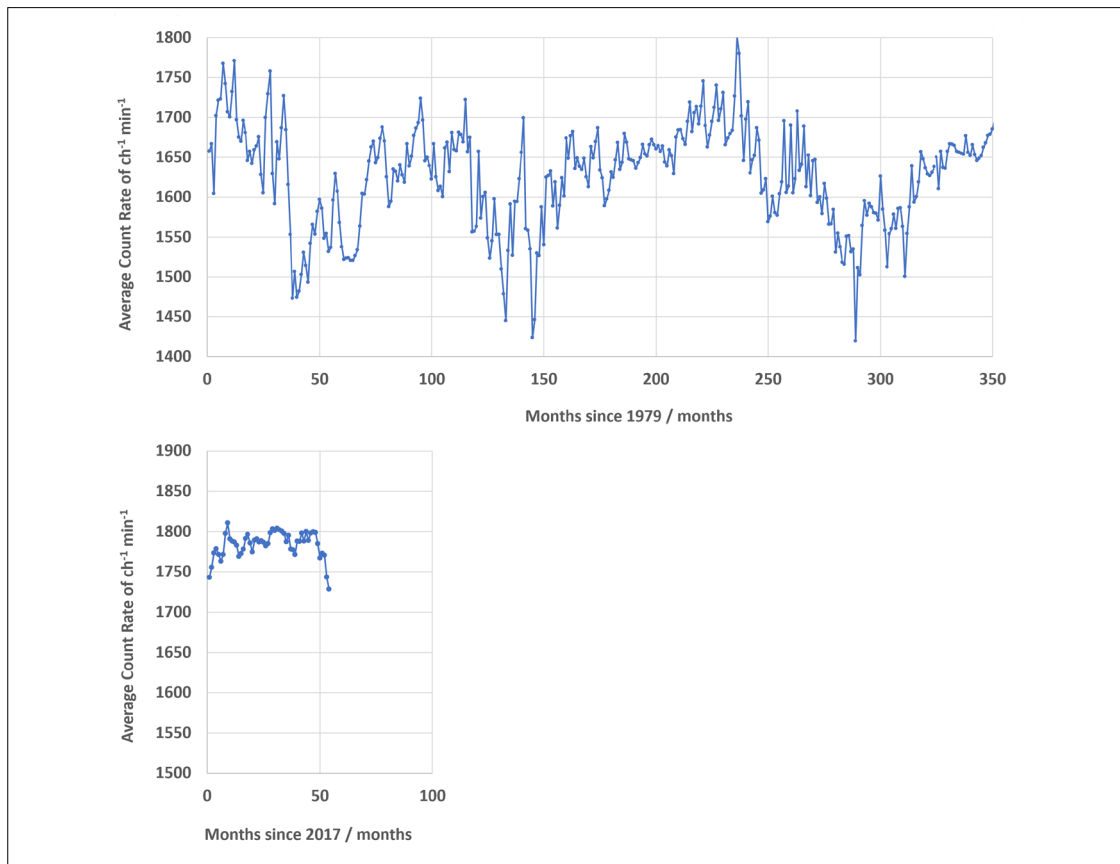


Fig. 2: Count rates after 1st order fit for solar activity.

Tab. 2: Multiple regression method validation results.

1979–1994	1994–2008
$S_1 = 0.996 \pm 0.046$	$S_2 = -1.133 \pm 0.039$
$T_1 = -0.309 \pm 0.073$	$T_2 = -0.250 \pm 0.047$
$E_1 = 1633.26 \pm 68.5$	$E_2 = 1664.6 \pm 54.7$

The ratio E_1/E_2 is, assuming the neutron monitor kept the same efficiency, should be close to unity. The value we obtained was:

$$E_1/E_2 = 0.981 \pm 0.052$$

Details are shown in [Fig. 3](#).

A further application of this method would provide relative baseline count rates for different neutron monitors and provide a means of estimating the effects of different cut-off rigidities, altitude, and instrumental differences. A trial has been made comparing data over the 29-year period (1979-2008) from the NMs at Oulu and Calgary yielding the result:

$$E_{\text{Oulu}}/E_{\text{Calgary}} = 0.325 \pm 0.014$$

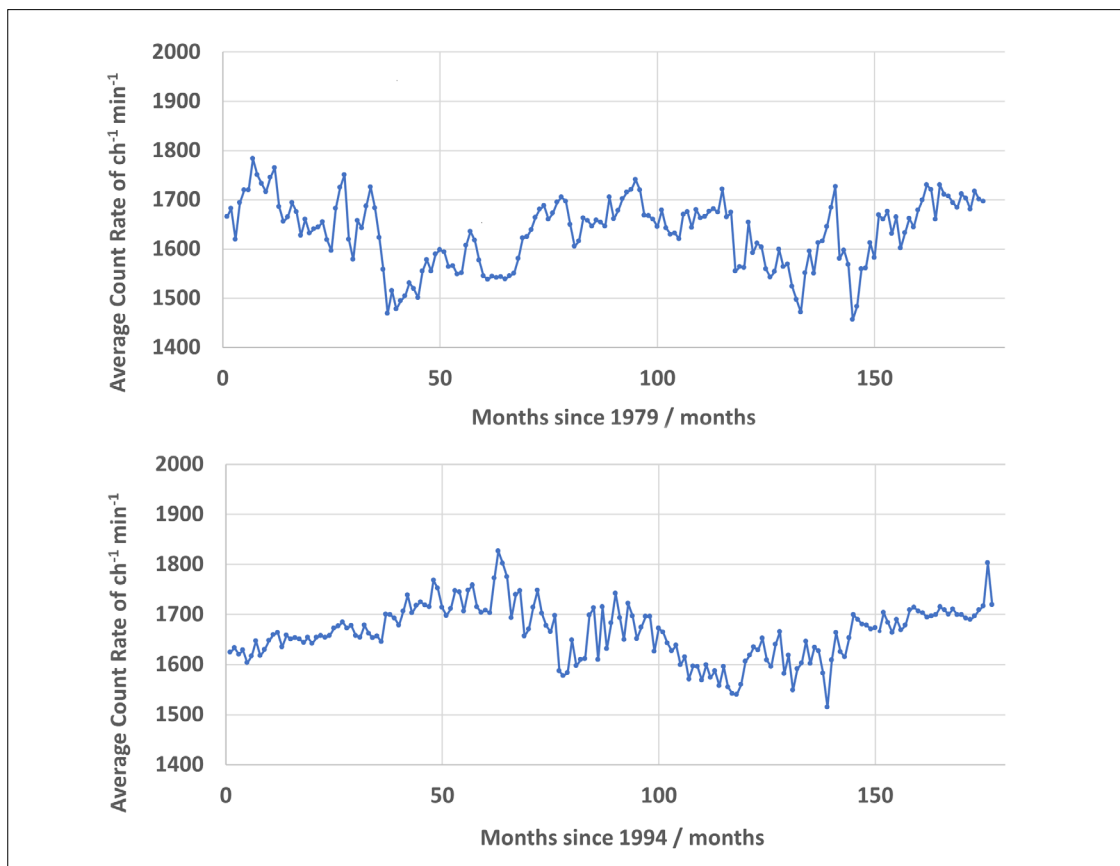


Fig. 3: Two halves of ~29 years data of Calgary NM were used to validate the method.

Upper panel: Count rate time series during the first half with 1st order correction for solar activity.

Lower panel: Count rate time series during the second half with 1st order correction for solar activity.

4. Conclusions

The use of multiple regression to obtain base-line count-rates for neutron monitors appears to offer a convenient way to correct for solar modulation and drift over the long term. Some improvement in accuracy might be achieved if days with larger short-term variations such as GLEs and Forbush decreases, were removed.

Acknowledgements

We thank Prof. David Knudsen for his support. Sunspot Numbers were provided by WDC-SILSO, Royal Observatory of Belgium. Oulu data downloaded from NMDB provided by Sodankyla Geophys. Observatory, University of Oulu.








References

Cooper B.E. 1969, Statistics for Experimentalists, Pergamon Press

Open Access

This paper is published under the Creative Commons Attribution 4.0 International license (<https://creativecommons.org/licenses/by/4.0/>). Please note that individual, appropriately marked parts of the paper may be excluded from the license mentioned or may be subject to other copyright conditions. If such third party material is not under the Creative Commons license, any copying, editing or public reproduction is only permitted with the prior consent of the respective copyright owner or on the basis of relevant legal authorization regulations.

Haleakala neutron monitor redeployment and calibration with AMS data

Cristina Consolandi ¹, Veronica Bindi ¹, Claudio Corti ¹, Nikolay Nikonov ¹, James Ryan ², Jason Legere ², Waraporn Nuntiyakul ³

Correspondence

1 Department of Physics and Astronomy, University of Hawaii at Manoa, Honolulu, USA, cconsola@hawaii.edu

2 College of Engineering and Physical Sciences, University of New Hampshire, Durham, USA

3 Department of Physics and Materials Science, Faculty of Science, Chiang Mai University, Thailand

Keywords

neutron monitor; observation; solar neutrons; cosmic rays; solar modulation

Abstract

Since the 1950s, neutron monitors (NMs) have successfully measured both the long-term and the short-term variation of Galactic Cosmic Rays (GCRs). NMs are also sensitive to solar energetic particles (SEPs) and solar neutron particles (SNPs), both detected as ground level enhancements. Since SNPs are not affected by the interplanetary magnetic field, they retain direct information about the nuclear reactions happening near the SEP acceleration site. The global NM network has still a huge gap over the equatorial Pacific for measuring high energy GCRs and SNPs which are best measured at low latitudes. We plan to extend the coverage of the world wide NM network for SNP and GCR observations by redeploying the Haleakala NM station (HLEA) on Maui, in time for the upcoming solar maximum (around 2025). Since NMs can only measure the total count rate, it is not trivial to derive the actual particle flux and to compare different station responses. We plan to calibrate the HLEA with the future AMS daily proton fluxes, extended until the ISS decommission date now planned in 2031, and to perform extensive Monte Carlo simulations of the detector and surrounding environment. The initial phase of the project has already started. Status of the upcoming HLEA NM detector is reported.

1. Introduction

Solar energetic particles (SEPs) are particles accelerated by the Sun during explosive events such as solar flares and Coronal Mass Ejections (CMEs). The highest-energy SEPs are primarily accelerated near the Sun; then they follow the complicated structure of the Interplanetary Magnetic Field (IMF) and the Earth's magnetosphere to reach Earth's atmosphere. Thus, their spatial distribution is greatly affected by

propagation processes, modifying their arrival time, intensity, duration, and anisotropy. During strong solar flares, the Sun can also emit energetic neutrons, called Solar Neutron Particles (SNPs), created in interactions of SEPs with nuclei in the Sun's atmosphere. Since SNPs are not affected by the IMF, they retain direct information about the nuclear reactions happening near the SEP acceleration site. When an SEP or an SNP event occurs, it may initiate a cascade of secondary particles in the Earth's atmosphere that can be detected on the ground by neutron monitors (NMs), i.e. ground level enhancement (GLE).

NM stations are distributed across the world, working together as a giant spectrometer, known as the global NM network. The global NM network, active since the 1950s, has successfully measured the long-term variation of Galactic Cosmic Rays (GCRs) due to the 11- and the 22-year solar cycle modulation, and the short-term variations of GCRs, e.g. diurnal variations or Forbush decreases (FDs), and the flux of particles accelerated by the Sun: SEPs and SNPs. Nevertheless, the Pacific Ocean represents a large gap in the equatorial coverage of the global NM network for SNP and GCR detection (Mishev & Usoskin 2020). Currently, this gap spans a longitudinal expanse of 162° from the Princess Sirindhorn NM in Thailand to Mexico City. To fill this gap, we will redeploy the Haleakala (HLEA) NM, which is strategically near the middle of this gap at an altitude of 3 km on the island of Maui. The HLEA position is ideal for SNP detection: the high-altitude minimizes SNP absorption in the atmosphere, and the low-latitude maximizes the Sun's elevation, thereby increasing exposure. In addition, space weather (SW) monitoring systems are becoming increasingly important for providing alerts to both the scientific community and private enterprise. For this reason, incorporating novel data from SNPs to advance SW alert systems is highly desirable.

Recently, the Payload for Antimatter Matter Exploration and Light-nuclei Astrophysics (PAMELA) and the Alpha Magnetic Spectrometer (AMS) have provided precise GCR measurements of different nuclei on various time scales (Galper et al. 2017; Aguilar et al. 2021a). AMS is a detector measuring charged particles in the energy range from 300 MeV to a few TeV on the International Space Station (ISS) since May 2011. As a space-borne experiment, AMS detects charged primary particles before their interaction with the atmosphere, enabling direct measurements of their spectra and chemical composition. The simultaneity of space-borne and ground-based detectors give us the possibility to compare and cross-calibrate the two kind of instruments and to understand the effects of the Earth's magnetosphere and atmosphere on charged particles propagation. In our past publication (Koldobskiy et al. 2019) we tested the stability versus time of some of the widely used NM yield functions (YFs) with the AMS monthly Proton and Helium fluxes (Aguilar et al. 2018). The new AMS publications on daily Proton and Helium fluxes (Aguilar et al. 2021b; Aguilar et al. 2022) give us the possibility to extend the same work on a shorter time scale and to set up a procedure for calibrating the forthcoming HLEA data with the future AMS fluxes extended until the ISS decommission date now planned in 2031.

2. Solar Neutron Particles with HLEA NM

J. A. Simpson, of the University of Chicago, deployed the first NMs in the early 1950s. Others followed with many at high altitude. The old HLEA NM, constructed in 1991, was part of the University of Chicago, then later the University of New Hampshire (UNH) system and continuously took data until its decommissioning (due to lack of funds) in 2006. This NM station is located on Haleakala mountain in the middle of the Pacific Ocean. SNPs are best observed by NM stations located at high altitude, to reduce atmospheric ab-

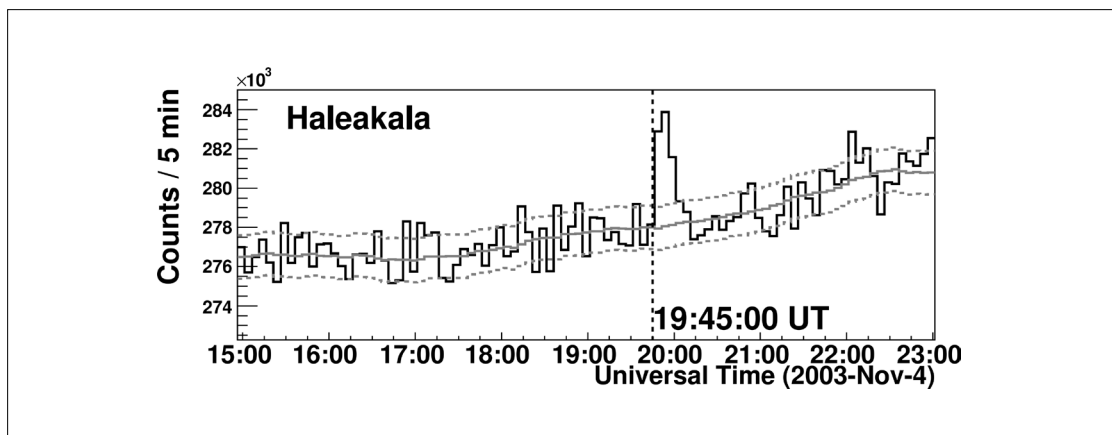


Fig. 1: Most recent SNP event observed by the old Haleakala NM station in 2003, November 4.

Picture taken from (Watanabe et al. 2006): *Five minute averages of the counting rate observed by the Haleakala. The smooth solid line is the averaged background, and the dashed lines are $\pm 1\sigma$ from the background.*

sorption, and low latitude, to maximize the elevation of the Sun. During its history, the old HLEA detector measured three SNP events (a list can be found in Yu et al. 2015). For demonstration purposes, Fig. 1 shows the five-minute average count rate for 2003, November 4, measured by the old HLEA station. At 19:45 UT, the detector measured a 2% increase over the background due to SNPs (Watanabe et al. 2006). The significance of this SNP event was 7.5σ . We now have funds to setup six-tubes which corresponds to one third of the old NM station and the new uncertainty on signal would scale roughly as, resulting in a significance of 4.3σ . Thanks to our collaboration with Chiang Mai University, we will have the possibility to expand HLEA NM with other three-tubes (see Sec. 3). In this case the significance would increase to 5.3σ . Therefore, a scaled-down version of HLEA would still be highly sensitive to SNP events with amplitude of 2% or more over the background. There are only a few NMs in the global NM network in a favorable location for detecting SNPs. The restoration of HLEA would fill a large gap between the Thailand and Mexico stations and will also provide information about FDs for GCRs with rigidity above 13 GV (Mangeard et al. 2017). The new HLEA NM will extend the ground coverage of GCR and SNP detection.

3. Redeployment of the Haleakala NM

Two standard sea containers will host the new HLEA NM and will be placed on Haleakala summit. Fig. 2 shows the facility location for the new HLEA NM. The area will cover a maximum of 50m^2 . It is located on the Haleakala summit in island of Maui, near the building that previously hosted the old HLEA NM. The new HLEA NM will be also near to the Daniel K. Inouye Solar Telescope (DKIST). DKIST telescope is imaging the Sun in several wavelengths. The direct observation of solar flares that produce SNPs will provide context for interpreting the new HLEA data.

Complementing HLEA will be a portable NM, Thimon provided by Chiang Mai University in Thailand. Fig. 3 shows a picture of the exterior of Thimon sea container hosting an NM instrument. This sea container was prepared and equipped in Thailand. Thimon NM will be one of the two sea containers that will constitute and expand HLEA NM instrument.

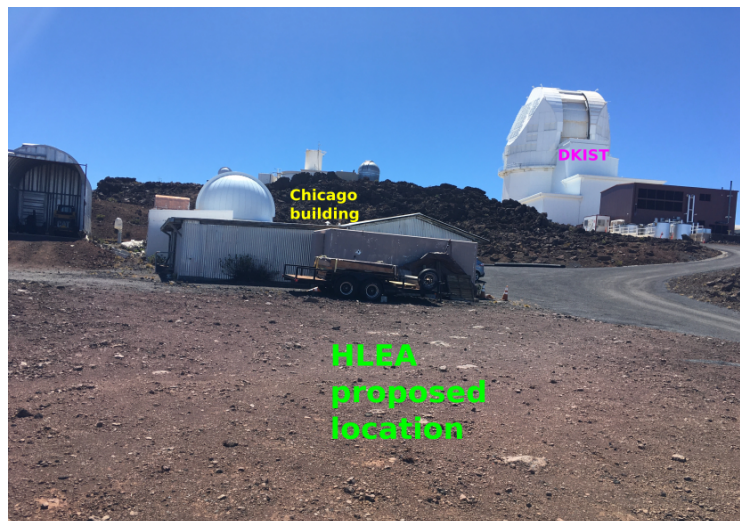


Fig. 2: Picture of new HLEA NM facility close to the Chicago building that previously hosted the old HLEA NM, on the Haleakala summit. The new HLEA will be also near to the DKIST telescope.



Fig. 3: Side view of Thimon shipping container. Logos of different institutes of the collaboration are well visible.

Fig. 4 shows a picture of the interior of Thimon shipping container. This container is already furnished with a 3-inch thick polyethylene (reflector) box and three pure lead rings that will host three Boron Tri-Fluoride (BF_3) NM tubes. We will reuse the original proportional counter tubes, with moderator, that were part of the previous HLEA NM. The Thimon container will be equipped with power cables, computers, temperature sensors, barometers, and lights. New electronic boards will be fabricated and tested at Bartol Research Institute. At the moment Thimon is located on the campus of the University of Hawaii (UH) on O'ahu. It will be shipped to Maui where it will be equipped with three BF_3 tubes and electronics.

A second shipping container with double doors will host the other six BF_3 tubes arranged such as three tubes will be reached at each side of the container independently. **Fig. 5** shows a model of this second

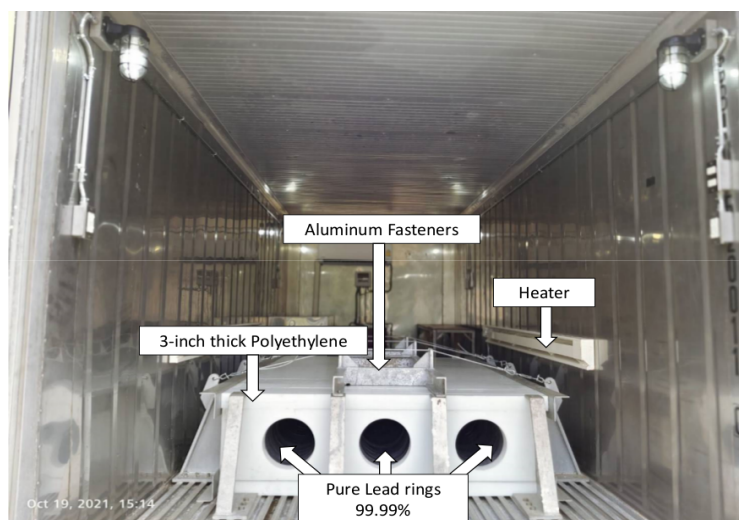


Fig. 4: Interior of Thimon, one of the two HLEA shipping containers minus the BF3 tubes. This container is equipped with a 3-inch thick polyethylene box and three pure lead rings. Aluminum fasteners and heaters are also marked.

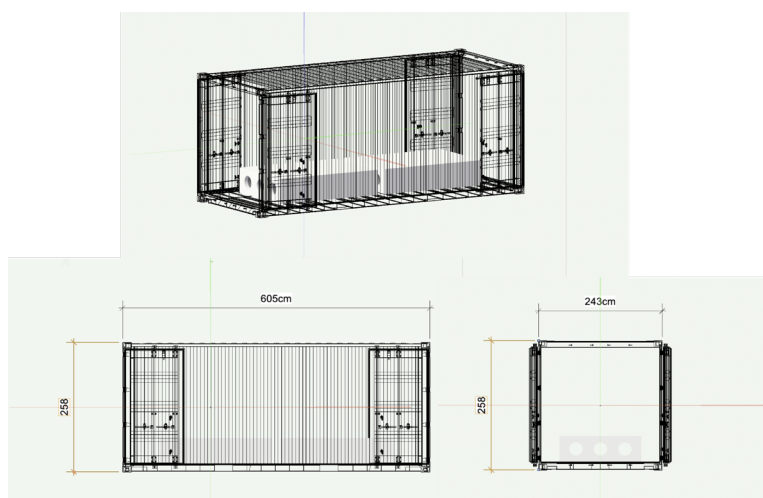


Fig. 5: Model of the second HLEA shipping container with double doors and two banks of 3-tubes at each side.

container seen from different angles. To minimize the operations at the summit, the second container will be assembled, equipped and tested at UNH. Also this second shipping container will be sent to Maui.

After the setup procedure is done, tests will be performed on Haleakala summit to check that the new HLEA NMs are running properly. We will take data and perform end-to-end tests. After these tests, normal operation will begin and the new HLEA NM will be remotely monitored. A monitoring system program will be developed and displayed at UH campus. Finally, HLEA data will be publicly available through the online NM database (NMDB) (<https://www.nmdb.eu>, last accessed July 4, 2023).

4. NM Calibration with AMS Data

The simultaneous measurements of AMS and NMs provide us the opportunity to validate and calibrate the NM YFs, i.e., the response of an NM to the particle flux with a given energy. The NM count rate at a time t , $N(t)$, can be related to the near-Earth spectrum, $J(R,t)$, as a function of rigidity R and time t ,

$$N(t) = \frac{1}{k} \sum_{i=p,He,\dots} \int_{R_c}^{\infty} J_i(R,t) Y_i(R) dR, \quad (1)$$

where R_c is the rigidity cutoff of the selected NM, k is a normalization factor that corrects for the realities of the NM (electronic efficiency, environmental effects, etc), $Y_i(R)$ is the YF, and the sum over the index i runs over all cosmic-ray elements. In our previous work (Koldobskiy et al. 2019), we tested the validity of different YFs commonly used in literature, by computing the normalization factor k as the ratio between the modeled and observed count rate. If a YF correctly describes the low-energy response of a NM, then the normalization factor k should be stable in time and uncorrelated to the level of solar activity. As $J_i(R,t)$, we used the monthly proton and helium fluxes measured by AMS from May 2011 to May 2016 (Aguilar et al. 2018). To correctly account for the contribution of $Z>2$ elements in GCRs, we used the fluxes of lithium, beryllium, boron, carbon, neon, and oxygen measured by AMS between May 2011 and May 2016 (Aguilar et al. 2021a), assuming that their spectrum has the same time dependence as that of helium. Recent AMS results on daily proton and helium fluxes (Aguilar et al. 2021b; Aguilar et al. 2022) give us the possibility to do the same work on a shorter time scale and to extend the YF validity. We will redo the same analysis testing different YFs on a daily basis until November 2019.

This job will serve as a starting point for calibrating the GCR spectra measured by the upcoming HLEA NM with future AMS publications.

5. Simulation of HLEA detector response

The particle environment on Haleakala, and the instrument itself, differs from all other stations in the Simpson network. Consequently, it is essential to understand in some detail how the detector responds to the particle spectrum. We will assess the realistic, energy-dependent effective area of HLEA, the so-called YF, for both GCRs and SNPs. To that end, we will embark on a thorough simulation of the instrument and its surrounding environment, which includes the overlying atmosphere. We will use GEANT-4 and PLANE-TOCOSMICS (Agostinelli 2023) simulation of the GCR and SNP magnetospheric and atmospheric transport with a realistic atmospheric depth profile. Variables that should be studied are: incident direction, solar cycle dependent cutoff, atmospheric overburden, and water content at the site of the instrument. To completely model the instrument requires an accurate representation of locations of the various components, i.e., the lead, low density polyethylene, other passive material, the sea container housing the instrument, and even the rock or soil lying beneath the monitor. We will characterize how the instrument responds to barometric pressure variations that affect the count rate. The elemental composition of GCRs affects the ground level neutron intensity. An NM responds to the number of hadronic interactions, so a ${}^4\text{He}$ cosmic ray will roughly generate four times the signal of a proton. NMs have typically assumed either pure protons or a mix of protons and helium. With AMS measurements available, we can now properly compute

the response from a cosmic-ray spectrum of variable composition. The effect of different species on the NM response will be simulated. As primary particle spectra, we will use the published AMS fluxes of the most abundant GCRs species: proton, helium, carbon, and others from oxygen up to a high-Z component, such as iron. The final simulated response will be compared to data. To check the validity of this YF, we will compare the measured count rate with the one calculated with Eq.1 of Sec.4.

For SNPs, the incident spectrum and composition is markedly different (softer) than that of the GCRs. The response of NMs is consequently different. Therefore, a complete air shower simulation will be performed for incoming neutrons of different energies. As SNP input spectra we will use a power law function with exponential rollover (Ellison & Ramaty 1985) as suggested by γ -ray measurements (Hurford et al. 2003; Ackermann et al. 2021). Because neutrons are not affected by the IMF and magnetosphere, they travel straight from Sun to Earth, and thus their distribution will be modeled as a point-like source coming from the Sun with different incident angles depending on the time of day at the detector and declination of the Sun. Earth's rotation will be taken into account and the particle distribution for seasonal and local time effects will be estimated at Haleakala location.

The entire process will serve as a calibration method for the HLEA detector.

Acknowledgements

The authors acknowledge the generous support of the National Science Foundation through grant 2149809 and 2149811.

References

- Ackermann, M., et al. (Fermi collaboration) 2021, Fermi detection of γ -ray emission from the M2 soft X-ray flare on 2010 June 12. *The Astrophysical Journal*, 745:144(11pp), <https://doi.org/10.1088/0004-637X/745/2/144>
- Agostinelli, S., et al. (Geant-4 collaboration) 2003, Geant-4 simulation toolkit. *Nucl. Instrum. Methods. Phys. Res. A*, 506:250-303, [https://doi.org/10.1016/S0168-9002\(03\)01368-8](https://doi.org/10.1016/S0168-9002(03)01368-8)
- Aguilar, M., et al. (AMS collaboration) 2018, Observation of fine time structures in the cosmic proton and helium fluxes with the Alpha Magnetic Spectrometer on the International Space Station. *Physical Review Letters*, 121(05), 051101, <https://doi.org/10.1103/PhysRevLett.121.051101>
- Aguilar, M. et al. (AMS collaboration), 2021a, The Alpha Magnetic Spectrometer (AMS) on the International Space Station: Part II - Results from the first seven years. *Physics Reports* 894:1-116, <https://doi.org/10.1016/j.physrep.2020.09.003>
- Aguilar, M., et al. (AMS collaboration) 2021b, Periodicities in the Daily Proton Fluxes: Results from the Alpha Magnetic Spectrometer. *Physical Review Letters* 127, p. 271102, <https://doi.org/10.1103/PhysRevLett.127.271102>
- Aguilar, M., et al. (AMS collaboration) 2022. Properties of Daily Helium Fluxes. *Physical Review Letters* 128, p. 231102, <https://doi.org/10.1103/PhysRevLett.128.231102>
- Ellison, D.C. and Ramaty, R., 1985. Shock acceleration of electrons and ions in solar flares. *The Astrophysical Journal*, 298:400-408, 1985, <https://doi.org/10.1086/163623>
- Galper, A.M., et al. (PAMELA collaboration) 2017 The PAMELA experiment: A decade of cosmic ray physics in space. *Journal of Physics, Conference Series*, 798(012033), <https://doi.org/10.1088/1742-6596/798/1/012033>
- Hurford, G. J., et al. 2003. First gamma-ray images of a solar flare. *The Astrophysical Journal*, 595:L77-L80, 2003, <https://doi.org/10.1086/378179>
- Koldobskiy, S.A., Bindi, V., Corti, C., Kovaltsov, G. A., and Usoskin, I. G. 2019, Validation of the neutron monitor yield function using data from AMS-02 experiment. *J. Geophys. Res. (Space Phys.)*, <https://doi.org/10.1029/2018JA026340>
- Mangeard, P.S., et al 2017, Cosmic ray modulation observed by the princess sirindhorn neutron monitor at high rigidity cutoff. 35th International Cosmic Ray Conference, <https://doi.org/10.22323/1.301.0036>

- Mishev, A., and Usoskin, I. 2020, Current status and possible extension of the global neutron monitor network. *J. Space Weather Space Clim.* 10:17, <https://doi.org/10.1051/swsc/2020020>
- Watanabe, K., et al. 2006, Solar neutron events of 2003 October–November. *The Astrophysical Journal* 636:1135–1144, <https://doi.org/10.1086/498086>
- Yu, X.X., Lu, H., Chen, G.T., Li, X.Q., Shi, J.K., Tan, C.M. 2015, Detection of solar neutron events and their theoretical approach. *New Astronomy* 39:25–35, <https://doi.org/10.1016/j.Newast.2014.12.010>

Open Access

This paper is published under the Creative Commons Attribution 4.0 International license (<https://creativecommons.org/licenses/by/4.0/>). Please note that individual, appropriately marked parts of the paper may be excluded from the license mentioned or may be subject to other copyright conditions. If such third party material is not under the Creative Commons license, any copying, editing or public reproduction is only permitted with the prior consent of the respective copyright owner or on the basis of relevant legal authorization regulations.

Session 4: Abstracts

New registration system of cosmic ray stations of ISTP SB RAS

Anna A. Lukovnikova

Correspondence

ISTP SB RAS - Institute of Solar-Terrestrial Physics, Siberian Branch of Russian Academy of Sciences, Irkutsk, Russia

Abstract

We consider the new registration system of cosmic ray stations. This system is based on a Raspberry Pi 3.

Neutron monitor electronics for spectral information from a single neutron monitor

David Ruffolo 

Correspondence



Department of Physics, Faculty of Science, Mahidol University, Bangkok, Thailand

Abstract

Neutron monitors have provided continuous tracking since about 1950 of the neutron count rate at various sites, with a precision as good as 0.1% for hourly rates, to monitor variations in the cosmic ray flux. Because different sites have different rigidity cutoffs (thresholds), ranging from about 1 GV to 17 GV, it is commonly thought that these sites also provide continuous monitoring of the cosmic ray spectrum over that rigidity range. However, in practice there are systematic uncertainties and local atmospheric effects that limit the accuracy of tracking spectral variations in that way, especially for time scales shorter than a year. Therefore, several techniques have been developed that can successfully measure spectral variations of galactic cosmic rays or solar energetic particles at a single site (or neighboring sites) or from a single neutron monitor. After a brief overview of such techniques, we will specifically describe techniques using special electronics to provide timing and multiplicity information. We describe technical problems with a common definition of multiplicity in terms of the number of events detected within a time window, because these are strongly affected by chance coincidences, which are sensitive to atmospheric pressure. A more successful technique is to statistically remove chance coincidences from the distribution of time delays between successive counts

to determine the “leader fraction” of counts that did not follow a temporally associated count from the same cosmic ray shower. This technique has been validated using data from latitude surveys and comparison with data from the space borne AMS-02 detector. At high cutoff rigidity, e.g., above 17 GV, the leader fraction provides superior resolution of spectral variations in comparison with spacecraft detectors. Electronics have been further developed to collect statistics on cross-counter time delays and events with high counter multiplicity. Partially supported by grant RTA6280002 from Thailand Science Research and Innovation.

Neural networks for identification of neutron monitor faulty tube-counts

Danislav T. Sapundjiev , Stanimir M. Stankov , Jean-Claude Jodogne

Correspondence

Royal Meteorological Institute of Belgium, Brussels, Belgium

Abstract

Neutron monitor data quality and control is fundamental for successful and reliable application of this instrument to space weather forecasting. The majority of the operating neutron monitors were built in the years 1965–1975. Despite all care and efforts to maintain their operation, noise and spurious peaks in one or more individual detector tubes are still observed in the output data. This requires data control and verification by an operator which is not suitable for real-time applications. The usual algorithm is to check the individual tube counts against the ratios with the remaining tubes [Sapundjiev et al. 2014](#). In some cases, more than half of the individual tubes do not pass the tube-ratio-test and the measurement cannot be accepted. In this work we are investigating the applicability and the advantages of neural networks (NNs) to detect faulty and good tube counts and the potency to recover erroneous data from as little as a single correct measurement. In order to evaluate this method, besides the real operational data for the training, we also used complex tailored data with as little as one good detector measurement. Finally, we are testing the NNs for real time data-control and correction complimentary to the tube ratios method.

Correction of snow effects on Oulu data using local snow depth data

Pauli Väisänen , Ilya Usoskin 


Correspondence

Space Physics and Astronomy, Faculty of Science, University of Oulu, Finland

Abstract

The University of Oulu neutron monitor (NM) started its operation in 1964 on the Kontinkangas campus, where it operated until 1974 and was located in a building with a roof where snow can be accumulated during winters. The amount of snow is known to affect count rates by reducing the NM count rate. Comparing the measured NM count rates to theoretical count rates determined by using a numerical model and the modulation potential, inferred independently from other NMs, deviations of up to 5 % can be observed on snowy winters. Although there are no recordings of snow depth on the building roof itself, digitized daily-snow-depth data from the Linnanmaa weather station, some 6 km north-northwest of the Kontinkangas location, are available. This has allowed us to determine corrections to the data. For individual snow periods, we found a good linear relation between the snow depth and deviation in the measured Oulu NM count rates from those theoretically expected. This relation can be used to correct the Oulu NM data for wintertimes before 1974. Since the move of the Oulu NM location to a new pyramid-shaped building in 1974, snow has never affected the NM count rate again.

Latitude surveys of time-delay histograms from a semi-leaded neutron monitor during 2018–2020

Panutda Yakum¹, Waraporn Nuntiyakul ¹, Sidarat Khamphakdee¹, Achara Seripienlert ², David Ruffolo ³, Alejandro Sáiz ³, Paul Evenson ⁴, Pierre-Simon Mangeard ⁴, Peng Jiang⁵, Pongpichit Chuanraksasat ², Chanoknan Banglieng ⁶, Kazuoki Munakata ⁷

Correspondence

- 1 Department of Physics and Materials Science, Faculty of Science, Chiang Mai University, Chiang Mai, Thailand
- 2 NARIT - National Astronomical Research Institute of Thailand, Chiang Mai, Thailand
- 3 Department of Physics, Faculty of Science, Mahidol University, Bangkok, Thailand
- 4 Bartol Research Institute and Department of Physics and Astronomy, University of Delaware, Newark, USA
- 5 Polar Research Institute of China, Pudong, Shanghai, China
- 6 Department of Physics, Faculty of Science and Technology, Rajamangala University of Technology Thanyaburi, Pathum Thani, Thailand
- 7 Physics Department, Shinshu University, Matsumoto, Nagano, Japan




Abstract

We have developed a portable neutron monitor with three counters for latitude surveys to investigate cosmic ray spectral variations. This “Changvan” uses the NM64 design, except that the middle counter lacks the lead producer, so we call this a “semi-leaded” neutron monitor. The Changvan was operated on two voyages of the Chinese icebreaker Xue Long between China and Antarctica in the 2018 and 2019. The standard measurement during a latitude survey is the count rate as a function of geomagnetic cutoff rigidity, i.e., the response function of the total count rate. Repeated measurements with the same detector over different solar cycle phases provide precise information about cosmic ray spectral variation. In addition, we have tested two techniques to track spectral variation, which have or could be implemented at fixed stations. First, histograms of the time delay between successive neutron counts determine the leader fraction, previously used to monitor short-term and solar-cycle spectral variations. Second, the count rate ratio of unleaded vs. leaded counters varies enormously with geomagnetic cutoff rigidity, indicating sensitivity to the cosmic ray spectrum. This may have advantage relative to using a “bare” counter in that this “unleaded” counter is shielded from the environment by the reflector and has a higher count rate due to the adjacent lead. We report measurement of the response function of the count rate and the leader fraction of the unleaded and leaded counters during these two latitude surveys. Partially supported by grant RTA6280002 from Thailand Science Resesarch and Innovation.

Session 5:

**Neutron detector
response functions**

Neutron monitor yield function: improved spectral computations of the Forbush decrease of June 2015

Maria Livada , Loukas Xaplanteris , Nafsika Dimosthenous , Helen Mavromichalaki 

Correspondence

Nuclear and Particle Physics Department, Faculty of Physics, National and Kapodistrian University of Athens, Greece, mairiliv@phys.uoa.gr, ksaplant@phys.uoa.gr, ndimosthen@phys.uoa.gr, emavromi@phys.uoa.gr

Keywords

galactic cosmic rays; spectral analysis; Forbush decreases; yield functions; neutron monitors

Abstract

In this work a new improved coupling function by Xaplanteris et al. (2021) based on Quantum Field Theory is applied for spectral analysis of cosmic rays. This new coupling function had already been confirmed in the application of cosmic rays with the calculation of primary cosmic ray intensity during Forbush decreases and ground level enhancements but this is the first time that it is used for the calculation of spectral index. To describe the rigidity spectrum of the galactic cosmic ray (GCR) during a Forbush decrease, a power law in rigidity is often used. The exponent of this power law, the spectral index, describes the hardness of the GCR spectrum. The spectrum of the GCR becomes harder during the Forbush decrease main phase. For this analysis the Forbush decrease of the cosmic ray intensity observed on June 2015 was chosen. Daily cosmic ray data of the neutron monitor stations obtained from the high-resolution neutron monitor database (NMDB) were used for calculating the cosmic ray density and anisotropy variations. For the spectral analysis of the galactic cosmic rays the technique of Wawrzynczak and Alania (2010) is applied, based on the coupling coefficient method. The obtained results of the Fd analysis by using the new coupling function by Xaplanteris et al. (2021) are compared with the results obtained based on the coupling function by Clem and Dorman (2000).

1. Introduction

Cosmic rays (CRs) that arrive at the top of the atmosphere are called primary cosmic rays. The cosmic rays that manage to penetrate the Earth atmosphere interact with its components and produce showers of secondary particles that are measured by the ground based detectors. The worldwide network of standard

neutron monitors (NMs) is of great importance for the detection and provision data of secondary neutrons produced by the interaction of cosmic rays and solar energetic particles with the atmospheric molecules to analyze CR variability (Shea & Smart 2000; Moraal et al. 2000).

The linking of the intensity of primary CRs with the NM count rates (secondary cosmic rays) requires high numerical simulations of the atmospheric cascade. One way to achieve this is with the NM yield function and it is crucial for Space Weather research. The yield function of a specific primary particle type is defined as the detector's response to this particle type at energy E and has dimensions of (counts m^2 sr), so it depends on the geometric characteristics of the NM detector. On the other hand the coupling function is defined as the differential count rate of the NM and has dimensions of counts $(GeV)^{-1}$ (Clem and Dorman 2000). There are several yield functions (or coupling function), some of which are calculated based on theoretical tools while others are defined by statistical and computational models. The FLUKA (Fasso et al. 1993) Monte-Carlo package was used by Clem and Dorman (2000) for simulations of particles transport through the atmosphere. The GEANT-4 (Agostinelli et al. 2003) Monte Carlo package was applied by Flückiger et al. (2008) and Matthiä et al. (2009) for the same reason. Also the GEANT-4 PLANETOCOSMICS Monte-Carlo tool and a realistic atmospheric model were used by Mishev et al. (2013) for the computation of an improved yield function. Recently, a new coupling function based on Quantum Field Theory (QFT) computations was published (Xaplanteris et al. 2021). Yield functions developed by different groups show different results in some energy regions due to the fact that they differ on the set of assumptions they are based on, the processes they take into account and the technique they are derived from (Heck 2006). The necessity of an accurate and suitable yield function has been presented in various publications (e.g. Clem & Dorman 2000; Mavromichalaki et al. 2012) especially for spectral analysis of important events of CRs such as Forbush decreases (Fds) and ground level enhancements (GLEs). In this work we focus on the case of Fds of GCRs.

Forbush decrease manifests itself in the fast decreases of the GCR intensity followed by a gradual recovery phase that happens over 8-10 days (Forbush 1954). Most of Fds occur due to coronal mass ejections (CMEs) which come from the Sun along with a shock wave (Cane 2000; Papailiou et al. 2013). The amplitude of the Fd (%) for each NM is defined as the difference between the cosmic ray intensity at the onset and the minimum point of this. A dependence of the observed difference on the GCR rigidity is one of the fundamental characteristics of Fds. It is given by Cane (2000) and can be expressed by a power law $R^{-\gamma}$, where γ is the spectral index.

In this work we focus on the calculation of the spectral index during the Fd using the technique of Wawrzynczak and Alania (2010) which is based on the coupling coefficient method (Clem and Dorman 2000), secondary cosmic ray measurements can be linked to the primary incident cosmic ray particles via specific mathematical functions. The Fd that took place on 22 June 2015 is studied and analyzed. For spectral analysis two coupling functions were applied to the case of the above Fd, the recently established coupling function based on QFT calculations (Xaplanteris et al. 2021) and the total response function of Clem and Dorman (2000). Our results are discussed.

2. Data selection

In this work daily cosmic ray data corrected for pressure and efficiency from middle latitude NM stations located over the world and obtained from the high resolution real time Neutron Monitor Database (NMDB) (<http://www.nmdb.eu>) were used. This study analyzes data from five stations with cut-off rigid-

ities above 1.67GV due to the limitations of the QFT coupling function: (Baksan (BKSJ) – $R_c = 5.60$ GV, Guadalajara (CALM) – $R_c = 6.95$ GV, Lomnický štít (LMKS) – $R_c = 3.84$ GV, Rome (ROME) – $R_c = 6.27$ GV, Jungfraujoch (JUNG1) – $R_c = 4.5$ GV).

The cosmic ray intensity recorded at each station was normalized according to Equation 1:

$$J_i^k = \frac{N_k - N_o}{N_o} \quad (1)$$

where J_i^k is the normalized cosmic ray intensity for the i^{th} station of the Fd, N_k is the daily cosmic ray intensity of each station for k days ($k=1,2,3,..$ days) and N_o is the average cosmic ray intensity for three days before the beginning of the Fd (Wawrzynczak & Alania 2010). Time profiles of daily values of the cosmic ray intensity of five middle latitude NM stations are presented in (Fig. 1) from 20 June 2015 to 03 July 2015. The first Fd in the studied period happened on 23 June 2015 and had an amplitude with a value of 6.51% for the JUNG1 NM station. The second one took place on 25 June 2015 with an amplitude value of 8.02% for the LMKS NM station. An increase in the counting rate of the JUNG1 NM station during 29-30 June 2015 (Fig.1) can be explained by the melting snow which may have started even before 29 June 2015 (Maurin et al. 2015) <http://cosray.unibe.ch> (last accessed May 12, 2023). We plan to make a new Fd analysis and publication in which we will not use the data of JUNG1, but the data of JUNG station.

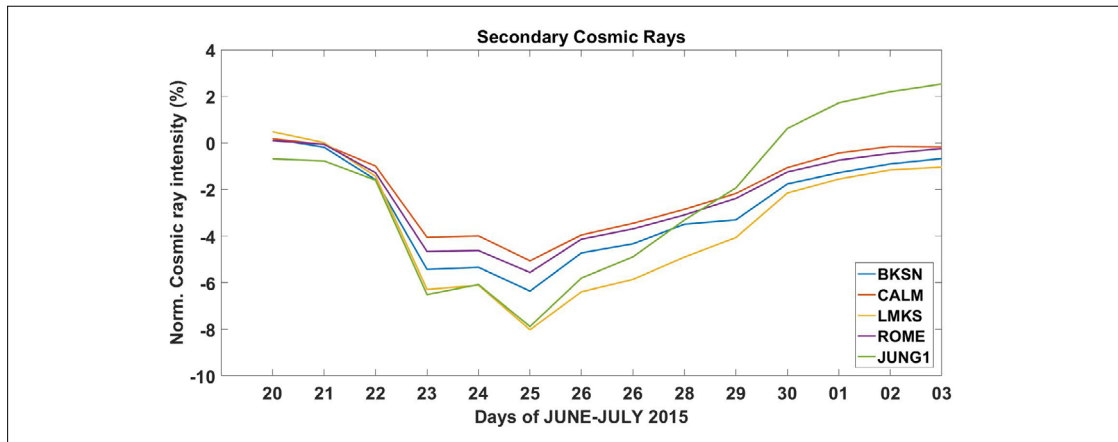


Fig. 1: The normalized CR intensity for middle latitude stations obtained from NMDB for the time period of 20 June 2015 to 03 July 2015.

During the studied period a series of solar events took place on the Sun. In general, 53 C-flares and 7 M-flares occurred on the solar atmosphere and 7 halo and partial halo CMEs at the solar corona, which had a linear velocity up to 1714 km/s. They were observed by GOES and SOHO/LASCO satellites <https://www.ngdc.noaa.gov/stp/space-weather/solar-data/>; <https://cdaw.gsfc.nasa.gov> (last accessed September 15, 2022). As for the geomagnetic indices the maximum value of the Kp index was equal to 8 on 22 June 2015 at 18:00-21:00 UT whereas the Dst index had two minimum values: a first one equal to -124nT that was on 22 June 2015 at 21:00-22:00 UT and a second one equal to -204nT that was on 23 June 2015 at 05:00–06:00 UT about a few hours after the minimum of the cosmic ray intensity (Samara et al. 2018) <https://www.spaceweatherlive.com>; Final Dst Index Monthly Plot and Table (kyoto-u.ac.jp) (last accessed May 12, 2023). It is thus concluded that two severe G4 geomagnetic storms occurred in the period 22–23 June 2015.

3. Data analysis and results

The method of Wawrzynczak and Alania (2010) used in previous works by Livada et al. (2018) and Livada and Mavromichalaki (2020) for spectral analysis of the Fd events was also applied in this work for the above selected Fds, complemented by the coupling function by Xaplanteris et al. (2021) based on QFT.

According to Wawrzynczak and Alania (2010), secondary cosmic ray data can be linked to the primary incident cosmic ray particles via specific mathematical functions that take into account the acceptance vectors for each detector (NM), based on its local characteristics (cut-off rigidity, altitude, geographic coordinates and detector's type). Each NM station is characterized by its asymptotic cone of acceptance which is a result of the modulation by the geomagnetic field of the cosmic rays (Dorman 2004).

Variations of GCRs intensity near Earth during Fds can be expressed by a power law in rigidity, according to Equation (2):

$$\frac{\delta D(R)}{D(R)} = \begin{cases} A \left(\frac{R}{R_0}\right)^{-\gamma} & R \leq R_{max} \\ 0 & R > R_{max} \end{cases} \quad (2)$$

where $R_0=10\text{GV}$ and $R_{max}=200\text{GV}$ is the rigidity above which the Fd of GCRs vanishes (Dorman 2004).

The cosmic ray intensity J_i^k of the Fd for the i^{th} detector with geomagnetic cut-off rigidity R_i at an atmospheric depth h_i (Dorman 1963) is defined as in Equation (3):

$$J_i^k = \int_{R_i}^{R_{max}} \left(\frac{\delta D(R)}{D(R)}\right)_k W_i(R, h_i) dR \quad (3)$$

where $W_i(R, h_i)$ is the coupling coefficient for the NM. In this study two coupling functions were studied the first is by Xaplanteris et al. (2021) and the second by Clem and Dorman (2000) which analyzed in section 3.1 and 3.2.

$$W(E) = 1.65 \times 10^{-2} \frac{1}{E} \left[\ln\left(\frac{E}{E_{cut}}\right) \right]^2 \left[\frac{5}{1 - 0.095 \ln\left(\frac{E}{E_{cut}}\right)} \right]^2 \text{ by Xaplanteris et al. (2021)}$$

$$w_T(R, h) = \alpha(h) (k(h)-1) \exp(-a(h) R^{-k(h)+1}) R^{-K(h)} \text{ by Clem and Dorman (2000)}$$

Inserting the power law of Equation (2) into Equation (3) and solving for the cosmic ray intensity of the Fd in free space (in the heliosphere) A_i^k , we can conclude the Equation (4) below:

$$A_i^k = \frac{J_i^k}{\int_{R_i}^{R_{max}} \left(\frac{R}{R_0}\right)^{-\gamma} W_i(R, h_i) dR} \quad (4)$$

where A_i^k should be independent of the local characteristics of the NM. Yasue et al. (1982) calculated the aforementioned coupling integral for discrete magnitudes and γ . In our analysis the cosmic ray intensity A_i^k of the Fd in the heliosphere was calculated for discrete values of γ ranging from 0.1 to 2 with step 0.01 using Matlab program (201 values) for 'i' NMs. According to our requirement an acceptable γ_o must correspond to the values of the A_i^k being almost the same for all NMs, i.e. $\Delta A_i^k = A_i^k - \bar{A}^k$ should be the minimal value. The errors $\Delta\gamma$ of each spectral index were calculated based on the previous ($k-1$) and the next value ($k+1$) of spectral index γ_o .

The technique of Wawrzynczak and Alania (2010) is based on the coupling function $W_i(R, h_i)$ between the intensity of NMs J_i^k and the primary cosmic rays A_i^k in the heliosphere that was described from Equation 4. In this work two types of coupling coefficient expressions are obtained.

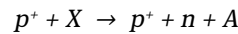
3.1 Theoretical coupling function

The first theoretical coupling function is the one proposed by Xaplanteris et al. (2021). It is derived purely analytically and aims to test the applicability of QFT computational tools to CRs phenomena. Initially a slight variation of the Lagrangian density L of a traditional Φ^4 theory is chosen (Peskin & Schroeder 1995; Srednicki 2007; Bilal 2011):

$$L = \frac{1}{2}(\partial_\mu \Phi_1)^2 + \frac{1}{2}(\partial_\mu \Phi_2)^2 + \frac{1}{2}m_1^2 \Phi_1^2 + \frac{1}{2}m_2^2 \Phi_2^2 - \frac{\lambda}{2!} \Phi_1^2 \Phi_2^2 \quad (5)$$

where Φ_1 and Φ_2 are scalar fields that describe the proton of mass m_1 and the neutron of mass m_2 respectively and are coupled with a coupling constant λ .

The interaction resulting in neutron production assumes that a primary proton, moving towards the Earth's surface, collide with a large atmospheric particle X and as a result a secondary proton (less energetic than the initial one) is produced alongside with a neutron and a large particle A . The large atmospheric particle X refers to an atmospheric molecule with large enough mass compared to the mass of a nucleon, so that in the equation of energy conservation it can be assumed at rest. More specifically in the calculation of the scattering amplitude using the Lehmann, Symmanzik, Zimmermann (LSZ) formula the particle used as X is nitrogen with mass $M=14 m_p=14 \text{ GeV}$ (Xaplanteris et al.2021).



Essentially, the model assumes that the produced neutron escapes from the particle X , meaning that particles X and A have masses differing by 1GeV. Furthermore, the secondary proton and neutron are assumed to travel towards the Earth's surface and particles X and A are considered at rest since their masses are much larger than the nucleons' masses. The final assumption that is made in this model is that after every interaction the secondary proton is left with 60% of its initial energy (Dorman 1974) whereas the remaining 40% is assigned to the neutron and particle A . Therefore, the energy cut-off is 1GeV corresponding to a rigidity cut-off of 1.71GV.

Using QFT principles in order to determine the scattering amplitude for the interaction considered the new coupling function can be derived as an expression of the energy E (Xaplanteris et al.2021):

$$W(E) = 1.65 \times 10^{-2} \frac{1}{E^3} \left[\ln\left(\frac{E}{E_{\text{cut}}}\right) \right]^2 \left[\frac{5}{1 - 0.095 \ln\left(\frac{E}{E_{\text{cut}}}\right)} \right]^2 \quad (6)$$

where E denotes the energy of the initial proton, $E_{\text{cut}} = 1 \text{ GeV}$ (or $R_{\text{cut}}=1.71 \text{ GV}$). This means that it can take into account incident protons with energy greater than 1 GeV. This limitation renders the coupling function applicable only to NM stations with energy cut-off value greater than 1 GeV.

It is important to note that the coupling function is not normalized since it can only be applied for energies $E \geq 1 \text{ GeV}$ and does not consider inelastic processes, thermalization and diffusion.

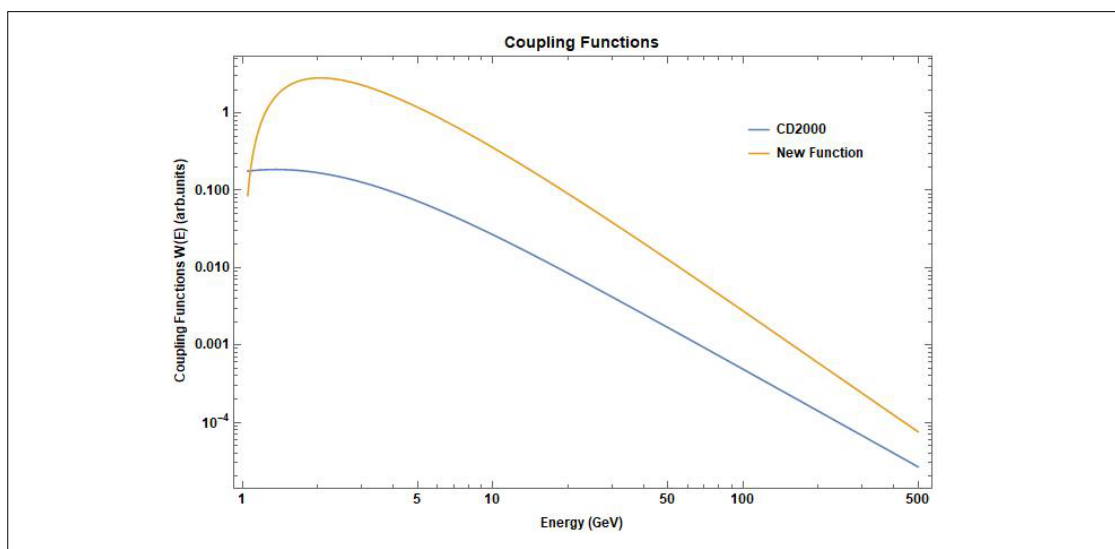


Fig. 2: Comparison of the newly computed coupling function based on QFT (Xaplanteris et al. 2021) with the function of Clem and Dorman (2000).

3.2 Total response function

The second coupling function is the total response function of Clem and Dorman (2000) given in Equation (7).

$$w_T(R, h) = \alpha(h) (k(h)-1) \exp(-a(h) R^{-k(h)+1}) R^{-K(h)} \quad (7)$$

where R is the cut-off rigidity of each station and a and κ are depth-dependent parameters which depend on solar activity (minimum or maximum).

In Fig. 2 the yield function of QFT (Xaplanteris et al. 2021) and the function of Clem and Dorman (2000) where the fit is adapted from Caballero-Lopez and Moraal (2012) are compared. The two curves follow the same behavior with a significant deviation in the lower energies between 2 GeV and 10 GeV. A more detailed justification between the new QFT coupling function and with other ones is given in the work of Xaplanteris et al. (2021).

4. Discussion and conclusions

The method of Wawrzynczak and Alania (2010) was applied using the above two coupling functions according to QFT (Xaplanteris et al. 2021) and Clem and Dorman (2000) respectively, for the calculation of cosmic ray intensity in the heliosphere near Earth for each station and the spectral index during the Fd of June 2015. For the calculation the daily data of five NM stations were used. In Figs. 3 and 4 the results of our calculations are presented.

- From our analysis it is concluded that during the events of June 2015, a temporal continuity between the solar events and the associated phenomena that were recorded on the Earth, exists. The observed Fds are directly associated with the production of CMEs on the Sun and the created shock waves.

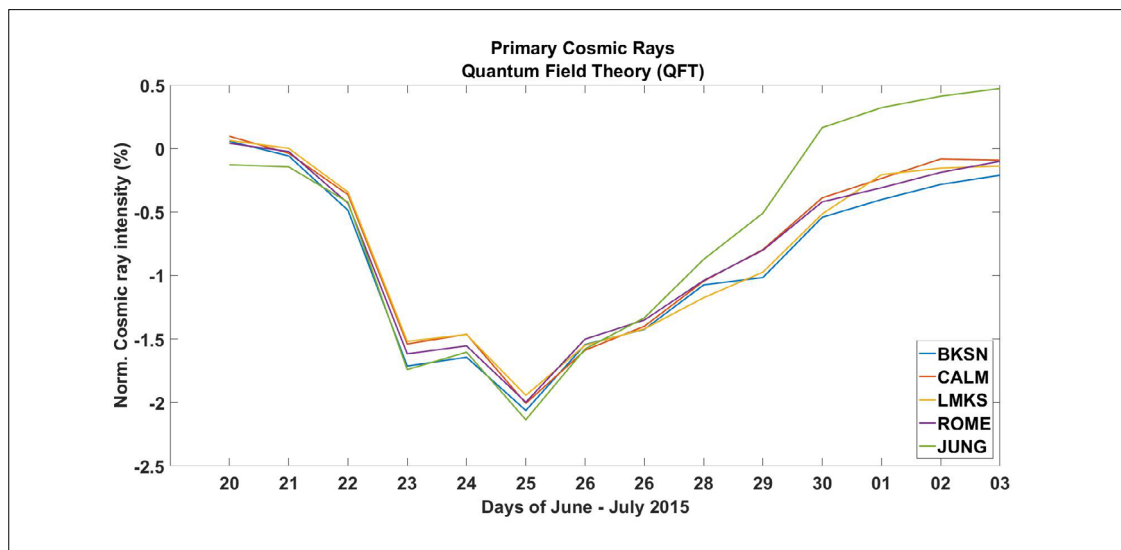


Fig. 3: Time profiles of the primary cosmic ray variations applying the coupling function of Xaplanteris et al. (2021) (above panel) and the function of Clem and Dorman (2000) (down panel) for the time period of 20 June 2015–03 July 2015.

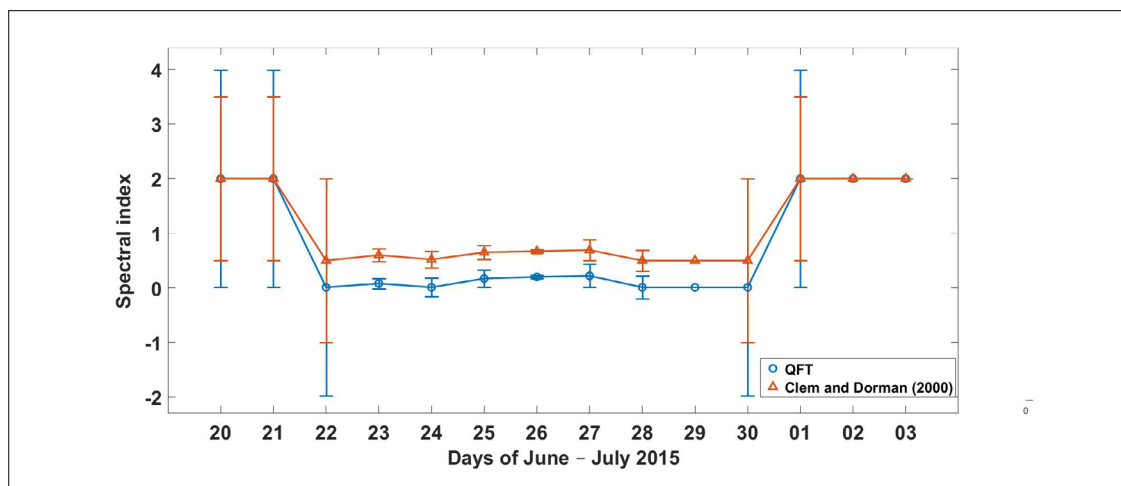


Fig. 4: Temporal changes of the rigidity spectrum exponent applying the coupling function of Xaplanteris et al. (2021) (blue line) and the function of Clem and Dorman (2000) (red line) for the time period of 20 June 2015–03 July 2015.

- According to the method of Wawrzynczak and Alania (2010) the calculated intensity of the primary cosmic rays is expected to be almost the same for the selected NMs due to the fact that it does not depend on the local characteristics of the detectors. This statement was confirmed by the two above coupling functions in Fig. 3 in the case of the selected Fd. In contrast the intensity of the secondary cosmic rays has different values in each station, with some stations having larger amplitude than others stations due to their cut-off rigidity (Fig. 1). However, the primary normalized cosmic ray intensity has difference when determined by the coupling function of Xaplanteris et al. (2021) and by the function of Clem and Dorman (2000) as well as the maximum GCR decrease is ~2% for the results of first coupling function and ~12% for the second Fig. 3. This is caused due to the fact that the calculated cosmic ray intensity depends on the using of coupling function. The newly computed function takes higher values for the energy region under study than the Clem and Dorman (2000) Fig. 2.

- The purpose of this work is to show that the time dependence of the calculated spectral index is in agreement with the fluctuations of the cosmic ray intensity during the Fds (Livada and Mavromichalaki 2020). This is achieved for the Fd of June 2015 for both coupling functions used. Specifically, the spectral index reached the minimum value during the main phase of Fd with the largest amplitude of the Fd (Fig. 4). It means that the spectrum of the GCR becomes harder during the Fd main phase. The deviations of the value of the daily spectral index are within the limit of the calculated error $\Delta\gamma$. In Fig. 4 and Tab. 1 the comparison of the results of the calculated spectral index with both cases of coupling functions is presented, in order to confirm that the new function produces similar results to the other.

Tab. 1: Daily values of the spectral index with the errors for the time period 20 June 2015–03 July 2015.

Date YYYY:MM:DD	Spectral index QFT (Xaplanteris et al. 2021)	Spectral index (Clem & Dorman 2000)
2015:06:20	2.00±1.99	2.00±1.50
2015:06:21	2.00±1.99	2.00±1.50
2015:06:22	0.01±1.99	0.50±1.50
2015:06:23	0.08±0.09	0.60±0.12
2015:06:24	0.01±0.17	0.52±0.15
2015:06:25	0.17±0.16	0.65±0.13
2015:06:26	0.20±0.03	0.67±0.03
2015:06:27	0.22±0.21	0.69±0.19
2015:06:28	0.01±0.21	0.50±0.19
2015:06:29	0.01±0.00	0.50±0.00
2015:06:30	0.01±1.99	0.50±1.50
2015:07:01	2.00±1.99	2.00±1.50
2015:07:02	2.00±0.00	2.00±0.00
2015:07:03	2.00±0.00	2.00±0.00

Acknowledgements

Special thanks are due to our colleagues of the Neutron Monitor stations (www.nmdb.eu) for kindly providing the cosmic ray data used in this study in the frame of the High resolution Neutron Monitor database NMDB, funded under the European Union's FP7 Program (contract no. 213007). Athens neutron Monitor station is supporting by the Special research account of the National and Kapodistrian University of Athens. Thanks are due to the IZMIRAN group of the Russian Academy of Sciences for kindly providing the Forbush decrease data.

References

- Agostinelli, S., Allison, J., Amako, K., Apostolakis, J., Araujo, H., et al. 2003, Geant4- a simulation toolkit, *Nucl Instr. Meth. Phys. Res. A*, 506, 250-303, [https://doi.org/10.1016/S0168-9002\(03\)01368-8](https://doi.org/10.1016/S0168-9002(03)01368-8)
- Bilal, A. 2011, Advanced quantum field theory: renormalization, non-abelian gauge theories and anomalies. In: *Lect. Notes Brus.*
- Caballero-Lopez, R.A., Moraal, H. 2012, Cosmic-ray yield and response functions in the atmosphere. *J. Geophys. Res. Space Phys.* 117, A12103, <https://doi.org/10.1029/2012JA017794>
- Cane, H.V. 2000, Coronal Mass Ejections and Forbush Decreases. *Space Sci. Rev.* 93, 55-77, <https://doi.org/10.1023/A:1026532125747>
- Clem, J.M., Dorman, L.I. 2000, Neutron Monitor Response Functions. *Space Sci. Rev.* 93, 335-359, <https://doi.org/10.1023/A:1026508915269>
- Dorman, L.I. 2004, *Cosmic Rays in the Earth's Atmosphere and Underground.* Kluwer Academic Publishers, Dordrecht, <https://doi.org/10.1007/978-1-4020-2113-8>
- Dorman, L.I. 1974, *Cosmic Rays Variations and Space Explorations.* North-Holland, Amsterdam.
- Dorman, L.I. 1963, *Cosmic Rays Variations and Space Exploration.* Nauka, Moscow.
- Flückiger, E.O., Moser, M.R., Pirard, B., Bütikofer, R., Desorgher, L. 2008, A parameterized neutron monitor yield function for space weather applications. *Proc. 30th ICRC Mexico*, ed. by R. Caballero, J. D'Olivo, G. Medina-Tanco, L. Nellen, F. Sánchez, and J. Valdés-Galicia, 1, 289-292, <https://indico.nucleares.unam.mx/event/4/session/78/contribution/1182/material/paper/0.pdf> (last accessed July 4, 2023).
- Fasso, A., Ferrari, A., Ranft, A., Sala, P. R., Stevenson, G. R., and Zazula, J.M. 1993, A comparison of Fluka Simulations with measurements of Fluence and Dose in Calorimeter structures, *Nucl. Inst. Meth.* A332, 459-468, [https://doi.org/10.1016/0168-9002\(93\)90301-W](https://doi.org/10.1016/0168-9002(93)90301-W)
- Forbush, S. E. 1954, World-wide cosmic-ray variations, 1937-1952. *J. Geophys. Res.* 59, 525-542, <https://doi.org/10.1029/JZ059i004p00525>
- Heck, D. 2006, Low-energy hadronic interaction models. *Nucl. Phys. B-Proc. Suppl.* 151, 127-134, <https://doi.org/10.1016/j.nuclphysbps.2005.07.024>
- Livada, M., Mavromichalaki, H. 2020, Spectral Analysis of Forbush Decreases Using a New Yield Function. *Solar Phys.* 295(115), <https://doi.org/10.1007/s11207-020-01679-z>.
- Livada, M., Mavromichalaki, H., Plainaki, C. 2018, Galactic cosmic ray spectral index: the case of Forbush decreases of March 2012. *Astrophys. Space Sci.* 363(8), <https://doi.org/10.1007/s10509-017-3230-9>.
- Matthiä, D., Heber, B., Reitz, G., Meier, M., Sihver, L., Berger, T., Herbst K. 2009, Temporal and spatial evolution of the solar energetic particle event on 20 January 2005 and resulting radiation doses in aviation. *J. Geophys. Res.* 114(A08104), <https://doi.org/10.1029/2009JA014125>
- Maurin, D., Cheminet, A., Derome, L., Ghelfi, A., Hubert, G. 2015, Neutron monitors and muon detectors for solar modulation studies: interstellar flux, yield function, and assessment of critical parameters in count rate calculations. *Adv. Space Res.* 55, 363-389, <https://doi.org/10.1016/j.asr.2014.06.021>
- Mavromichalaki, H. 2012, The physics of cosmic rays applied to space weather. *Advances in Solar and Solar-Terrestrial Physics*, ed. by G. Maris, C. Demetrescu, 135-161.
- Mishev, A.L., Usoskin, I.G., Kovaltsov, G.A. 2013, Neutron monitor yield function: New improved computations. *J. Geophys. Res.* 118, 2783-2788, <https://doi.org/10.1002/jgra.50325>
- Moraal, H., Belov, A., Clem, J. M. 2000, Design and co-Ordination of Multi-Station International Neutron Monitor Networks. *Space Sci. Rev.* 93, 285-303, <https://doi.org/10.1023/A:1026504814360>
- Papailiou, M., Mavromichalaki, H., Abunina, M., Belov, A., Eroshenko, E., Yanke, V., Kryakunova, O. 2013, Forbush Decreases Associated with Western Solar Sources and Geomagnetic Storms: A Study on Precursors. *Solar Phys.* 283, 557-563, <https://doi.org/10.1007/s11207-013-0231-x>
- Peskin, M.E., Schroeder, D.V. 1995, *An Introduction to Quantum Field Theory.* Perseus Books, Cambridge.
- Samara, E., Smpionias, A., Lytrosyngounis, I., Lingri, D., Mavromichalaki, H., Sgouropoulos, C. 2018, Unusual Cosmic Ray Variations During the Forbush Decreases of June 2015. *Solar Phys.* 293(67), <https://doi.org/10.1007/s11207-018-1290-9>
- Shea, M. A., Smart, D. F. 2000, Fifty Years of Cosmic Radiation Data. *Space Sci. Rev.* 93, 229-262, <https://doi.org/10.1023/A:1026500713452>
- Srednicki, M. 2007, *Quantum Field Theory.* Cambridge University Press, Cambridge, <https://doi.org/10.2277/0521864496>
- Wawrzynczak, A., Alania, M.V. 2010, Modeling and data analysis of a Forbush decrease. *Adv. Space Res.* 45, 622-631, <https://doi.org/10.1016/j.asr.2009.09.005>
- Xaplanteris, L., Livada, M., Mavromichalaki, H., Dorman, L., Georgoulis, M.K., Sarris, T.E. 2021 Improved Approach in the Coupling Function Between Primary and Ground Level Cosmic Ray Particles Based on Neutron Monitor Data. *Solar Phys.* 296(91), <https://doi.org/10.1007/s11207-021-01836-y>
- Yasue, S., Mori, S., Sakakibara, S. et al. 1982, Coupling coefficients of cosmic rays daily variations for neutron monitors. 7, Nagoya

Open Access

This paper is published under the Creative Commons Attribution 4.0 International license (<https://creativecommons.org/licenses/by/4.0/>). Please note that individual, appropriately marked parts of the paper may be excluded from the license mentioned or may be subject to other copyright conditions. If such third party material is not under the Creative Commons license, any copying, editing or public reproduction is only permitted with the prior consent of the respective copyright owner or on the basis of relevant legal authorization regulations.

Session 5: Abstracts

Neutron monitor response functions

Alexander Mishev 

Correspondence

Space Physics and Astronomy, Faculty of Science, University of Oulu, Finland

Abstract

Neutron monitors (NMs) provide continuous ground-based recording of the hadronic component of secondary cosmic ray radiation. The introduction of an NM as a continuous recorder of cosmic ray (CR) intensity followed the design by Simpson in 1953, introduced during the International Geophysical Year (IGY) 1957-1958. The IGY neutron monitor was used worldwide as a detector to study CR variations. Lately, in the mid-sixties, the design of the IGY NM was optimized resulting in increased counting rates. This second generation of NM design is known as NM64 or supermonitor, in practice the standard device nowadays. At recent, mini-NM has been installed at several stations, showing good performance, specifically at low cut-off rigidity and high-altitude locations. Standard NM consists of sensitive to thermal neutrons proportional counters based on ^3He or boron-trifluoride enriched to ^{10}B , surrounded by a moderator, usually paraffin wax or polyethylene, a reflector made of the same material as the moderator and a lead producer. In order to use the NM as a ground-based detector to study CRs, it is necessary to establish a connection between the primary cosmic ray particles at the top of the Earth's atmosphere and the count rate of the device. Since the secondary CRs, resulting from the primary cascade in the Earth's atmosphere, can reach the ground level and eventually be registered by an NM, the corresponding NM response incorporates the full complexity of the atmospheric cascade development including secondary particle propagation in the atmosphere and the efficiency of the detector itself to register the secondaries. Here, different methods of determining the neutron monitor response function to primary CRs are reviewed and discussed including early and recent results as well as several applications.

Session 6:

**Data bases
and catalogues**

Accessing NMDB data using NEST and pandas

Christian T. Steigies ¹, Nicolas Fuller ²

Correspondence

1 Extraterrestrial Physics, Institute of Experimental and Applied Physics, Kiel University, Germany,
steigies@physik.uni-kiel.de

2 Observatoire de Paris, LESIA, Université PSL, CNRS, Sorbonne Université, Université Paris Cité, France,
nicolas.fuller@obspm.fr

Keywords

cosmic rays; neutron monitor; database; python; data science

Abstract


The Neutron Monitor database (NMDB) was created by teams from 12 different countries in 2008. Data from neutron monitors worldwide is pooled and made available, for many stations in real-time. The NMDB Event Search Tool (NEST) started as a quick-look interface to the data in NMDB, but by now has become the main interface to all NMDB data. NEST does not only enable you to plot data from one or several NMDB stations in a very customizable way, it also allows you to retrieve the data in ASCII format for further processing or creating your own plots. Downloading data can be scripted using 'wget' or 'curl' as documented in '3 ways 2 use NEST'. Here we are presenting python functions to read in data from one or several stations directly from NEST into a pandas dataframe. Once your data is in a 'dataframe', you can easily sort, modify or plot data with python.

1. Introduction

The main goal of the Neutron Monitor Database (NMDB) is to make neutron monitor data easily accessible, in a common format. This includes real-time data (for example available at <http://rt.nmdb.eu>, last accessed July 4, 2023) as well as historical data. The data in NMDB is typically available at 1-minute resolution, but also in 1-hour resolution to study long-term variations. For intermediate resolutions, the database can provide averaged data as well.

While NMDB stores all data in an SQL database, only few users have (and need) direct access to the database: Neutron Monitor stations sending real-time data to NMDB, and applications that work with real-time data, for example GLE Alert tools. Regular users do not want to work with SQL commands to access the data, so a graphical user interface, the NMDB event search tool NEST (shown in [Fig. 1](#)), has been developed that allows users to interactively select stations and time ranges, datatypes and additional data like sunspot numbers and provides the results as configurable plot, or in ASCII format to download for further processing.

3 ways 2 use NEST





? Quick Plots


conditions & information to use data


top


[jul 2022] In memoriam: Pr. Lev I. Dorman (1929-2022)


[jul 2022] Warning: All lines of the ascii files.


Last 3 days


Basic Plot Example


GLE&FD Plot Examples


Kp Ri p+ Plot Examples

? Stations

(When selecting multiple stations, note that only one variable can be plotted)

<input type="checkbox"/> AATA	<input type="checkbox"/> AATB	<input type="checkbox"/> APTY	<input type="checkbox"/> ARNM	<input type="checkbox"/> ATHN
<input type="checkbox"/> BKSJ	<input type="checkbox"/> CALG	<input type="checkbox"/> CALM	<input type="checkbox"/> DJON	<input type="checkbox"/> DOMB
<input type="checkbox"/> DOMC	<input type="checkbox"/> DRBS	<input type="checkbox"/> ESOI	<input type="checkbox"/> FSMT	<input type="checkbox"/> HRMS
<input type="checkbox"/> INVK	<input type="checkbox"/> IRK2	<input type="checkbox"/> IRK3	<input type="checkbox"/> IRKT	<input type="checkbox"/> JBGO
<input type="checkbox"/> JUNG	<input type="checkbox"/> JUNG1	<input type="checkbox"/> KERG	<input type="checkbox"/> KIEL	<input type="checkbox"/> KIEL2
<input type="checkbox"/> LMKS	<input type="checkbox"/> MCRL	<input type="checkbox"/> MGDN	<input type="checkbox"/> MOSC	<input type="checkbox"/> MRNY
<input type="checkbox"/> MWSN	<input type="checkbox"/> MXCO	<input type="checkbox"/> NAIN	<input type="checkbox"/> NANM	<input type="checkbox"/> NEU3
<input type="checkbox"/> NEWK	<input type="checkbox"/> NRLK	<input type="checkbox"/> NVBK	<input type="checkbox"/> OULU	<input type="checkbox"/> PSNM
<input type="checkbox"/> PTFM	<input type="checkbox"/> PWNK	<input type="checkbox"/> ROME	<input type="checkbox"/> SANB	<input type="checkbox"/> SNAE
<input type="checkbox"/> SOPB	<input type="checkbox"/> SOPO	<input type="checkbox"/> TERA	<input type="checkbox"/> THUL	<input type="checkbox"/> TSMB
<input type="checkbox"/> TXBY	<input type="checkbox"/> YKTK			

Online* stations in green

? Date Selection (UTC)

Last days hours mins
 From
 To
 GLE number/date [detailed list](#)
 FD number/date

? Resolution

Time resolution:
 Force**
 Smooth window:

? Data variables

Pressure & efficiency corr.
 Pressure corrected
 Uncorrected
 Pressure

? Scale

Relative scale
 Counts/s*
 Log scale
 (* mbar for pressure)

? Output

Plot
 Ascii
 Plot & ascii

read.nmdb.eu via TCP/IP

* online means some data (realtime or not) have been uploaded during the last 15mn

** force parameter: Read note 1 and note 3 of the help file

Contact: questions@nmdb.eu

? NMDB tables

? Overplot main

? Overplot Ri

? Proton / Kp plots

? Env. & meta data

? Scaling Options

? Event Options

? Ascii Options

? Style Options

NEST is provided by




Fig. 1: NEST web interface to NMDB data.

While this is excellent for occasional browsing the data, it is a bit cumbersome for serious data analysis. To enable automated downloads of NMDB data the NEST manual ‘3 ways 2 use NEST’ (Fuller 2022) provides also instructions on retrieving data in ASCII format without having to fill in a webform. A query string can be created and the data can be accessed with a tool like ‘wget’ or ‘curl’. When the data has been downloaded, it can be further processed by the user.

The python programming language has become the de-facto standard for Data Science (VanderPlas 2016) at most universities, even some proprietary software can use functions written in python (Origin 2022). So instead of downloading NMDB data with hand-created queries, or with simple shell scripts, it makes sense to download the data directly in python, where the data will be analyzed. Here we present some python functions to easily access user selected data from NMDB, and some examples on how to work with this data using the pandas library, a popular tool among data scientists (The pandas development team 2022).

2. NEST queries

NMDB data can be downloaded with a special URL, as explained in the NEST manual. This URL defines the Neutron Monitor station, the datatable, the datatype, and the timerange of the requested data. One query can either combine data for several stations (and one datatype), or one station with several datatypes (like uncorrected, pressure, and corrected data). We have created separate python functions for these use cases: `nest.multi` for querying multiple stations, and `nest.single` for querying a single station. Both functions use the same parameters:

- `station`: station shortname as used in NMDB (four or five letters, list of strings for multi, string for single)
- `table`: data table used in NMDB with the following abbreviations:
 - `e`: `corr_for_efficiency`
 - `c`: `corr_for_pressure`
 - `u`: `uncorrected`
 - `p`: `pressure_mbar`
- `data`: `ori`, `revori` (revised and original data merged), or `1h`
- `start`: datetime of the start of the requested data
- `end`: datetime of the end of the requested data

The functions include no error checking for valid station names or datetimes or the amount of data that will be returned by NEST. The data will be returned in the highest available resolution (1-min for `ori` and `revori`), or, for longer time periods, averaged to longer durations by NEST. For details, see the NEST manual (Fuller 2022).

2.1 `nmdb.multi`

The `nmdb.multi` function allows to access one datatype for multiple stations. The required arguments are a list with the station names, the datatable which can be one of `revori`, `ori`, or `1h`, the datatype, which can be one of `e`, `c`, `u`, `p`, and the datetimes for the start and the end of the requested data. See Fig. 2 for an example using the `nest.multi` function.

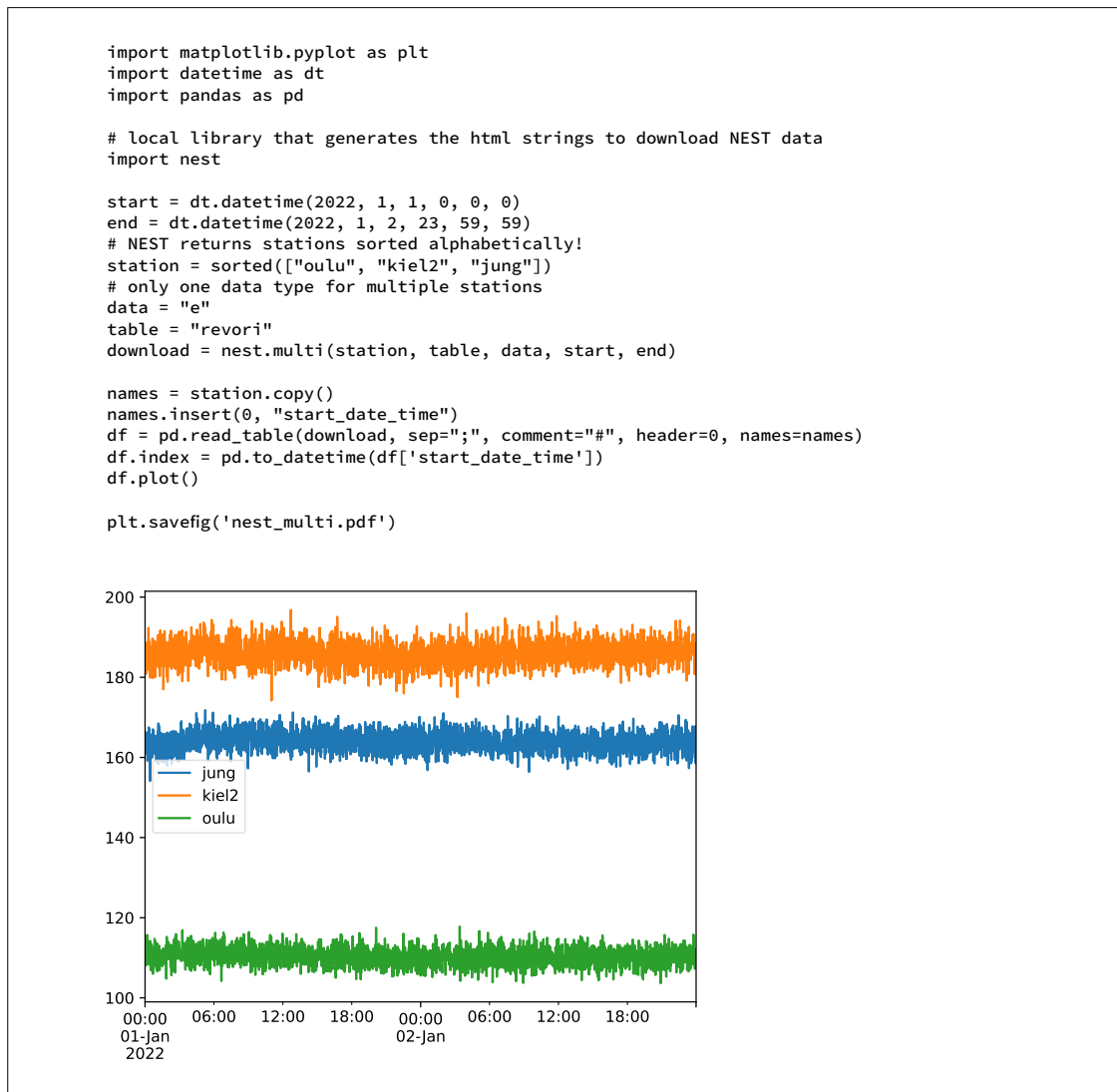


Fig. 2: Example using the `nest.multi` function.

2.2 `nmdb.single`

The `nmdb.single` function allows to access several datatypes for a single station. The required arguments are a string with the station name, the datatable, which can be one of `revori`, `ori`, or `1h`, a list with the datatype (which can be one of `e`, `c`, `u`, `p`), and the datetimes for the start and the end of the requested data. See Fig. 3 for an example using the `nest.single` function.

2.3 `nmdb.header`

NEST returns meta data together with the requested data as comments, however this is currently not stored in the pandas dataframe. To access the meta data a separate `nmdb.header` function is provided. This function takes the url created by either `nmdb.multi` or `nmdb.single` and extracts the meta data into a string. The meta data contains information such as if the data has been averaged or revised and how to cite the data. See Fig. 4 for an example using the `nest.header` function.

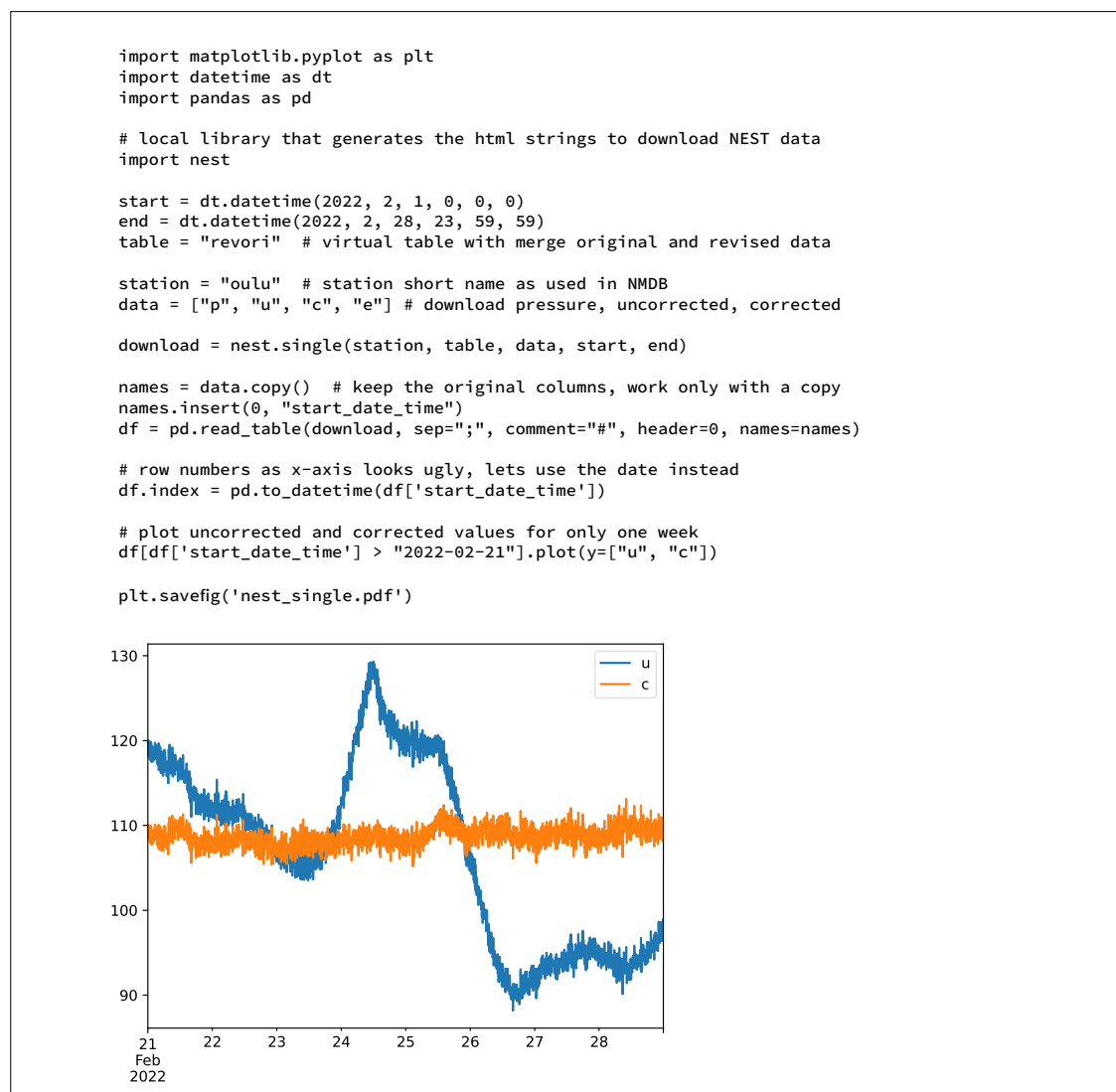


Fig. 3: Example using the nest.single function.

3. Installation

The python sourcecode for the nest module, the examples for the multi, single and header function, as well as a jupyter notebook with further examples are available on the NMDB website at <https://www.nmdb.eu/software/python/nest> (last accessed July 4, 2023). Updates to the nest module as well as extensions, for example an option to select the resolution of the data, will be made available on that webpage.

To install the nest module, simply copy the module nest.py and any example scripts you want to use into your working directory. If you execute the example scripts in an Integrated Development Environment (IDE) like spyder, or use the jupyter notebook, you can interactively work with the dataframes and immediately display the plots without adding further commands that would be necessary to execute in a stand-alone python script.

```

In [1]: import datetime as dt
import pandas as pd

# local library that generates the html strings to download NEST data
import nest

start = dt.datetime(2022, 2, 1, 0, 0, 0)
end = dt.datetime(2022, 2, 28, 23, 59, 59)
table = "revori" # virtual table with merge original and revised data

station = "oulu" # station short name as used in NMDB
# download pressure, uncorrected, corrected (for pressure) and efficiency corrected data
data = ["p", "u", "c", "e"]

download = nest.single(station, table, data, start, end)
header = nest.header(download)
print(header)

-----QUERY RESULTS SUMMARY-----
STATION: OULU
START TIME: 2022-02-01 00:00:00 UTC
END TIME: 2022-02-28 23:55:00 UTC
NMDB TABLE: revised original
REV EQ. ORI: Yes, revised data are identical to the original data for this period
DATA TYPE: pressure_mbar(RPRESS)
OTHER DATA: uncorrected(RUNCORR)corr_for_pressure(RCORR_P) corr_for_efficiency(RCORR_E)
AVERAGING: Yes / 5 min
ORIGINAL RES: 1 min

-----
Timestamps always correspond to the beginning of the time interval
-----

Data retrieved via NMDB are the property of the individual data providers. These data are free for non commercial use to within the restriction imposed by the providers. If you use such data for your research or applications, please acknowledge the origin by a sentence like 'We acknowledge the NMDB Database (www.nmdb.eu) founded under the European Union's FP7 programme (contract no. 213 007), and the PIs of individual neutron monitors at: Oulu (Sodankyla Geophysical Observatory of the University of Oulu, Finland)

```

Fig. 4: Example using the nest.header function.

4. Conclusion

We have presented an open source python module that enables easy access to NMDB data via the NEST webinterface. Users can access all NMDB data simply by specifying stations, time-periods and datatypes to create a URL to the data and read in the data using this URL into a pandas dataframe. With the data in a dataframe users can plot the data or further analyse it using all the powers provided by pandas and the entire python ecosystem.

References

- Fuller, N. 2023, 3 ways 2 use NEST, <https://www.nmdb.eu/nest/help.php#howto> (last accessed January 16, 2023)
- NMDB 2008, the Neutron Monitor Database, <https://nmdb.eu> (last accessed January 16, 2023)
- Origin 2022, <https://www.originlab.com/doc/python/Run-Python-in-Origin> (last accessed January 16, 2023)
- The pandas development team 2022, pandas-dev/pandas: Pandas (v1.5.2), <https://doi.org/10.5281/zenodo.3509134>
- VanderPlas, J. 2016. The Python Data Science Handbook. O'Reilly.

Open Access

This paper is published under the Creative Commons Attribution 4.0 International license (<https://creativecommons.org/licenses/by/4.0/>). Please note that individual, appropriately marked parts of the paper may be excluded from the license mentioned or may be subject to other copyright conditions. If such third party material is not under the Creative Commons license, any copying, editing or public reproduction is only permitted with the prior consent of the respective copyright owner or on the basis of relevant legal authorization regulations.

Session 6: Abstracts

The catalog of the thunderstorm ground enhancement events registered on Mt. Aragats

Davit Aslanyan 

Correspondence

Yerevan Physics Institute, Cosmic Ray Division, Yerevan, Armenia

Abstract

The new phenomena in atmospheric physics are the high-energy processes culminating in huge fluxes of electrons and gamma rays incident on the earth's surface. We have continuously monitored elementary particle fluxes on the Mt. Aragats high-altitude research station of the Cosmic Ray Division of A. Alikhanyan National Laboratory discovered a powerful electron accelerator in the thunderclouds. To reach a complete understanding of high-energy processes in the terrestrial atmosphere and to find new and easily measured indicators of the global change in the climate system, we form a database of these rather rare events. Throughout the years 2009–2022, we have registered nearly 500 thunderstorm ground enhancement events (TGEs). We recover energy spectra of TGE electrons and gamma rays, calculate the significances of peaks relative to fair-weather values, measure geomagnetic and near-surface electric fields, distances to lightning flashes, and register atmospheric discharges. As well we monitor skies above the research station on Mt. Aragats by panoramic cameras. As a result of the measurements, a database was created containing data from continuous observations of fluxes of neutral and charged particles together with data on disturbances of the near-surface electric field measured by a network of BOLTEK's EFM-100 electric field mills and meteorological conditions from automatic weather stations from DAVIS Instruments. Now we form an EXCEL catalog of 237 TGE events observed in 2013–2022 containing 11 parameters including the peak intensity of TGE as registered by detectors with 0.7 MeV, 3 MeV, 7 MeV energy thresholds, temperature, and dew point during the TGE and atmospheric electric field parameters. From the catalog one can directly access the data analysis ADEI platform with its rich possibilities of multivariate visualizations and statistical tools for the multivariate correlation analysis of particle fluxes, lightning flashes, and numerous environmental parameters.

NMDB status, a brief tutorial

Christian T. Steigies 

Correspondence

Extraterrestrial Physics, Institute of Experimental and Applied Physics, Kiel University, Germany

Abstract

Since 2008 the EU FP7 funded Neutron Monitor database (NMDB) is providing access to 1-minute neutron monitor data in real-time as well as different neutron monitor data products for the public. Over the years, several data products have disappeared or had to be disabled for security reasons, others have been extended or set up from scratch to make accessing the data easier for the user. After an overview of the status of the NMDB, I will give an interactive tutorial on accessing real-time data from NMDB using python and pandas. We will use a Jupyter Notebook that runs in your web browser without you having to install additional software on your computer. If you want to participate in this exercise, please mention this in your registration email so that we can set up an account for you in our JupyterHub server.

Program of the meeting

Monday, September 26

CR and the atmosphere, data bases, catalogues

Chairperson: Ilya Usoskin

Session manager: Maria Abunina

Time [UTC]	Presenter	Title
Tutorials		
08:00 - 09:00	S. Poluianov	Cosmic rays and the atmosphere
09:00 - 10:00	C. Steigies	NMDB status, a brief tutorial
Contributed talks		
11:00 - 11:05	H. Mavromichalaki	Opening
11:10 - 11:15	L. Pustilnik	Obituaries
11:15 - 11:35	A. Chilingarian	Neutron monitors detecting cores of extensive air showers
11:35 - 11:55	P. Makrantonis et al.	Atmospheric cosmic ray induced ionization and radiation affecting aviation
11:55 - 12:05	D. Aslanyan	The catalog of the thunderstorm ground enhancement events registered on Mt. Aragats
12:05 - 12:20		General discussion
12:40 - 13:00	H. Martoyan	Forbush decrease observed by nodes of SEVAN East-European particle detector network on November 2021
13:00 - 13:10	R. Kataoka et al.	Local environmental effects on cosmic ray observations at Syowa Station in the Antarctic: PARMA-based snow cover correction for neutrons and machine learning approach for neutrons and muons
13:10 - 13:30	C. Steigies and N. Fuller	Accessing NMDB data using NEST and pandas
13:30 - 14:00		General discussion

Tuesday, September 27

CR in the Heliosphere: spatial and time variability

Chairperson: Olga Kryakunova

Session manager: Agnieszka Gil-Świdarska

Time [UTC]	Presenter	Title
Tutorials		
09:00 - 10:00	M. Laurenza	CR in the Heliosphere
Contributed talks		
11:00 - 11:20	K. Munakata et al.	Large amplitude bidirectional anisotropy of cosmic-ray intensity observed in November, 2021
11:20 - 11:40	V. Yanke et al.	Residual modulation of galactic cosmic rays in the heliosphere
11:40 - 11:50	P. Gololobov et al.	Cosmic ray angular distribution dynamics during Forbush decrease in 3-4 November 2021

11:50 – 12:00	E. Ntina et al.	Magnetospheric effects on cosmic rays during the magnetic storm of March 2015
12:00 – 12:10	K. Poopakun et al.	Solar magnetic polarity effect on neutron monitor count rates: comparing latitude surveys and antarctic stations
12:10 – 12:25		General discussion
12:40 – 13:00	P. Väisänen et al.	Revised neutron monitor scaling factor and modulation potential determination for 1964-2021
13:00 – 13:20	P. Muangha et al.	Cosmic ray intensity and spectral changes during 27-day variations using time-delay measurements from Antarctic neutron monitors
13:20 – 13:40	S. Belov and A. Belov	Real time monitoring of the angular distribution of cosmic rays with Ring of Stations method using NMDB data
13:40 – 14:00		General discussion

Wednesday, September 28

Neutron detector instrumentation, stability, and response function

Chairperson: David Ruffolo

Session manager: Ludwig Klein

Time [UTC]	Presenter	Title
Tutorials		
08:00 – 09:00	D. Ruffolo	Neutron monitor electronics for spectral information from a single neutron monitor
09:00 – 10:00	A. Mishev	Neutron detector response functions
Contributed talks		
11:00 – 11:20	D. Sapundjiev and S. Stankov	Neural networks for identification of neutron monitor faulty tube-counts
11:20 – 11:40	R.D. Strauss et al.	First results of the SA Agulhas II mobile mini-neutron monitor: Instrumental characterization and environmental sensitivity
11:40 – 11:50	P. Väisänen and I. Usoskin	Correction of snow effects on Oulu data using local snow depth data
11:50 – 12:00	P. Yakum et al.	Latitude surveys of time-delay histograms from a semi-leaded neutron monitor during 2018-2020
12:00 – 12:10	M. Livada et al.	Neutron monitor yield function: improved spectral computations of the Forbush decrease of June 2015
12:10 – 12:25		General discussion
12:40 – 13:00	J. Ryan et al.	US-based Simpson neutron monitor network
13:00 – 13:10	A. Lukovnikova	New registration system of cosmic ray stations of ISTP SB RAS
13:10 – 13:30	C. Bland and A. Kouznetsov	Calgary neutron monitor efficiency factor estimation after major renovation
13:30 – 13:40	C. Consolandi et al.	Haleakala neutron monitor redeployment and calibration with AMS data
13:40 – 14:00		General discussion

Thursday, September 29**GLE analysis**

Chairperson: Monica Laurenza
 Session manager: Maria Gerontidou

Time [UTC]	Presenter	Title
Tutorials		
08:00 – 09:00	A. Papaioannou	What do we learn from ground level enhancements?
09:00 – 10:00	E. Flückiger, R. Bütikofer	40 years of neutron observations
Contributed talks		
11:00 – 11:20	A. Sáiz et al.	Magnetic field line path length variations and effects on solar energetic particle transport
11:20 – 11:40	J. Rodriguez and B. Kress	GOES observations of solar protons during ground level enhancements
11:40 – 12:00	J. J. Blanco et al.	Solar activity as observed by neutron monitors and muon telescopes in the same location
12:00 – 12:20		General discussion
12:40 – 13:00	A. Papaioannou et al.	Investigating GLE73, the first ground level enhancement of solar cycle 25
13:00 – 13:20	A. Mishev et al.	The GLE #73 on 28 October 2021: spectra, angular distribution and terrestrial effects
13:30 – 13:40	R. Bütikofer and C. Steigies	Solar energetic particle event on 28 October 2021 as observed by the neutron monitor network
13:40 – 14:00		General Discussion

Friday, September 30**GLE analysis and space weather services**

Chairperson: Du Toit Strauss
 Session manager: Athanasios Papaioannou

Time [UTC]	Presenter	Title
Tutorials		
09:00 – 10:00	M. Abunina	Cosmic rays and space weather
Contributed talks		
11:00 – 11:20	S. Koldobskiy et al.	A new reconstruction of solar energetic particle fluence for GLE events
11:20 – 11:40	N. Shlyk et al.	Solar energetic particle events and Forbush decreases driven by the same solar sources
11:40 – 12:00	H. Mavromichalaki et al.	The updated GLE alert system by ANEMOS
12:00 – 12:20		General discussion
12:40 – 13:00	K.-L. Klein et al.	A relationship between rise times and decay times of relativistic solar particle events observed by neutron monitors
13:00 – 13:20	P. Gololobov et al.	NMDB and space weather forecasting
13:20 – 13:40	O. Kryakunova et al.	Behaviour of galactic cosmic rays density and vector anisotropy before and during high-energy magnetospheric electron flux enhancements
13:40 – 13:55		General discussion
13:55 – 14:00		Closing

